



JACOBS
UNIVERSITY

Cucurbituril Complexes and their Spectral Characterization

by

Mohammad A. Alnajjar

A thesis submitted in partial fulfillment

of the requirements for the degree of

Doctor of Philosophy

in Chemistry

Approved Dissertation Committee

Prof. Dr. Werner M. Nau, Jacobs University Bremen

Prof. Dr. Detlef Gabel, Jacobs University Bremen

Prof. Dr. Andreas Hennig, Osnabrück University

Prof. Dr. Uwe Pischel, University of Huelva

Date of Defense: 29-07-2021

Department of Life Sciences and Chemistry

Statutory Declaration

Family Name, Given/First Name	Al Najjar, Mohammad
Matriculation number	20331542
What kind of thesis are you submitting: Bachelor-, Master- or PhD-Thesis	Ph.D. Thesis

English: Declaration of Authorship

I hereby declare that the thesis submitted was created and written solely by myself without any external support. Any sources, direct or indirect, are marked as such. I am aware of the fact that the contents of the thesis in digital form may be revised with regard to usage of unauthorized aid as well as whether the whole or parts of it may be identified as plagiarism. I do agree my work to be entered into a database for it to be compared with existing sources, where it will remain in order to enable further comparisons with future theses. This does not grant any rights of reproduction and usage, however.

The thesis has been written independently and has not been submitted at any other university for the conferral of a Ph.D. degree; neither has the thesis been previously published in full.

German: Erklärung der Autorenschaft (Urheberschaft)

Ich erkläre hiermit, dass die vorliegende Arbeit ohne fremde Hilfe ausschließlich von mir erstellt und geschrieben worden ist. Jedwede verwendeten Quellen, direkter oder indirekter Art, sind als solche kenntlich gemacht worden. Mir ist die Tatsache bewusst, dass der Inhalt der Thesis in digitaler Form geprüft werden kann im Hinblick darauf, ob es sich ganz oder in Teilen um ein Plagiat handelt. Ich bin damit einverstanden, dass meine Arbeit in einer Datenbank eingegeben werden kann, um mit bereits bestehenden Quellen verglichen zu werden und dort auch verbleibt, um mit zukünftigen Arbeiten verglichen werden zu können. Dies berechtigt jedoch nicht zur Verwendung oder Vervielfältigung.

Diese Arbeit wurde in der vorliegenden Form weder einer anderen Prüfungsbehörde vorgelegt noch wurde das Gesamtdokument bisher veröffentlicht.

.....
Date, Signature

To my beloved family and parents

*“If we did all the things we are
capable of, we would literally
astound ourselves.”*

Thomas Edison

Abstract

This doctoral thesis provides insights into the chemistry of host-guest complexes of hydrophobic amino molecules or hydrophobic amines attached with dyes, and their characteristics after complexation with cucurbit[n]urils ($n = 7$ and 8) was studied. It describes how to calculate the binding constants by different methods and techniques with minimum error and propagation error. Different types of complex can be formed, accompanied by changes in guest luminescence properties after complexation.

The first project in the thesis presents a new fluorophore class for the design of reporter dyes for supramolecular host-guest complex formation with cucurbit[7]uril (CB7). The boron-dipyrromethene group (BODIPY) contains protonatable aniline nitrogen in the meso-position of the BODIPY chromophore, which was functionalized with known binding motifs for CB7.

The second project in the thesis describes the formation of supramolecular complexation between cucurbit[n]urils ($n = 7$ and 8) and an amphiphilic pyridinium-functionalized anthracene (AnPy) in aqueous solution. The host-guest complexation between CB n and AnPy was studied in detail by using optical spectroscopy.

The third project in the thesis describes how to use different techniques to calculate accurate and precise binding constants with CB7, and how to establish a series of reference compounds to determine CB7 binding affinities by direct and competitive titrations. The compounds have been selected according to their commercial availability to be suitable for various measurement techniques. The binding affinity of berberine chloride was established as a central reference point, which could be measured by fluorescence spectroscopy, ITC, and ^1H NMR. The sensitivity of its K_a value to trace impurities in Millipore water was observed in direct titrations but not in competitive titrations. The particular impurities appeared to have similar effects on the reference compounds and the competitors. Within a series of competition experiments, reference compounds were established to cover a wide range of affinities (mM-fM).

Acknowledgments

I would like to express my sincere gratitude to my supervisor Prof. Dr. Werner M. Nau, for allowing me to carry out the Doctor of Philosophy in his research group. I am so profoundly grateful for his help, professionalism, valuable guidance, encouragement, and financial support throughout my Ph.D. study. Indeed, I do not have enough words to express my deep and warm appreciation.

I would also like to thank Dr. Andreas Hennig for his continuous support, encouragement, follow-up, guidance, and encouragement throughout the research work. I appreciate his patience and motivation. I am very grateful for his assistance in writing this thesis and working in the projects.

Special thanks go to Dr. Khaleel Assaf to collaborate on different projects with me and share his knowledge and skills in various topics and for always being helpful and supportive. I would like to gratefully acknowledge Prof. Dr. Detlef Gabel and Prof. Dr. Uwe Pischel for their acceptance to become members of my thesis committee.

I am also thankful to all former and present members of the Nau group for collaborative work, fruitful discussions, friendly relations, support, help, and advice. I thank Dr. Mohamed Nilam, Dr. Alexandra Lazar, Dr. Suhang He, Dr. Chusen Huang, Dr. Shuai Zhang, Dr. Maik Jacob, Dr. Andrea Barba-Bon, Dr. Yan-Cen Liu, Thomas Schwarzlose, Yao Chen, Jinling Zhang, and Ruixue Jiang. Also, I thank all my friends for sharing with me a nice moment and pleasant time in Bremen.

I would like to also thank Deutsche Forschungsgemeinschaft (DFG) for the financial support and continuous effort in making sure all projects were well funded.

Last but not least, I must express my profound gratitude to my parents and my wife, providing me with unfailing support and continuous encouragement throughout my years of studies. This aim would not have been achieved without them.

Thank you to everyone

List of Publications

1. Assaf, K. I.; **Alnajjar, M. A.**; Nau, W. M., Supramolecular Assemblies through Host-Guest Complexation between Cucurbiturils and an Amphiphilic Guest Molecule. *Chem. Commun.* **2018**, *54*, 1734-1747.
2. **Alnajjar, M. A.**; Bartelmeß, J.; Hein, R.; Ashokkumar, P.; Nilam, M.; Nau, W. M.; Rurack, K.; Hennig, A., Rational Design of Boron-dipyrromethene (BODIPY) Reporter Dyes for Cucurbit[7]uril. *Beilstein J. Org. Chem.* **2018**, *14*, 1961-1971.
3. Nilam, M.; Ahmed, M.; **Alnajjar, M. A.**; Hennig, A., Characterization of Mixed-Ligand Shells on Gold Nanoparticles by Transition Metal and Supramolecular Surface Probes. *Analyst* **2019**, *144*, 579-586.
4. Assaf, K. I.; Abed alfattah, H.; Eftaiha, A. F.; Bardaweel, S. K.; **Alnajjar, M. A.**; Alsoubani, A. F.; Qaroush, K. A.; El-Barghouthi, I. M.; Nau, W. M., Encapsulation of Ionic Liquids inside Cucurbiturils. *Org. Biomol. Chem.* **2020**, *18*, 2120-2128.

Manuscript in Preparation

- 1- **Alnajjar, M. A.**, Hennig, A., and Nau, W. M., A Reference Scale of Cucurbit[7]uril Binding Affinities.

List of Attended Conferences

I have attended the following conference during my Ph.D. studies.

- 1- Suprachem, 24-26.02.2019, Würzburg. Poster: “Rational design of boron-dipyrromethene (BODIPY) reporter dyes for cucurbit[7]uril”.

Table of Contents

Abstract.....	xi
Acknowledgments	xiii
List of Publications	xv
Manuscript in Preparation	xv
List of Attended Conferences.....	xvii
Chapter 1. Introduction	3
1.1 Supramolecular Host-Guest Complexes	3
1.2 Cucurbit[<i>n</i>]urils	3
1.3 Cucurbituril Guest Binding	4
1.4 Host-Guest Pairs and Binding Constants	5
1.5 Host-Guest Complexes of Fluorescent Dyes with Macrocyclic Receptors	8
1.6 Indicator Displacement Assays	9
1.7 Limitations of Binding Titrations.....	10
1.8 High-Affinity Binders	11
1.9 New Reporter Pairs for Molecular Recognition.....	12
Chapter 2. Rational Design of Boron-dipyrromethene (BODIPY) Reporter Dyes for Cucurbit[7]uril.....	17
2.1 Introduction	17
2.2 Synthesis of Different BODIPY Derivatives	21
2.3 Spectroscopic Characterization of Dyes.....	22
2.4 Complexation with CB7.....	25
2.5 Applications of BODIPY-CB7 Complexes.....	28
Chapter 3. Supramolecular Assemblies through Host-Guest Complexation between Cucurbiturils and an Amphiphilic Guest Molecule.....	35
3.1 Introduction	35
3.2 Formation of Supramolecular Assemblies between Pyridinium-Functionalized Anthracene and Cucurbiturils.....	36

3.3 Investigation of Supramolecular Assemblies by Optical Spectroscopy.....	36
3.4 Investigation of Supramolecular Assemblies by ¹ H NMR Spectroscopy	39
3.5 Binding Modes for AnPy with CB7 and CB8.....	40
3.6 Investigation the Supramolecular Assemblies by DLS and TEM.....	42
3.7 Supramolecular Assembly Responses to External Stimuli	43
Chapter 4. A Reference Scale of Cucurbit[7]uril Binding Affinities	47
4.1 Introduction	47
4.2 Reference Compounds for μM Affinity	50
4.3 Reference Compounds for nM Affinity	54
4.4 Reference Compounds for pM Affinity	58
4.5 Reference Compounds for fM Affinity	60
4.6 Reference Compounds for mM Affinity	61
4.7 Binding Constants of High-Affinity Guests	61
Summary and Outlook	67
References.....	Error! Bookmark not defined.
Appendices.....	83
A.1 Supporting Information for Chapter 2.....	83
A.1.1 Materials and Instrumentation	83
A.1.2 Abbreviations.....	84
A.1.3 Synthesis	85
A.1.4 NMR Spectra of Synthesized Compounds	93
A.1.5 Determination of Fluorescence Quantum Yields.....	102
A.1.6 Global Fitting Procedure.....	103
A.1.7 Supporting Figures.....	105
A.2 Supporting Information for Chapter 3.....	107
A.2.1 Methods	107
A.2.2 Synthesis and Characterization of AnPy	107
A.2.3 Job's Plots of the CBn•AnPy Complexes.....	111

A.2.4	ITC Experiments	111
A.2.5	Competitive Titrations	112
A.2.6	Photo-oxidation Reaction of AnPy	115
A.3	Supporting Information for Chapter 4	116
A.3.1	Materials and Instrumentation	116
A.3.2	Abbreviations	116
A.3.3	Binding Constant Determinations and Error Calculations	117
A.3.5	Berberine Chloride (BE)	122
A.3.6	Hexamethylenediamine (HMD)	124
A.3.7	<i>p</i> -Xylylenediamine (PXD)	127
A.3.8	Putrescine (Put)	130
A.3.9	Tetrabutylammonium Chloride (TBA)	132
A.3.10	Cyclohexylmethylamine (CHMA)	135
A.3.11	<i>Cis</i> -1,4-Bis(aminomethyl)-cyclohexane (CBAMC)	137
A.3.12	(2,3-Diazabicyclo[2.2.2]oct-2-enyl) Methylamine (DBO-A)	138
A.3.13	Adamantylamine (ADA)	140
A.3.14	Aminomethyladamantane (AMADA)	143
A.3.15	<i>N,N</i> -Dimethylaminomethylferrocene (FDMA)	146
A.3.16	(<i>S</i>)-2-(Adamantan-1-yl)-2-aminoacetic Acid Hydrochloride (AMADA-aa)	149
A.3.17	Aminomethyladamantane-putrescine (AMADA-Put)	150
A.3.18	<i>Trans</i> -1,4-Bis(aminomethyl)-cyclohexane (TBAMC)	152
Curriculum Vitae		Error! Bookmark not defined.

Chapter 1

Introduction

Chapter 1. Introduction

1.1 Supramolecular Host-Guest Complexes

Supramolecular host-guest chemistry is focuses on the study of intermolecular interactions among others, on selective interactions between host and guest molecules.^[1] Frequently, a host is a molecular container with a large cavity volume such as cyclodextrin (CD),^[2] calixarene (CX),^[3] and cucurbituril (CB).^[4-5] Guest molecules display both a complementary shape and significant interaction with host molecules. The formation of the host-guest complexes involves non-covalent interactions, including hydrogen bonding, electrostatic, hydrophobic, and Van der Waals interactions.^[5] These interactions provide selectivity between host and guest, which presents a form of molecular recognition.^[4]

Fluorescent dyes are well-known molecular probes to assess microenvironmental parameters, membrane translocations, and enzymatic transformations.^[6] In addition, fluorescent dye molecules are suitable for monitoring the formation of host-guest complexes.^[7] The encapsulation of the dye molecules inside a macrocyclic cavity leads to large changes in their photophysical properties, including their UV-visible absorption and fluorescence.^[5,7] Such changes are utilized in supramolecular chemistry to determine thermodynamic and kinetic parameters. Also, the binding of fluorescent dyes with macrocyclic host molecules provides useful information about the structures of supramolecular assemblies.^[8-9]

The present thesis focuses on water-soluble macrocycles with a perspective of using them in molecular recognition. Also, it discusses the effect of host-guest complexation on the UV-vis absorption and emission properties, and how their complex formation can be used in sensing and imaging applications. Further, binding constants, ¹H NMR spectral shifts, fluorescent enhancements, and quenching effects have been accurately quantified.

1.2 Cucurbit[n]urils

Cucurbit[n]urils (CB_n, *n* = 5-14) are rigid, symmetric macrocycles, which are composed of two identical carbonyl-linked portals with a hydrophobic cavity. Initially, CB6 were discovered by Behrend in 1905.^[10] As for CDs, and CXs, they exist in different sizes such as CB5, CB6, CB7, CB8, CB10, and CB14 (**Figure 1.1**).^[11-12] CB_n have been used in several applications due to their ability to form

binary and ternary host-guest complexes in aqueous solution. Several previous studies have focused on the CB synthesis,^[13] functionalization,^[14] host-guest binding properties,^[4] membrane translocation,^[15] enzymatic transformations,^[16-17] drug delivery,^[18] and nanotechnology.^[19] Numerous applications of CBs rely on the formation of dynamic complexes with different guest molecules. Research efforts by the CB community focused on identifying and characterizing suitable guest molecules. However, tailoring functional systems including CBs would not be possible without proper knowledge of binding affinity and kinetics of complexation of the host molecules.

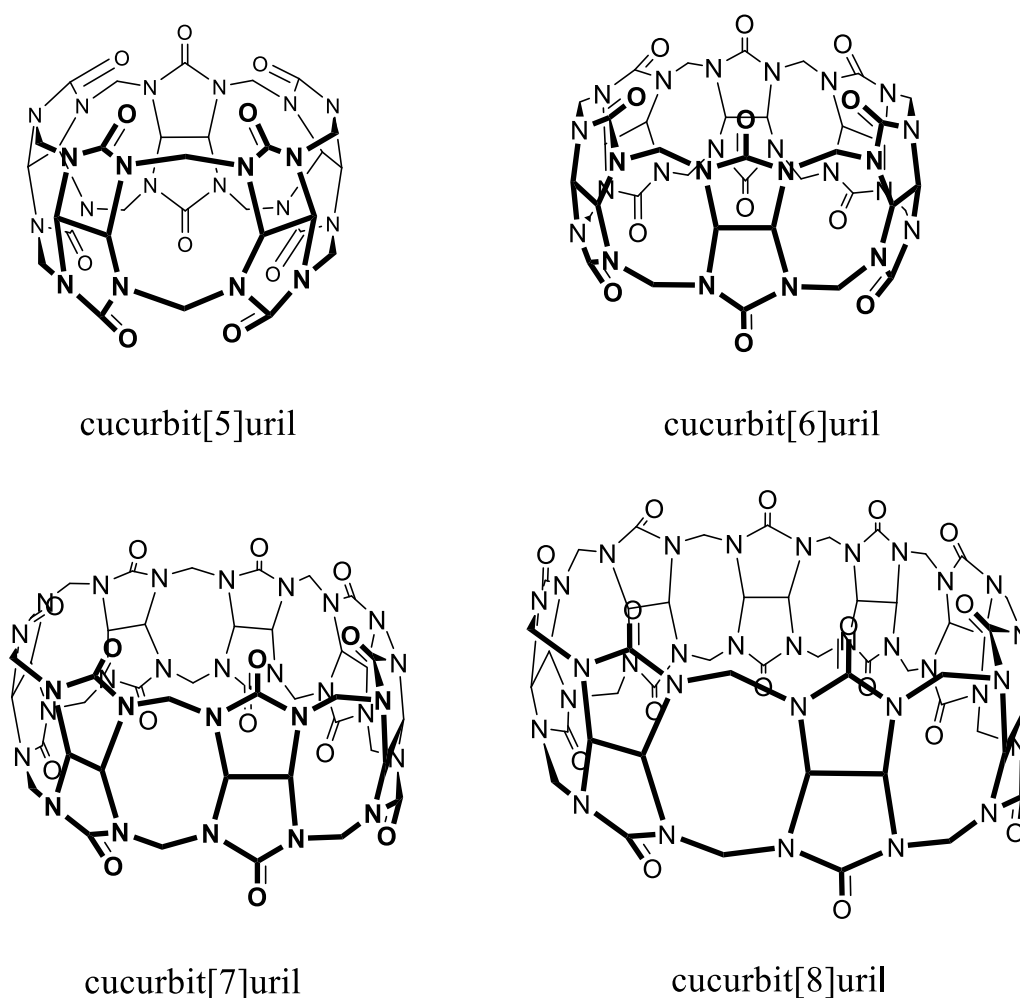


Figure 1.1 Chemical structures of cucurbituril homologues.

1.3 Cucurbituril Guest Binding

CBs are composed from n glycoluril units, which are laced in a ring-like arrangement through methylene bridges.^[5] The orientation of the glycoluril subunits is an essential factor for understanding the encapsulation properties of CBs. The

number of glycoluril repeat units limits the portal size and cavity volume.^[20] Further, the arrangement of the glycoluril repeat units results in a hydrophobic cavity including carbonyl-lined portals. Factors that influence the binding include 1) portal interactions, 2) cavity interactions, 3) cavity size fit. The dipolar nature of the carbonyl portal of the CBs are highly attractive for cation binding via ion-dipole interactions.^[21] Alkaline earth metals,^[22] transition metals,^[23] lanthanides and actinides,^[23-24] imidazolium ions,^[25] and ammonium ions^[26] have been reported to bind to the portals of CBs. The inner cavity of CBs possesses outstanding hydrophobicity suitable for encapsulating hydrophobic guests.^[27] For instance, alkylated ammonium ions bind to the portal of CBs, while the alkyl chain is accommodated inside the CB cavity.^[5]

Moreover, dicationic species can be selectively separated by CBs, due to their hydrophobic region. For example, CB6, CB7, and CB8 bind strongly to putrescine, cadaverine, and bis-amino adamantane, respectively.^[5] Another key factor for the binding of guest molecules inside the CB cavity is the packing coefficient, which is the ratio between guest and cavity volume. A packing coefficient value of *ca.* 55% was found to be ideal for the formation of stable host-guest complexes.^[5] Either a smaller or larger value of the packing coefficient is associated with lower binding affinities.^[5,28]

1.4 Host-Guest Pairs and Binding Constants

The association constant between host and guest is a significant benchmark to assess the potential host-guest/reporter pairs.^[6,29] A high binding affinity allows low reporter pair concentrations and ensures the function of a sensor as a non-interfering part in the sensing of analytes.^[6,30] The binding affinity between host and guest can be determined with different methods based on the intrinsic properties of the host-guest pair. For instance, since most of the investigated fluorescent dyes (**Figure 1.2**) are weakly fluorescent, the method of choice is “direct fluorescence titrations”.^[31-32] In this direct titration, the change of the fluorescence response at a constant dye concentration is monitored by subsequently increasing the concentrations of host.^[9] The binding constant (K_a) can be calculated by considering the total fluorescence signal (ΔI) during the titrations that represents the combined fluorescence intensity of the guest (G) and host-guest complex ($H.G$).^[33] The binding constant K_a is given by the equilibrium of host-guest complex formation and the concentrations of host-

guest complex $[HG]$, free (unbound) host $[H]$, and free (unbound) guest $[G]$ (Equation 1).

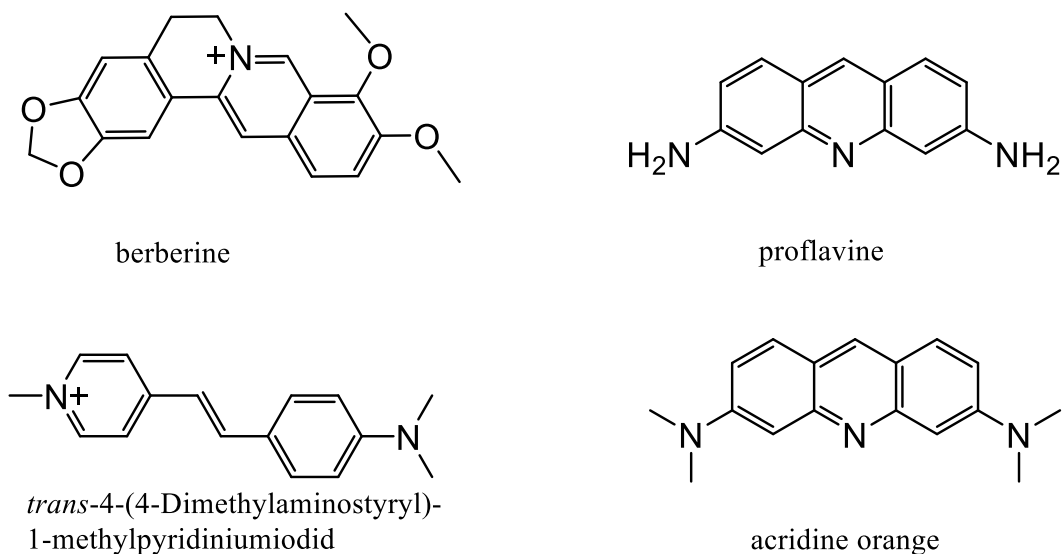


Figure 1.2 Selected dyes used in reporter pairs with CB7.

An equation was derived to analyse data from a spectroscopic binding titration to obtain the binding constant. The respective law of mass action is given in Equation 1.^[34]

$$K_a = \frac{[HG]}{[H][G]} \Leftrightarrow [HG] = K_a[H][G] \quad (\text{eq. 1})$$

Conservation of mass requires that the total host and guest concentration $[H]_0$ and $[G]_0$ are:

$$[H] = [H]_0 - [HG] \quad (\text{eq. 2})$$

$$[G] = [G]_0 - [HG] \quad (\text{eq. 3})$$

Combining Equations 1 to 3 gives a quadratic equation, in which $[HG]$ and K_a are the only unknown.

$$0 = [HG]^2 - ([G]_0 + [H]_0 + 1/K_a)[HG] + [H]_0[G]_0 \quad (\text{eq. 4})$$

Equation 4 has the form of $0 = x^2 + px + q$ and can thus be easily solved:

$$[HG] = \frac{([G]_0 + [H]_0 + 1/K_a)}{2} \pm \sqrt{\frac{([G]_0 + [H]_0 + 1/K_a)^2}{4} - [H]_0[G]_0} \quad (\text{eq. 5})$$

The contributions of the free guest (a dye molecule) and the host-guest complex to the spectrum must be considered to analyze absorption spectral or fluorescence

changes. For example, in absorption spectroscopy, the Beer-Lambert law relates the absorbance at a particular wavelength to the extinction coefficients of the guest, ε_G , and the host-guest complex, ε_{HG} , and the respective concentrations and the optical pathlength, d :

$$A = \varepsilon_G[G]d + \varepsilon_{HG}[HG]d \quad (\text{eq. 6})$$

In particular, the extinction coefficient of the host-guest complex is not exactly known, but we can consider that the absorbance of the guest only, A_G , is under the same experimental conditions $A_G = \varepsilon_G[G]_0d$, and that if all guest, i.e. $[G]_0$, is fully complexed with host, then $A_{HG} = \varepsilon_{HG}[G]_0d$. This gives:

$$A = \frac{[G]}{[G]_0} A_G + \frac{[HG]}{[G]_0} A_{HG} \quad (\text{eq. 7})$$

Using Equations 3 and 5 with Equation 7, gives us an equation, which can be used by data analysis programs to analyze a titration curve. The change of absorbance of a solution is plotted against varying concentrations of added host $[H]_0$. Similar considerations can be made for the varying fluorescence intensities at a particular wavelength FI :

$$FI = \frac{[G]}{[G]_0} FI_G + \frac{[HG]}{[G]_0} FI_{HG} \quad (\text{eq. 8})$$

In contrast, other analytes of interest or guest may not contain any intrinsic fluorescence. In these cases, their binding affinity can be calculated by “competitive fluorescence titrations” using an indicator displacement assay. This is done in a displacement (or competitive) titration, in which increasing amounts of the molecule of interest (the competitor) is added, while the concentrations of host and dye are kept constant (**Figure 1.3**). Since both dye and competitor are capable of binding to the cavity of the host, increasing concentrations of the competitor lead to a successive displacement of the dye from the host. Thereby, the fluorescent or absorption spectral properties of the dye in the solution are being restored. The concomitant changes of fluorescence response, combined with knowledge of the known host-guest binding constant (K_a), can be used to calculate the competitor binding affinity (K_c). The fitting model for competitive binding is derived from the direct binding model with the addition of a competitor term $[C]$, and the respective competitor binding constant, K_c .

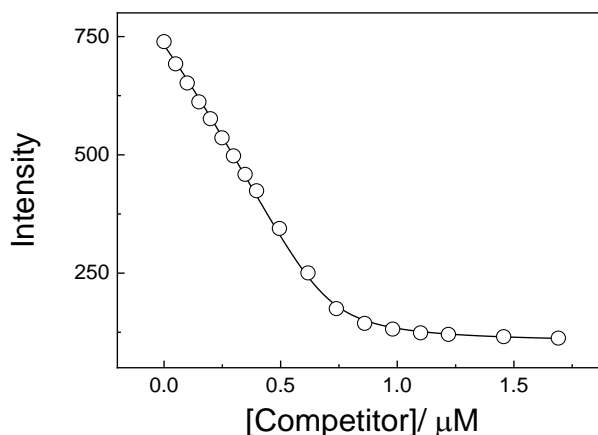


Figure 1.3 Example of a competitive displacement titration.



1.5 Host-Guest Complexes of Fluorescent Dyes with Macrocyclic Receptors

When dyes bind to macrocyclic receptors, they are exposed to an altered microenvironment, which is frequently accompanied by a change in their spectroscopic properties.^[6] We have used fluorescent dyes to sound out the polarizability inside supramolecular binding cavities (**Figure 1.4**),^[35] and found that certain dyes are much more stable towards photobleaching when encapsulated by a macrocyclic receptor.^[36] Combinations of macrocyclic receptors with fluorescent dyes that change their spectroscopic properties upon binding can also serve as reporter pairs to allow optical sensing.^[37] The addition of an analyte, which competes with the dye for binding to the receptor, leads to a restoration the spectroscopic properties of the unbound dye.

This principle allows one to detect and quantify the analyte and has been termed as an indicator displacement assay (IDA).^[38] Over the years, we have identified various combinations of fluorescent dyes and macrocyclic receptors suitable for IDAs. A library of reporter pairs has since then become available.^[6]

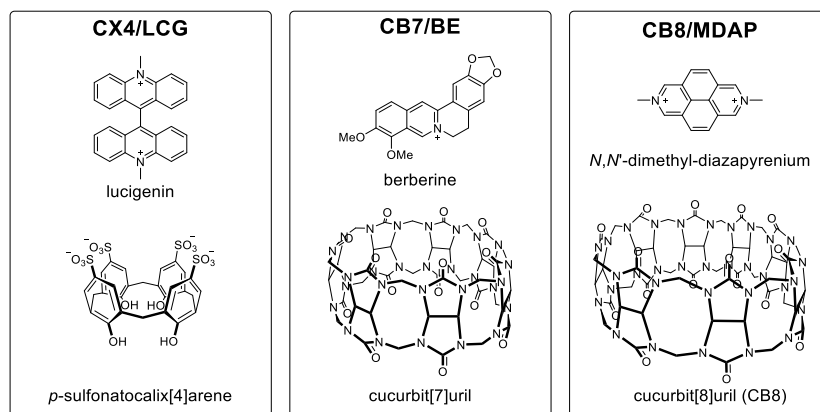
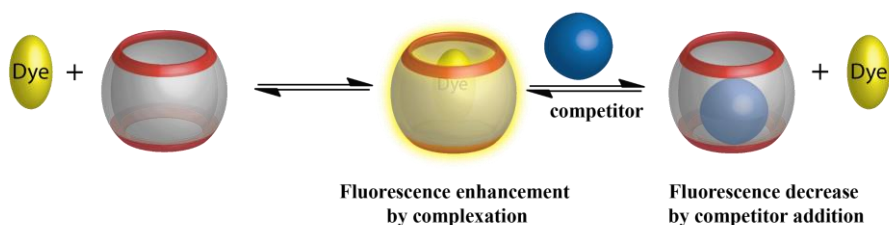


Figure 1.4 Chemical structures of selected reporter pairs used for molecular recognition.

1.6 Indicator Displacement Assays

Indicator displacement assays (IDAs) have become very popular for optical sensing applications,^[39] because they allow sensing analytes at low concentrations using optical methods. IDAs are based on an indicator bound to a receptor through noncovalent interactions resulting in changes of the optical properties of the indicator. Such chemosensing ensembles have been referred to as reporter pairs.^[40] An analyte can displace the indicator and bind to the receptor, whereby the indicator restores its original optical properties.^[38-39,41]

IDAs using synthetic host molecules (**Scheme 1.1**) become a powerful tool in the field of supramolecular chemistry, because IDAs have many advantages over other sensing methods. First, covalent attachment of the receptor and the indicator is not required; second, one receptor can bind several different indicators or analyte molecules, and third, the IDA is applicable in organic solvents and aqueous media, it can be adjusted by varying the solvent to “tune” the desired K_a value for analyte and indicator.^[38-39]



Scheme 1.1 The general principle of an indicator displacement assay.

In classical applications of IDAs, the goal was to determine static concentrations of analytes or even just qualitatively to detect an analyte. More recently, time-

resolved versions of IDAs were developed, in which concentration changes of analytes can be conveniently followed in real time.^[38] This advancement has been used for enzyme assays, membrane transport assays, and is now referred to as supramolecular tandem assays.^[40,42-43] Numerous macrocyclic hosts have been used in IDAs, e.g., cucurbiturils, cyclodextrins, and calixarenes.^[42,44]

1.7 Limitations of Binding Titrations

It is often worth considering the outcome of the binding equilibria, which leads to two limiting cases, i.e., 1) quantitative binding, when the concentrations are much larger than $1/K_a$, and 2) low binding when the concentrations are much lower than $1/K_a$.^[45]

Simulated competitive titrations are shown in **Figure 1.5** to illustrate the outcome of the two limiting cases.

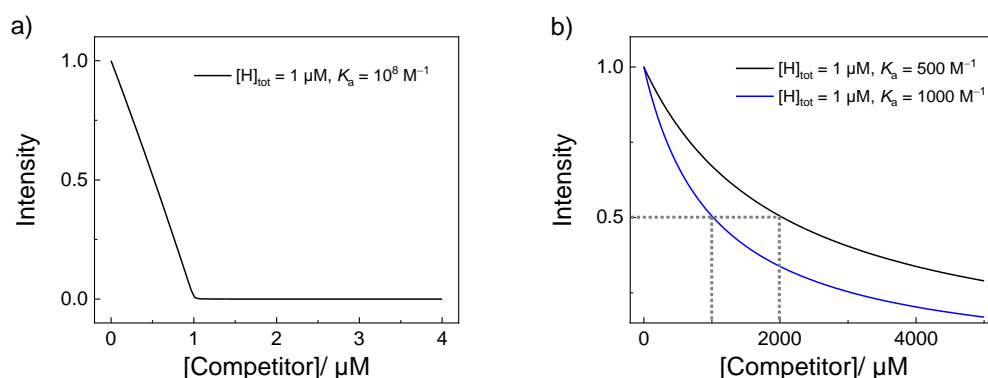


Figure 1.5 Simulated binding titration curves for the limiting cases of a) quantitative binding ($[H]_{\text{tot}} \gg 1/K_a$) and b) very low K_a ($[H]_{\text{tot}} \ll 1/K_a$).

In case of quantitative binding, the added competitor quantitatively binds to the host molecule. The result is that the binding titration curve is mostly linear and shows an intersection point with the plateau region when the total competitor concentration is equal to the total host concentration $[H]_{\text{tot}}$.

Moreover, it is extremely difficult, if not impossible, to accurately determine the binding constant under (nearly) quantitative binding conditions. The opposite case, when the concentrations are much lower than $1/K_a$, is also worthwhile to consider (**Figure 1.5**). The intensity has decreased to exactly 50% of its initial value, when the total competitor concentration is $1/K_a$ (1 mM for $K_a = 1000 \text{ M}^{-1}$ and 2 mM for $K_a = 500 \text{ M}^{-1}$). These conditions are thus ideally suited to determine binding constants with highest accuracy. However, with respect to the sensitivity in

analytical sensing applications, it also means that the sensitivity is ultimately limited by a low binding constant.

Isothermal titration calorimetry (ITC) is the preferred choice to assess the binding affinity between host and guest molecules. The complexation enthalpy (reaction heat) is used as a signalling method; thus, no labelling of the interacting analytes is required. An ITC experiment provides the stoichiometry (n), binding constant (K_a), and the thermodynamic parameters (ΔH , ΔS , ΔG) of the host-guest complexation process. The microcalorimeter measures the host-guest binding owing to the release (exothermal) or absorption (endothermal) of heat upon binding. Complexation results in a gain in free energy, ΔG , and, thus, a binding constant, K_a , which is related to the free energy via $\Delta G = R T \ln K_a$, can be calculated.^[46-49] However, analysis of the requires the assumption of the binding affinity involves complex stoichiometry, which requires additional experimental techniques such as Job's plot, NMR, XRD, MS, etc.^[4-5,50] Frequently, a 1:1 host-guest binding model is used to fit the data. When the binding does not follow this model, an expected 1:2 host-guest binding model is resonable with larger host molecules such as γ -CD, CB8, and CX6.^[51-53] Higher-order stiochiometries are not considered in this thesis and will not be discussed further.

1.8 High-Affinity Binders

CBs can bind guests of various size/shape with high affinity ($K_a > 10^{12} \text{ M}^{-1}$).^[4] For instance, CB7 forms 1:1 stable inclusion complexes with amino-adamantane,^[14,54] ferrocene,^[55-56] and bicyclooctanes.^[57] The previously reported binding affinities for such guest molecules exceed strong noncovalent interactions found for biological systems such as the biotin-avidin pair.^[56] Amino-adamantane, for example, binds to CB7 with picomolar affinity ($K_a = 10^{12} \text{ M}^{-1}$).^[57] Recently, Isaacs demonstrated that monovalent molecular recognition in water between CB7 and the diamantane diammonium ion resulted in a so-called "ultra-high" affinity with $K_a = 7.2 \times 10^{17} \text{ M}^{-1}$ in D_2O and $1.9 \times 10^{15} \text{ M}^{-1}$ in 50 mM NaO_2CCD_3 , by using ^1H NMR competition experiments.^[56,58]

The near-perfect size and shape match between diamantane and the rigid CB7 cavity led to an attomolar dissociation constant.^[56] Also, Mock and coworkers reported on the structure-selectivity relationship between CB6 and various alkyl-substituted ammonium ions. The CB6-related studies indicated that CB6 exhibits a

chain length-dependent selectivity.^[59-60] Diammonium ions, including a hexano or pentano bridge, bind stronger ($K_a \sim 10^8 \text{ M}^{-1}$) than shorter or longer alkyl chains ($K_a \sim 10^7 \text{ M}^{-1}$).^[5,16] For instance, the alkyl chain of 1,6-diammoniumhexane, folds inside the cavity to optimize the cavity filling and maximize ion-dipole interactions.^[61] Also, the CB6 cavity volume is 142 \AA^3 , showing a size- and shape-complementarity for 1,6-diammoniumhexane.^[61-63]

1.9 New Reporter Pairs for Molecular Recognition

Until now, a large variety of different combinations of hosts and dyes have been explored for their use in homogeneous solution,^[6] but there are additional requirements regarding to be used for sensing reporter pairs. As a simple example, acridine orange (AO) has proven to be a versatile dye in IDAs and supramolecular tandem enzyme assays,^[19,64] but it is also well-known as a staining reagent for cells because it crosses lipid membranes easily, and this renders it also unsuitable for encapsulation into liposomes. Moreover, only very few fluorescent dyes established in supramolecular tandem assays have an absorption above 450 nm (**Figure 1.6**). However, long-wavelength absorption is a prerequisite for excitation with standard lasers, e.g., the shortest wavelength of an Ar laser is 488 nm and of a He-Ne laser 543 nm. So far, only *trans*-4-[4-(dimethylamino)styryl]-1-methylpyridinium iodide (DSMI) and AO would meet the wavelength requirement; but AO is unsuitable (see above), and DSMI can only be used with CB6 as host and it has not yet been tested whether it is compatible with liposomes.^[16-17]

Additionally, it was noted during live-cell experiments that the fluorescent dye lucigenin (LCG), which can be excited with a diode laser at 405 nm, is rapidly photobleached.^[65] This prevented confocal laser scanning microscopy and only allowed the use of epifluorescence microscopy, using a Xe lamp as excitation source. Consequently, highly photostable fluorescent dyes with absorption above 450 nm are needed to afford the next generation of reporter pairs for supramolecular sensing applications.

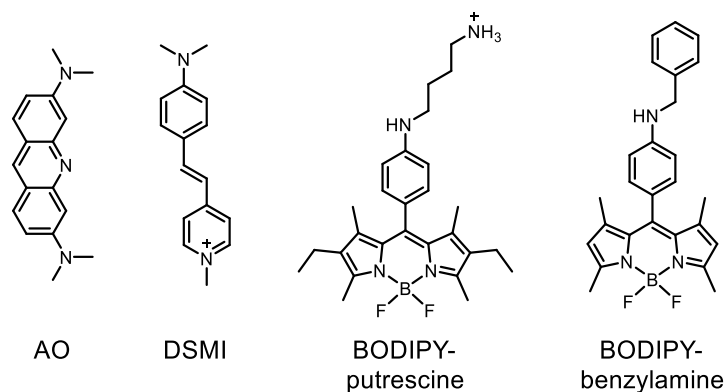


Figure 1.6 Selected fluorescent dyes for reporter pairs with absorption above 450 nm.

We have continuously expanded the library of reporter pairs to match the diverse requirements of different supramolecular tandem assays, but only a few are promising candidates for membrane assays. Previously, a strategy was suggested, which allows designing suitable fluorescent dyes to respond to supramolecular encapsulation in a predictable manner.^[64] This design strategy utilizes well-known binding motifs to position protonatable groups such that a pK_a shift results (**Figure 1.7**). This can be exploited to modulate the protonation state and, thus, the fluorescence of the dye upon binding to afford a generic approach to design suitable dyes for reporter pairs. BODIPYs are particularly well-known for their high photostability and show a large fluorescence response upon protonation of an arylamino group in the *meso* position of the BODIPY core.^[66]

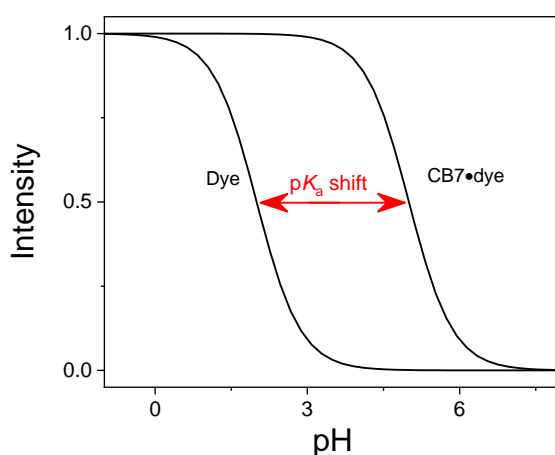


Figure 1.7 Simulated pH titration curves of a dye and the corresponding CB7•dye complex.

Chapter 2

Rational Design of Boron-dipyrromethene (BODIPY) Reporter Dyes for Cucurbit[7]uril

Chapter 2. Rational Design of Boron-dipyrromethene (BODIPY) Reporter Dyes for Cucurbit[7]uril

This chapter is derived from the content of the following publication:

Alnajjar, M. A.; Bartelmeß, J.; Hein, R.; Ashokkumar, P.; Nilam, M.; Nau, W. M.; Rurack, K.; Hennig, A., Rational Design of Boron-dipyrromethene (BODIPY) Reporter Dyes for Cucurbit[7]uril. *Beilstein J. Org. Chem.* **2018**, *14*, 1961-1971.

2.1 Introduction

Cucurbit[*n*]urils (CB*n*, *n* = 5-8, 10, and 14) are a class of macrocyclic host molecules which are water-soluble, nontoxic, and able to bind a large variety of neutral and cationic guests in their inner cavity with high binding affinity.^[4-5,67-68] This unique combination of properties has enabled numerous applications in the life sciences, for example, for protein binding,^[69-70] stabilization,^[71] immobilization,^[72] isolation,^[73] self-assembly,^[74-75] and regulation,^[76] or for drug solubilization and delivery.^[77-79]

The combination of CBs with fluorescent dyes directly enables (bio)sensing applications through the indicator displacement principle.^[6,80] Therein, the fluorescence properties of a dye are altered when encapsulated by the host, and when a competitive binder displaces the dye from the cavity, the properties of the non-encapsulated dye are regenerated. This principle has enabled, for example, real-time monitoring of enzymatic activity,^[44,81-82] the detection of membrane transport activity^[83] and membrane fusion,^[84] and even cellular imaging appears to be a potential future prospect.^[65,85]

However, most combinations of macrocyclic hosts and dyes that have so far been reported^[6] are only of limited use for these currently emerging life science applications of CBs. Many of the fluorescent dyes which bind to CBs with significant fluorescence changes, have a limited photostability, in particular under intense laser light illumination in confocal laser scanning microscopy,^[30,65] or absorb at shorter wavelengths, where biological samples show a high background

from autofluorescence.^[86-87] An ideal fluorescent dye would be highly photostable in biological media, have long-wavelength absorption to minimize background fluorescence from biological samples, and it would have a high fluorescence quantum yield in either bound or unbound state with a large difference in fluorescence intensity between both. In addition, a tuneable hydrophobicity to render the dye•CB complex membrane-permeable or not, and a tuneable affinity for the macrocycle would be desirable.

One possibility is the use of monofunctionalized CBs with outer cavity-attached fluorescent dyes.^[84-85] This principally allows the modular construction of various Förster resonance energy transfer (FRET) pairs as demonstrated with a Cy3-attached CB7, or the design of self-inclusion complexes, in which an outer cavity-attached rhodamine was intramolecularly bound in the CB7 cavity. As an alternative, it has been previously suggested that host-assisted protonation of a cavity-binding functional moiety (an “anchor group”) and a suitably attached protonation-sensitive fluorescent dye yields a rational and modular approach towards CB–dye pairs.^[30] This strategy had been previously applied to carbazole, aminonaphthalenesulfonate, and aminopyrene as fluorescent dyes.^[30,86-88]

Herein, we systematically explore the utility of boron-dipyrromethenes (BODIPYs) with an aniline substituent in the *meso*-position as fluorescent dyes in this type of anchor approach (**Figure 2.1**). BODIPYs are a class of fluorescent dyes that are particularly suitable for applications in medical imaging, and as fluorescent labels in biology, biochemistry and related fields.^[89-90] They are characterized by narrow absorption and fluorescence emission bands with small Stokes shifts, high molar absorption coefficients, and high quantum yields. Their excitation and emission maxima are in the visible region, usually above 470 nm, and they show high thermal, and photochemical stability under various conditions, particularly under physiological conditions.

Although, most BODIPYs are insensitive to pH changes, pH-activatable optical probes for cancer imaging have been reported, in which an aniline substituent in the *meso*-position of the BODIPY core led to efficient fluorescence quenching by photoinduced electron transfer (PET), whereas the protonated form was brightly fluorescent.^[91] We report herein the synthesis and photophysical characterization of BODIPY derivatives with an aniline substituent in the *meso*-position to which

different anchor groups have been attached, and we investigate their complexation behaviour with CB7. The goal was to explore the suitability of this approach, the possibility to fine-tune binding constants with different anchor groups and to provide BODIPYs with different absorption and emission wavelengths as well as pK_a values of the aniline substituent.

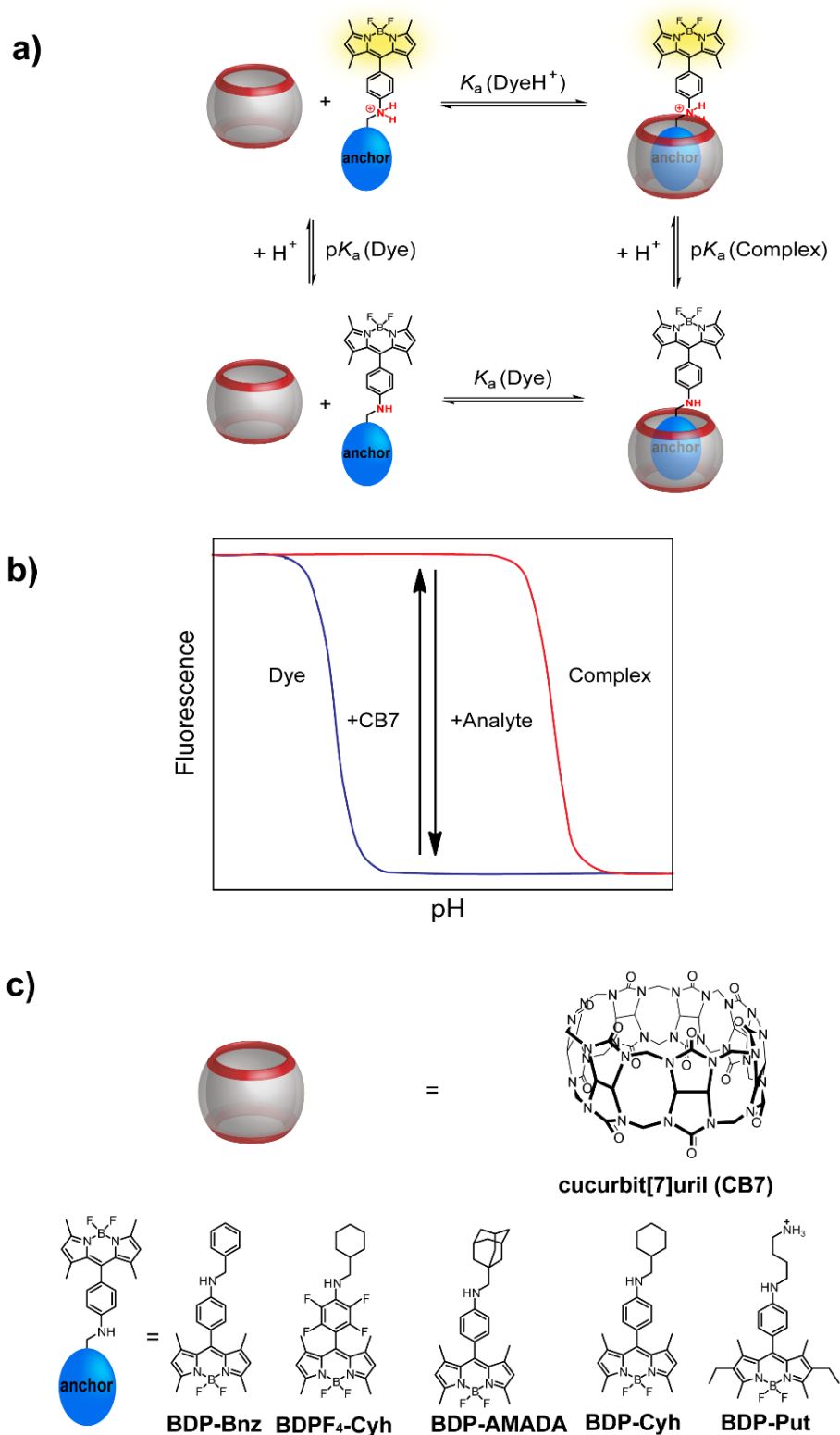
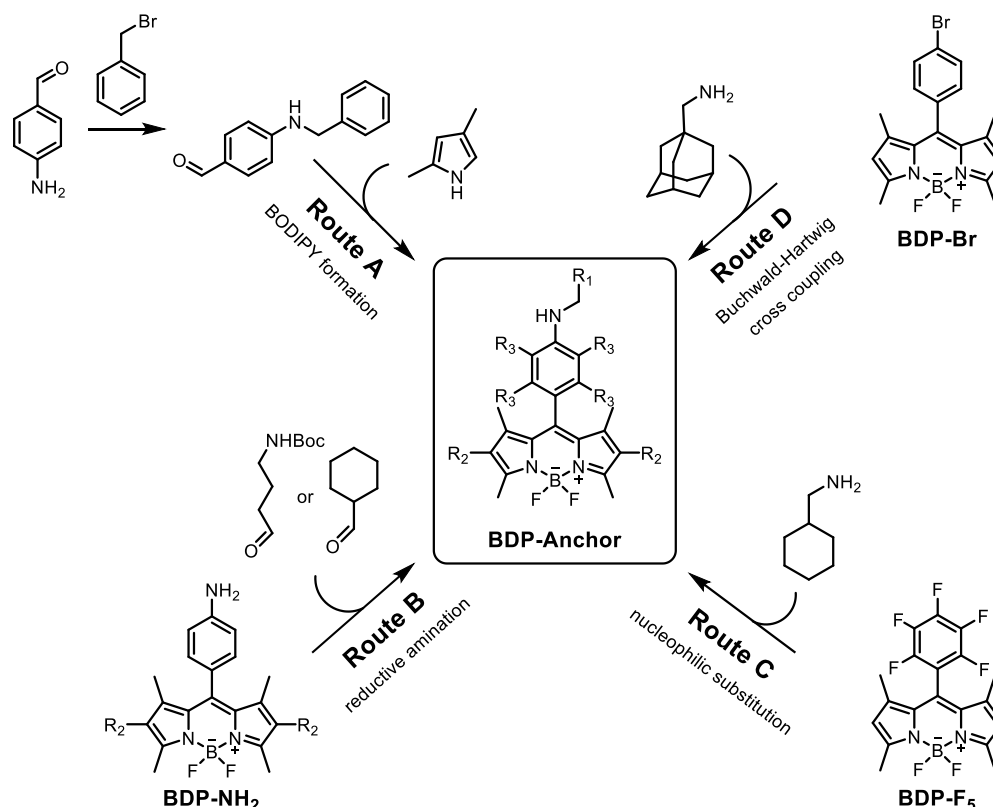


Figure 2.1 a) The “anchor group” approach for a rational design of CB–dye pairs involving a thermodynamic cycle of protonation and binding. b) Simulated pH titration curves of dye (blue) and CB7•dye complex (red) demonstrating the sensing principle based on pK_a of dye and complex in presence and absence of analyte c) Structures of CB7 and BODIPY derivatives.

2.2 Synthesis of Different BODIPY Derivatives

In this section, various routes were explored to synthesize the desired BODIPY dyes bearing an anchor group for binding to CB7 (**Figure 2.1**). **BDP-Bnz** was obtained by alkylation of *p*-amino benzaldehyde with benzylbromide and subsequent reaction of the obtained 4-(benzylamino)benzaldehyde with 2,4-dimethylpyrrole to afford the BODIPY dye by condensation under acidic conditions (Route A, **Scheme 2.1**).^[92] Since all efforts to obtain **BDP-Cyh** via Route A were not successful, even using Finkelstein conditions in aprotic solvents with high boiling points with various bases,^[93-94] BDP-NH₂ was synthesized according to a reported literature procedure,^[95] and then converted into the desired BODIPY anchor dye by reductive amination with the respective aldehyde using sodium triacetoxyborohydride as a mild reducing agent (Route B, **Scheme 2.1**).^[96] **BDP-Put** was also synthesized by reductive amination by reacting BDP-NH₂ with 4-[*N*-(tert-butyloxycarbonyl)]amino-1-butanal^[97] followed by Boc deprotection with trifluoroacetic acid (TFA). **BDPF₄-Cyh** was prepared by a substitution reaction from the parent *meso*-pentafluorobenzyl-BODIPY BDP-F₅ with aminomethylcyclohexane (Route C), following an established synthetic approach.^[98] For the preparation of the aminomethyladamantane derivative **BDP-AMADA**, a route *via* a bromo-benzyl-BODIPY BDP-Br followed by a Buchwald-Hartwig-coupling was performed. For the latter, a previously published Pd/XPhos containing catalytic system was successfully utilized (Route D).^[99]



Scheme 2.1 Synthesis of BODIPY derivatives.

2.3 Spectroscopic Characterization of Dyes

To ensure that the dyes do not aggregate under the conditions used for further measurements, concentration-dependent absorption and fluorescence spectra were measured first. In neutral water containing either 5% or 30% (v/v) acetonitrile (ACN), the aniline nitrogen in the *meso*-position of all BODIPY dyes is deprotonated (see below) and with 30% ACN, a linear dependence of the fluorescence intensity on the concentration of the dyes with no significant alterations of the shape of the absorption and emission bands was observed over the whole range of concentrations used herein (up to 5 μ M). In 5% ACN, however, dye aggregation was indicated by a downward curvature in the fluorescence intensity plots at dye concentrations above 60 to 120 nM. Further experiments were therefore conducted in 30% ACN.

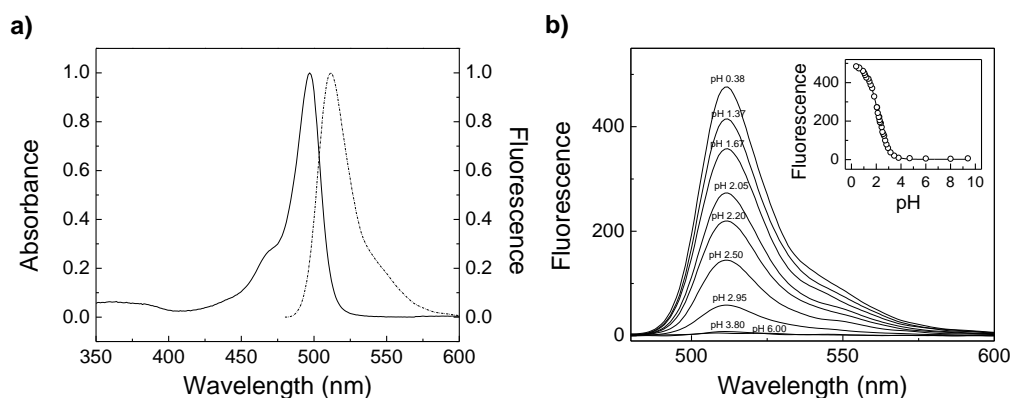


Figure 2.2 a) Normalized absorption (solid line) and normalized fluorescence emission spectrum (dotted line) of 0.72 μM BDP-Bnz in 30% (v/v) ACN in water, pH 7.0, and b) fluorescence spectra in 30% (v/v) ACN in water with varying pH. Insert: Fluorescence pH titration measured with $\lambda_{\text{exc}} = 470 \text{ nm}$ and $\lambda_{\text{em}} = 510 \text{ nm}$.

The absorption maximum was centred at *ca.* 500 nm for all aniline dyes (**Figure 2.2a** and **Tabel 2.1**) and the emission maximum was centred at *ca.* 510 nm for **BDP-Bnz** and **BDP-Cyh**, whereas **BDP-Put** showed a significantly red-shifted emission maximum at 540 nm, because we used the hexaalkylated instead of the tetraalkylated BODIPY core for this dye, trying to achieve maximum fluorescence output. The spectra of the tetrafluorinated **BDPF4-Cyh** showed an overall red shift with the absorption maximum at 510 nm and the emission maximum at 530 nm. The molar absorption coefficients of the BODIPY derivatives were around 90,000 $\text{M}^{-1}\text{cm}^{-1}$, which agrees well with related BODIPY derivatives in the literature.^[90,100-104]

With decreasing pH, a strong increase in fluorescence was observed for all dyes (**Figure 2.1b**), which is due to the protonation of the aniline nitrogen in the *meso*-position of the BODIPY core lowering the HOMO energy level of the aniline group. Negligible changes in absorption spectra and in the position of the emission maxima were in accordance with the anticipated PET mechanism.^[91] Further, the change in free energy, ΔG , associated with PET was calculated using the Rehm–Weller equation.^[105] Therefore, we used a reduction potential of -1.55 V for the 1,3,7,9-tetramethyl-BODIPY core acceptor of 1, 2, and 5^[106] and of -1.81 V for the 2,8-diethyl-1,3,7,9-tetramethylBODIPY core acceptor of 3 in acetonitrile,^[106] an oxidation potential of $+0.0625 \text{ V}$ for the aniline donor,^[107-108] and the vibrational zero electronic energy was determined as 2.46 eV from absorption and emission

spectra. This gave ΔG values of $-87.6 \text{ kJ mol}^{-1}$ for 1, 2, and 5 and of $-62.5 \text{ kJ mol}^{-1}$ for 3, which clearly demonstrates that PET is energetically favourable.

Fitting of the pH titration curves revealed pK_a values in the range of 2-3 for the aniline nitrogen and a pK_a value of -0.14 for the tetrafluoroaniline nitrogen of BODIPYs (Table 2.1). This range agrees well with the electron-withdrawing nature of the BODIPY core and with reported pK_a values, for example, for aniline ($pK_a = 4.58$), 4-nitroaniline ($pK_a = 1.02$), 4-cyanoaniline ($pK_a = 1.74$), or pentafluoroaniline ($pK_a = -0.30$).^[109-110] At basic pH values, no spectroscopic changes were noted except for **BDP-Put**, which showed a broadening and a marked decrease of the absorption band (see appendices **Figure A1.17**). This presumably originates from a deprotonation of the terminal alkyl ammonium group of the putrescine chain, which could fold back and enable an intramolecular charge transfer state of the amine lone pair with the BODIPY chromophore. In accordance with this hypothesis, a positive solvatochromism with varying contents of ACN was observed (see appendices **Figure A1.18**).

The fluorescence quantum yields of the deprotonated BODIPY dyes were determined in 30% ACN in water (at pH 7.4) and of the protonated BODIPY dyes in 30% ACN in 0.1 M HCl. For both, fluorescein in 0.1 M NaOH was used as the reference ($\Phi_f = 0.89$).^[111] These measurements revealed an increase in fluorescence by a factor of 7 to 50 upon protonation for the investigated BODIPYs, which is sufficient for the desired sensing applications (**Table 2.1**).^[44,112] Surprisingly, and despite the hexaalkylated core was used, the fluorescence quantum yields of protonated as well as deprotonated **BDP-Put** were more than 100-fold lower than the quantum yields of the other derivatives. Such reduced quantum yields have been previously reported for some BODIPYs substituted with diamines in the aniline *meso*-position, and the decreased quantum yields were ascribed to the loose-bolt effect.^[101,113-114]

Tabel 2.1 Photophysical properties of the synthesized BODIPY derivatives.^a

	BDP-Put	BDP-Bnz	BDP-cyH	BDPF ₄ -cyH	BDP-AMADA
ε / M ⁻¹ cm ⁻¹	93,000	97,000	97,000	85,300	99,000
$\lambda_{\text{abs.max}}$ / nm	500	496	497	510	497
$\lambda_{\text{em.max}}$ / nm	540	511	510	530	510
Φ_f (Dye) / %	0.017	1.1	6.2	2.0	2.4
Φ_f (DyeH ⁺) %	0.12	54	51	41 ^b	30.5
p <i>K</i> _a (Dye)	2.7	2.2	2.6	– 0.3	3.6

^a Measured in 30% (v/v) ACN in water except for the extinction coefficient ε , which was determined in neat ACN. ^b Determined from the CB7 complex at 4 mM CB7.

2.4 Complexation with CB7

Addition of excess CB7 to the BODIPY dyes at low pH values, in which the dyes are fully protonated, or at high pH values above the p*K*_a value of the BODIPY•CB7 complex (see below) had no effect on the spectroscopic properties of the dyes. At intermediate pH values, however, the fluorescence of the dyes increased upon addition of CB7 (**Figure 2.4**). This result is in accordance with the anticipated anchor group mechanism leading to a complexation-induced protonation of the dye (**Figure 2.1**). It also suggests that the BODIPY core is not encapsulated in the macrocyclic cavity and that encapsulation of the anchor group by CB7 has no effect on the spectroscopic properties of the dyes. At intermediate pH, the protonated fraction of the dye will be strongly bound by CB7, which affects the protonation equilibrium of the dye and leads to more protonated dye being produced. The net outcome is an increase in fluorescence intensity (upward arrow in “detection window” in (**Figure 2.1b**)). Multiple binding titrations performed at different pH values were fully consistent with the mechanism (**Figure 2.3b**). At low pH values, the fluorescence intensity in absence of CB7 was higher and the fluorescence increase upon addition of CB7 was steeper, because more dye molecules are already protonated, whereas at higher pH values more CB7 was required to reach the final fluorescence intensity of the fully protonated dyes.

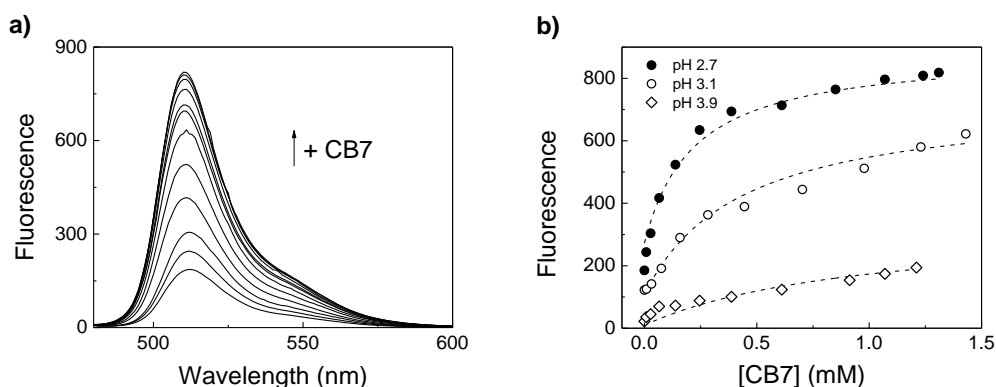


Figure 2.3 a) Fluorescence spectral changes ($\lambda_{\text{exc}} = 470$ nm) upon addition of CB7 to 50 nM BDP-Bnz in 10 mM citrate buffer, pH 2.7, containing 30% (v/v) ACN, and b) respective titration plot ($\lambda_{\text{em}} = 510$ nm) at varying pH. The dashed lines were obtained by a global fitting according to the thermodynamic cycle (see appendices 3 for details).

Unfortunately, the absence of any detectable changes for the fully protonated or unprotonated dyes upon addition of CB7 prevented a direct determination of the respective binding constants, K_a (DyeH⁺) and K_a (DyeH), at low and high pH values. We therefore developed a global fitting procedure (see appendices A.1.6), in which the binding titrations at different pH values are simultaneously analysed to provide the values for the binding constants of the protonated and unprotonated dye, K_a (DyeH⁺) and K_a (Dye), as well as the pK_a values of the BODIPY•CB7 complex pK_a (Complex), see **Table 2.2** The pK_a value of the uncomplexed dye, pK_a (Dye), was obtained from a simple pH titration and fixed during the global fitting procedure.

Table 2.2 Properties of the CB7–BODIPY host–guest complexes.^a

	BDP-Bnz	BDP-cyH	BDPF ₄ -cyH	BDP-AMADA
$pK_a(\text{Complex})^b$	5.0	5.3	1.5	8.2
ΔpK_a	2.8	2.7	1.8	4.6
$K_a(\text{Dye})^c / \text{M}^{-1}$	30	5000	240	n.a. ^d
$K_a(\text{DyeH}^+)^c / \text{M}^{-1}$	1.9×10^4	2.6×10^6	1.5×10^4	n.a. ^d

^a Measured in 30% (v/v) ACN/H₂O. ^b Error ± 0.2 pK_a units. ^c Error in K_a ca. 20%. ^d Binding constants could not be determined due to the very slow exchange kinetics of the BDP-AMADA•CB7 complex. see also **Figure A1.19** in appendices.

The binding affinities of the BODIPY dyes were significantly lower than the reported binding constants of the respective anchor groups in water.^[4] To allow a better comparison, we determined the binding constants of the benzylammonium (Bnz) and cyclohexylmethylammonium (cyH) cations by displacement titrations (see below) in our 30% (v/v) ACN/H₂O mixture, which gave $K_a(\text{Bnz}) = 1.4 \times 10^5 \text{ M}^{-1}$ and $K_a(\text{cyH}) = 1.5 \times 10^7 \text{ M}^{-1}$. This indicated that the binding affinity is lowered 100- to 1000-fold by reducing the hydrophobic effect in presence of 30% acetonitrile as also previously noted for water/DMSO mixtures.^[115] The attachment of the BODIPY chromophore to the anchor groups thus reduces the binding constant by an additional factor of 10 for the aniline *meso*-group and by factor of 1000 for the tetrafluoroaniline group in **BDPF₄-Cyh**. We ascribe this to steric hindrance between the carbonyl-fringed CB7 rim and the fluorine atoms in the tetrafluoroaniline, which are slightly larger than the hydrogen atoms.^[116] The data obtained with **BDP-Put** could not be fitted satisfactorily, which is presumably due to the more complex photophysics of this dye (see above) and the exchange of **BDP-AMADA** was too slow to equilibrate during the titration within reasonable time (**Figure A1.19** see in appendices).

The pK_a values of the host–dye complex was independently determined by pH titrations in presence of excess CB7 and analysed assuming quantitative complex formation (**Figure 2.4**). Overall, the pK_a values from the direct titration and from the global fitting agreed reasonably well, and the complexation-induced pK_a shifts were in the typical range reported for CB7 host–guest complexes.^[117]

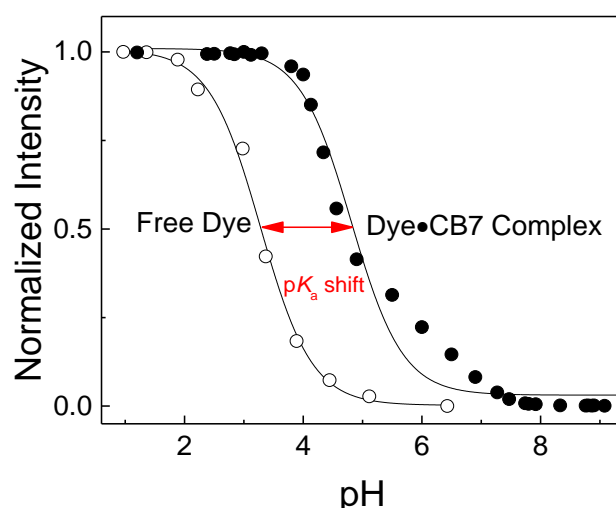
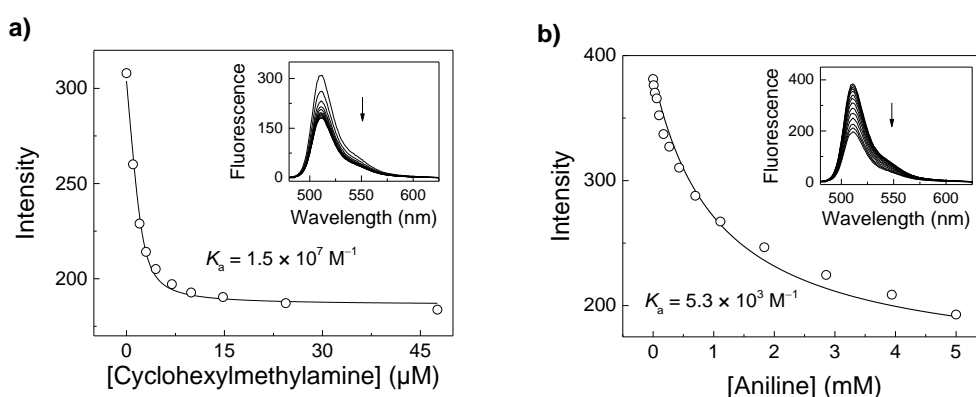


Figure 2.4 Fluorescence pH titration of BDP-cyH and the respective complex (in presence of 3 mM CB7) in 30% (v/v) ACN in water with varying pH. Fluorescence was measured with $\lambda_{\text{exc}} = 470$ nm and $\lambda_{\text{em}} = 510$ nm.

2.5 Applications of BODIPY-CB7 Complexes

The availability of BODIPY dyes, which respond towards complexation by CB7, enables a large variety of potential applications of the resulting host–dye reporter pairs. As first example, the CB7–BODIPY pairs can be applied as sensors using the indicator displacement principle.^[80-81,83,118] This is demonstrated by sensing of cyclohexylmethylamine and aniline as model analytes (**Figure 2.5**). In order to determine the binding constants of the two analytes, the apparent binding constant of **BDP-CyH** at pH 3.1 was taken ($K_{\text{app}} = 6.7 \times 10^5 \text{ M}^{-1}$) and the displacement titrations were analysed with a competitive titration model.^[30,81] This gave binding constants of $1.5 \times 10^7 \text{ M}^{-1}$ for the cyclohexylmethylammonium cation, $5.3 \times 10^3 \text{ M}^{-1}$ for the anilium cation and $1.4 \times 10^5 \text{ M}^{-1}$ for the benzylammonium cation in the 10 mM citrate buffer in 30% (v/v) acetontirile in water.



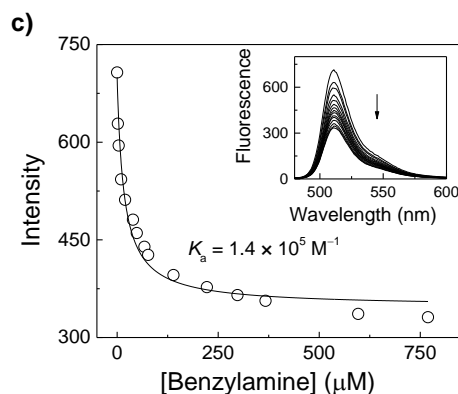


Figure 2.5 Fluorescence displacement titrations ($\lambda_{\text{ex}} = 470$ nm, $\lambda_{\text{em}} = 510$ nm) of a) 5 μM BDP-cyH and 2.5 μM CB7 with cyclohexylmethylamine, b) 7 μM BDP-cyH and 2.5 μM CB7 with aniline and c) 0.5 μM BDP-cyH and 0.2 μM CB7 with benzylamine and in 10 mM citrate buffer in 30% (v/v) ACN in water, pH 3.1.

As another advantage over previously established supramolecular reporter dyes, the absorption maximum of the BODIPYs introduced herein matches the emission wavelength of an Ar laser, which is still the most common excitation source in fluorescence correlation spectroscopy (FCS) and fluorescence microscopy. FCS has been established to study dynamic processes in biological systems and, more recently, also in materials science, but its use in supramolecular chemistry is so far very rare.^[29,119-122] It can be applied to investigate translational and rotational diffusion of supramolecules as well as exchange kinetics. To demonstrate the compatibility of the new BODIPY dyes with FCS, we have now determined the diffusion coefficient of the **BDP-Cyh**•CB7 complex in comparison to the free **BDP-Cyh** dye. Therefore, FCS autocorrelation curves (**Figure 2.6**) were analysed to obtain the diffusion times t_{diff} of **BDP-Cyh** and the **BDP-Cyh**•CB7 complex and then converted into diffusion coefficients D using the reported standard Rhodamine 6G ($D = 2.80 \times 10^{-6} \text{ cm}^2 \text{ s}^{-1}$).^[119,123] This gave $D = 4.87 \times 10^{-6} \text{ cm}^2 \text{ s}^{-1}$ for **BDP-Cyh** and $D = 3.39 \times 10^{-6} \text{ cm}^2 \text{ s}^{-1}$ for the **BDP-Cyh**•CB7 complex, which perfectly matches the range reported for other dyes and their respective CB7 complexes.^[119]

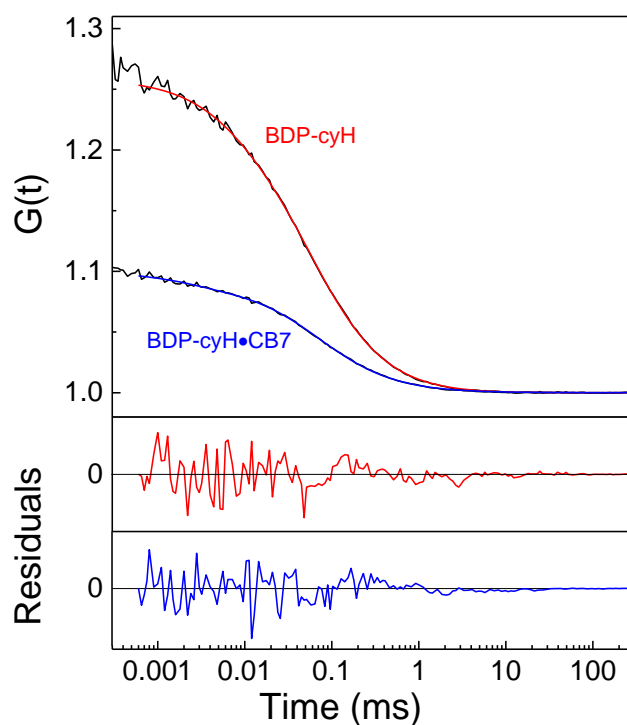


Figure 2.6 FCS autocorrelation curves obtained with 10 nM BDP-cyH in the absence (red fitted line) and presence (blue fitted line) of 100 μ M CB7 at pH 1.5 (7:3 water:ACN). The fitted diffusion times for free dye and complex were 54.1 and 77.9 μ s, respectively.

The compatibility of BODIPYs with common excitation sources and filter sets also enables their use in fluorescence microscopy. To demonstrate, we have used polymer microparticles with surface-bound CB7^[14] and added them with a solution containing a mixture of **BDP-AMADA** and 1-(aminomethyl)adamantane (AMADA). The latter was added to reduce the surface group density of the dye and prevent undesired self-quenching at high surface concentrations of the fluorophore. After centrifugation and washing of the polymer particles, surface-bound **BDP-AMADA** could be clearly visualized by fluorescence microscopy on CB7-functionalized polymer particles, whereas polymer particles lacking CB7 on the surface did not show any fluorescence (**Figure 2.7**). This result is consistent with specific host-guest binding of **BDP-AMADA** to CB7 on the surface, which suggests the use of **BDP-AMADA** for straightforward surface functionalization to create nanophotonic devices as well as for multimodal surface group quantifications, e.g. using their optical properties for fluorescence and their fluorine heteroatom for x-ray photoelectron spectroscopy.^[124-126]

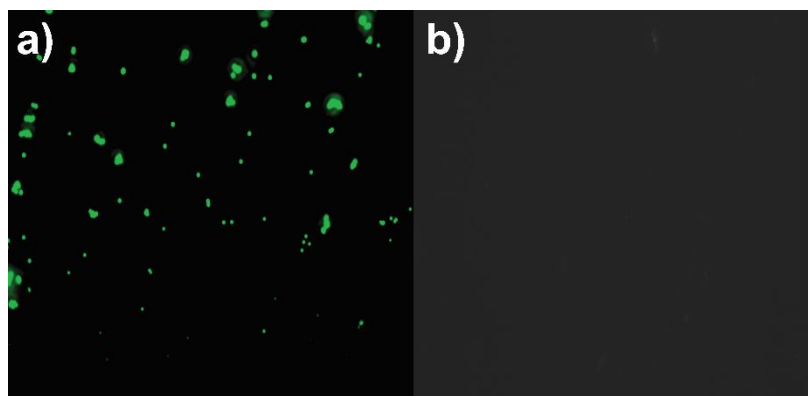


Figure 2.7 Fluorescence microscopy images of 1 mg/ml polymer microspheres a) with or b) without surface-bound CB7 after incubation with 10 nM BDP-AMADA and 1 μ M AMADA in 10 mM citrate, pH 3.3 (7:3 (v/v) water:ACN) and centrifugation to immobilize BDP-AMADA through supramolecular host-guest binding.

The license is subject to the Beilstein Journal of Organic Chemistry terms and conditions: (<https://www.beilstein-journals.org/bjoc>)

<https://creativecommons.org/licenses/by/4.0/>

Chapter 3

Supramolecular Assemblies through Host-Guest Complexation between Cucurbiturils and an Amphiphilic Guest Molecule

Chapter 3. Supramolecular Assemblies through Host-Guest Complexation between Cucurbiturils and an Amphiphilic Guest Molecule

This chapter is derived from the content of the following publication:

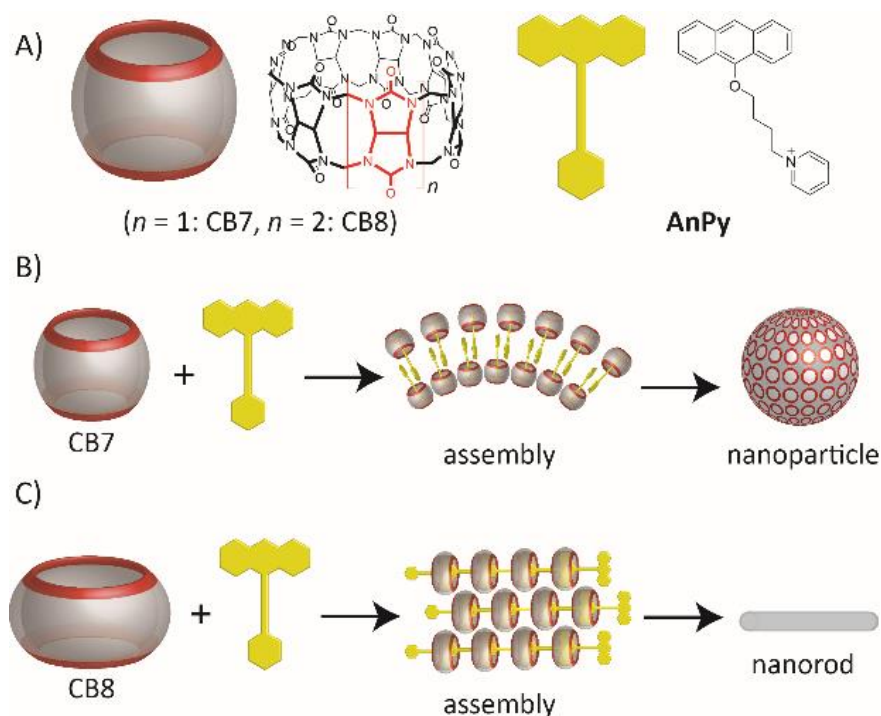
Assaf, K. I.; **Alnajjar, M. A.**; Nau, W. M., Supramolecular Assemblies through Host-Guest Complexation between Cucurbiturils and an Amphiphilic Guest Molecule. *Chem. Comm.* **2018**, 54, 1734-1747.

3.1 Introduction

Supramolecular chemistry has paved the way for designing and generating functional materials through multiple reversible non-covalent interactions, including hydrogen bonding, electrostatic, and dispersion forces.^[127-128] Among supramolecular systems, host-guest complexation has emerged as a novel strategy to construct nanoassemblies in water, which in principle can be controlled by external stimuli, e.g., light, heat, pH, and additives.^[129-132] Several macrocyclic host molecules (cucurbiturils, cyclodextrins, calixarenes, and pillararenes) have been used to construct multifunctional nanoarchitectures, e.g., hydrogels, nanoparticles, and polymeric structures, through the formation of stable host-guest complexes in aqueous solution.^[132-137] These nanoassemblies are associated with potential applications ranging from sensing to drug delivery.^[6,133,136,138] Amphiphilic molecules consisting of hydrophobic and hydrophilic groups have been used as scaffolds for constructing nanometer-sized assemblies.^[139-143] By combining amphiphilicities with macrocyclic molecules, new nanoassemblies with unique properties can be obtained.^[144-146] Cucurbit[*n*]urils (CB*n*) are a novel class of water-soluble macrocycles with versatile recognition properties.^[5,133,147-148] They are able to accommodate different organic guest molecules in aqueous solution with exceptional high binding affinity.^[56,58,149]

3.2 Formation of Supramolecular Assemblies between Pyridinium-Functionalized Anthracene and Cucurbiturils

We report that host-guest complexation between an amphiphilic pyridinium-functionalized anthracene (**AnPy**) with CB_n ($n = 7$ and 8) in aqueous solution allows the formation of supramolecular assemblies (**Scheme 3.1**). **AnPy** consists of a hydrophobic electron-rich anthracene ring and a hydrophilic electron-deficient pyridinium moiety, with an alkyl spacer between them.^[150-151] **AnPy**-based amphiphiles can self-assemble through charge-transfer interactions.^[150-151] Recently, Liu and co-workers have reported that the complexation of **AnPy** with *p*-sulfonatocalix[4]arene (CX4) in water leads to the formation of light-responsive nanoparticles, in which CX4 lowers the critical aggregation concentration of the **AnPy**.^[152]



Scheme 3.1 A) Cartoon and chemical representations of the CB_n (left) and **AnPy** (right) structures. Schematic illustration of the proposed supramolecular assemblies between **AnPy** and CB_7 (B) and CB_8 (C).

3.3 Investigation of Supramolecular Assemblies by Optical Spectroscopy

The host-guest complexation between CB_n and **AnPy** was studied in detail by using optical spectroscopy (**Figure 3.1** and **Figure 3.2**). The complexation of **AnPy** with CB_7 afforded a small hyperchromic shift in the course of the absorption titrations

(**Figure 3.1A**). On the other hand, the fluorescence intensity decreases upon addition of CB7 (**Figure 3.1C**). In contrast to the experiments with CB7, the complexation of **AnPy** with CB8 showed a large bathochromic and hypochromic shift in the absorption spectra. The large bathochromic shift is attributed to a charge-transfer process upon complexation with CB8, which indicated the encapsulation of both components inside the CB8 cavity. As **AnPy** showed a distinct absorption response with CB7 and CB8, the differentiation between the two hosts was readily possible (see in appendices). The fluorescence of **AnPy** significantly decreases upon complexation with CB8. A Job's plot analysis for the complexation indicated a 1:1 binding mode with both hosts (see appendices **Figure A2.5**). Optical titration data could be well-fitted according to a 1:1 complexation stoichiometry. The resulting binding constants were $8.6 \times 10^4 \text{ M}^{-1}$ and $9.2 \times 10^6 \text{ M}^{-1}$ for CB7 and CB8, respectively (**Figure 3.1** and **Figure 3.2**, B and D). Further, isothermal titration calorimetry (ITC) was used to study the thermodynamics of the host-guest complexes. The ITC results (see appendices **Figure A2.6**) supported the binding affinities obtained by optical titrations and verified the postulated 1:1 binding mode. The complexation process for both hosts was found to be enthalpically driven, with favorable entropic contributions for CB7 and unfavorable ones for CB8.

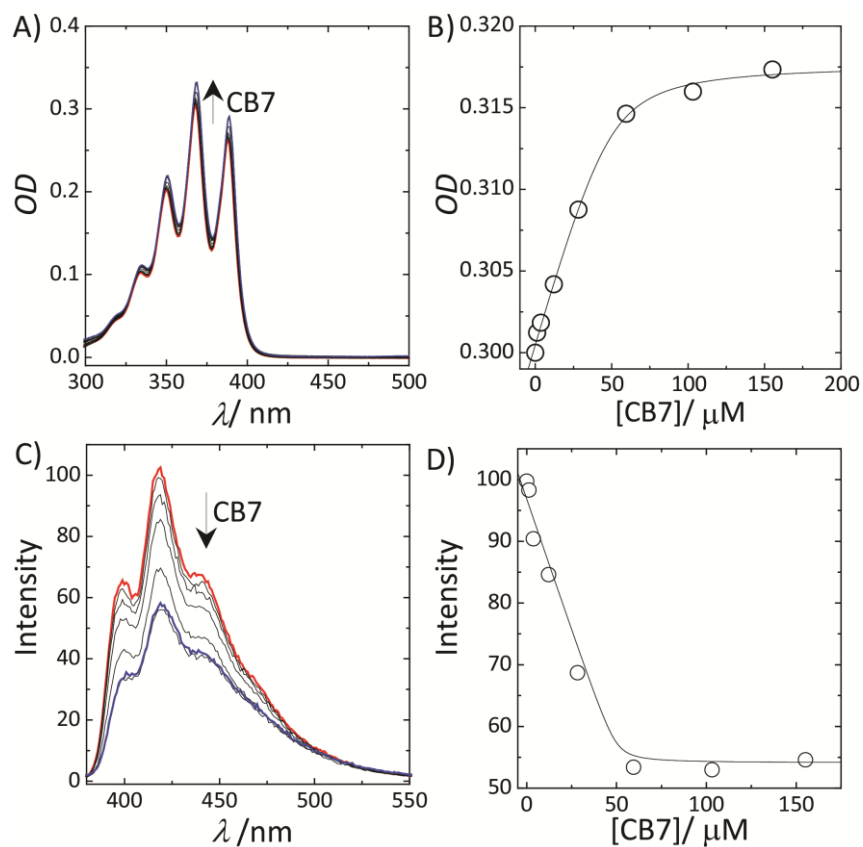


Figure 3.1 UV-Vis (top) and fluorescence (bottom) titrations of AnPy (35 μM) with CB7 ($\lambda_{\text{ex}} = 365$); the fittings (right) were done by assuming a 1:1 binding model from which the association constant was derived.

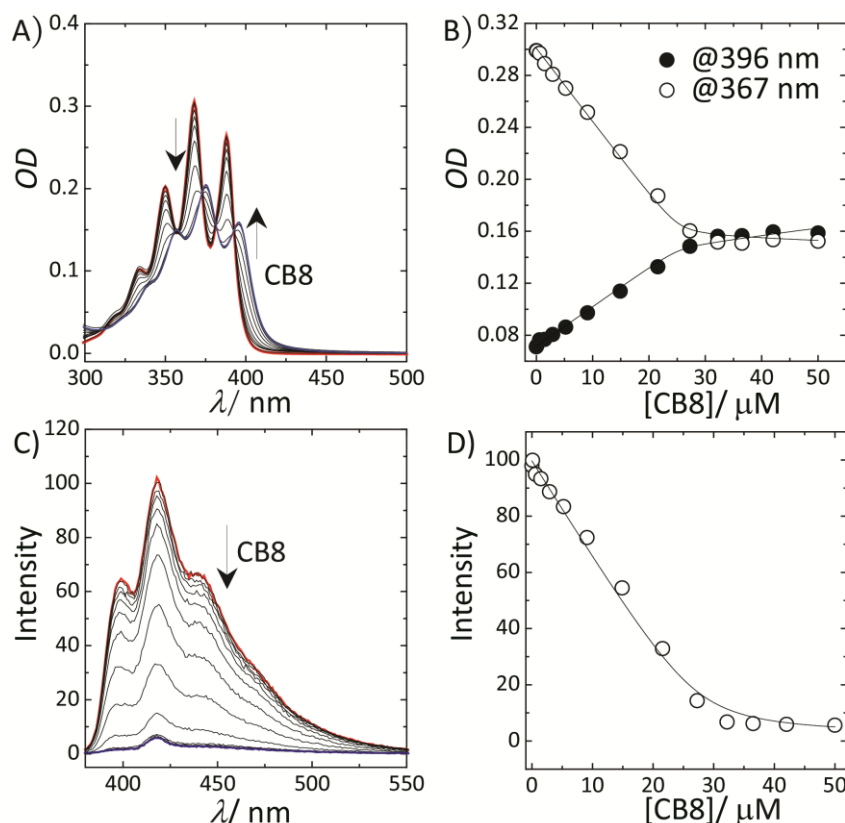


Figure 3.2 UV-Vis (top) and fluorescence (bottom) titrations of AnPy (35 μM) with CB8 ($\lambda_{\text{ex}} = 365$); the fittings (right) were done by assuming a 1:1 binding model from which the association constant was derived.

3.4 Investigation of Supramolecular Assemblies by ^1H NMR Spectroscopy

The depth of the inclusion of **AnPy** into the host cavity can be followed by ^1H NMR spectroscopy, where the complexation of the guest inside the hydrophobic cavity of the host leads to complexation-induced chemical shifts.^[59] Upon mixing CB7 with **AnPy** (2 mM), significant changes were observed for the **AnPy** protons (**Figure 3.3**). In particular, a marked upfield shift of the protons and broadening of the peaks were observed. This is attributed to the formation of a supramolecular assembly through the stacking of the anthracene residues, as expected for the formed nanoparticles (see below). When DMSO was added to the solution, only the pyridinium protons were upfield shifted, indicative for the complexation of the pyridinium ring inside the CB7 cavity, as well as the deaggregation of the anthracene residues. For CB8, the anthracene and the pyridinium protons were shifted upfield (**Figure 3.4**). In addition, the protons of the alkyl-spacer exhibited a large upfield shift. This indicates that **AnPy** is fully encapsulated inside the large

cavity of CB8, in which the pyridinium ring is back-folded inside the cavity,^[153] in accordance with the optical data.

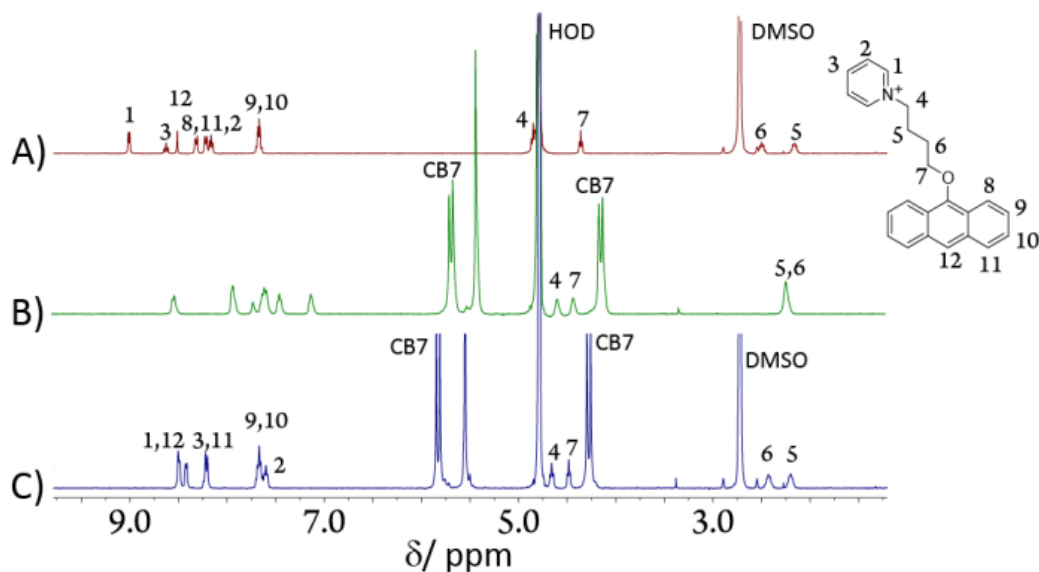


Figure 3.3 ¹H NMR spectra of A) free AnPy (2 mM) in a D₂O/DMSO-d₆ (4:1) mixture, B) CB7•AnPy (2mM) in D₂O, C) CB7•AnPy (2 mM) in a D₂O/DMSO-d₆ (4:1) mixture.

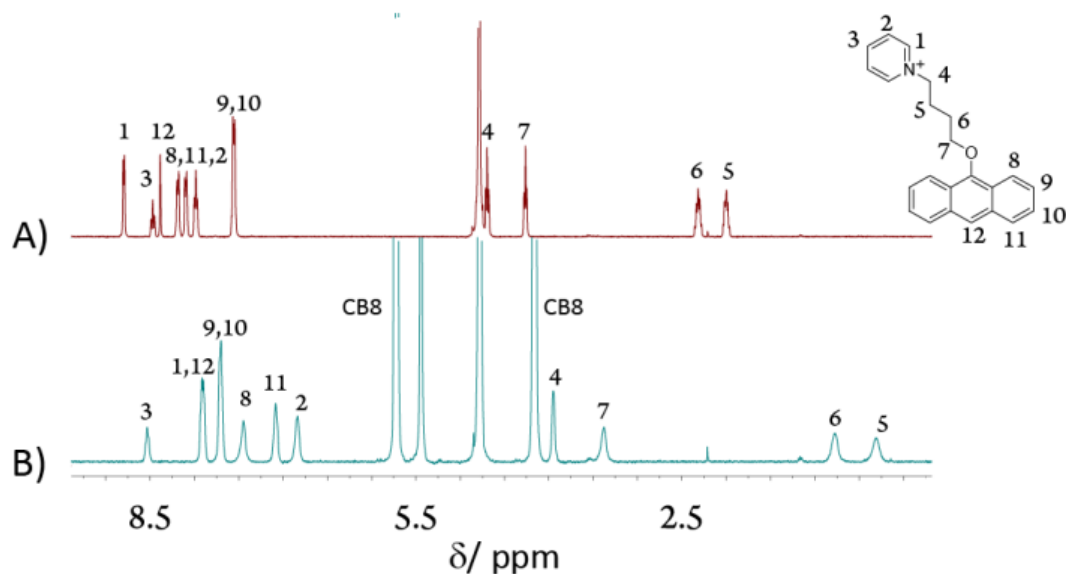


Figure 3.4 ¹H NMR spectra of A) free AnPy (2 mM) and B) CB8•AnPy (2 mM: 2 mM) in D₂O.

3.5 Binding Modes for AnPy with CB7 and CB8

The experimentally observed different binding modes for AnPy with CB7 and CB8 were modelled by quantum-chemical calculations (wB97xD/6-31G*). The optimized structures (Figure 3.5A) showed that CB7 can encapsulate the pyridinium ring, while the anthracene part remains excluded, suggestion exposure

to bulk water in solution. The larger cavity of CB8 allowed the encapsulation of both residues, the pyridinium and the anthracene rings, in a folded structure (**Figure 3.5B**). **Figure 3.5C** shows a different binding mode for the CB8•AnPy that is expected in the extended polymeric structure (see below). The calculated binding energies for the CB7 and CB8 complexes (see **Figure 3.5**) were in accordance with the experimental binding affinities, that is, the CB8•AnPy was found to be more stable than the CB7•AnPy complex. Furthermore, the calculations indicated that the 1:1 CB8•AnPy complex was more stable than the 1:2 one.

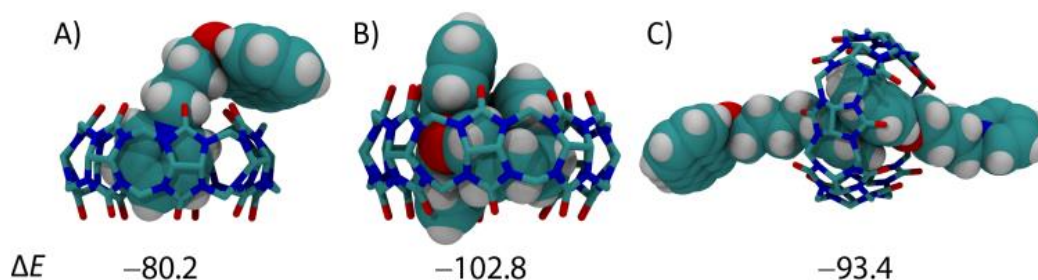


Figure 3.5 DFT-optimized structures of A) CB7•AnPy, B) CB8•AnPy, and C) CB8•AnPy, the later as expected for the extended polymeric structure. Binding energies are given below the structures in kcal mol⁻¹.

The remarkable optical changes upon complexation of AnPy with CB n and its high binding affinity make it an excellent choice for sensing applications.^[17,149,154-155] It is always a challenge to find suitable dyes for macrocycles with large cavity sizes, such as for CB8, whose cavity is sufficiently large to encapsulate simultaneously two dye molecules by formation of ternary complexes. This frequently complicates the analysis of indicator displacement titration data.^[156] As shown in **Figure 3.5B**, once the anthracene part is complexed inside the cavity of CB8, the pyridinium ring back-folds to occupy the empty space under formation of a 1:1 complex.^[153] The addition of a small aromatic guest molecule is expected to displace the pyridinium ring by forming a ternary complex. The displacement can be monitored by the optical properties of the CB8•AnPy reporter pair. Competitive titrations are shown in **Figure 3.6** and the appendices 6.2.5. For example, the binding constant of D-phenylalanine could be readily determined in this manner by absorption and fluorescence, affording values of 3750 and 1020 M⁻¹ at pH 2 and 6.5, respectively. The higher affinity at pH 2 is due to the protonation of the carboxylic acid residue ($pK_a = 2.2$). The binding affinities of aniline (17000 M⁻¹) and phenol (160 M⁻¹) were determined accordingly (see appendices **Figure A2.10** and **Figure A2.11**).

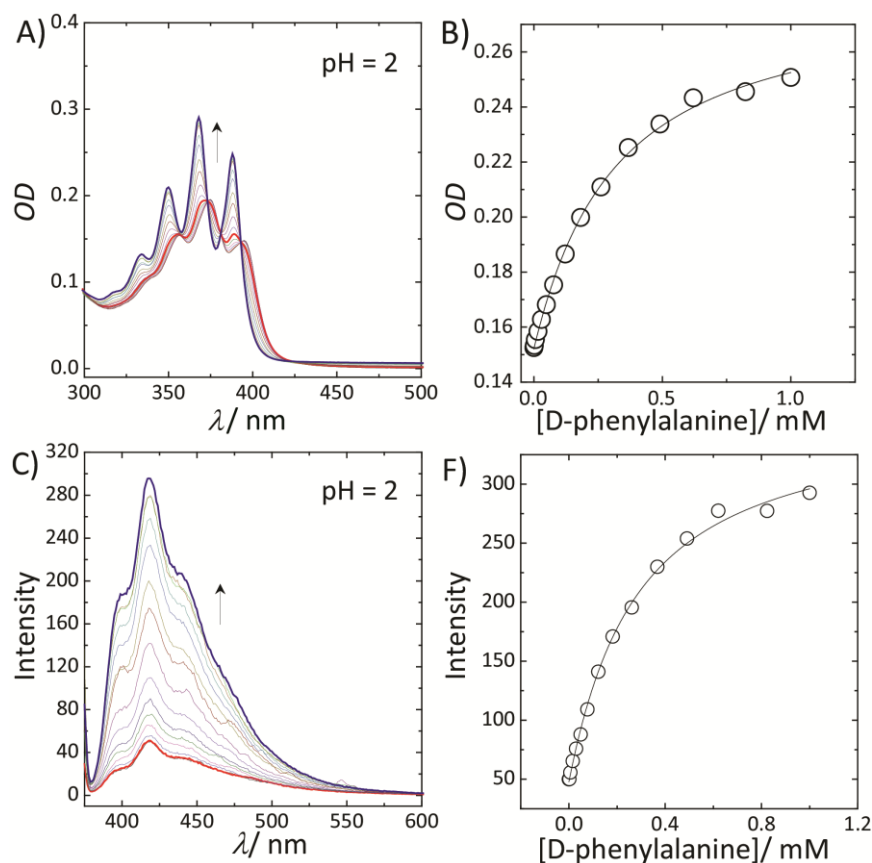


Figure 3.6 UV-Vis (A) and fluorescence (C) competitive titrations for the reporter pair CB8•AnPy (35:35 μ M) complex with D-phenylalanine at pH 2. The fittings are shown in B and D.

3.6 Investigation the Supramolecular Assemblies by DLS and TEM

The shielding of the pyridinium ring inside the CB7 cavity promotes π - π stacking between the anthracene rings of **AnPy** resulting in the formation of nanoparticles (**Scheme 3.1B**). The critical aggregation concentration of the **AnPy**-CB7 assembly was measured by monitoring the dependence of the transmittance at 600 nm on the ratio of **AnPy** to CB7. In the absence of CB7, optical measurements showed no visible aggregation even at high mM concentration of **AnPy**. The same observation was made at low concentration of the CB7•**AnPy** complex (≤ 2 mM). However, upon increasing the concentration of **AnPy** and CB7 to > 3 mM, the optical transmittance decreased, indicating the formation of large assemblies (**Figure 3.7A**). The formation of the assemblies was confirmed by DLS measurements, which yielded homogenous size distributions with an average diameter of 500 nm (**Figure 3.7B**). Moreover, spherical nanoparticles with diameters ranging from 400-

1000 nm were observed in the transmission electron microscopy (TEM) images (**Figure 3.8A**). The formed nanoparticles were stable for several days.

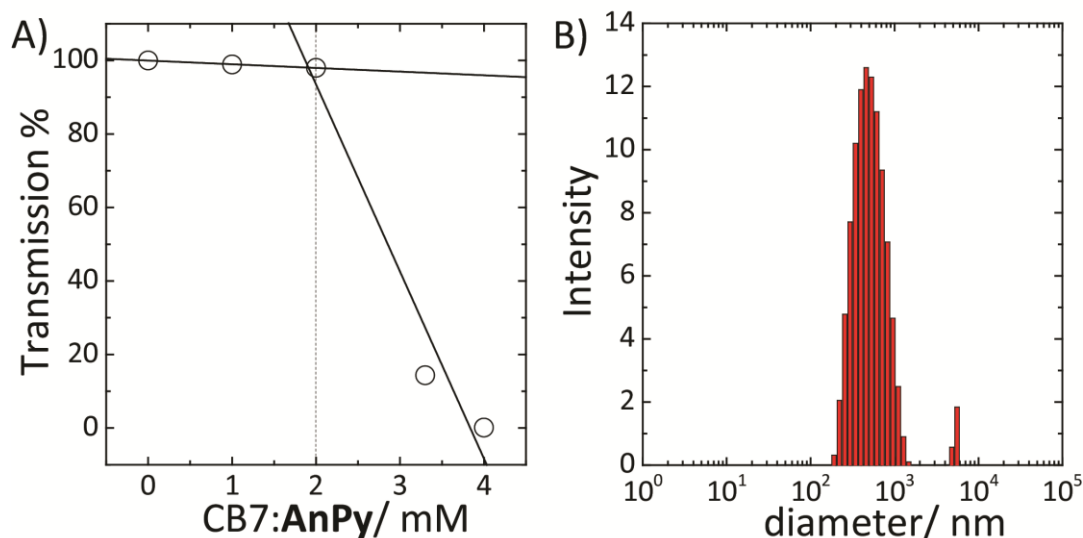


Figure 3.7 A) Dependence of the optical transmittance at 600 nm on the AnPy•CB7 concentration in water at 25 °C. B) DLS data of the CB7•AnPy assembly at 25 °C.

When **AnPy** and CB8 were mixed at millimolar concentrations, a dark yellow solution developed followed by the formation of aggregates, which were stable for several weeks. TEM images indicated the formation of a linear supramolecular polymeric structure (**Scheme 3.1C** and **Figure 3.8B**). The postulated aggregation involves the formation of polymeric chains through the complexation of pyridinium and anthracene residues from different units (see **Figure 3.5C**). The lengths of these polymeric chains were of several micrometers, while their width was 700 ± 50 nm. The large width of the assemblies is attributed to outer-surface interactions occurring through the convex surface of CB8 (see **Scheme 3.1C**).^[157]

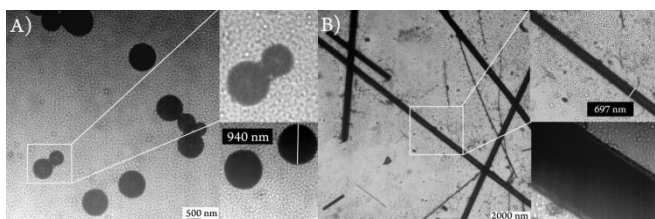


Figure 3.8 TEM images of A) the CB7-AnPy assembly and B) the CB8-AnPy assembly.

3.7 Supramolecular Assembly Responses to External Stimuli

The new assemblies respond to external stimuli. For example, the **CB7-AnPy** nanoparticles can be assembled and disassembled by changing the temperature

(**Figure 3.9**) within a very narrow range (25-40 °C) around ambient conditions. After heating the CB7-**AnPy** nanoparticles to 40 °C for few minutes, the optical transmittance increased to approximately 80% of the initial value, suggesting the destruction of the CB7-**AnPy** nanoparticles. The assembly/disassembly process is fully reversible (**Figure 3.9**). **AnPy** can also undergo photo-oxidation, which leads to the formation of anthraquinone upon reaction with oxygen and subsequent cleavage of the alkanol part. This reaction was followed as a function of time for free and complexed **AnPy** (see appendices **Figure A2.14**). The results indicated that the reaction is much faster in the presence of the host.^[152] The CB7-**AnPy** aggregates can be destroyed upon UV-irradiation at 365 nm. ¹H NMR spectra (see appendices **Figure A2.15**) indicated that **AnPy** is decomposed upon UV-irradiation leading to the formation of anthraquinone and the 1-(4-hydroxybutyl)-pyridinium, in which only the 1-(4-hydroxybutyl)-pyridinium residue that remains complexed to CB7, while the anthraquinone product precipitates out. The addition of strong competitive guest molecules (e.g., adamantylamine) to the aggregates results also in the dissociation of the assemblies as well. This exemplary experiment demonstrates that the assemblies response sensitively to physical, photonic, and chemical stimuli.

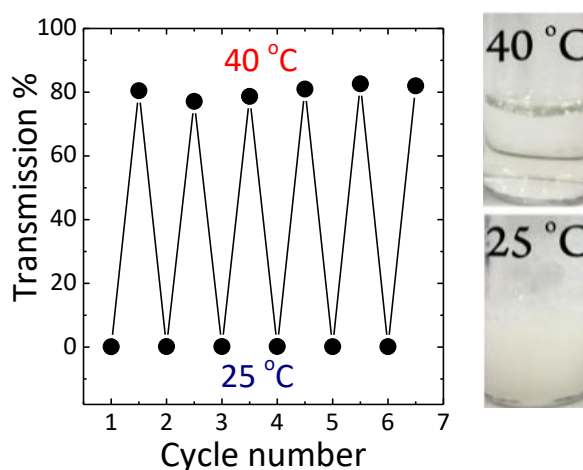


Figure 3.9 Optical transmittance changes of the CB7-**AnPy** assembly at 600 nm over multiple cycles of thermal equilibration in water at 25 °C and 40 °C (left). Photograph visualizing the assembly/disassembly of the CB7-**AnPy** nanoparticles (right).

Chapter 4

A Reference Scale of
Cucurbit[7]uril Binding Affinities

Chapter 4. A Reference Scale of Cucurbit[7]uril Binding Affinities

This chapter is derived from the content of the submitted manuscript:

Alnajjar, M. A., Hennig, A., and Nau, W. M., A. Reference Scale of Cucurbit[7]uril Binding Affinities.

4.1 Introduction

The determination of binding constants is quintessential in supramolecular host-guest chemistry, because it provides a direct measure for analyzing the strength of intermolecular interactions between host and guest.^[4-5,158] Commonly, binding constants are determined by titrations, in which a physical property such as the chemical shift in NMR spectroscopy or the absorbance or fluorescence in optical spectroscopy is monitored, while the concentrations of the binding partners (host or guest) are being varied.^[34,159-161] The resulting binding titration curves are subsequently fitted to a suitable binding model to obtain the association constant, K_a , and, thereby, the interaction energy, ΔG , via $\Delta G = R \cdot T \ln K_a$, where T is the absolute temperature and R the universal gas constant. Alternatively, isothermal titration calorimetry (ITC) is used to determine the thermodynamics of binding processes by measuring the heat evolved or absorbed upon association between guest and host to afford K_a , the complexation stoichiometry, n , and the binding enthalpy, ΔH . The binding entropy, ΔS , can be extracted according to $\Delta G = \Delta H - T\Delta S$.^[46-47,49,162]

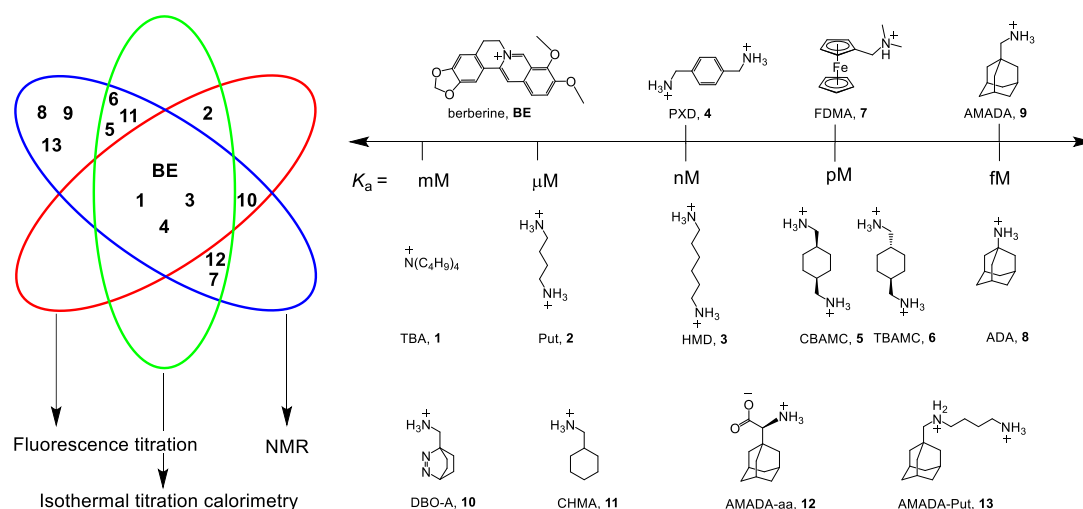
The reliability of the results gained from these titrations depends on a number of factors, which have been comprehensively summarized.^[34] For example, the analysis of more involved binding phenomena, such as the formation of ternary complexes involving different modes of cooperativity, requires a careful experimental planning and a critical data analysis. As another example, Benesi-Hildebrand plots remain popular, although it has often been noted that data linearization by (double)-reciprocal plots introduces large errors, which are not considered by standard least-squares fitting methods.^[34]

However, even with careful consideration of all these factors, binding constants with high reliability and, ideally, inter-laboratory reproducibility are often challenging to obtain. As an example from our own research, we have performed numerous binding titrations with cucurbit[7]uril (CB7) and acridine orange (AO) and obtained values that ranged from $5.7 \times 10^4 \text{ M}^{-1}$ to $3.1 \times 10^6 \text{ M}^{-1}$.^[163-166] We could finally trace this back to an undesirable interaction of AO with the walls of quartz glass cuvettes, which could be reduced, but not completely eliminated, in poly(methylmethacrylate) cuvettes.^[166]

With respect to the family of the pumpkin-shaped cucurbit[*n*]urils (CBs with *n* = 5-8, 10 and 14),^[68,167-169] numerous host-guest binding constants have been reported for hydrocarbons, dyes, drugs, amino acids, and even for selected amino acid residues or sequences in peptides and proteins.^[17,170-171] The resulting data compilations are of indisputable scientific merit, but the reported individual values are occasionally difficult to compare due to variations in experimental conditions while in other cases they appear contradictory even if reported for the same conditions. For example, several binding constants have only been measured in buffer solutions with high salt concentrations;^[172] the associated data points can only be considered as apparent binding constants due to the competitive binding of cations at CB portals.^[173-174] A particular challenge arises from the very high binding affinities of CBs ($K_a > 10^9 \text{ M}^{-1}$).^[56,58] These preclude direct host-guest titrations, because the required nanomolar concentrations are typically too low to afford a detectable spectroscopic or calorimetric response.^[34,159-161] Access to CB binding constants is further limited by the very slow host-guest exchange rates at ultra-high affinities ($K_a > 10^{12} \text{ M}^{-1}$), which have been noted at several instances, for example for the protonated forms of amino-substituted cyclohexanes, adamantanes, diamantanes, and ferrocenes.^[54,56,58,175-178]

Among the CB homologues, the focus is on the intermediary sized CB7, which is notoriously known for its extremely strong binding (up to $K_a = 7.2 \times 10^{17} \text{ M}^{-1}$).^[56] This ultrahigh affinity has immense potential in biotechnology as well as analytical chemical applications,^[179-182] for example, CB7-beads can selectively capture proteins labelled with 1-trimethylammoniomethylferrocene from complex heterogenous protein mixtures.^[183]

In an effort to obtain structure-activity relationships and to tune the binding affinities with CB7, Isaacs and co-workers have used competitive titrations with sub-stoichiometric amounts of the host and an excess of two competing guest molecules and established a reference scale of binding affinities in order to determine ultra-high binding affinities by multistep ^1H NMR competition experiments.^[54,58,175] However, their key reference compound to assess binding constants with nanomolar and higher affinity, (3-aminopropyl)[(trimethylsilyl)methyl]amine, is not readily available.^[54,56,58,172]



Scheme 4.1 Structures of established reference compounds **BE** and **1-8** to determine the affinity of guests **9-13**.

In order to facilitate the determination of CB7 host-guest binding affinities, we introduce herein a series of reference compounds that allow affinity determinations by competitive titrations in the range from $<10^3 \text{ M}^{-1}$ to $>10^{15} \text{ M}^{-1}$ (**Scheme 4.1**). The purpose of our rather analytical-chemical supramolecular study was not to measure new affinities of additional compounds, but rather to provide robust, mutually cross-checked, and reproducible values for already studied compounds that are readily and broadly accessible.

As a central entry point to this series, we have selected berberine (**BE**), for which we could confirm a recently reported and very thoroughly determined binding constant.^[184] Based on direct fluorescence and ITC titrations as well as competitive NMR titrations against putrescine (Put, **2**), we propose a reference value of $(2.36 \pm 0.20) \times 10^7 \text{ M}^{-1}$ for **BE**. Competitive fluorescence titrations with **BE** and control experiments by NMR and ITC suggested hexamethylenediamine (HMD, **3**) and *p*-xylylenediamine (PXD, **4**) as the desirable reference compounds with nM affinity.

For pM affinity, the *cis*- and *trans*-isomers of 1,4-bis(aminomethyl)-cyclohexane (CBAMC, **5** and TBAMC, **6**) as well as *N,N*-dimethylaminomethylferrocene (FDMA, **7**) were explored. At the upper end, adamantylamine (ADA, **8**) could serve as potential reference compound with fM affinity. The proposed binding constants of all reference compounds and their errors are based on repeated measurements with various methods, and we discuss herein the advantages and limitations of each reference compound. Finally, we use our reference scale to report the binding affinities of compounds **10-13**, which we have previously used in various contexts without accurately determining their binding affinities.^[19,81,166,170,177,185-186]

4.2 Reference Compounds for μ M Affinity

The most desirable property of a potential reference compound for binding constant determinations is the possibility to directly measure its affinity by various methods. This suggests to establish a fluorescent dye as a first reference compound, which allows one to combine the results from optical spectroscopy, ITC, and, eventually, NMR spectroscopy. The possibility to jointly use these methods with the same compound is, however, rarely met, because many dyes tend to aggregate at the millimolar concentrations required for NMR. For example, acridine orange, which has been widely used with CB7,^[9,81,163] shows clear signs of aggregation around 10 μ M in water, which renders it unsuitable for binding constant determinations by NMR.^[187-188] Isaacs and co-workers explored the fluorescent dye 3,6-diaminoacridine (proflavine) as a reference compound,^[56] which also showed significant peak broadening at concentrations higher than 0.5 mM, even in the presence of CB7.^[56]

Based on these considerations, we selected **BE** as an alternative fluorescent reference compound. The fluorescence of **BE** is insensitive to pH and complex formation with CB7 is known to enhance the fluorescence intensity about 500-fold, ITC gives a pronounced heat response, ¹H NMR spectroscopy shows well-separated peaks of complexed and free **BE**, a slow exchange on the ¹H NMR timescale, and no signs of aggregation up to its solubility limit of ca. 2.5 mM.^[32] This rather unique combination affords easily detectable signals upon complexation and allows a mutual verification of binding constants measured by fluorescence, ITC, and NMR.

In order to determine the binding constant of **BE** with minimal uncertainty, we have initially re-evaluated data sets from eight randomly selected fluorescence titrations ($n = 8$), which were performed by different individuals in our lab during the previous years with different commercial and self-synthesized CB7 batches. Global fitting of this extended data set gave a binding constant of $(1.91 \pm 0.14) \times 10^7 \text{ M}^{-1}$ (**Figure A3.1**), whereas measurements from ITC ($K_a = (1.20 \pm 0.10) \times 10^7 \text{ M}^{-1}$, $n = 3$, **Figure A3.2**) suggested a slightly lower binding constant with non-overlapping error ranges.

When we compared our result with the CB7•**BE** binding constants reported in the literature, we noted that Miskolczy and Biczók found a binding constant of $(2.4 \pm 0.3) \times 10^7 \text{ M}^{-1}$ in purified water, which had been freshly distilled from a diluted KMnO_4 solution.^[184] They noted that trace impurities in commercial HPLC-quality water could give a lower binding affinity, and we were intrigued whether our Millipore “ultrapure” water could be responsible for the observed deviations in the measured CB7•**BE** binding affinity. Indeed, when we re-measured the binding constant of **BE** with CB7 in water distilled from KMnO_4 , our value ($K_a = (2.43 \pm 0.39) \times 10^7 \text{ M}^{-1}$, **Figure A3.3**) was in perfect agreement with the value documented by Miskolczy and Biczók. Moreover, ITC measurements with water distilled from KMnO_4 also gave a higher binding constant of $(2.26 \pm 0.40) \times 10^7 \text{ M}^{-1}$ (**Figure A3.4**), in very good agreement with the value from fluorescence spectroscopy. The detrimental influence on the apparent binding affinity was also noted with putrescine (Put, **2**), which gave $K_a = (1.42 \pm 0.14) \times 10^6 \text{ M}^{-1}$ with water from our Millipore purification system and $(1.85 \pm 0.10) \times 10^6 \text{ M}^{-1}$ with water distilled from KMnO_4 by ITC (see Appendix A.4 in Appendices). Combining the results from fluorescence and ITC gave the binding affinity of **BE** to CB7 and its error as $K_a = (2.36 \pm 0.20) \times 10^7 \text{ M}^{-1}$ (see Appendix A.3.3.2 in Appendices for error calculation), which we propose as the first reference value of a reference scale of CB7 binding affinities (**Table 4.1** and **Figure 4.1**).^[32,172,184,189-191]

The value of the CB7•**BE** binding constant was therefore additionally confirmed by NMR spectroscopy. Competitive NMR measurements, in which an excess of a competitor is added to displace a sizeable fraction of the reference compound from a sub-stoichiometric amount of the host,^[54,172] were considered as the only suitable approach, because a direct determination of the binding constant is prevented by the high affinity of the CB7•**BE** complex. The latter would require low micromolar

concentrations, which are incompatible with standard ^1H NMR instruments operating at 400 or 500 MHz.

As potential competitors, tetrabutylammonium chloride (TBA, **1**) and Put (**2**) were considered with binding affinities in the millimolar and micromolar range. TBA was immediately disregarded due to precipitation in the NMR tube containing a mixture of TBA (**1**), BE, and CB7, which singled out Put. As a starting point, the binding constant of Put (**2**) was determined by a direct ITC titration as $(1.85 \pm 0.11) \times 10^6 \text{ M}^{-1}$ ($n = 1$) and by competitive fluorescence titrations as $(1.79 \pm 0.18) \times 10^6 \text{ M}^{-1}$ ($n = 6$, see Appendix A.3.5 in Appendices for data and A.3.3.2 for error calculation). Combining the values and errors of these titrations led to a reference value for Put of $(1.82 \pm 0.11) \times 10^6 \text{ M}^{-1}$. In the next step, the relative binding affinity ($K_{\text{rel}} = K_{\text{a, BE}} / K_{\text{a, Put}}$) of Put (**2**) was determined by competitive NMR. This requires the identification of well-resolved peaks of complexed and free **BE** or Put,^[189] and we considered the ^1H NMR signals of protons 1, 2, 3, and 5+11 in their free (without prime) and complexed form (with prime) as suitable (**Figure 4.2**). Integration of the ^1H NMR peak areas of the signals gave K_{rel} by equation SI-A4.6, and the average and standard deviation of these four sets of peaks was next calculated from triplicate measurements (see Appendix A.3.3.4.3 in Appendices), which gave a value of $K_{\text{rel}} = 13.18 \pm 0.60$; by using the reference K_{a} values of Put (**2**), we obtained a K_{a} value of $(2.40 \pm 0.22) \times 10^7 \text{ M}^{-1}$ for BE by competitive NMR (eq. A4.18). This value is in perfect agreement with the proposed reference value for **BE** from the direct titrations, such that we confidently recommend it as a reference compound with micromolar affinity (see lower part of **Figure 4.1**), which can conversely be used to conduct measurements with higher-affinity binders, those in the nanomolar range.

Table 4.1 Binding constants of proposed reference compounds investigated in this study.

Compound	K_a (M^{-1})			Recommended K_a (M^{-1})	Literature value(s)	Ref.
	NMR ^a	ITC	Fluorescence ^b			
TBA, 1	$(4.10 \pm 0.52) \times 10^3$ ^c	$(4.75 \pm 0.56) \times 10^3$ ^d	$(4.67 \pm 0.52) \times 10^3$	$(4.51 \pm 0.31) \times 10^3$	2.8×10^3 ^c	[192]
Put, 2	n.d.	$(1.85 \pm 0.11) \times 10^6$ ^d	$(1.79 \pm 0.18) \times 10^6$	$(1.82 \pm 0.11) \times 10^6$	7.9×10^5 ^d	[193]
BE	$(2.40 \pm 0.22) \times 10^7$	$(2.26 \pm 0.39) \times 10^7$ ^d	$(2.43 \pm 0.39) \times 10^7$ ^e	$(2.36 \pm 0.20) \times 10^7$	2.4×10^7 ^d	[184]
HMD, 3	$(1.34 \pm 0.26) \times 10^9$	$(1.29 \pm 0.13) \times 10^9$ ^f	$(1.22 \pm 0.25) \times 10^9$	$(1.28 \pm 0.13) \times 10^9$	2.1×10^9 ^f 1.4×10^8 ^f	[175,194] [193]
PXD, 4	$(2.27 \pm 0.30) \times 10^{10}$	$(2.20 \pm 0.40) \times 10^{10}$ ^f	$(2.00 \pm 0.35) \times 10^{10}$	$(2.16 \pm 0.21) \times 10^{10}$	3.3×10^9 ^f 1.2×10^{10} ^f	[193] [56]
CBAMC, 5	$(6.01 \pm 0.67) \times 10^{12}$	$(5.62 \pm 0.68) \times 10^{12}$ ^f	n.d. ^g	$(5.81 \pm 0.48) \times 10^{12}$	n.a. ^h	n.a. ^h
TBAMC, 6	$(6.57 \pm 0.48) \times 10^{12}$	$(6.62 \pm 0.77) \times 10^{12}$ ^f	n.d. ^g	$(6.60 \pm 0.46) \times 10^{12}$	n.a. ^h	n.a. ^h
FDMA, 7	$(2.40 \pm 0.30) \times 10^{12}$	$(2.38 \pm 0.34) \times 10^{12}$ ^f	n.d. ^g	$(2.39 \pm 0.23) \times 10^{12}$	2.0×10^{12} ^f 2.4×10^{12} ^f 1.7×10^{14} ^f	[194] [57] [57]
ADA, 8	$(1.04 \pm 0.15) \times 10^{15}$	n.d. ⁱ	n.d. ^g	$(1.04 \pm 0.15) \times 10^{15}$	4.2×10^{12} ^a 1.1×10^{11} ^f	[54] [193]
AMADA, 9	$(5.26 \pm 0.61) \times 10^{15}$	n.d. ⁱ	n.d. ^g	$(5.26 \pm 0.61) \times 10^{15}$	7.7×10^{14} ^a 9×10^{14} ^a	[57]j [57]j

^a Measured by competitive NMR (unless indicated differently). ^b Measured by fluorescence displacement with **BE** (except for **BE** itself). ^c Measured by direct NMR titration. ^d Measured by direct ITC. ^e Measured by direct fluorescence titration. ^f Measured by competitive ITC. ^g Binding constants could not be determined due to the quantitative displacement of **BE**. ^h No literature value available. ⁱ Binding constants could not be determined due to slow exchange. ^j Different values reported in main text and SI

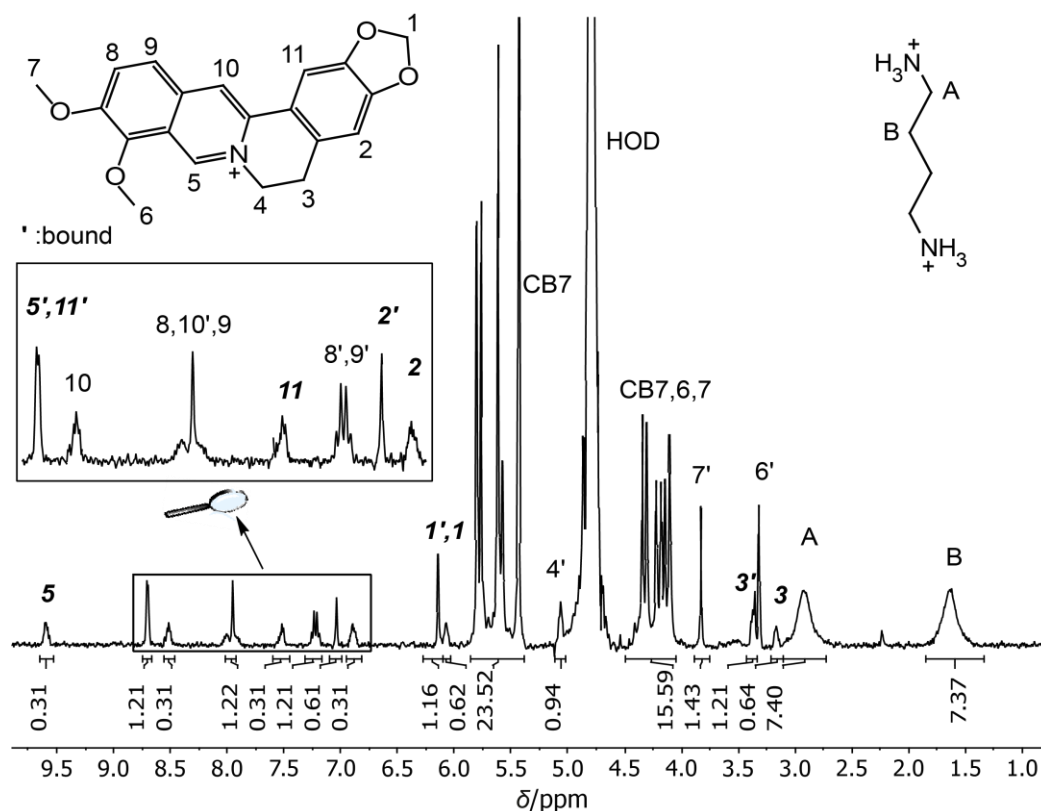


Figure 4.1 ^1H NMR spectrum for 0.84 mM CB7, 1.16 mM Put and 0.91 mM BE in D_2O at pH 7.4. Signals marked in bold were used for integration and determination of K_{rel} .

4.3 Reference Compounds for nM Affinity

In order to establish reference compounds with nanomolar affinity, we decided for HMD (**3**) and PXD (**4**), with reported binding constants of $2.1 \times 10^9 \text{ M}^{-1}$ and $1.8 \times 10^9 \text{ M}^{-1}$.^[54,175-176] The trimethylsilylated reference compound synthesized by the Isaacs group was elegantly selected for its well-separated NMR peak in the region around 0 ppm,^[56] whereas HMD (**3**) and PXD (**4**) complement each other by covering the aliphatic and aromatic regions of the NMR spectrum. Consequently, the aliphatic HMD (**3**) can be used to determine binding affinities of aromatic competitors with minimal probability of overlapping NMR peaks and the aromatic PXD (**4**) can be used for aliphatic competitors (**Figure 4.1**).

As a first step, we have determined the binding affinity of HMD (**3**) by competitive fluorescence titrations with **BE** (**Figure A3.6**), which yielded a value of $K_a = (1.22 \pm 0.25) \times 10^9 \text{ M}^{-1}$ ($n = 6$, see Appendix A.3.3.2 in Appendices for error calculation), whereas the displacement titration with PXD (**4**) was more challenging. With typical concentrations of **BE** and CB7, we noted that the titration curve could not be

reliably fitted, because the strong binding of PXD (**4**) led to quantitative displacement under the standard conditions. To remedy, we increased the concentration of **BE** from 2 μM to 25 μM to account for the high affinity of PXD. To eliminate potential interferences from the inner filter effect at this high concentration, the commonly used 10×10 mm cuvette was replaced with a 10×4 mm cuvette. When **BE** was excited along the 4 mm path, a linear dependence of fluorescence intensity on concentration was obtained (**Figure A3.11**). In this way, competitive fluorescence titrations with PXD (**Figure 4.4**) gave a binding constant of $K_a = (2.00 \pm 0.35) \times 10^{10} \text{ M}^{-1}$ ($n = 6$, see Appendix A.3.3.2 in Appendices for error calculation).

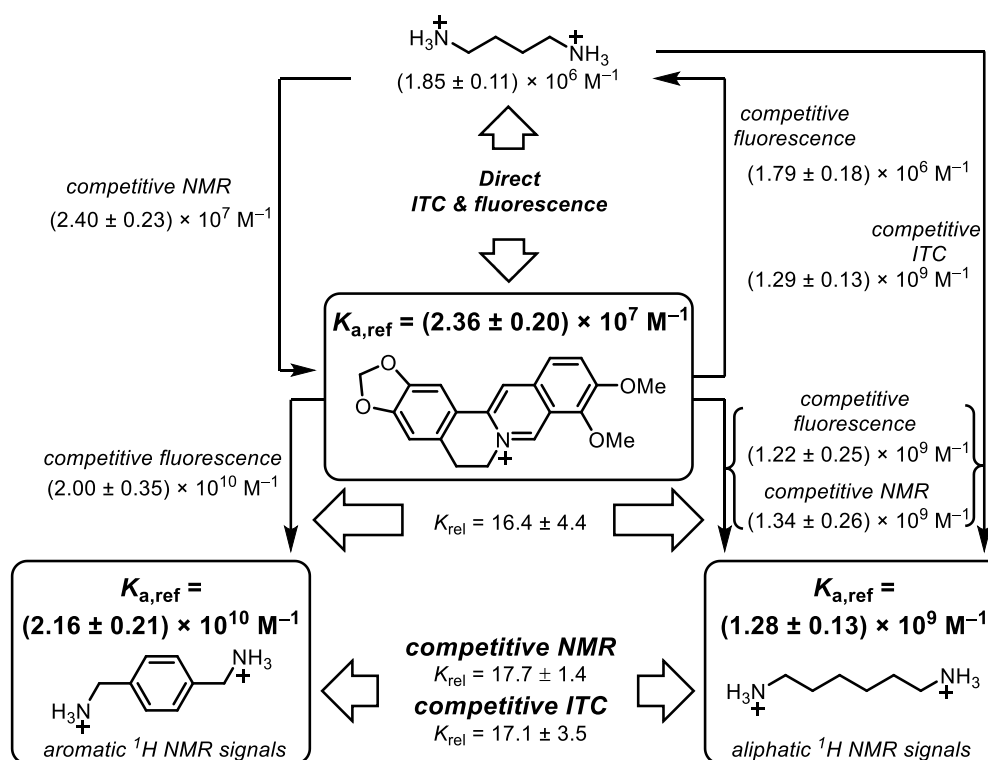


Figure 4.2 Flow scheme for determination and mutual verification of binding constants in the range of 10^6 to 10^{10} M^{-1} .

Our results revealed some discrepancies with the reported literature values.^[54,175] For example, it had been reported that HMD (**3**) ($K_a = 2.1 \times 10^9 \text{ M}^{-1}$) binds about equally strong to CB7 than PXD (**4**) ($2.1 \times 10^9 \text{ M}^{-1}$ versus $1.8 \times 10^9 \text{ M}^{-1}$), whereas we found an order of magnitude higher affinity for PXD (**4**, $K_{\text{rel}} = 16.4 \pm 4.4$, by fluorescence titration). To obtain an independent confirmation, competitive ^1H NMR measurements with HMD (**3**) and PXD (**4**) were performed next. The ^1H NMR spectra of mixtures of HMD (**3**), PXD (**4**), and a limiting quantity of CB7,

exhibited clear spectral differentiation with no overlap between the peak positions of free and complexed HMD (**3**) and PXD (**4**); only the peaks ascribed to the benzylic protons of uncomplexed PXD (**4**) overlapped with the CB7 peaks at 4.20 ppm (**Figure 4.1**). The relative binding constant and its standard deviation could accordingly be calculated by using all six combinations of the integrated peak areas of the two PXD (**4**) peak pairs (the CB7 peak area was subtracted from the integrated peak area of B) and three HMD (**3**) peak pairs (equation A4.11). This gave $K_{\text{rel}} = K_{\text{a,PXD}}/K_{\text{a,HMD}} = 17.7 \pm 1.4$, which agrees very well with the K_{rel} value obtained by fluorescence (16.4 ± 4.4) and clearly confirmed that PXD (**4**) binds more strongly to CB7 than HMD (**3**).

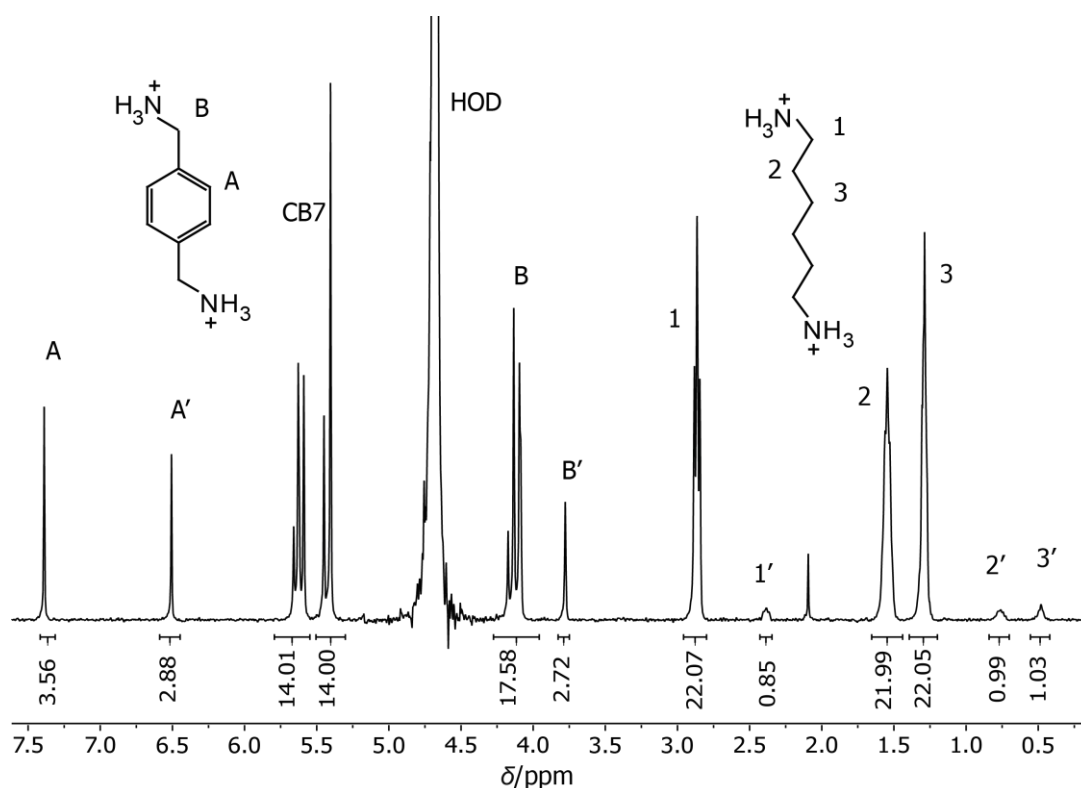


Figure 4.3 ^1H NMR competition experiment with 1.0 mM CB7, 1.6 mM PXD, and 5.7 mM HMD in D_2O at pD 7.4. Signals for PXD are assigned with uppercase letters and those for HMD with Arabic numerals. Dashes indicate the respective CB7 complexes. The integrated peak areas are given below the x-axis.

The binding constant of HMD (**3**) was further confirmed by ^1H NMR using BE as a competitive binder (**Figure A3.9**), which afforded $K_{\text{a}} = (1.34 \pm 0.26) \times 10^9 \text{ M}^{-1}$, and by ITC by using Put (**2**) as a competitive binder (**Figure A3.7**, $K_{\text{a}} = (1.29 \pm 0.13) \times 10^9 \text{ M}^{-1}$). Both values agree very well with our fluorescence value, such that we suggest to use a reference value of $(1.28 \pm 0.13) \times 10^9 \text{ M}^{-1}$ for HMD (**3**).

(see eq.A4.2 and eq.A4.3). This value lies within the range of reported literature values for HMD (**3**) binding to CB7, which varied from $1.4 \times 10^8 \text{ M}^{-1}$ to $2.1 \times 10^9 \text{ M}^{-1}$ (see **Figure 4.1** and **Table 4.1** for an overview).^[175,193]

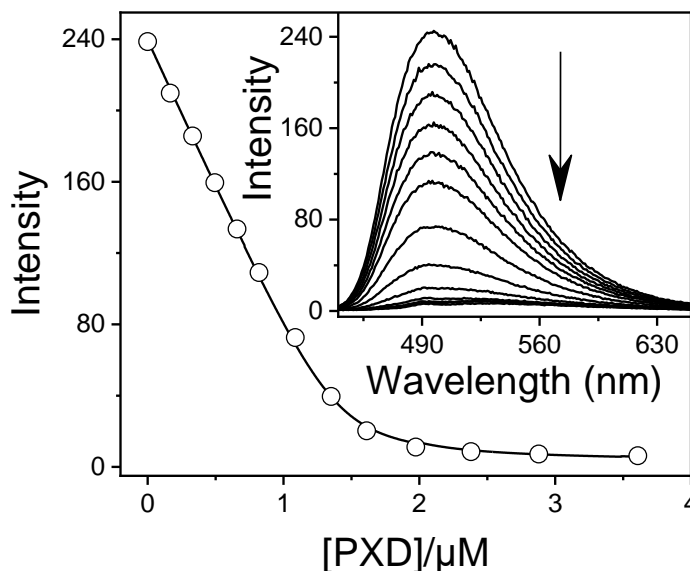


Figure 4.4 Fluorescence displacement titration ($\lambda_{\text{ex}} = 420 \text{ nm}$, $\lambda_{\text{em}} = 490 \text{ nm}$) of $25.0 \mu\text{M}$ berberine and $1.4 \mu\text{M}$ CB7 upon adding different concentrations of PXD (**4**).

The absolute K_a value of PXD (**4**) cannot be measured against berberine by NMR, because the required concentration of berberine exceeds the solubility limit of **BE**, but it was further confirmed by competitive ITC against HMD (**3**) (**Figure A3.12**, $K_a = (2.20 \pm 0.40) \times 10^{10} \text{ M}^{-1}$). Combining the results from ITC, NMR, and fluorescence suggests a reference value of $(2.16 \pm 0.21) \times 10^{10} \text{ M}^{-1}$ for the binding affinity of PXD (**4**) to CB7 (**Figure 4.1**), which lies above the range of previously reported binding affinities (**Table 4.1**).^[56,194]

It is noteworthy that we scrutinized our results in water distilled from KMnO_4 and data obtained in initial exploration experiments with Millipore water. A re-evaluation of the data in our Millipore water clearly suggested that the potential trace impurities had only a small, but sizeable influence on direct titrations, whereas the influence in competitive titrations was negligible. For example, when **BE** displacement titrations with HMD (**3**) in Millipore water were re-evaluated with the reference K_a value of **BE** in water distilled from KMnO_4 , the obtained binding constants of HMD were identical, within error, to the results from titrations in water

distilled from KMnO_4 . Also, for Put (**2**), direct ITC titrations revealed differences in Millipore water and in water distilled from KMnO_4 (see previous section), whereas fluorescence displacement titrations with Put (**2**) and BE in Millipore water gave the same binding constants as in water distilled from KMnO_4 , when the reference K_a value of BE in water distilled from KMnO_4 was used in the fitting. It is further interesting to note, that the *relative* binding constants of Put (**2**) and BE in H_2O at pH 7.0 (by fluorescence) and in D_2O at pD 7.4 (by NMR) were identical within our rigorously determined error ranges, which excludes any undesirable interferences in our commercial D_2O in competitive NMR titrations. From these observations, one may jump to the conclusion that competitive titrations always afford reliable relative binding constants even if the concentrations of known or unknown impurities (such as buffer salts or the unknown impurity in the employed Millipore water) vary. However, this is correct only if the impurity or salt competes with both analytes of interest in the same manner. In reality, this is certainly not always the case, e.g. the presence of cations affects the binding of different hydrocarbons to CB6 to a different degree, likely due to the variable involvement of ternary complexes.^[87]

4.4 Reference Compounds for pM Affinity

With increasing affinity, competitive titrations become more and more time-demanding, because of the slow exchange kinetics associated with high-affinity guests. This prevents the use of reference compounds with $K_a > 10^{12} \text{ M}^{-1}$ in competitive ITC titrations, because equilibration times of hours to days would be required after every injection. As an alternative, competitive ITC titrations have been performed with high millimolar concentrations of the more rapidly exchanging guests PXD (**4**) or HMD (**3**) with nanomolar affinity by Kaifer^[193] and by Kim, Inoue and Gilson.^[57] This strategy is, however, not possible with competitive ^1H NMR titrations, because the determination of ratios of components in a mixture with small peak areas (low concentration of the complex) and large peak areas (high concentration of the free competitor) is often lacking accuracy.^[172,195] The Isaacs group has therefore utilized 1-adamantyl-pyridinium as a relatively fast exchanging high-affinity reference compound with picomolar affinity for competitive ^1H NMR titrations.^[56,58]

As potential alternatives, we introduce herein *cis*- and *trans*-1,4-bis(aminomethyl)-cyclohexane (CBAMC, **5**, and TBAMC, **6**) as well as *N,N*-dimethylaminomethyl-ferrocene (FDMA, **7**) as potential reference compounds for CB7 binding affinities in the pM range. As an initial experiment, the relative binding constant of CBAMC (**5**) and TBAMC (**6**) were assessed by NMR and ITC against PDX (**Table 4.1**, see **Figure A3.23**, **Figure A3.25**, **Figure A3.48**, and **Figure A3.49**), which indicated that the affinity of both isomers to CB7 is very similar and that the affinity of the *trans* isomer is only 1.1-fold higher than that of the *cis* isomer. Interestingly, the *cis* isomer CBAMC (**5**) showed, however, more rapid exchange kinetics (**Figure A3.50**) and was thus further investigated in more detail.

CBAMC (**5**) shows clearly separated free and bound peaks for the CH₂-N methanaminium (at 2.87 and 2.55 ppm), the C–H group of the cyclohexane ring (at 1.64 and 0.71 ppm), and for four cyclohexane CH₂ protons at 1.85 and 0.15 ppm (**Figure A3.24**). The competitive NMR titration of CBAMC (**5**) against PDX (**4**) (**Figure A3.25**) was evaluated as described above by considering all six combinations of the three CBAMC (**5**) compound peak pairs and two PDX (**4**) reference peak pairs with equation A.3.11. This gave a K_{rel} value of 278 ± 14 , which was converted into a binding constant of $(6.01 \pm 0.67) \times 10^{12} \text{ M}^{-1}$ by NMR using equations A.3.16 and A.3.18. We also determined the binding affinity of CBAMC (**5**) by ITC ($n = 2$) by titrating CBAMC (**5**) into a solution containing the PDX•CB7 complex (**Figure A3.23**). This furnished a binding constant of $(5.62 \pm 0.68) \times 10^{12} \text{ M}^{-1}$, in good agreement with the NMR value, which leads us to propose a reference value of $(5.81 \pm 0.48) \times 10^{12} \text{ M}^{-1}$ for CBAMC (**5**). In addition, FDMA (**7**) was measured against PDX (**4**) by NMR and ITC (**Figure A3.39** and **Figure A3.40**), which yielded binding constants of $(2.40 \pm 0.30) \times 10^{12} \text{ M}^{-1}$ and $(2.38 \pm 0.34) \times 10^{12} \text{ M}^{-1}$, respectively; we suggest a reference value of $(2.39 \pm 0.23) \times 10^{12} \text{ M}^{-1}$ for FDMA (**7**) (**Table 4.1**).

The 1-ferrocenyl-trimethylmethanaminium cation had been used previously within a series of binding constant determinations,^[54] but based on our results, we consider ferrocene derivatives, such as FDMA (**7**), to be overall less useful than CBAMC (**5**). First, we noted that many of the ferrocene peaks overlap with the CB7 peaks in ¹H NMR spectroscopy (Figure S38), such that only a single peak appeared

suitable for integration. Second, FDMA (**7**) has a limited solubility (<12 mM), which is too low for competitive titrations of guests with femtomolar affinity (see below). And third, we noted that the ^1H NMR peaks of a FDMA (**7**) solution in D_2O became significantly broadened after a few days, which may be due to slow decomposition of FDMA. The advantage of FDMA (**7**) compared to CBAMC (**5**) is its significantly faster exchange rate (compare **Figure A3.32** and **Figure A3.33**), which is, however, still too slow to be useful for competitive ITC. As a consequence, FDMA (**7**) may be a useful reference compound when high binding affinities need to be rapidly screened, whereas CBAMC (**5**) will likely provide more accurate affinities. A literature value for CBAMC (**5**) has, so far, not been reported, but our value for FDMA (**7**) is gratifyingly in excellent agreement with the value reported by Kim, Inoue, and Gilson ($2.4 \times 10^{12} \text{ M}^{-1}$) and in very good agreement with the value by Kaifer ($2.0 \times 10^{12} \text{ M}^{-1}$).^[57,194]

4.5 Reference Compounds for fM Affinity

Several guests with femtomolar and higher affinity have been reported for CB7, which include diamantane, adamantane, and bicyclooctane derivatives,^[56-57] but the extremely slow exchange kinetics in combination with the lack of established reference compounds renders the determination of these ultrahigh affinities often challenging and time-consuming. For example, adamantylamine (ADA, **8**) has been very often used as a prototypical ultrahigh-affinity guest, but its reported binding constant varies largely and ranges from $1.1 \times 10^{11} \text{ M}^{-1}$ over $1.7 \times 10^{12} \text{ M}^{-1}$ to $4.2 \times 10^{14} \text{ M}^{-1}$.^[54,57,193]

With the goal to extend our reference scale to compounds with binding affinities in the femtomolar range, we considered ADA (**8**) as well as aminomethyladamantane (AMADA, **9**), also because they are both commercially available. The K_{rel} values of both compounds were determined by ^1H NMR competition experiments with CBAMC (**5**) as the reference. To ensure full relaxation of the host-guest equilibration mixtures, two samples were prepared for each competitor, in which, first, CBAMC was pre-mixed with CB7, and second, the competitor was pre-mixed with CB7 before addition of the other compound. Subsequently, ^1H NMR spectra were recorded after varying time periods until both mixtures were fully equilibrated, as indicated by both having reached the same degree of complexation (**Figure A3.32** and **Figure A3.37**). Integration of three

peaks per spectrum gave $K_{\text{rel}} = 179 \pm 14$ for ADA (**7**) and 906 ± 73 for AMADA (**9**) using equations A4.11- A4.15. This value was converted into a binding constant of $(1.04 \pm 0.15) \times 10^{15} \text{ M}^{-1}$ for ADA (**8**) and $(5.26 \pm 0.61) \times 10^{15} \text{ M}^{-1}$ for AMADA (**9**) by NMR using equations A4.16 and A4.18. Notably, our value for ADA is about fivefold higher than the originally reported values in the literature,^[54,57,193] which underlines the challenge to accurately measure such ultra-high binding affinities.

When comparing the principal suitability of ADA (**8**) and AMADA (**9**) as potential reference compounds, it is apparent that the dissociation kinetics of ADA (**8**) is much faster than that of AMADA (**9**) (**Figure A3.32** and **Figure A3.37**). In fact, the chemical exchange of AMADA in ^1H NMR competition experiment is so slow that it would require unreasonably long equilibration times in routine binding titrations (**Figure A3.37**). This is unfortunate, because the peaks of the $\text{CH}_2\text{-N}$ methanaminium protons of AMADA (**9**) and its CB7 complex are very well separated (at 2.68 and 2.46 ppm for the free complexed form) and can thus be very reliably integrated.

4.6 Reference Compounds for mM Affinity

To complete the list of suitable reference compounds also at the lower end of the affinity scale, we included TBA (**1**), which could serve as a potential reference in the mM range for important biological molecules such as carnitine, trimethyllysine, or amino acids.^[192-193,196-197] The binding constant of TBA (**1**) was measured by ITC, fluorescence displacement with **BE** and by a direct ^1H NMR titration (see **Table 4.1** and Appendix A.3.9 in Appendices). This provided an average binding constant of $(4.51 \pm 0.31) \times 10^3 \text{ M}^{-1}$, which we propose as the reference value for this low affinity range.

4.7 Binding Constants of High-Affinity Guests

After setting up a reference scale of binding affinities, we determined the binding constant of compounds **10-13** (see **Table 4.2**). (2,3-diazabicyclo[2.2.2.]oct-2-enyl)methylamine (DBO-A, **10**) and the putrescine derivative of aminomethyladamantane (AMADA-Put, **13**) are guests with a supposedly high binding affinity to CB7. For example, AMADA-Put was previously introduced by us to determine the number of reactive surface functional groups on micro- and nanoparticles^[19,166,185] and as a ditopic guest in a supramolecular switch,^[177] and

DBO-A may be useful in time-resolved assays with CB7.^[198-199] However, the binding constants of **10** and **13** have so far not been reported. In addition, we were interested in the binding affinity of an amino acid derivative of AMADA (*S*)-2-(adamantan-1-yl)-2-aminoacetic acid hydrochloride (AMADA-aa, **12**) to CB7, and in the affinity of cyclohexylmethylamine (CHMA, **11**). The latter was previously explored by us as an anchor group in the design of reporter dyes for CB7-based sensor systems.^[186]

With the now set up reference scale and the respective uncertainty ranges, the binding constant for each compound was measured by competition experiments using the reference values and errors in **Table 4.1**. The binding constant of DBO-A (**10**) was measured by ¹H NMR competition with PXD (**4**) and by fluorescence displacement titration with **BE**. ¹H NMR, using the integrated peak areas of eight peaks (**Figure A3.28**), gave a K_a value of $(2.18 \pm 0.31) \times 10^{10} \text{ M}^{-1}$ and global fitting ($n = 6$) of fluorescence titrations (**Figure A3.26**) gave a binding constant for DBO-A (**10**) of $(2.07 \pm 0.21) \times 10^{10} \text{ M}^{-1}$. Noteworthy, the fluorescence displacement titration was performed as described above for PXD to avoid quantitative binding and the fluorescence of DBO-A itself was undetectable under these conditions due to the low brightness of the azo chromophore. The binding constant of DBO-A (**10**) is lower than the analogous aliphatic bicyclooctane,^[57] which is in agreement with a decreased hydrophobicity of DBO derivatives due to the significant dipole moment and high water-solubility resulting from the azo group.^[200]

The K_a value of AMADA-Put (**13**) was expected to be in the femtomolar range and was accordingly determined against CBAMC (**5**) as a competitor. AMADA-Put (**13**) exhibited extremely slow exchange kinetics. Especially, when CBAMC (**5**) was added to the AMADA-Put (**13**) complex with CB7, more than six months were required to reach equilibrium. The obtained K_{rel} of AMADA-Put (**13**) against CBAMC was $(3.47 \pm 0.59) \times 10^3$, which gave a K_a value of $(2.02 \pm 0.39) \times 10^{16} \text{ M}^{-1}$ (see **Table 4.2**, **Figure A3.43** and **Figure A3.45**). The increased affinity of aminoalkylated adamantane derivatives compared to the unsubstituted amines was previously noted and explained through a primary ammonium looping model.^[58,201] In agreement with this model, the ratio of the K_{rel} values of **13** and **9** agrees very well with the related aminoalkylated adamantylamines from Isaacs.^[58]

Table 4.2 Binding constants values of amines measured or re-measured in this study.

Compound	Method	K_a/M^{-1}	Literature value
DBO-A, 10	NMR	$(2.18 \pm 0.31) \times 10^{10 \text{ a}}$	n.a. ^c
CHMA, 11	Fluorescence	$(2.07 \pm 0.21) \times 10^{10 \text{ b}}$	
	NMR	$(8.80 \pm 1.10) \times 10^{10 \text{ a}}$	
	ITC	$(8.43 \pm 0.43) \times 10^{10 \text{ d}}$	$1.3 \times 10^{11 \text{ e}}$
AMADA-aa, 12	NMR	$(1.55 \pm 0.32) \times 10^{12 \text{ f}}$	n.a. ^c
AMADA-Put, 13	NMR	$(2.02 \pm 0.39) \times 10^{16 \text{ f}}$	n.a. ^c

^a Measured by competition NMR against PXD. ^b Measured by fluorescence displacement with BE. ^c Literature value not available. ^d Measured by competitive ITC against HMD. ^e Measured by competitive ITC in ref. ^[175]. ^f Measured by competition NMR against CBAMC.

The amino acid AMADA-aa (**12**) has two ionizable functional groups, and typical pK_a values for the α -carboxylic acid (<2.5) and α -amino groups (>8.5) in amino acids suggest that AMADA-aa (**12**) prevails in its zwitterionic, neutral form at neutral pH. Using PXD (**4**) as a competitor, the relative binding constant was measured by ^1H NMR competition using six integratable peaks, which gave $K_{\text{rel}} = 72 \pm 13$ and $K_a = (1.55 \pm 0.32) \times 10^{12} \text{ M}^{-1}$ (see **Table 4.2**, **Figure A3.41** and **Figure A3.42**). As expected, AMADA-aa (**12**) has a significantly lower binding affinity than AMADA (**9**), because the negatively charged carboxylate anion introduces repulsive ion-dipole interactions with the carbonyl groups at the CB7 rim.^[81,202]

Finally, the affinity of CHMA (**11**) to CB7 was obtained via competitive ITC by injecting CHMA into a solution containing the HMD•CB7 complex, which established $K_a = (8.43 \pm 0.43) \times 10^{10} \text{ M}^{-1}$ (see **Table 4.2**, **Figure A3.21**). This value is slightly lower than the literature value, which is attributed to the higher K_a value of HMD (**3**) used in the competition experiment in the literature;^[175] the relative binding constants of our experiments and the ITC titration in the literature differ only by 10%. To additionally confirm the revised value, the binding constant of CHMA (**11**) was also measured by ^1H NMR competition using PXD (**4**) as a competitor, which gave $K_a = (8.8 \pm 1.1) \times 10^{10} \text{ M}^{-1}$ (**Figure A3.22**).

Summary and Outlook

Summary and Outlook

The doctoral thesis, in the first part, describes the use of BODIPYs as fluorophores via an anchor group strategy towards the design of reporter dyes for CB7. The resulting dyes have absorption and emission wavelengths which are compatible with established instrumentation in life science applications and show pronounced fluorescence changes upon host binding. The affinity of the dyes for the CB7 host was successfully adjusted by using different anchor groups and was only minimally reduced in comparison with the unmodified anchor groups. This strategy enables several applications of fluorescent host-guest complexes, for example, indicator displacement assays with absorption and emission wavelengths in the visible spectral region, fluorescence correlation spectroscopy, and noncovalent surface functionalization with fluorophores. Furthermore, the strategy is similarly applicable to pH-sensitive fluoresceins, cyanines, or rhodamines, in which protonation and deprotonation of suitably positioned amino groups can also modulate their fluorescence properties. It can also be used to design dyes which reduce their fluorescence upon binding, e.g., when electron-deficient groups are generated by protonation which are quenched intramolecularly by donor-excited PET.^[203-207]

In the second part, we have investigated the host-guest complexation of AnPy with CB n in aqueous solution. Two different binding modes are observed for the differently sized CB n homologues. CB7 can bind the pyridinium ring, while the large cavity of CB8 can simultaneously encapsulate the anthracene and the pyridinium rings. The CB7•AnPy aggregates form nanoparticles at high concentrations, while the CB8•AnPy pair assembles in a cylindrical shape. Both assemblies show responsive properties. For example, the CB7•AnPy particles can be assembled and disassembled by changing the temperature. This approach can be used to potentially construct various responsive CB n -based self-assembled materials for drug-delivery applications.

In the third part, we have established a series of reference compounds for the determination of CB7 binding affinities by competitive host-guest titrations. The compounds have been selected to cover a wide range of affinities (mM-fM), to be amenable to various measurement techniques, and to allow ready and broad access as well as high reproducibility on account of commercial sample availability. The

fluorescent dye berberine was established as a central compound with μM affinity, which was measured by fluorescence spectroscopy, ITC, and ^1H NMR. Within a series of cross-validated competition experiments, we next established hexamethylenediamine and *p*-xylylenediamine as references with nM affinity, *cis*-1,4-bis(aminomethyl)-cyclohexane and *N,N*-dimethylaminomethylferrocene as references with pM affinity (with the latter showing faster exchange), and we propose adamantylamine as reference compound with fM affinity.

To illustrate an immediate application of the reference scale, we determined the binding constants of four compounds of interest, DBO-A, AMADA-aa, AMADA-Put, and CHMA, by the corresponding competitive titrations with the respective reference compounds. For example, CHMA was tested as an anchor group in the design of new host-dye reporter pairs with CB7^[186] and AMADA-Put was used to determine the number of reactive surface functional groups^[19,166,185] and as a ditopic guest in a supramolecular switch.^[177] The amino acid AMADA-aa could be introduced into peptides and become useful in sensing applications, for example in supramolecular tandem membrane and enzyme assays.^[15,17,81,199,208-210]

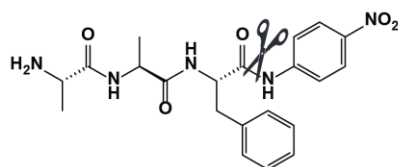
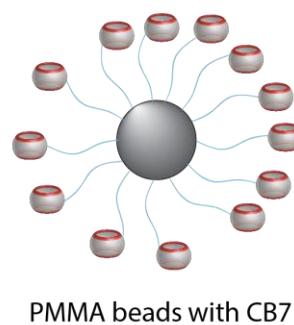
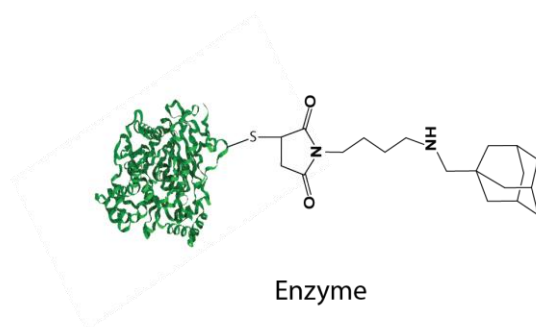
As a future prospective Mono-functionalized CB7 and its supramolecular host-guest complexes can be used to study bioconjugations.^[211] The streptavidin-biotin protein-ligand interaction occurs in nature. This has been successfully utilized in several applications, including sensing of nucleic acids, proteins, lipids, and protein purifications.^[212] The strongest binding interaction of biotin-avidin is 10^{15} M^{-1} . The complex formation between biotin and avidin occurs rapidly. The complex is stable under wide range of pH values, temperature, organic solvents, and other denaturing agents.^[212]

Although the avidin-biotin system is simple to set up and use, it does have certain limitations. For example, avidin can nonspecifically bind to negatively charged residues on cell surfaces and nucleic acids, or membrane sugars receptors, in addition to the background problems caused by avidin, in particular, for histochemical and cytochemical applications.^[213] With supramolecular high-affinity host-guest complexes, new labelling and bioconjugation strategy is now available.^[14]

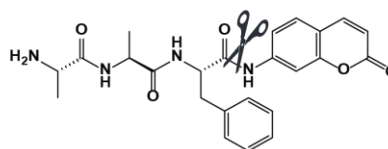
We have previously prepared polymethylmethacrylate (PMMA) beads modified with the macrocycle CB7, via well-known copper-catalyzed azide-alkyne click chemistry, which have been used for quantitatively determine surface coverage.^[14]

Herein, we have introduced the applicability of the polymethylmethacrylate (PMMA) beads modified with CB7 to conjugate biomolecules such as proteins.^[14] In details, chymotrypsin is attached with maleimide through a thiol group, and further tethered to aminomethyladamantane (AMADA), which is recognized by the macrocyclic receptor CB7. Based on the binding affinity value of AMADA with CB7,^[5,214] we predict the CB7 modified beads will bind strongly to an AMADA-protein.

Chymotrypsin is known to specifically cleave peptide bonds after bulky nonpolar side chains, such as the aromatic amino acid phenylalanine. The hydrolysis of a peptide substrate carrying a chromophore can now be investigated using the chymotrypsin modified beads (see **Scheme 1**). Initially, mixing the CB7 modified PMMA beads with AMADA-chymotrypsin will insure the formation of CB7-AMADA inclusion complex and therefore the successful coverage of the beads with chymotrypsin. Subsequently, known amount of substrate is added into the CB7-AMADA-chymotrypsin mixture. This led to an enzymatic reaction that can be monitored in real-time due to the cleavage of the chromophore and consequently changing the optical properties. After the reaction is completed, reaction mixture is centrifuged and obtained the pellet, which is washed with Millipore water. This pellet contains CB7-AMADA-chymotrypsin. Subsequently addition of AMADA into the pellet resulted in unbound AMADA-chymotrypsin, which represents the major advantage of using beads, as heterogenous systems over homogenous ones.



Substrate: H-Ala-Ala-Phe-pNA



H-Ala-Ala-Phe-AMC

Scheme 1 Chemical structures of a potential supramolecular chemosensor composed of PMMA beads attached with macrocycle host CB7 and an enzyme (chymotrypsin) attached with an adamantane moiety, which has femtomolar affinity to CB7. Substrate (peptide) attached with chromophore.

References

References

- [1] J.-M. Lehn, *Science* **1985**, 227, 849-856.
- [2] G. Crini, *Chem. Rev.* **2014**, 114, 10940-10975.
- [3] A. F. Danil de Namor, R. M. Cleverley, M. L. Zapata-Ormachea, *Chem. Rev.* **1998**, 98, 2495-2526.
- [4] S. J. Barrow, S. Kasera, M. J. Rowland, J. del Barrio, O. A. Scherman, *Chem. Rev.* **2015**, 115, 12320-12406.
- [5] K. I. Assaf, W. M. Nau, *Chem. Soc. Rev.* **2015**, 44, 394-418.
- [6] R. N. Dsouza, U. Pischel, W. M. Nau, *Chem. Rev.* **2011**, 111, 7941-7980.
- [7] F. Biedermann, D. Hathazi, W. M. Nau, *Chem. Commun.* **2015**, 51, 4977-4980.
- [8] N. J. Turro, J. D. Bolt, Y. Kuroda, I. Tabushi, *Photochem. Photobiol.* **1982**, 35, 69-72.
- [9] B. D. Wagner, N. Stojanovic, G. Leclair, C. K. Jankowski, *J. Inclusion Phenom. Macrocyclic Chem.* **2003**, 45, 275-283.
- [10] R. Behrend, E. Meyer, F. Rusche, *Justus Liebigs Annalen der Chemie* **1905**, 339, 1-37.
- [11] K. I. Assaf, W. M. Nau, in *Cucurbiturils and Related Macrocycles*, The Royal Society of Chemistry, **2020**, pp. 54-85.
- [12] S. Li, D. H. Macartney, R. Wang, in *Cucurbiturils and Related Macrocycles*, The Royal Society of Chemistry, **2020**, pp. 31-53.
- [13] A. I. Day, A. S. Atthar, in *Cucurbiturils and Related Macrocycles*, The Royal Society of Chemistry, **2020**, pp. 238-282.
- [14] S. Zhang, Z. Domínguez, K. I. Assaf, M. Nilam, T. Thiele, U. Pischel, U. Schedler, W. M. Nau, A. Hennig, *Chem. Sci.* **2018**, 9, 8575-8581.
- [15] A. Barba-Bon, Y.-C. Pan, F. Biedermann, D.-S. Guo, W. M. Nau, A. Hennig, *J. Am. Chem. Soc.* **2019**, 141, 20137-20145.
- [16] M. Nilam, P. Gribbon, J. Reinshagen, K. Cordts, E. Schwedhelm, W. M. Nau, A. Hennig, *SLAS Discov.* **2017**, 22, 906-914.
- [17] G. Ghale, W. M. Nau, *Acc. Chem. Res.* **2014**, 47, 2150-2159.
- [18] D. Das, K. I. Assaf, W. M. Nau, *Front. Chem.* **2019**, 7.
- [19] M. Nilam, M. Ahmed, M. A. Alnajjar, A. Hennig, *Analyst* **2019**, 144, 579-586.
- [20] D. Bardelang, K. A. Udachin, D. M. Leek, J. C. Margeson, G. Chan, C. I. Ratcliffe, J. A. Ripmeester, *Cryst. Growth Des.* **2011**, 11, 5598-5614.
- [21] S. Zhang, L. Grimm, Z. Miskolczy, L. Biczók, F. Biedermann, W. M. Nau, *Chem. Commun.* **2019**, 55, 14131-14134.
- [22] J.-X. Liu, L.-S. Long, R.-B. Huang, L.-S. Zheng, *Cryst. Growth Des.* **2006**, 6, 2611-2614.
- [23] O. A. Gerasko, E. A. Mainicheva, M. I. Naumova, M. Neumaier, M. M. Kappes, S. Lebedkin, D. Fenske, V. P. Fedin, *Inorg. Chem.* **2008**, 47, 8869-8880.
- [24] J.-X. Liu, L.-S. Long, R.-B. Huang, L.-S. Zheng, *Inorg. Chem.* **2007**, 46, 10168-10173.
- [25] P. Montes-Navajas, A. Corma, H. Garcia, *J. Mol. Catal. A: Chem.* **2008**, 279, 165-169.
- [26] K. Jansen, H.-J. Buschmann, A. Wego, D. Döpp, C. Mayer, H.-J. Drexler, H.-J. Holdt, E. Schollmeyer, *J. Inclusion Phenom.* **2001**, 39, 357-363.
- [27] J. Murray, K. Kim, T. Ogoshi, W. Yao, B. C. Gibb, *Chem. Soc. Rev.* **2017**, 46, 2479-2496.
- [28] S. Mecozzi, J. Rebek, Julius, *Chem. Eur. J.* **1998**, 4, 1016-1022.

- [29] A. L. Koner, W. M. Nau, *Supramol. Chem.* **2007**, *19*, 55-66.
- [30] A. Praetorius, D. M. Bailey, T. Schwarzlose, W. M. Nau, *Org. Lett.* **2008**, *10*, 4089-4092.
- [31] Z. Miskolczy, L. Biczók, M. Megyesi, I. Jablonkai, *J. Phys. Chem. B* **2009**, *113*, 1645-1651.
- [32] M. Megyesi, L. Biczók, I. Jablonkai, *J. Phys. Chem. C* **2008**, *112*, 3410-3416.
- [33] A. E. Hargrove, Z. Zhong, J. L. Sessler, E. V. Anslyn, *New J. Chem.* **2010**, *34*, 348-354.
- [34] P. Thordarson, *Chem. Soc. Rev.* **2011**, *40*, 1305-1323.
- [35] C. Marquez, W. M. Nau, *Angew. Chem. Int. Ed.* **2001**, *40*, 4387-4390.
- [36] J. Mohanty, W. M. Nau, *Angew. Chem. Int. Ed.* **2005**, *44*, 3750-3754.
- [37] L. You, D. Zha, E. V. Anslyn, *Chem. Rev.* **2015**, *115*, 7840-7892.
- [38] S. L. Wiskur, H. Ait-Haddou, J. J. Lavigne, E. V. Anslyn, *Acc. Chem. Res.* **2001**, *34*, 963-972.
- [39] B. T. Nguyen, E. V. Anslyn, *Coord. Chem. Rev.* **2006**, *250*, 3118-3127.
- [40] R. N. Dsouza, U. Pischel, W. M. Nau, *Chem. Rev.* **2011**, *111*, 7941-7980.
- [41] A. Buryak, F. Zaubitzer, A. Pozdnoukhov, K. Severin, *J. Am. Chem. Soc.* **2008**, *130*, 11260-11261.
- [42] M. Florea, S. Kudithipudi, A. Rei, M. J. González-Álvarez, A. Jeltsch, W. M. Nau, *Chem. Eur. J.* **2012**, *18*, 3521-3528.
- [43] J. Zhang, S. Umemoto, K. Nakatani, *J. Am. Chem. Soc.* **2010**, *132*, 3660-3661.
- [44] R. N. Dsouza, A. Hennig, W. M. Nau, *Chem. Eur. J.* **2012**, *18*, 3444-3459.
- [45] G. Krainer, J. Broecker, C. Vargas, J. Fanghänel, S. Keller, *Anal. Chem.* **2012**, *84*, 10715-10722.
- [46] M. M. Pierce, C. S. Raman, B. T. Nall, *Methods* **1999**, *19*, 213-221.
- [47] L. Mazzei, S. Ciurli, B. Zambelli, in *Methods Enzymol.*, Vol. 567 (Ed.: A. L. Feig), Academic Press, **2016**, pp. 215-236.
- [48] M. R. Duff, Jr., J. Grubbs, E. E. Howell, *J. Vis. Exp.* **2011**, 2796.
- [49] S. Leavitt, E. Freire, *Curr. Opin. Struct. Biol.* **2001**, *11*, 560-566.
- [50] S. He, F. Biedermann, N. Vankova, L. Zhechkov, T. Heine, R. E. Hoffman, A. De Simone, T. T. Duignan, W. M. Nau, *Nat. Chem.* **2018**, *10*, 1252-1257.
- [51] K. I. Assaf, M. A. Alnajjar, W. M. Nau, *Chem. Commun.* **2018**, *54*, 1734-1737.
- [52] K. I. Assaf, O. Suckova, N. Al Danaf, V. von Glasenapp, D. Gabel, W. M. Nau, *Org. Lett.* **2016**, *18*, 932-935.
- [53] D.-S. Guo, V. D. Uzunova, K. I. Assaf, A. I. Lazar, Y. Liu, W. M. Nau, *Supramol. Chem.* **2016**, *28*, 384-395.
- [54] S. Liu, C. Ruspic, P. Mukhopadhyay, S. Chakrabarti, P. Y. Zavalij, L. Isaacs, *J. Am. Chem. Soc.* **2005**, *127*, 15959-15967.
- [55] J. W. Lee, S. Samal, N. Selvapalam, H.-J. Kim, K. Kim, *Acc. Chem. Res.* **2003**, *36*, 621-630.
- [56] L. Cao, M. Šekutor, P. Y. Zavalij, K. Mlinarić-Majerski, R. Glaser, L. Isaacs, *Angew. Chem. Int. Ed.* **2014**, *53*, 988-993.
- [57] S. Moghaddam, C. Yang, M. Rekharsky, Y. H. Ko, K. Kim, Y. Inoue, M. K. Gilson, *J. Am. Chem. Soc.* **2011**, *133*, 3570-3581.
- [58] D. Sigwalt, M. Šekutor, L. Cao, P. Y. Zavalij, J. Hostaš, H. Ajani, P. Hobza, K. Mlinarić-Majerski, R. Glaser, L. Isaacs, *J. Am. Chem. Soc.* **2017**, *139*, 3249-3258.
- [59] W. L. Mock, N. Y. Shih, *J. Org. Chem.* **1986**, *51*, 4440-4446.
- [60] W. L. Mock, N. Y. Shih, *J. Am. Chem. Soc.* **1988**, *110*, 4706-4710.
- [61] T. Krasia, S. Khodabakhsh, D. Tuncel, J. Steinke, Berlin Heidelberg, 2004, **2004**, pp. 41-59.

- [62] W. L. Mock, N. Y. Shih, *J. Am. Chem. Soc.* **1989**, *111*, 2697-2699.
- [63] C. Márquez, R. R. Hudgins, W. M. Nau, *J. Am. Chem. Soc.* **2004**, *126*, 5806-5816.
- [64] G. Ghale, V. Ramalingam, A. R. Urbach, W. M. Nau, *J. Am. Chem. Soc.* **2011**, *133*, 7528-7535.
- [65] A. Norouzy, Z. Azizi, W. M. Nau, *Angew. Chem. Int. Ed.* **2015**, *54*, 792-795.
- [66] M. A. Alnajjar, J. Bartelmeß, R. Hein, P. Ashokkumar, M. Nilam, W. M. Nau, K. Rurack, A. Hennig, *Beilstein J. Org. Chem.* **2018**, *14*, 1961-1971.
- [67] J. Lagona, P. Mukhopadhyay, S. Chakrabarti, L. Isaacs, *Angew. Chem. Int. Ed.* **2005**, *44*, 4844-4870.
- [68] J. Kim, I.-S. Jung, S.-Y. Kim, E. Lee, J.-K. Kang, S. Sakamoto, K. Yamaguchi, K. Kim, *J. Am. Chem. Soc.* **2000**, *122*, 540-541.
- [69] J. M. Chinai, A. B. Taylor, L. M. Ryno, N. D. Hargreaves, C. A. Morris, P. J. Hart, A. R. Urbach, *J. Am. Chem. Soc.* **2011**, *133*, 8810-8813.
- [70] W. Li, A. T. Bockus, B. Vinciguerra, L. Isaacs, A. R. Urbach, *Chem. Commun.* **2016**, *52*, 8537-8540.
- [71] M. J. Webber, E. A. Appel, B. Vinciguerra, A. B. Cortinas, L. S. Thapa, S. Jhunjhunwala, L. Isaacs, R. Langer, D. G. Anderson, *Proc. Natl. Acad. Sci. U. S. A.* **2016**, *113*, 14189-14194.
- [72] J. F. Young, H. D. Nguyen, L. Yang, J. Huskens, P. Jonkheijm, L. Brunsveld *ChemBioChem* **2010**, *11*, 180-183.
- [73] D.-W. Lee, K. M. Park, M. Banerjee, S. H. Ha, T. Lee, K. Suh, S. Paul, H. Jung, J. Kim, N. Selvapalam, S. H. Ryu, K. Kim, *Nat. Chem.* **2010**, *3*, 154.
- [74] C. Hou, J. Li, L. Zhao, W. Zhang, Q. Luo, Z. Dong, J. Xu, J. Liu, *Angew. Chem. Int. Ed.* **2013**, *52*, 5590-5593.
- [75] H. D. Nguyen, D. T. Dang, J. L. J. van Dongen, L. Brunsveld, *Angew. Chem. Int. Ed.* **2010**, *49*, 895-898.
- [76] D. T. Dang, H. D. Nguyen, M. Merckx, L. Brunsveld, *Angew. Chem. Int. Ed.* **2013**, *52*, 2915-2919.
- [77] G. Hettiarachchi, D. Nguyen, J. Wu, D. Lucas, D. Ma, L. Isaacs, V. Briken, *PLOS ONE* **2010**, *5*, e10514.
- [78] Y. Jin Jeon, S.-Y. Kim, Y. Ho Ko, S. Sakamoto, K. Yamaguchi, K. Kim, *Org. Biomol. Chem.* **2005**, *3*, 2122-2125.
- [79] Y. Zhao, D. P. Buck, D. L. Morris, M. H. Pourgholami, A. I. Day, J. G. Collins, *Org. Biomol. Chem.* **2008**, *6*, 4509-4515.
- [80] B. T. Nguyen, E. V. Anslyn, *Coord. Chem. Rev.* **2006**, *250*, 3118-3127.
- [81] A. Hennig, H. Bakirci, W. M. Nau, *Nat. Methods* **2007**, *4*, 629-632.
- [82] F. Biedermann, D. Hathazi, W. M. Nau, *Chem. Commun.* **2015**, *51*, 4977-4980.
- [83] G. Ghale, A. G. Lanctôt, H. T. Kreissl, M. H. Jacob, H. Weingart, M. Winterhalter, W. M. Nau, *Angew. Chem. Int. Ed.* **2014**, *53*, 2762-2765.
- [84] B. Gong, B.-K. Choi, J.-Y. Kim, D. Shetty, Y. H. Ko, N. Selvapalam, N. K. Lee, K. Kim, *J. Am. Chem. Soc.* **2015**, *137*, 8908-8911.
- [85] A. T. Bockus, L. C. Smith, A. G. Grice, O. A. Ali, C. C. Young, W. Mobley, A. Leek, J. L. Roberts, B. Vinciguerra, L. Isaacs, A. R. Urbach, *J. Am. Chem. Soc.* **2016**, *138*, 16549-16552.
- [86] M. Schnurr, J. Sloniec-Myszk, J. Döpfert, L. Schröder, A. Hennig, *Angew. Chem. Int. Ed.* **2015**, *54*, 13444-13447.
- [87] M. Florea, W. M. Nau, *Angew. Chem. Int. Ed.* **2011**, *50*, 9338-9342.
- [88] A. I. Lazar, J. Rohacova, W. M. Nau, *J. Phys. Chem. B* **2017**, *121*, 11390-11398.
- [89] N. Boens, V. Leen, W. Dehaen, *Chem. Soc. Rev.* **2012**, *41*, 1130-1172.

- [90] A. Loudet, K. Burgess, *Chem. Rev.* **2007**, *107*, 4891-4932.
- [91] Y. Urano, D. Asanuma, Y. Hama, Y. Koyama, T. Barrett, M. Kamiya, T. Nagano, T. Watanabe, A. Hasegawa, P. L. Choyke, *Nat. Med.* **2009**, *15*, 104-109.
- [92] J. Neres, P. Bonnet, P. N. Edwards, P. L. Kotian, A. Buschiazzi, P. M. Alzari, R. A. Bryce, K. T. Douglas, *Bioorg. Med. Chem.* **2007**, *15*, 2106-2119.
- [93] B. Wang, F. Yu, P. Li, X. Sun, K. Han, *Dyes Pigm.* **2013**, *96*, 383-390.
- [94] C. Lu, Y. Guo, J. Li, M. Yao, Q. Liao, Z. Xie, X. Li, *Bioorg. Med. Chem.* **2012**, *22*, 7683-7687.
- [95] R. W. Wagner, J. S. Lindsey, *Pure Appl. Chem.* **1996**, *68*, 1373-1380.
- [96] A. F. Abdel-Magid, K. G. Carson, B. D. Harris, C. A. Maryanoff, R. D. Shah, *J. Org. Chem.* **1996**, *61*, 3849-3862.
- [97] T. Zhao, K. Kurpiewska, J. Kalinowska-Tluscik, E. Herdtweck, A. Domling, *Chem. Eur. J.* **2016**, *22*, 3009-3018.
- [98] G. Vives, C. Giansante, R. Bofinger, G. Raffy, A. Del Guerzo, B. Kauffmann, P. Batat, G. Jonusauskas, N. D. McClenaghan, *Chem. Commun.* **2011**, *47*, 10425-10427.
- [99] Y. Zhang, H. M. Fang, X. T. Zhang, S. Wang, G. W. Xing, *ChemistrySelect* **2016**, *1*, 1-6.
- [100] S. Guo, L. Ma, J. Zhao, B. Kucukoz, A. Karatay, M. Hayvali, H. G. Yaglioglu, A. Elmali, *Chem. Sci.* **2014**, *5*, 489-500.
- [101] Y. Volkova, B. Brizet, P. D. Harvey, F. Denat, C. Goze, *Chem. Eur. J.* **2014**, *2014*, 2268-2274.
- [102] W. Wu, J. Zhao, H. Guo, J. Sun, S. Ji, Z. Wang, *Chem. Eur. J.* **2012**, *18*, 1961-1968.
- [103] S. G. Awuah, J. Polreis, V. Biradar, Y. You, *Org. Lett.* **2011**, *13*, 3884-3887.
- [104] W. K. Hagmann, *J. Med. Chem.* **2008**, *51*, 4359-4369.
- [105] D. Rehm, A. Weller, *Isr. J. Chem.* **1970**, *8*, 259-271.
- [106] J. C. Suatoni, R. E. Snyder, R. O. Clark, *Anal. Chem.* **1961**, *33*, 1894-1897.
- [107] R. Lincoln, L. E. Greene, K. Krumova, Z. Ding, G. Cosa, *J. Phys. Chem. A* **2014**, *118*, 10622-10630.
- [108] P. Winget, E. J. Weber, C. J. Cramer, D. G. Truhlar, *Phys. Chem. Chem. Phys.* **2000**, *2*, 1231-1239.
- [109] L. C. T. Shoute, J. P. Mittal, P. Neta, *J. Phys. Chem.* **1996**, *100*, 3016-3019.
- [110] K. C. Gross, P. G. Seybold, *Int. J. Quantum Chem.* **2000**, *80*, 1107-1115.
- [111] C. Würth, M. Grabolle, J. Pauli, M. Spieles, U. Resch-Genger, *Nat. Protoc.* **2013**, *8*, 1535-1550.
- [112] R. Gotor, P. Ashokkumar, M. Hech, K. Keil, K. Rurack, *Anal. Chem.* **2017**, *89*, 8437-8444.
- [113] S. Mula, K. Elliott, A. Harriman, R. Ziessel, *J. Phys. Chem. A* **2010**, *114*, 10515-10522.
- [114] N. J. Turro, V. Ramamurthy, J. Scaiano, *Modern Molecular Photochemistry of Organic Molecules*, 1st ed., University Science Books, Sausalito California **2010**.
- [115] S. Senler, B. Cheng, A. E. Kaifer, *Org. Lett.* **2014**, *16*, 5834-5837.
- [116] H. J. Böhm, D. Banner, S. Bendels, M. Kansy, B. Kuhn, K. Müller, U. Obst-Sander, M. Stahl, *ChemBioChem* **2004**, *5*, 637-643.
- [117] N. Barooah, J. Mohanty, H. Pal, A. C. Bhasikuttan, *P. Natl. A. Sci. India A* **2014**, *84*, 1-17.
- [118] C. P. Carvalho, V. D. Uzunova, J. P. Da Silva, W. M. Nau, U. Pischel, *Chem. Commun.* **2011**, *47*, 8793-8795.

- [119] J. Mohanty, W. M. Nau, *Angew. Chem. Int. Ed.* **2005**, *117*, 3816-3820.
- [120] W. Al-Soufi, B. Reija, M. Novo, S. Felekyan, R. Kühnemuth, C. A. M. Seidel, *J. Am. Chem. Soc.* **2005**, *127*, 8775-8784.
- [121] D. Granadero, J. Bordello, M. J. Pérez-Alvite, M. Novo, W. Al-Soufi, *Int. J. Mol. Sci.* **2010**, *11*, 173.
- [122] S.-C. Cui, T. Tachikawa, M. Fujitsuka, T. Majima, *J. Phys. Chem. C* **2011**, *115*, 1824-1830.
- [123] R. Rigler, Ü. Mets, J. Widengren, P. Kask, *Eur. Biophys. J.* **1993**, *22*, 169-175.
- [124] T. Fischer, P. M. Dietrich, W. E. S. Unger, K. Rurack, *Anal. Chem.* **2016**, *88*, 1210-1217.
- [125] A. Hennig, P. M. Dietrich, F. Hemmann, T. Thiele, H. Borcharding, A. Hoffmann, U. Schedler, C. Jager, U. Resch-Genger, W. E. S. Unger, *Analyst* **2015**, *140*, 1804-1808.
- [126] P. M. Dietrich, A. Hennig, M. Holzweber, T. Thiele, H. Borcharding, A. Lippitz, U. Schedler, U. Resch-Genger, W. E. S. Unger, *J. Phys. Chem. C* **2014**, *118*, 20393-20404.
- [127] J. M. Lehn, *Angew. Chem. Int. Ed.* **1990**, *29*, 1304-1319.
- [128] J.-M. Lehn, *Chem. Soc. Rev.* **2007**, *36*, 151-160.
- [129] X. Ma, H. Tian, *Acc. Chem. Res.* **2014**, *47*, 1971-1981.
- [130] S. Dong, B. Zheng, F. Wang, F. Huang, *Acc. Chem. Res.* **2014**, *47*, 1982-1994.
- [131] P. Wei, X. Yan, F. Huang, *Chem. Soc. Rev.* **2015**, *44*, 815-832.
- [132] D.-S. Guo, Y. Liu, *Chem. Soc. Rev.* **2012**, *41*, 5907-5921.
- [133] S. J. Barrow, S. Kasera, M. J. Rowland, J. del Barrio, O. A. Scherman, *Chem. Rev.* **2015**, *115*, 12320-12406.
- [134] J. Zhang, P. X. Ma, *Nano today* **2010**, *5*, 337-350.
- [135] Y. Kang, K. Guo, B. J. Li, S. Zhang, *Chem. Commun.* **2014**, *50*, 11083-11092.
- [136] A. Harada, Y. Takashima, M. Nakahata, *Acc. Chem. Res.* **2014**, *47*, 2128-2140.
- [137] P. Xing, H. Chen, M. Ma, X. Xu, A. Hao, Y. Zhao, *Nanoscale* **2016**, *8*, 1892-1896.
- [138] I. Ghosh, W. M. Nau, *Adv. Drug Delivery Rev.* **2012**, *64*, 764-783.
- [139] M. Lee, S. J. Lee, L. H. Jiang, *J. Am. Chem. Soc.* **2004**, *126*, 12724-12725.
- [140] C. Wang, Z. Wang, X. Zhang, *Acc. Chem. Res.* **2012**, *45*, 608-618.
- [141] X. Zhang, C. Wang, *Chem. Soc. Rev.* **2011**, *40*, 94-101.
- [142] T. Shimizu, M. Masuda, H. Minamikawa, *Chem. Rev.* **2005**, *105*, 1401-1443.
- [143] K. I. Assaf, A. Hennig, S. Peng, D.-S. Guo, D. Gabel, W. M. Nau, *Chem. Commun.* **2017**, *53*, 4616-4619.
- [144] X. Wu, Y.-M. Zhang, Y. Liu, *RSC Adv.* **2016**, *6*, 99729-99734.
- [145] G. Yu, K. Jie, F. Huang, *Chem. Rev.* **2015**, *115*, 7240-7303.
- [146] H. Zhang, F. Xin, W. An, A. Hao, X. Wang, X. Zhao, Z. Liu, L. Sun, *Colloids Surf., A* **2010**, *363*, 78-85.
- [147] W. M. Nau, M. Florea, K. I. Assaf, *Isr. J. Chem.* **2011**, *51*, 559-577.
- [148] D. Shetty, J. K. Khedkar, K. M. Park, K. Kim, *Chem. Soc. Rev.* **2015**, *44*, 8747-8761.
- [149] A. I. Lazar, F. Biedermann, K. R. Mustafina, K. I. Assaf, A. Hennig, W. M. Nau, *J. Am. Chem. Soc.* **2016**, *138*, 13022-13029.
- [150] J. Hu, P. Wang, Y. Lin, J. Zhang, M. Smith, P. J. Pellechia, S. Yang, B. Song, Q. Wang, *Chem. Eur. J.* **2014**, *20*, 7603-7607.

- [151] J. Hu, L. Gao, Y. Zhu, P. Wang, Y. Lin, Z. Sun, S. Yang, Q. Wang, *Chem. Eur. J.* **2017**, *23*, 1422-1426.
- [152] Y. X. Wang, Y. M. Zhang, Y. Liu, *J. Am. Chem. Soc.* **2015**, *137*, 4543-4549.
- [153] G. H. Aryal, K. I. Assaf, K. W. Hunter, W. M. Nau, L. Huang, *Chem. Commun.* **2017**, *53*, 9242-9245.
- [154] B. T. Nguyen, E. V. Anslyn, *Coord. Chem. Rev.* **2006**, *250*, 3118-3127.
- [155] K. I. Assaf, O. Suckova, N. Al Danaf, V. von Glasenapp, D. Gabel, W. M. Nau, *Org. Lett.* **2016**, *18*, 932-935.
- [156] M. Sayed, F. Biedermann, V. D. Uzunova, K. I. Assaf, A. C. Bhasikuttan, H. Pal, W. M. Nau, J. Mohanty, *Chem. Eur. J.* **2015**, *21*, 691-696.
- [157] F. Lin, T.-G. Zhan, T.-Y. Zhou, K.-D. Zhang, G.-Y. Li, J. Wu, X. Zhao, *Chem. Commun.* **2014**, *50*, 7982-7985.
- [158] F. Biedermann, H.-J. Schneider, *Chem. Rev.* **2016**, *116*, 5216-5300.
- [159] K. A. Connors, *Binding Constants: The Measurement of Molecular Complex Stability*, John Wiley & Sons, New York, Chichester, Brisbane, Toronto, Singapore, **1987**.
- [160] K. Hirose, *J. Inclusion Phenom. Macrocyclic Chem.* **2001**, *39*, 193-209.
- [161] I. Jarmoskaite, I. AlSadhan, P. P. Vaidyanathan, D. Herschlag, *eLife* **2020**, *9*, e57264.
- [162] M. R. Duff, Jr., J. Grubbs, E. E. Howell, *J Vis Exp* **2011**, 2796.
- [163] P. Montes-Navajas, A. Corma, H. Garcia, *ChemPhysChem* **2008**, *9*, 713-720.
- [164] G. Ghale, N. Kuhnert, W. M. Nau, *Nat. Prod. Commun.* **2012**, *7*, 343-348.
- [165] M. Shaikh, J. Mohanty, P. K. Singh, W. M. Nau, H. Pal, *Photochem. Photobiol. Sci.* **2008**, *7*, 408-414.
- [166] A. Hennig, A. Hoffmann, H. Borcherdig, T. Thiele, U. Schedler, U. Resch-Genger, *Chem. Commun.* **2011**, *47*, 7842-7844.
- [167] W. A. Freeman, W. L. Mock, N. Y. Shih, *J. Am. Chem. Soc.* **1981**, *103*, 7367-7368.
- [168] A. I. Day, R. J. Blanch, A. P. Arnold, S. Lorenzo, G. R. Lewis, I. Dance, *Angew. Chem. Int. Ed.* **2002**, *41*, 275-277.
- [169] A. Day, A. P. Arnold, R. J. Blanch, B. Snushall, *J. Org. Chem.* **2001**, *66*, 8094-8100.
- [170] W. M. Nau, G. Ghale, A. Hennig, H. Bakirci, D. M. Bailey, *J. Am. Chem. Soc.* **2009**, *131*, 11558-11570.
- [171] F. Biedermann, W. M. Nau, *Angew. Chem. Int. Ed.* **2014**, *53*, 5694-5699.
- [172] L. Cao, L. Isaacs, *Supramol. Chem.* **2014**, *26*, 251-258.
- [173] S. Zhang, L. Grimm, Z. Miskolczy, L. Biczók, F. Biedermann, W. M. Nau, *Chem. Commun.* **2019**, *55*, 14131-14134.
- [174] H. Tang, D. Fuentealba, Y. H. Ko, N. Selvapalam, K. Kim, C. Bohne, *J. Am. Chem. Soc.* **2011**, *133*, 20623-20633.
- [175] M. V. Rekharsky, T. Mori, C. Yang, Y. H. Ko, N. Selvapalam, H. Kim, D. Sobransingh, A. E. Kaifer, S. Liu, L. Isaacs, W. Chen, S. Moghaddam, M. K. Gilson, K. Kim, Y. Inoue, *Proc. Natl. Acad. Sci. U.S.A.* **2007**, *104*, 20737-20742.
- [176] D. Ma, P. Y. Zavalij, L. Isaacs, *J. Org. Chem.* **2010**, *75*, 4786-4795.
- [177] Y.-C. Liu, W. M. Nau, A. Hennig, *Chem. Commun.* **2019**, *55*, 14123-14126.
- [178] C. Marquez, W. M. Nau, *Angew. Chem. Int. Ed.* **2001**, *40*, 3155-3160.
- [179] A. E. Kaifer, W. Li, S. Yi, *Isr. J. Chem.* **2011**, *51*, 496-505.
- [180] J. Murray, J. Sim, K. Oh, G. Sung, A. Lee, A. Shrinidhi, A. Thirunarayanan, D. Shetty, K. Kim, *Angew. Chem. Int. Ed.* **2017**, *56*, 2395-2398.

- [181] X. Zhou, X. Su, P. Pathak, R. Vik, B. Vinciguerra, L. Isaacs, J. Jayawickramarajah, *J. Am. Chem. Soc.* **2017**, *139*, 13916-13921.
- [182] S.-R. Wang, J.-Q. Wang, G.-H. Xu, L. Wei, B.-S. Fu, L.-Y. Wu, Y.-Y. Song, X.-R. Yang, C. Li, S.-M. Liu, X. Zhou, *Adv. Sci.* **2018**, *5*, 1800231.
- [183] D.-W. Lee, K. M. Park, M. Banerjee, S. H. Ha, T. Lee, K. Suh, S. Paul, H. Jung, J. Kim, N. Selvapalam, S. H. Ryu, K. Kim, *Nat. Chem.* **2011**, *3*, 154-159.
- [184] Z. Miskolczy, L. Biczók, *J. Phys. Chem. B* **2014**, *118*, 2499-2505.
- [185] A. Hennig, H. Borchering, C. Jaeger, S. Hatami, C. Würth, A. Hoffmann, K. Hoffmann, T. Thiele, U. Schedler, U. Resch-Genger, *J. Am. Chem. Soc.* **2012**, *134*, 8268-8276.
- [186] M. A. Alnajjar, J. Bartelmeß, R. Hein, P. Ashokkumar, M. Nilam, W. M. Nau, K. Rurack, A. Hennig, *Beilstein J. Org. Chem.* **2018**, *14*, 1961-1971.
- [187] J. Liu, N. Jiang, J. Ma, X. Du, *Eur. J. Org. Chem.* **2009**, *2009*, 4899-4899.
- [188] M. Sayed, S. Jha, H. Pal, *Phys. Chem. Chem. Phys.* **2017**, *19*, 24166-24178.
- [189] Z. Miskolczy, L. Biczók, M. Megyesi, I. Jablonkai, *J. Phys. Chem. B* **2009**, *113*, 1645-1651.
- [190] D. Bhowmik, M. Hossain, F. Buzzetti, R. D'Auria, P. Lombardi, G. S. Kumar, *J. Phys. Chem. B* **2012**, *116*, 2314-2324.
- [191] G.-Q. Wang, L. Guo, L.-M. Du, Y.-L. Fu, *Microchem. J.* **2013**, *110*, 285-291.
- [192] A. D. St-Jacques, I. W. Wyman, D. H. Macartney, *Chem. Commun.* **2008**, *40*, 4936-4938.
- [193] N. Dong, J. He, T. Li, A. Peralta, M. R. Avei, M. Ma, A. E. Kaifer, *J. Org. Chem.* **2018**, *83*, 5467-5473.
- [194] W. S. Jeon, K. Moon, S. H. Park, H. Chun, Y. H. Ko, J. Y. Lee, E. S. Lee, S. Samal, N. Selvapalam, M. V. Rekharsky, V. Sindelar, D. Sobransingh, Y. Inoue, A. E. Kaifer, K. Kim, *J. Am. Chem. Soc.* **2005**, *127*, 12984-12989.
- [195] T. D. W. Claridge, S. G. Davies, M. E. C. Polywka, P. M. Roberts, A. J. Russell, E. D. Savory, A. D. Smith, *Org. Lett.* **2008**, *10*, 5433-5436.
- [196] Z.-Z. Gao, J.-L. Kan, L.-X. Chen, D. Bai, H.-Y. Wang, Z. Tao, X. Xiao, *ACS Omega* **2017**, *2*, 5633-5640.
- [197] I. W. Wyman, D. H. Macartney, *Org. Biomol. Chem.* **2010**, *8*, 253-260.
- [198] C. Marquez, F. Huang, W. M. Nau, *IEEE Trans. Nanobiosci.* **2004**, *3*, 39-45.
- [199] A. Hennig, W. M. Nau, *Front. Chem.* **2020**, *8*.
- [200] W. M. Nau, M. Florea, K. I. Assaf, *Isr. J. Chem.* **2011**, *51*, 559-577.
- [201] J. Hostaš, D. Sigwalt, M. Šekutor, H. Ajani, M. Dubecký, J. Řezáč, P. Y. Zavalij, L. Cao, C. Wohlschlager, K. Mlinarić-Majerski, L. Isaacs, R. Glaser, P. Hobza, *Chem. Eur. J.* **2016**, *22*, 17226-17238.
- [202] D. Sobransingh, A. E. Kaifer, *Chem. Commun.* **2005**, 5071-5073.
- [203] P. Zhou, J. Liu, S. Yang, J. Chen, K. Han, G. He, *Phys. Chem. Chem. Phys.* **2012**, *14*, 15191-15198.
- [204] M. Kucki, T. Fuhrmann-Lieker, *J. Royal Soc. Interface* **2012**, *9*, 727-733.
- [205] T. Kobayashi, Y. Urano, M. Kamiya, T. Ueno, H. Kojima, T. Nagano, *J. Am. Chem. Soc.* **2007**, *129*, 6696-6697.
- [206] Y. Urano, M. Kamiya, K. Kanda, T. Ueno, K. Hirose, T. Nagano, *J. Am. Chem. Soc.* **2005**, *127*, 4888-4894.
- [207] X. Peng, F. Song, E. Lu, Y. Wang, W. Zhou, J. Fan, Y. Gao, *J. Am. Chem. Soc.* **2005**, *127*, 4170-4171.
- [208] S. Peng, A. Barba-Bon, Y.-C. Pan, W. M. Nau, D.-S. Guo, A. Hennig, *Angew. Chem. Int. Ed.* **2017**, *129*, 15948-15951.
- [209] F. Biedermann, G. Ghale, A. Hennig, W. M. Nau, *Commun. Biol* **2020**, *3*, 383.

- [210] M. Nilam, S. Collin, S. Karmacharya, A. Hennig, W. M. Nau, *ACS Sensors* **2021**, *6*, 175-182.
- [211] J. Han, A. Schmidt, T. Zhang, H. Permentier, G. M. M. Groothuis, R. Bischoff, F. E. Kühn, P. Horvatovich, A. Casini, *Chem. Commun.* **2017**, *53*, 1405-1408.
- [212] A. Chilkoti, P. S. Stayton, *J. Am. Chem. Soc.* **1995**, *117*, 10622-10628.
- [213] A. T. Marttila, O. H. Laitinen, K. J. Airenne, T. Kulik, E. A. Bayer, M. Wilchek, M. S. Kulomaa, *FEBS Letters* **2000**, *467*, 31-36.
- [214] L. Cao, M. Sekutor, P. Y. Zavalij, K. Mlinaric-Majerski, R. Glaser, L. Isaacs, *Angew. Chem. Int. Ed.* **2014**, *53*, 988-993.
- [215] C. Marquez, H. Fang, W. M. Nau, *IEEE Trans. Nanobiosci.* **2004**, *3*, 39-45.
- [216] U. Resch-Genger, D. Pfeifer, C. Monte, W. Pilz, A. Hoffmann, M. Spieles, K. Rurack, J. Hollandt, D. Taubert, B. Schönenberger, P. Nording, *J. Fluoresc.* **2005**, *15*, 315-336.
- [217] U. Resch-Genger, K. Hoffmann, W. Nietfeld, A. Engel, J. Neukammer, R. Nitschke, B. Ebert, R. Macdonald, *J. Fluoresc.* **2005**, *15*, 337-362.
- [218] K. Hoffmann, U. Resch-Genger, R. Mix, J. F. Friedrich, *J. Fluoresc.* **2006**, *16*, 441-448.
- [219] U. Resch-Genger, K. Hoffmann, A. Hoffmann, *Ann. N. Y. Acad. Sci.* **2008**, *1130*, 35-43.
- [220] C. Monte, W. Pilz, U. Resch-Genger, *Linking fluorescence spectroscopy to the scale of spectral sensitivity: the BAM reference fluorometer*, Vol. 5880, SPIE, **2005**.
- [221] J. E. Bertie, Z. Lan, *J. Phys. Chem. B* **1997**, *101*, 4111-4119.
- [222] C. Marquez, F. Huang, W. M. Nau, *IEEE Trans. Nanobiosci.* **2004**, *3*, 39-45.
- [223] R. R. Hudgins, F. Huang, G. Gramlich, W. M. Nau, *J. Am. Chem. Soc.* **2002**, *124*, 556-564.
- [224] P. K. Glasoe, F. A. Long, *J. Phys. Chem.* **1960**, *64*, 188-190.
- [225] P. R. Bevington, & Robinson, D. K., *Data reduction and error analysis for the physical sciences*, New York: McGraw-Hill., **2003**.

Appendices

Appendices

A.1 Supporting Information for Chapter 2

A.1.1 Materials and Instrumentation

Materials. Reagents and compounds for synthesis, buffer preparation and analytical measurements were from Sigma-Aldrich (Steinheim, Germany). Deuterated solvents for NMR measurements were from Deutero (Kastellaun, Germany), Sigma-Aldrich (Steinheim, Germany) or Merck (Mannheim, Germany). Cucurbit[7]uril (CB7) was from Strem Chemicals Int. (Massachusetts, United States) or synthesized as previously reported.^[17,215] Buffers were prepared from solid citric acid monohydrate and the pH was adjusted by addition of NaOH.

Instrumentation. NMR spectra were recorded on a JEOL ECX 400 spectrometer and are reported as chemical shifts (δ) in ppm relative to TMS ($\delta = 0$) or residual protonated solvent signals as internal standard. Spin multiplicities are reported as singlet (s), doublet (d), triplet (t), quartet (q), and quintet (quint) with coupling constants (J) given in Hz, or as multiplets (m). FTIR spectra were recorded on a Bruker IR Spectrometer VECTOR 33 and are reported as wavenumbers in cm^{-1} with band intensities indicated as s (strong), m (medium), w (weak), and br (broad). ESI-HRMS was performed on a Bruker HCT ultra mass spectrometer, and spectra are reported as mass-per-charge ratio m/z . Absorbance measurements were performed with a Varian Cary 4000 spectrophotometer. Fluorescence was measured either with a Varian Eclipse or a Jasco FP-8500 spectrofluorometer equipped with temperature controllers. Correction curves for the fluorescence measurements were generated with a dye kit certified by the Federal Institute for Materials Research and Testing (BAM, Germany).^[216-220] All spectroscopic measurements were performed in 3.5 ml quartz glass cuvettes from Hellma Analytics (Müllheim, Germany). pH values were measured with a Weilheim 3110 pH meter and the pH values in ACN/water mixtures are reported as uncorrected, apparent pH values. Fluorescence correlation spectroscopy (FCS) was performed with an Insight Cell 3D microscope from Evotec Technologies (Hamburg, Germany, now Perkin Elmer), equipped with a 543-nm continuous-wave HeNe and a 635-nm pulsed diode laser (~ 80 -ps pulse width; PicoQuant, Berlin, Germany), and a 40fold water immersion objective

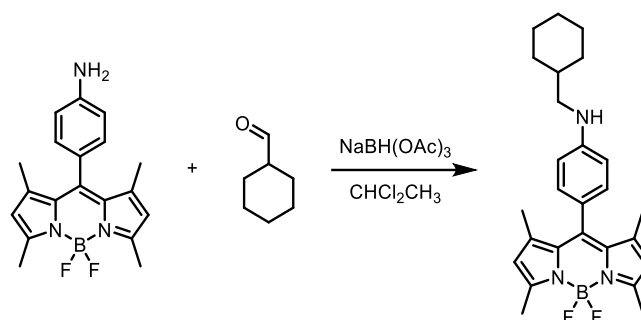
(UApo340 40×, NA 1.15, Olympus, Tokyo, Japan), and avalanche photodiode detectors (SPCM-AQR-13-FC; Perkin Elmer Optoelectronics, Fremont, CA). Fluorescence excitation was performed with linear polarized light, and the laser power was adjusted to 5–20 mW. Fluorescence microscopy images were captured by a Zeiss Axiovert 200 with a BP 455-495/LP 515 filter set through an Evolution QEi Media Cybernetics camera by using a 40x objective, and processed with the software imageJ V1.48 (<https://imagej.nih.gov/ij/index.html>).

A.1.2 Abbreviations

ACN: acetonitrile, AMADA: 1-(aminomethyl)adamantane, BODIPY: 4,4-difluoro-4-bora-3a,4a-diaza-s-indacene, CB7: cucurbit[7]uril, DCM: dichloromethane, DCE: dichloroethane, DDQ: 2,3-dichloro-5,6-dicyano-*p*-benzoquinone, DMF: dimethylformamide, EtOAc: ethyl acetate, EtOH: ethanol, ESI-HRMS: electrospray ionization high resolution mass spectrometry, Et₂O: diethyl ether, ESI: electrospray ionization, DiPEA: Diisopropylethylamine, HOMO: highest occupied molecular orbital, FT-ICR: Fourier transform ion cyclotron resonance, FTIR: Fourier transform infrared spectroscopy, HRMS: high resolution mass spectrometry, IR: infrared spectroscopy, MeOH: methanol, MS: mass spectrometry, NIR: near-infrared, NMR: nuclear magnetic resonance spectroscopy, PE: petroleum ether 40-60 °C, PET: photoinduced electron transfer, TEA: triethylamine, TFA: trifluoroacetic acid, TMS: tetramethylsilane.

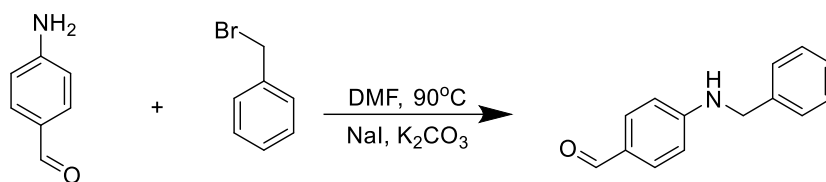
A.1.3 Synthesis

A.1.3.1 Synthesis of BDP-cyH

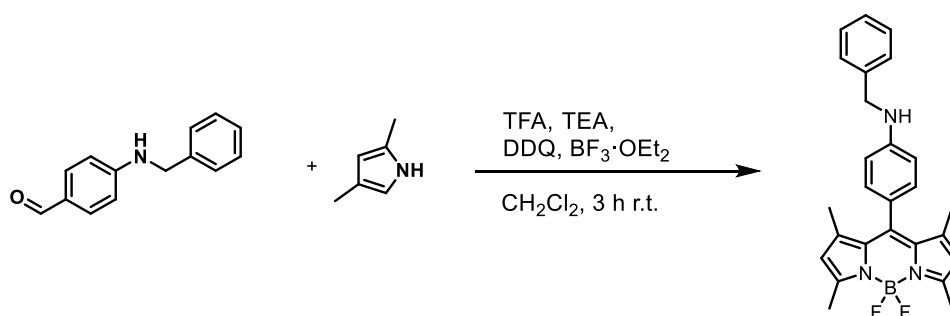


BDP-CyH. 69 mg Me₄BDP-NH₂ (0.203 mmol) and 27 μ L cyclohexanecarbaldehyde (0.223 mmol) were dissolved in 5 mL 1,2-dichloroethane. Then, 60 mg NaBH(OAc)₃ (0.283 mmol) and 12 μ L AcOH (0.210 mmol) were added and the mixture was reacted for 2 days (48 h) at room temperature under N₂. Afterwards, 1 mL of 0.1 M NaOH and then 45 mL Et₂O were added. The organic phase was washed twice with 20 mL brine and dried over anhydrous Na₂SO₄. Removal of diethylether by rotary evaporation and purification on a silica column (PE/EtOAc 10:1) gave 38 mg (43%) BDP-cyH as an orange-red product. *R*_f = 0.79 with PE/EtOAc (2:1). M.p 217 °C; ¹H NMR 400 MHz, CDCl₃ δ (ppm) = 6.99 (d, *J* = 6.2 Hz, 2H, Ar-H), 6.68 (d, *J* = 5.9 Hz, 2H, Ar-H), 5.96 (s, 2H, Pyr-H), 2.99 (d, *J* = 6.6 Hz, 2H, Cy-CH₂-NH), 2.54 (s, 6H, Pyr-CH₃), 1.88-1.67 (m, 5H, cyH), 1.43 (s, 6H, Pyr-CH₃), 1.35- 0.95 (m, 6H, cyH). ¹³C NMR (100 MHz, CDCl₃) δ = 154.9, 149.1, 143.4, 143.2, 132.3, 129.0, 123.2, 121.0, 113.2, 50.8, 45.0, 37.8, 31.4, 29.8, 26.7, 26.1, 14.8, 14.7. ¹⁹F NMR (376 MHz, CDCl₃) δ = -146.0. ATR-IR cm⁻¹ 3383 (w), 2924 (m), 2852 (w), 1741 (w), 1613 (w). MS (ESI, DCM): 436.2731 m/z ([M+H]⁺).

A.1.3.2 Synthesis of BDP-Bnz



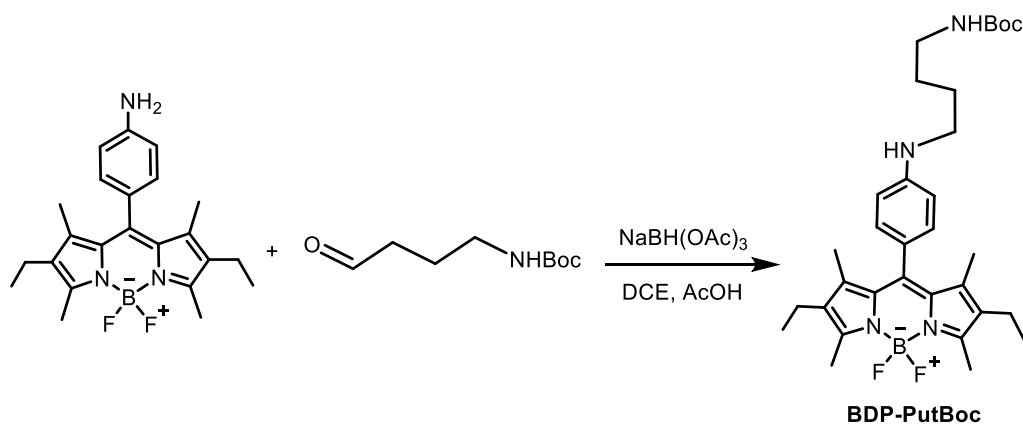
***p*-(benzylamino)benzaldehyde.** 200 mg (1.65 mmol) *p*-amino benzaldehyde was dissolved in 40 ml of anhydrous dimethylformamide (DMF). 1.14 g (8.25 mmol) NaI and 1.14 g (8.25 mmol) K₂CO₃ was added and the mixture was stirred for 1 h at ambient temperature. 197 mg (1.65 mmol) (bromomethyl)benzene was added dropwise within 15 min and the reaction was subsequently heated to 90 °C for 3 d. After that, the reaction mixture allowed to cool down to room temperature and 50 ml water were added. 40 ml DCM added and the organic phase was separated and subsequently washed 2 times with 50 ml saturated brine solution. The combined organic phases dried with MgSO₄ and the solvent removed by rotary evaporation and purified by column chromatography using a solvent gradient from PE/EtOAc 50:1 to 1:2 (v/v) to afford 170 mg (48%) *p*-(benzylamino)benzaldehyde were obtained as a yellow solid. *R*_f = 0.51 with PE/EtOAc (2:1). Mp: 125 °C; ¹H NMR (400 MHz, acetone-d₆): δ (ppm) = 9.67 (s, 1H, COH), 7.64 (d, *J* = 8.4 Hz, 2H, Ar-H), 6.77 (d, *J* = 8.4 Hz, 2H, Ar-H), 7.52-7.11 (m, 5H, Ar-H), 4.49 (2H, Ar-CH₂-NH). ¹³C NMR (100 MHz, acetone-d₆) δ (ppm) = 190.0, 154.9, 140.1, 132.6, 129.5, 128.2, 127.3, 112.8, 47.4; MS (ESI⁺, ACN: 234 m/z ([M+Na]⁺).



BDP-Bnz. 100 mg (0.47 mmol) *p*-(benzylamino)benzaldehyde were dissolved in 10 ml DCM and 97 μl 2,4-dimethylpyrrole (0.95 mmol) and 5 μl TFA were added to the reaction. After 50 min reaction at room temperature, 0.107 g (0.47 mmol) DDQ were added, the reaction mixture was stirred for another 50 min and 2 ml (14.35 mmol) TEA were added. After 30 min, 2 ml (16.2 mmol) boron trifluoride diethyl etherate were added and the reaction mixture was stirred for 3 hours. Evaporation of the solvent gave a dark-purple solid, which was further purified by column

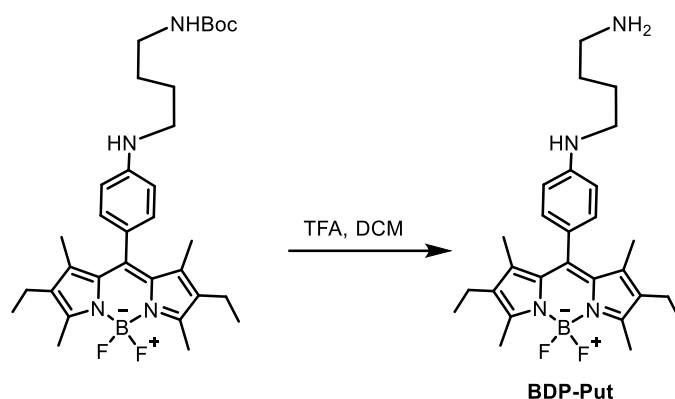
chromatography using a gradient from PE/EtOAc 4:1 to 1:1 to afford 35 mg (17%) BDP-Bnz as a purple solid. $R_f = 0.3$ with PE/EtOAc (2:1). Mp: 227 °C; ^1H NMR 400 MHz, acetone- d_6 δ (ppm) = 7.43-7.20 (m, 5H, Ar-H), 7.04 (d, $J = 8.3$ Hz, 2H, Ar-H) 6.86 (d, $J = 8.3$ Hz, 2H, Ar-H), 6.08 (s, 2H, Pyr-H), 4.44 (s, 2H, Ar- CH_2 -NH), 2.84 (s, 6H, Pyr- CH_3), 1.52 (s, 6H, Pyr- CH_3). ^{13}C NMR (100 MHz, CDCl_3) δ = 155.0, 143.3, 142.8, 132.2, 129.1, 128.8, 127.7, 121.1, 113.9, 100.0, 48.6, 14.8. ^{19}F NMR (376 MHz, CDCl_3) δ = -146.2. ATR-IR cm^{-1} 3418 (m), 2924 (w), 2852 (w), 1738 (w), 1613 (s). MS (ESI, DCM): 430.30 m/z ($[\text{M}+\text{H}]^+$).

A.3.2.3 Synthesis of BDP-Put



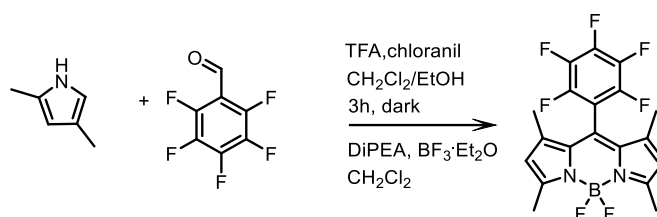
BDP-PutBoc. To a stirred solution of $\text{Me}_4\text{Et}_2\text{BDP-NH}_2$ (100 mg, 0.253 mmol) in 1,2-dichloroethane (10 mL), 4-[*N*-(*tert*-butoxycarbonyl)]amino-1-butanal (62 mg, 0.329 mmol)^[97] and AcOH (25 μL , 0.430 mmol) were added under an argon atmosphere. To this mixture, $\text{NaBH}(\text{OAc})_3$ (70 mg, 0.329 mmol) was added in small portions over a 10 min period and stirring continued for 24 hrs in Ar atmosphere. After completion, the reaction was quenched by the slow addition of sat. NaHCO_3 (10 mL) and extracted three times with ethyl acetate (3×25 mL). The combined organic layers were washed with H_2O and brine (30 mL each), dried over anhydrous Na_2SO_4 , filtered, and evaporated under reduced pressure. Purification on silica column (DCM/MeOH 95:5) gave 89 mg (62 %) of BDP-PutBoc. ^1H NMR (400 MHz, $\text{DMSO}-d_6$): δ (ppm) 7.07 (d, $J = 8.8$ Hz, 2H, Ar-H), 6.78 (d, $J = 8.6$ Hz, 2H, Ar-H), 3.15-3.28 (m, 4H, $\text{PhNH-CH}_2\text{-CH}_2$ & $\text{CH}_2\text{-CH}_2\text{-NHBoc}$), 2.38 (q, $J = 7.2$ Hz, 4H, Pyr- $\text{CH}_2\text{-CH}_3$), 2.32 (s, 6H, Pyr- CH_3), 1.75-1.59 (m, 4H, $\text{NHCH}_2\text{-CH}_2\text{-CH}_2\text{-CH}_2$), 1.56 (s, 6H, Pyr- CH_3), 1.42 (s, 9H, Boc- CH_3), 1.04 (t, $J = 7.4$ Hz, 6H, Pyr- $\text{CH}_2\text{-CH}_3$). ^{13}C NMR (100 MHz, $\text{DMSO}-d_6$): δ (ppm) 155.4, 152.5, 146.7, 141.1, 138.6, 132.8, 131.2, 130.0, 122.8, 112.3, 79.7, 53.2, 36.1, 28.6, 26.2, 25.4,

17.1, 14.6, 12.4, 11.4. HR-MS (ESI⁺): m/z calculated for C₃₂H₄₆BF₂N₄O₂ [M+H]⁺: 567.3682, found 567.3678.

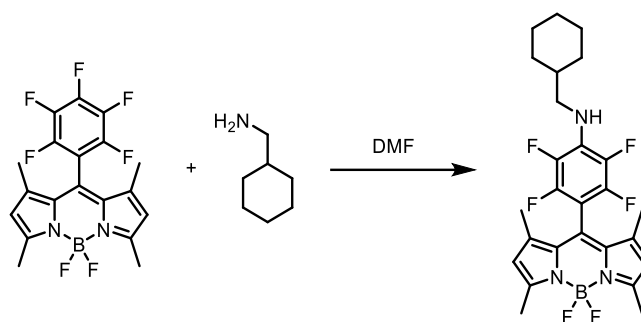


BDP-Put. To a solution of BDP-PutBoc (80 mg, 0.141 mmol) in dichloromethane (2 mL), TFA (2 mL) was added and stirred for 3 h. The solvent was removed from the reaction mixture by rotary evaporation. Now methanol is added and evaporation continued for 3 more times to remove traces of TFA. Purification on neutral alumina column (DCM/MeOH 90:10) gave 58 mg (88 %) of BDP-Put. ¹H NMR (400 MHz, DMSO-d₆): δ (ppm) 7.08 (d, J = 8.8 Hz, 2H, Ar-H), 6.79 (d, J = 8.4 Hz, 2H, Ar-H), 3.19 (t, J = 6.8 Hz, 2H, PhNH-CH₂-CH₂), 2.78 (t, J = 6.8 Hz, 2H, CH₂-CH₂-NH₂), 2.40 (q, J = 7.2 Hz, 4H, Pyr-CH₂-CH₃), 2.33 (s, 6H, Pyr-CH₃), 1.69-1.62 (m, 4H, NHCH₂-CH₂-CH₂-CH₂), 1.58 (s, 6H, Pyr-CH₃), 1.05 (t, J = 7.6 Hz, 6H, Pyr-CH₂-CH₃). ¹³C NMR (100 MHz, DMSO-d₆) δ = 152.7, 146.9, 140.9, 138.7, 132.8, 131.0, 130.2, 122.9, 112.4, 53.1, 41.9, 25.4, 25.1, 17.0, 14.6, 12.4, 11.4. HR-MS (ESI⁺): m/z calculated for C₂₇H₃₈BF₂N₄ [M+H]⁺: 467.3158, found 467.3160.

A.1.3.3 Synthesis of BDPF4-cyH

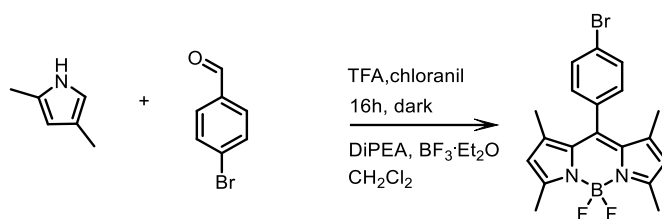


BDP-F5. 0.9 mg (9.4 mmol) of 2,4-dimethylpyrrole and 0.87 mg (4.7 mmol) of pentafluorobenzaldehyde were dissolved in a mixture 280 mL of dichloromethane and 20 mL of absolute ethanol and deoxygenated with Ar. Some drops of trifluoroacetic acid were added and the reaction mixture was stirred for 3h in the dark. 1125 mg (4.65 mmol) of chloranil were added, followed by stirring for 1h. The solvents were removed and the solid was dissolved in 200 mL of dichloromethane. Then, 4.9 mL of diisopropylethylamine were added and after 5 min of stirring, 5.2 mL of boron trifluoride diethyletherate were added, followed by stirring for 30 min. The reaction mixture was filtered through a pad of silica, eluted with dichloromethane and the solvents were evaporated to dryness. The crude product was purified on a silica column (PE/DCM 2:1 with increasing amounts of DCM). After recrystallization from DCM layered with methanol and washing of the crystals with a small amount of methanol, 561 mg (1,35 mmol, 19%) of a crystalline red solid were recovered. ^1H NMR 400 MHz, DMSO- d_6 δ (ppm) = 6.30 (s, 2H, Pyr-H), 2.48 (s, 6H, Pyr- CH_3), 1.64 (s, 6H, Pyr- CH_3). ^{13}C NMR (100 MHz, DMSO- d_6) δ = 157.5, 144.4, 142.1, 130.1, 122.5, 14.3, 13.2. HRMS-ESI: m/z: calculated for $\text{C}_{19}\text{H}_{15}\text{BF}_7\text{N}_2^+$: 415.1211 $[\text{M}+\text{H}]^+$, found: 415.1253.

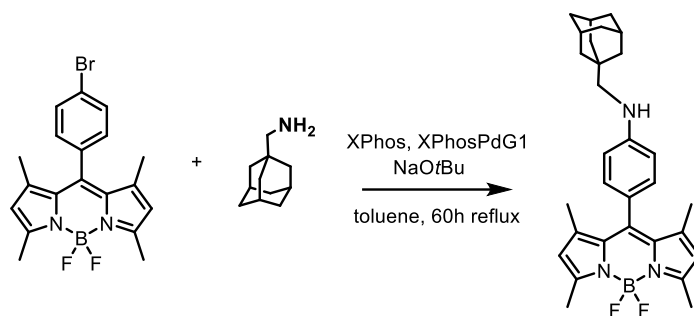


BDPF4-Cyh. 50 mg (0.12 mmol) of BDP-F₅ were dissolved in 5 mL of dimethylformamide and 130 mL (113 mg, 1.0 mmol) of cyclohexylmethanamine were added. After stirring for 3h at RT, the reaction mixture was extracted with water/diethylether and the organic phase was dried over MgSO₄. After removal of the solvents, the crude product was purified on a column of neutral alumina (PE/DCM 3:1), eluting the product as second yellow-colored band (after some residual starting material). Yield: 39 mg (0.077 mmol, 64%) of a red solid. ¹H NMR 400 MHz, DMSO-d₆ δ (ppm) = 6.27 (s, 2H, Pyr-H), 3.03 (t, *J* = 6.6 Hz, 2H, Cy-CH₂-NH), 2.46 (s, 6H, Pyr-CH₃), 1.70-1.60 (m, 5H, cyH), 1.66 (s, 6H, Pyr-CH₃), 1.29- 1.01 (m, 6H, cyH). ¹³C NMR (100 MHz, DMSO-d₆) δ = 156.5, 141.9, 131.1, 124.9, 122.0, 49.5, 38.2, 30.1, 26.0, 25.3, 14.3, 12.9. HRMS-ESI: *m/z*:calcd for C₂₆H₂₉BF₆N₃⁺: 508,2353 [M + H]⁺, found: 508,2356.

A.1.3.4 Synthesis of BDP-AMADA



BDP-Br. 0.9 mg (9.4 mmol) of 2,4-dimethylpyrrole and 0.87 mg (4.7 mmol) of 4-bromobenzaldehyde were dissolved in 200 mL of dichloromethane and deoxygenated with Ar. Some drops of trifluoroacetic acid were added and the reaction mixture was stirred for 16h in the dark. 1125 mg (4.65 mmol) of chloranil were added, followed by stirring for 2h. Then, 4.9 mL of diisopropylethylamine were added and after 5 min of stirring, 5.2 mL of boron trifluoride diethyletherate were added, followed by stirring for 2h. The reaction mixture was filtered through a pad of silica, eluted with dichloromethane and the solvents were evaporated to dryness. The crude product was purified on a silica column (PE/EtOAc 9:1) yielding 335 mg (0,83 mmol, 18%) of a red solid. ¹H NMR 400 MHz, DMSO-d₆ δ (ppm) = 7.77 (d, J = 8.6 Hz, 2H, Ar-H), 7.36 (d, J = 8.6 Hz, 2H, Ar-H), 6.20 (s, 2H, Pyr-H), 2.45 (s, 6H, Pyr-CH₃), 1.38 (s, 6H, Pyr-CH₃). ¹³C NMR (100 MHz, DMSO-d₆) δ = 155.1, 142.5, 140.3, 133.1, 132.2, 130.4, 130.1, 122.5, 121.4, 14.1, 14.0. HRMS-ESI: m/z:calcd for C₁₉H₁₉BBBrF₂N₂⁺: 403.0787 [M + H]⁺, found: 403.0793.



BDP-AMADA. Under an argon atmosphere, 60.2 mg (0.15 mmol) of BDP-Br, 16.2 mg (0.034 mmol) of 2-dicyclohexylphosphino-2',4',6'-triisopropylbiphenyl (XPhos), 23.6 mg (0.032 mmol) of (2-dicyclohexylphosphino-2',4',6'-triisopropyl-1,1'-biphenyl)[2-(2-aminoethyl)phenyl] palladium(II) chloride (XPhos Pd G1) and 29 mg (0.30 mmol) of sodium *tert*-butoxide were added to 6 mL of dry toluene. Subsequently, 28 mL (26 mg, 0.23 mmol) of 1-adamantanemethylamine were added. The reaction mixture was heated under reflux for 40h and after cooling to RT filtered through a pad of silica. The crude product was eluted with DCM and evaporated to dryness. After purification on a neutral alumina column (PE/DCM 3:1 with increasing amounts of DCM), the product was eluted as second, non-fluorescent yellow-colored fraction (after some residual BDP-Br starting material) in 12% yield (9 mg, 0.018 mmol). ^1H NMR 400 MHz, CDCl_3 δ (ppm) = 7.32 (d, J = 8.8 Hz, 2H, Ar-H), 7.21 (d, J = 8.8 Hz, 2H, Ar-H), 5.99 (s, 2H, Pyr-H), 2.58-2.54 (m, 8H, Cy- CH_2 -NH, Pyr- CH_3), 1.78-1.60 (m, 3H, ADAMA), 1.51 (s, 6H, Pyr- CH_3 ; (m, 2H, ADAMA)), 1.29-1.57 (m, 5H, ADAMA), 0.94-0.82 (m, 4H, ADAMA). ^{13}C NMR (100 MHz, CDCl_3) δ = 155.2, 146.2, 144.6, 131.5, 128.8, 127.1, 126.5, 125.2, 121.1, 119.6, 117.2, 108.5, 51.9, 40.8, 37.1, 29.7, 28.4, 28.1, 14.7, 14.6, 14.5. HRMS-ESI: m/z : calcd for $\text{C}_{30}\text{H}_{37}\text{BF}_2\text{N}_3^+$: 488.3043 [$\text{M} + \text{H}$] $^+$, found: 488.3078.

A.1.4 NMR Spectra of Synthesized Compounds

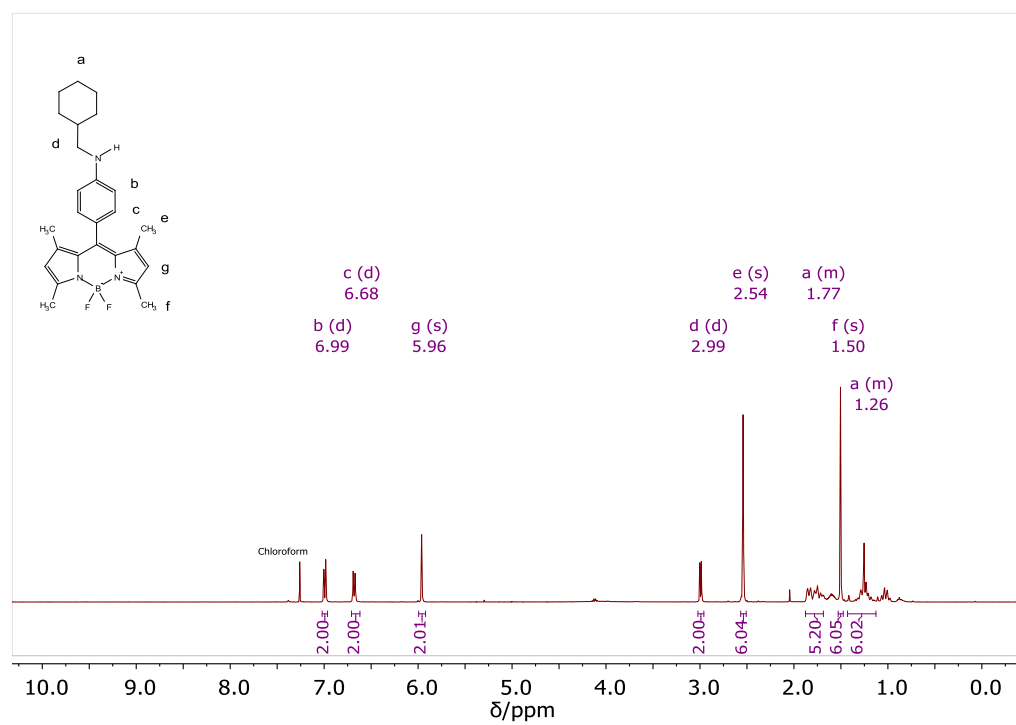


Figure A1.1 ^1H NMR spectrum of BDP-Cyh.

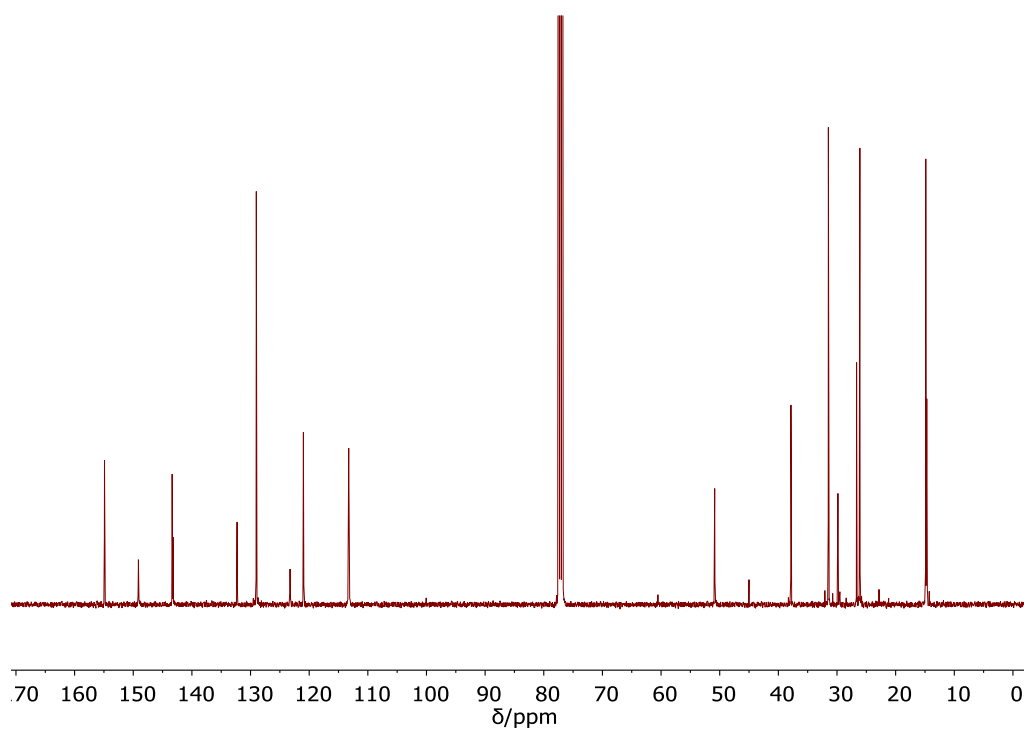


Figure A1.2 ^{13}C NMR spectrum of BDP-Cyh.

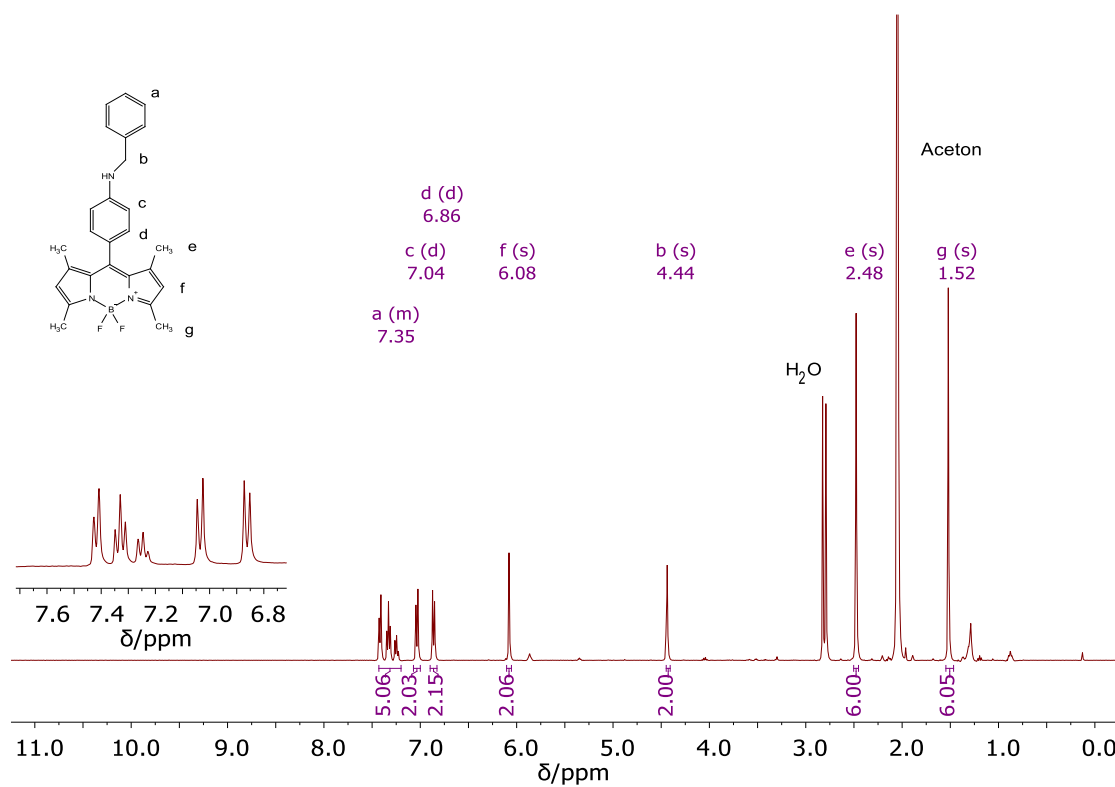


Figure A1.3 ^1H NMR spectrum of BDP-Bnz.

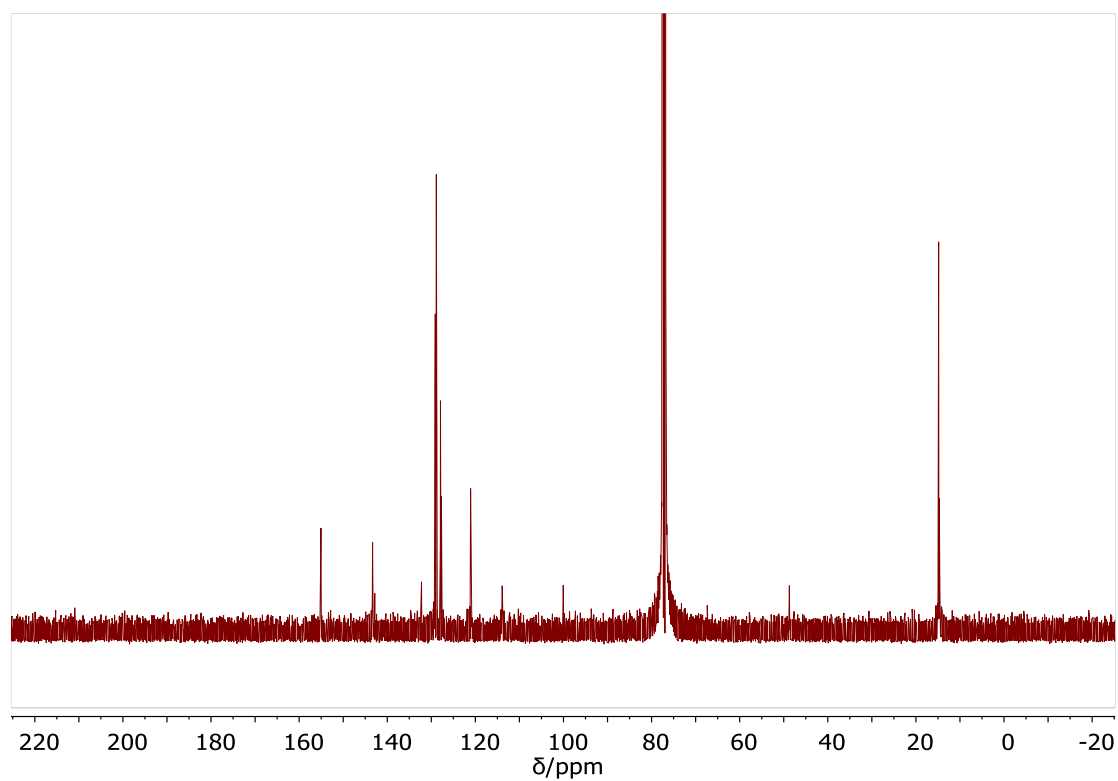


Figure A1.4 ^{13}C NMR spectrum of BDP-Bnz.

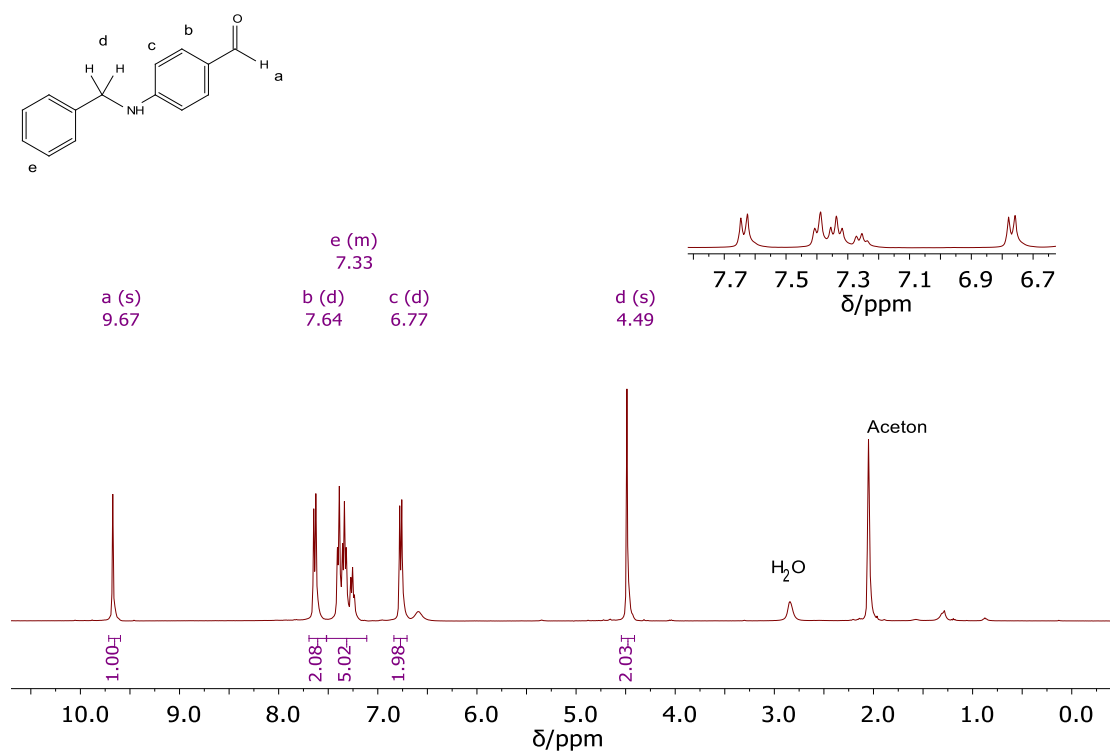


Figure A1.5 ^1H NMR spectrum of p-(benzylamino)benzaldehyde.

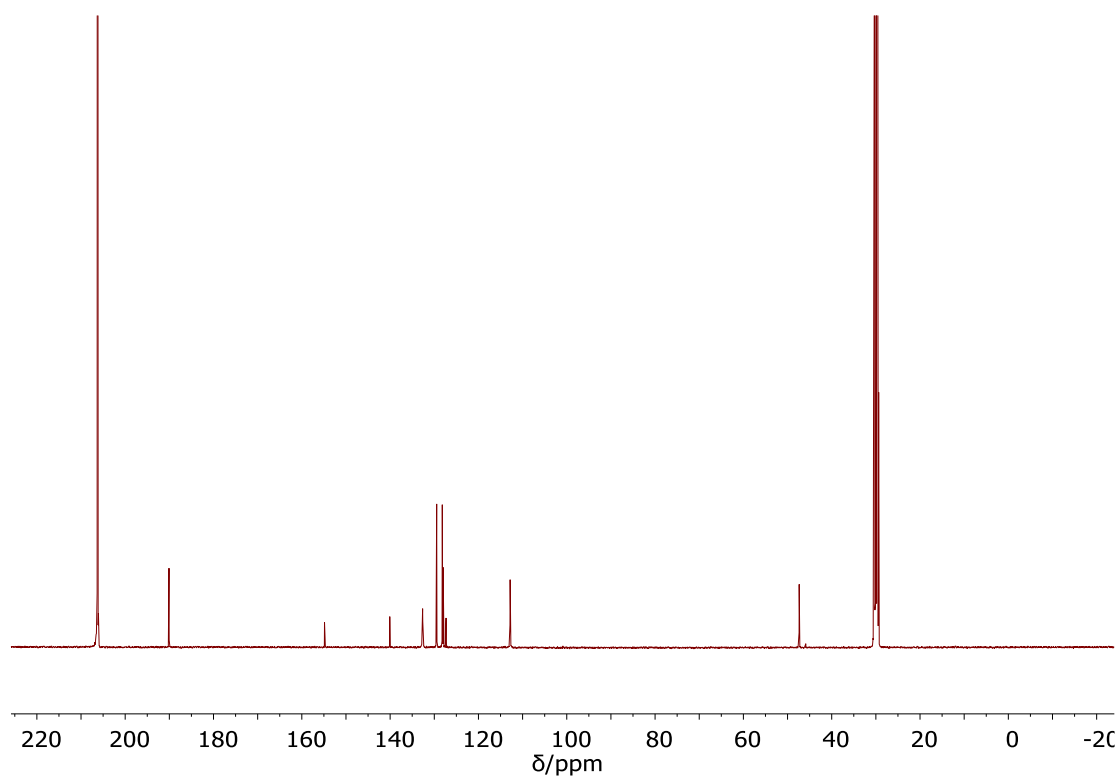


Figure A1.6 ^{13}C NMR spectrum of *p*-(benzylamino)benzaldehyde.

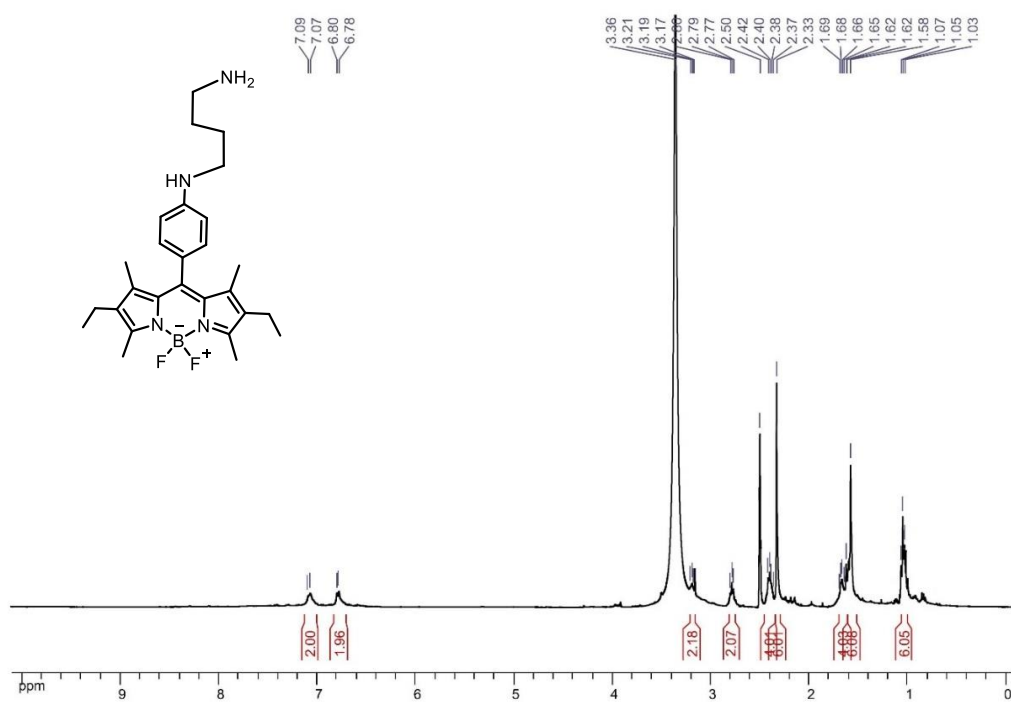


Figure A1.7 ^1H NMR spectrum of BDP-Put.

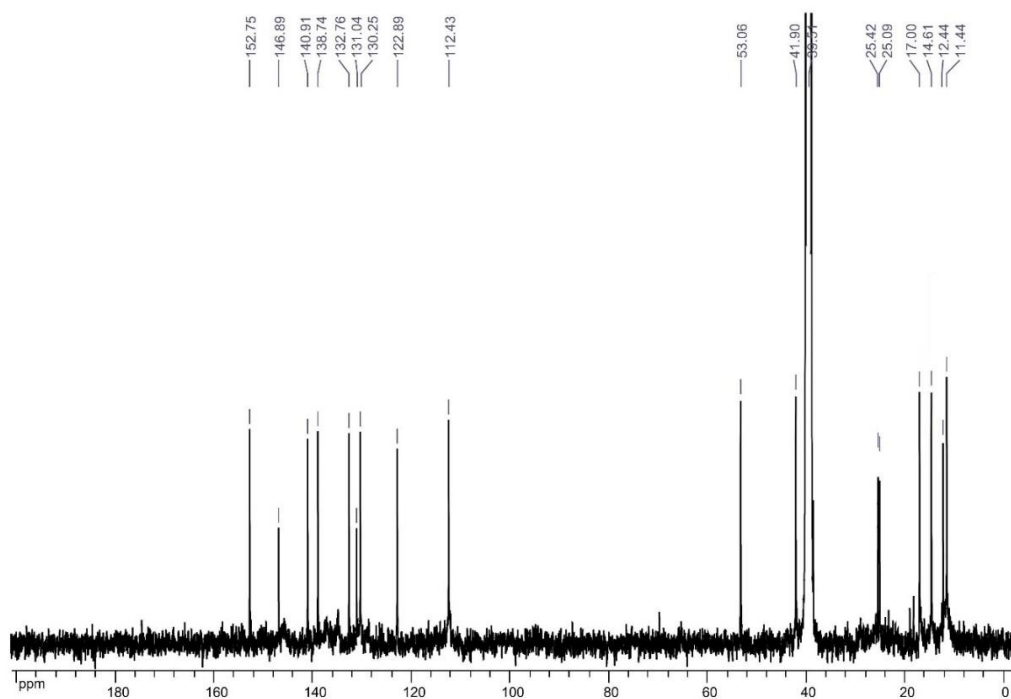


Figure A1.8 ¹³C NMR spectrum of BDP-Put.

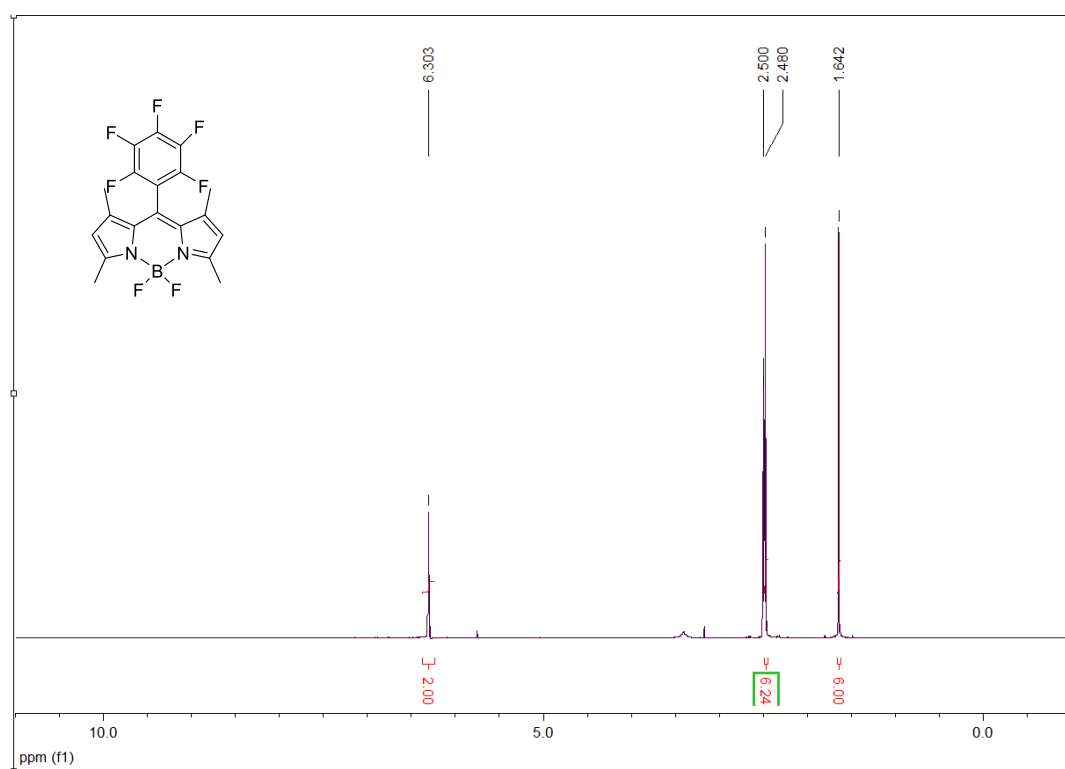


Figure A1.9 ¹H NMR spectrum of BDP-F₅.

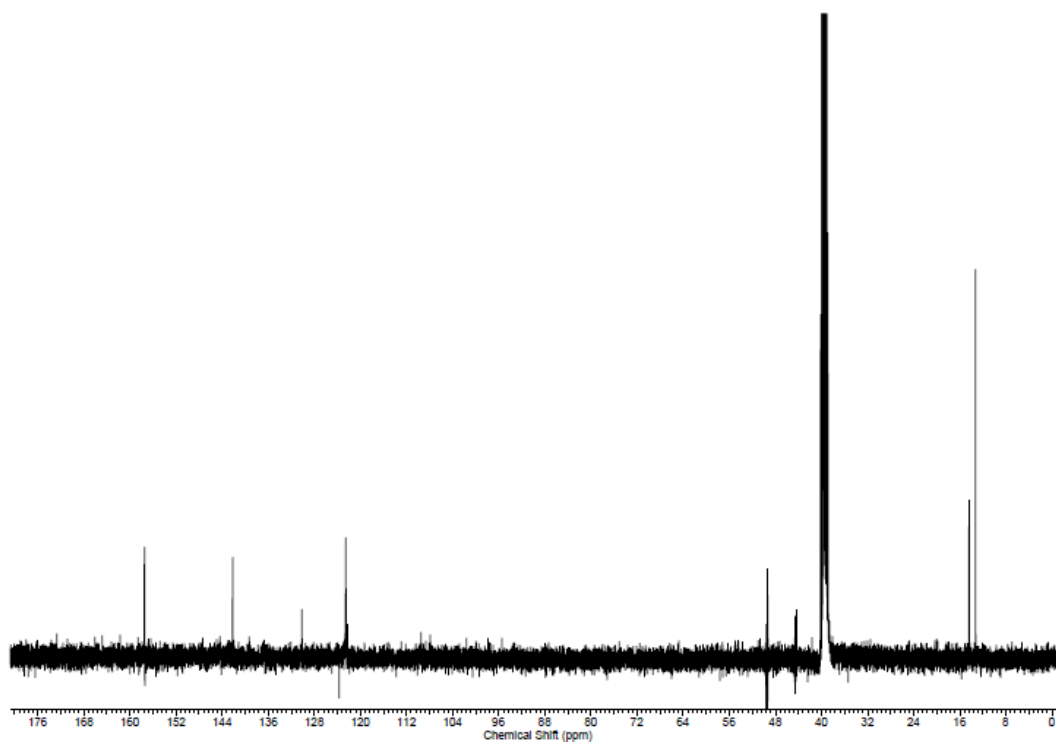


Figure A1.10 ¹³C NMR spectrum of BDP-F₅.

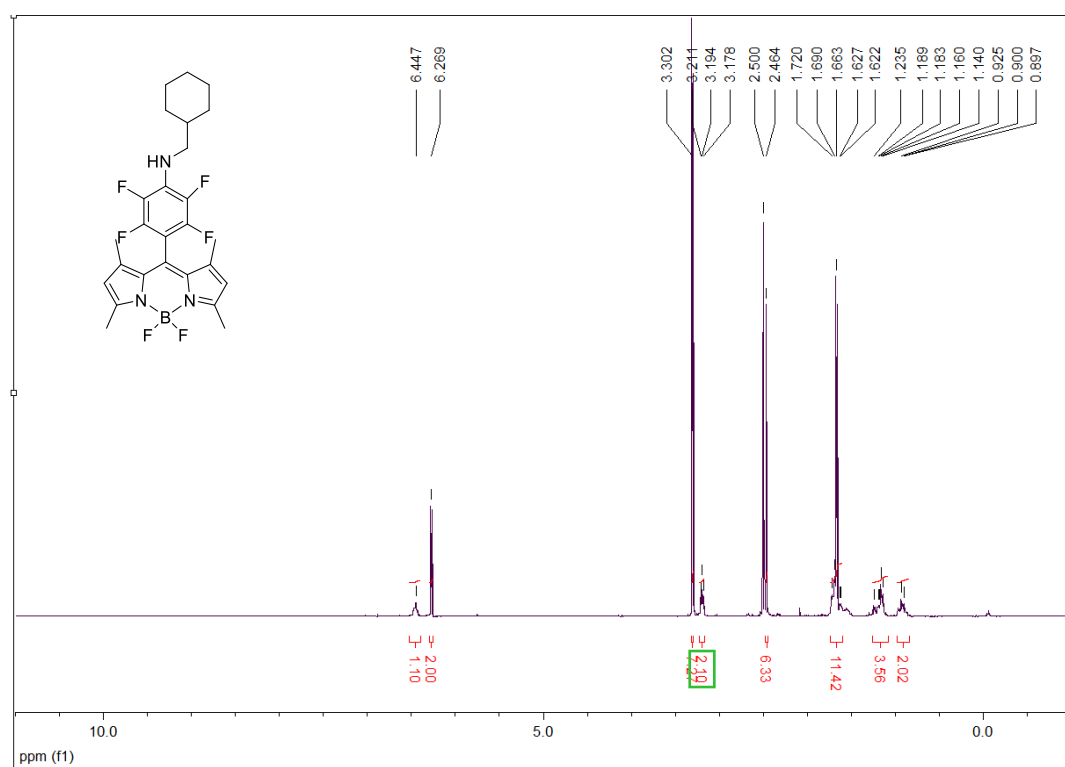


Figure A1.11 ¹H NMR spectrum of BDPF₄-Cyh.

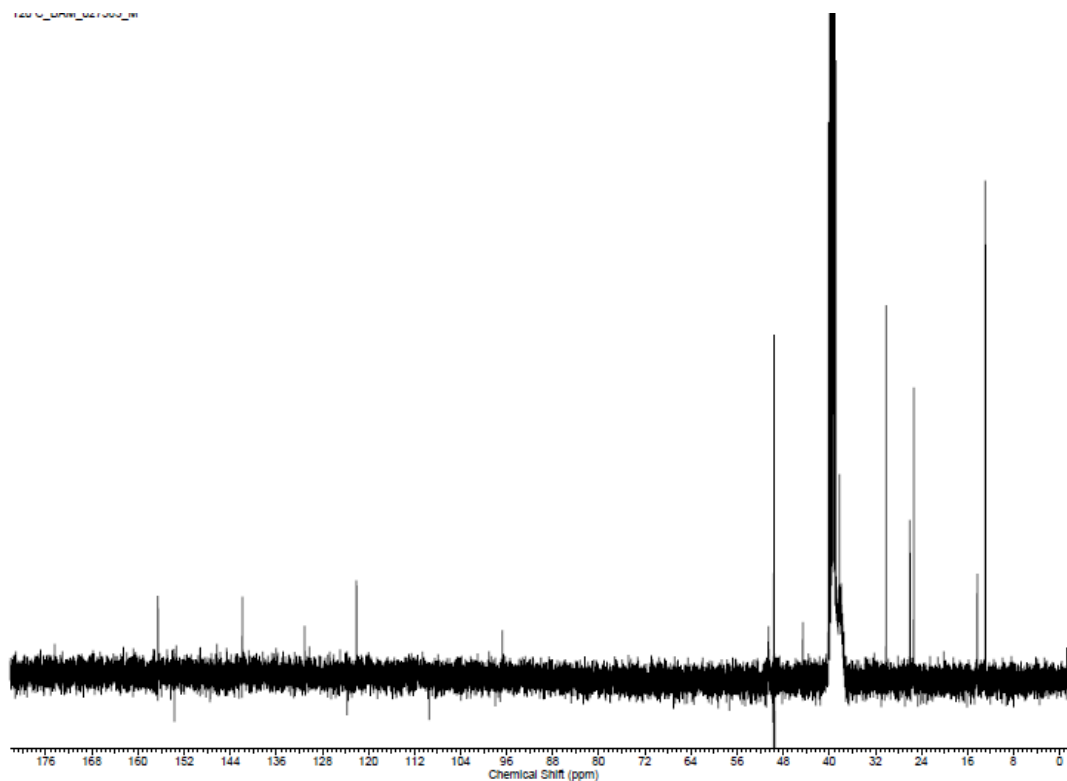


Figure A1.12 ¹³C NMR spectrum of BDPF₄-Cyh.

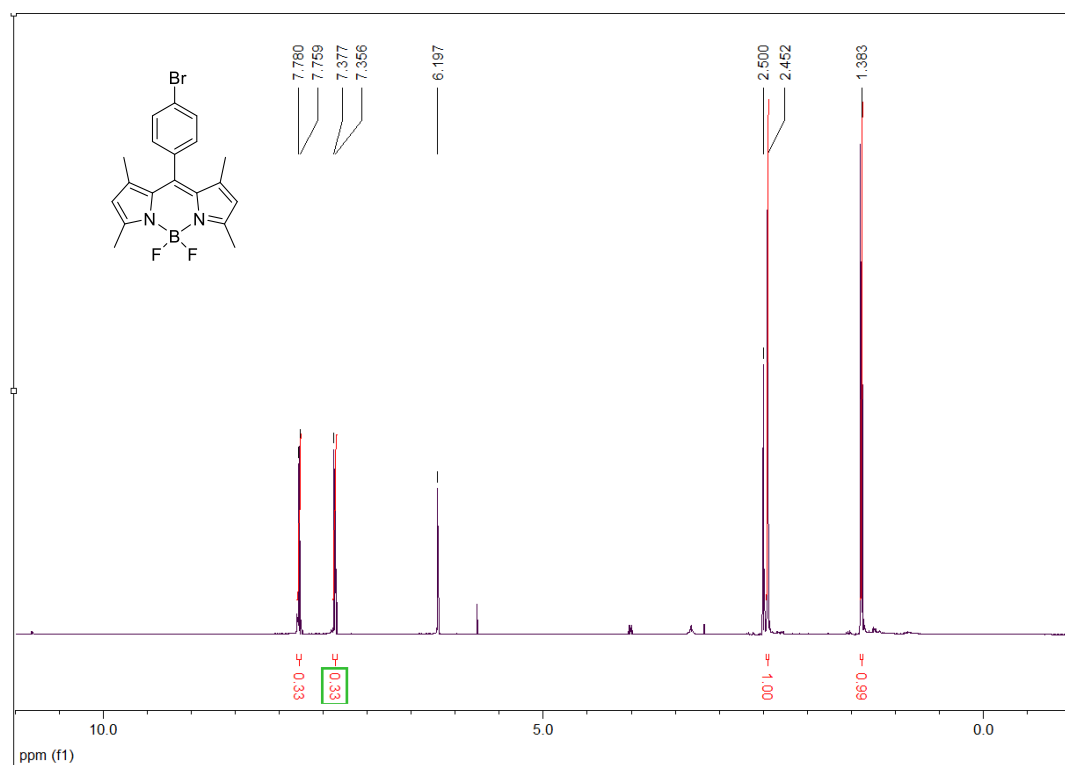


Figure A1.13 ¹H NMR spectrum of BDP-Br.

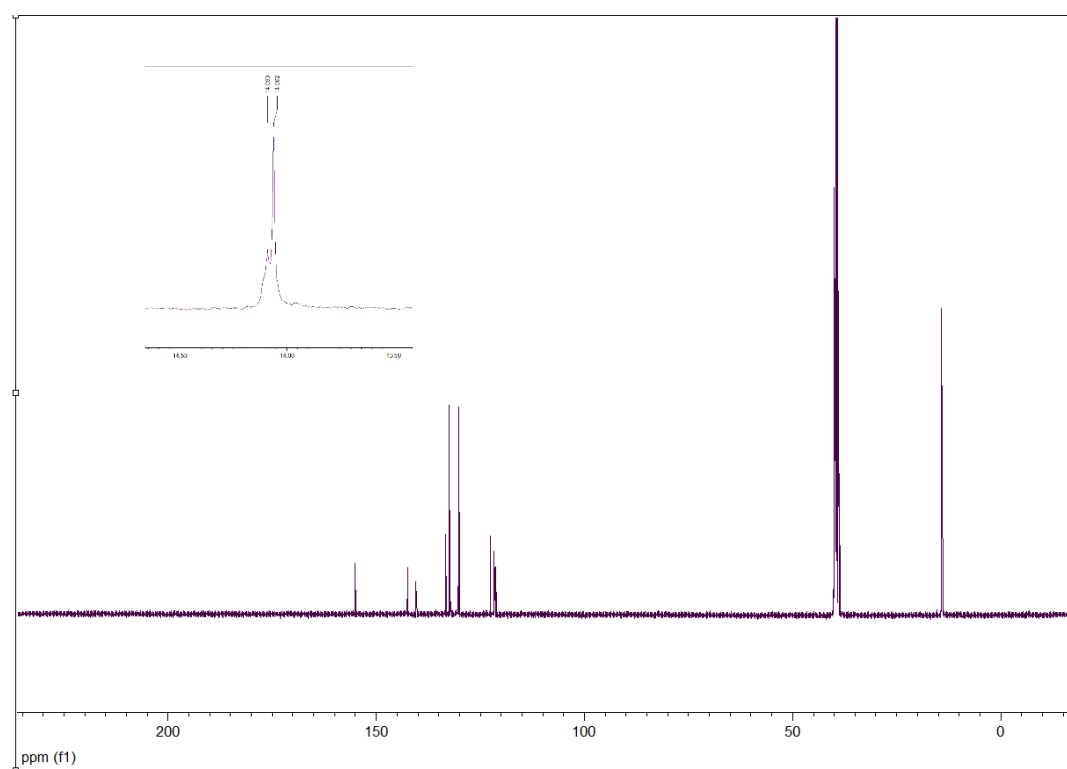


Figure A1.14 ^{13}C NMR spectrum of BDP-Br. Inset: 2 Peaks at around 14 ppm.

101

A.1.5 Determination of Fluorescence Quantum Yields

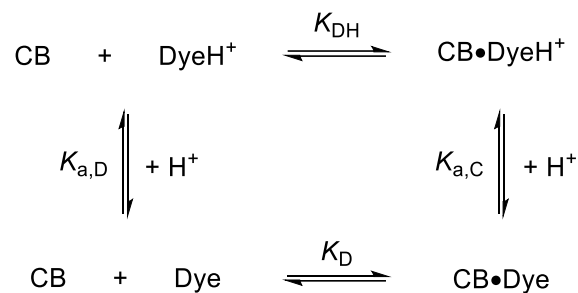
Quantum yields were determined according to established literature methods.^[111] In brief, the integrated area of the fluorescence emission bands of the BODIPY samples, I_{BDP} , and the standard, I_{St} , their respective absorbance at the excitation wavelength, A_{BDP} and A_{St} , and the refractive index of the solvents, η_{BDP} and η_{St} , were used in conjunction with the fluorescence quantum yield of the standard, Φ_{St} , to calculate the quantum yields of the BODIPYS, Φ_{BDP} , according to the following equation:

$$\phi_{BDP} = \phi_{St} \times \frac{I_{BDP} A_{St}}{I_{St} A_{BDP}} \times \frac{\eta_{BDP}^2}{\eta_{St}^2}$$

Specifically, fluorescein in 0.1 M NaOH was taken as standard ($\Phi_{St} = 0.89$) and the refractive index of the ACN/water mixtures was calculated by considering a linear dependence of the refractive index on the mole fraction of the solvent mixture.^[221] Correction curves for the fluorescence measurements were generated with a dye kit certified by Federal Institute for Materials Research and Testing (BAM, Germany).^[216-219]

A.1.6 Global Fitting Procedure

Binding between CB7 and protonated as well as deprotonated BODIPY dyes is described by the following thermodynamic cycle (see also **Figure 2.1**):



From the law of mass action, it follows:

$$K_{\text{D}} = \frac{[\text{CB}\bullet\text{Dye}]}{[\text{CB}][\text{Dye}]} \quad [\text{eq A1.1}]$$

$$K_{\text{DH}} = \frac{[\text{CB}\bullet\text{DyeH}^+]}{[\text{CB}][\text{DyeH}^+]} \quad [\text{eq A1.2}]$$

$$K_{\text{a,D}} = \frac{[\text{Dye}][\text{H}^+]}{[\text{DyeH}^+]} \quad [\text{eq A1.3}]$$

$$K_{\text{a,C}} = \frac{[\text{CB}\bullet\text{Dye}][\text{H}^+]}{[\text{CB}\bullet\text{DyeH}^+]} \quad [\text{eq A1.4}]$$

Law of conservation of mass requires for the total concentrations of CB, $[\text{CB}]_0$, and BODIPY dye, $[\text{Dye}]_0$, that:

$$[\text{CB}\bullet\text{Dye}] + [\text{CB}\bullet\text{DyeH}^+] = [\text{CB}]_0 - [\text{CB}] \quad [\text{eq A1.5}]$$

$$[\text{CB}\bullet\text{Dye}] + [\text{CB}\bullet\text{DyeH}^+] = [\text{Dye}]_0 - [\text{Dye}] - [\text{DyeH}^+] \quad [\text{eq A1.6}]$$

Combining eq A1.5 with eq A1.1 to and eq A1.4 affords:

$$\frac{K_{\text{a,C}}[\text{CB}\bullet\text{DyeH}^+]}{[\text{H}^+]} + [\text{CB}\bullet\text{DyeH}^+] = [\text{CB}]_0 - \frac{K_{\text{a,C}}[\text{CB}\bullet\text{DyeH}^+]}{K_{\text{D}}[\text{Dye}][\text{H}^+]} \quad [\text{eq A1.7}]$$

Combining eq A1.6 with eq A1.3 and eq A1.4 affords:

$$\frac{K_{\text{a,C}}[\text{CB}\bullet\text{DyeH}^+]}{[\text{H}^+]} + [\text{CB}\bullet\text{DyeH}^+] = [\text{Dye}]_0 - [\text{Dye}] \left(1 + \frac{[\text{H}^+]}{K_{\text{a,D}}} \right) \quad [\text{eq A1.8}]$$

Equations A2.7 and A2.8 can now be solved for $[\text{Dye}]$ and combined to afford:

$$0 = a[\text{CB}\bullet\text{DyeH}^+]^2 + b[\text{CB}\bullet\text{DyeH}^+] \quad [\text{eq A1.9}]$$

where

$$a = \frac{K_{a,C}^2}{[H^+]} + 2K_{a,C} + [H^+]$$

$$b = -\left((K_{a,C} + [H^+])[Dye]_0 + (K_{a,C} + [H^+])[CB]_0 + \frac{K_{a,C}K_{a,D} + K_{a,C}[H^+]}{K_{a,D}K_D}\right)$$

$$c = [Dye]_0[H^+][CB]_0$$

EqA1.9 can be solved analytically to afford $[CB \bullet DyeH^+]$.

The fluorescence intensity is obtained from the mole fraction of each species (unprotonated dye D and complex DCB as well as protonated dye DH+ and complex DCBH+) and their respective intensities at the applied concentration:

$$FI = \frac{[Dye]}{[Dye]_0} I_D + \frac{[CB \bullet Dye]}{[Dye]_0} I_{DCB} + \frac{[DyeH^+]}{[Dye]_0} I_{DH+} + \frac{[CB \bullet DyeH^+]}{[Dye]_0} I_{DCBH+} \quad [\text{eq A1.10}]$$

In our case, the fluorescence is only affected by protonation and not by complexation such that $I_D = I_{DCB}$ and $I_{DH+} = I_{DCBH+}$. Eq10 can thus be simplified and combined with eq 3 and eq8 to afford:

$$FI = I_D + (I_{DH+} - I_D) \left(\frac{[Dye]_0[H^+] - K_{a,C}[CB \bullet DyeH^+] - [CB \bullet DyeH^+][H^+]}{(K_{a,D} + [H^+])[Dye]_0} + \frac{[CB \bullet DyeH^+]}{[Dye]_0} \right) \quad [\text{eq A1.11}]$$

Eq A1.11 and eq A1.9 were then implemented into Origin 9 and titration data at various pH (see for example **Figure 2.3** in main text) was simultaneously analyzed using the Global Fitting procedure from Origin 9.

A.1.7 Supporting Figures

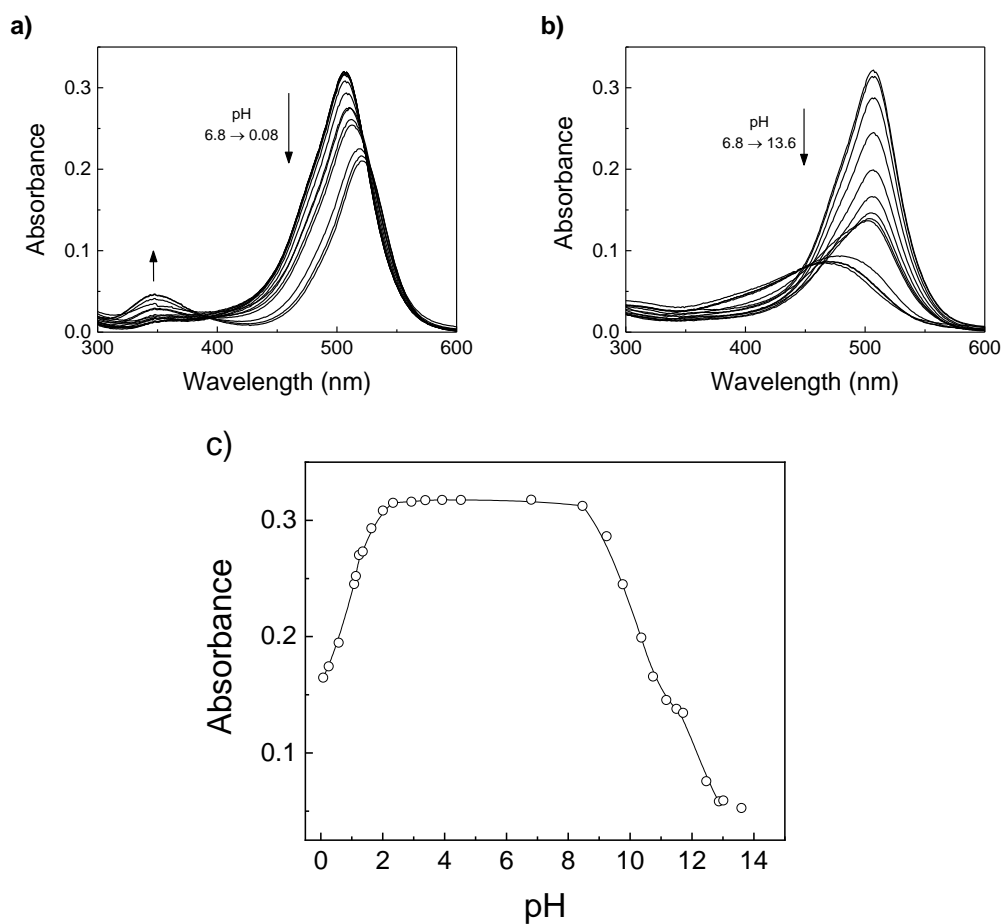


Figure A1.17 Absorption spectral changes with varying pH for BDP-Put. H₂O/ACN 98:2, $\lambda_{\text{obs}} = 506$ nm.

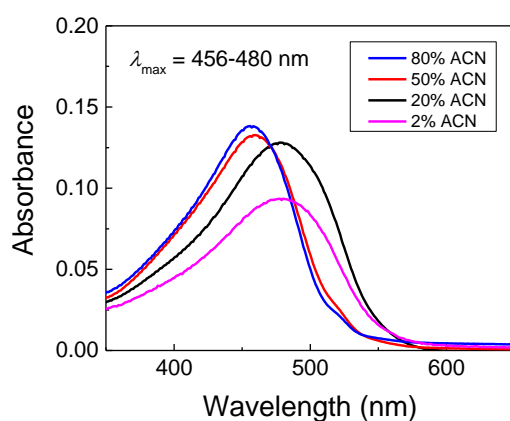


Figure A1.18 Solvatochromism of 10 μ M BDP-Put in varying H₂O/ACN mixtures at pH 12.0.

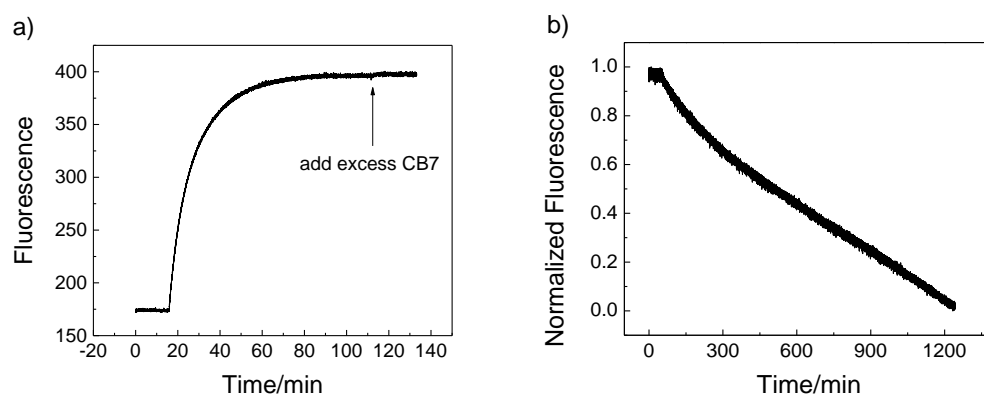


Figure A1.19 Fluorescence association and dissociation kinetic for 200nM BDP-AMADA in 10 mM citrate, pH 3.33 (7:3 water:ACN). a) Association kinetics with 200 nM CB7. b) Competitive dissociation kinetics of 200 nM BDP-AMADA•CB7 complex with 1.5 mM adamantylamine as a competitor.

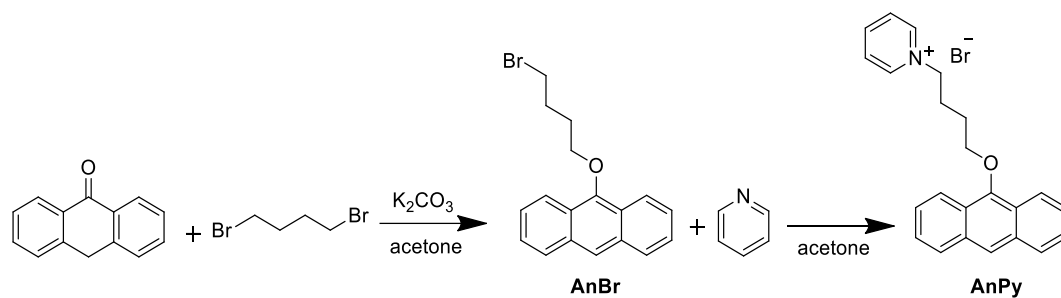
A.2 Supporting Information for Chapter 3

A.2.1 Methods

Cucurbit[7]uril and cucurbit[8]uril were synthesized according to literature procedures.^[215] The CB8 sample contains traces of HCl from recrystallization, which enhances its water-solubility (up to 0.1 mM). NMR spectra were recorded on a JEOL JNM-ECX 400 spectrometer working at 400 MHz. Quantum-chemical calculations were performed with the Gaussian 09 package, utilizing density functional theory (DFT) with dispersion corrected method (wB97xd) in combination with 6-31G* basis set. ITC experiments were carried out on a VIP ITC from Microcal Inc. (Northampton, MA, United States) at 25 °C. The solutions were degassed and thermostated by a ThermoVac accessory for all experiments. The data was analyzed by Origin 7.0 software with the one set of sites model. UV-Vis absorption measurements were performed with a Varian Cary 4000 spectrophotometer and the fluorescence spectra were recorded on a Varian Cary Eclipse or a JASCO FP-8500 spectrofluorometer. All measurements were performed at ambient temperature, in rectangular SUPRASIL® quartz glass cuvettes (Hellma Analytics) with 1-cm optical path length. DLS and zeta potential measurements were performed on a Malvern Zetasizer Nano ZS instrument. TEM images were recorded with a Zeiss EM900 transmission electron microscope, in which the sample was put on the Cu-grid with carbon support film (carbon-film on 3.05 nm Cu-network 200 nm mesh) purchased from PLANO GmbH. An accelerating voltage of 80 kV was applied.

A.2.2 Synthesis and Characterization of AnPy

AnBr and **AnPy** were synthesized according to the literature (**Scheme A2.1**).^[152]



Scheme A2.1 Synthesis of **AnBr** and **AnPy**.

Synthesis of 9-(4-Bromobutoxy)anthracene (**AnBr**): 2.0 g (10.3 mmol) anthrone and 9.0 g (41.7 mmol) 1,4-dibromo butane, and 14.0 g (101.3 mmol) K₂CO₃ were mixed in 120 mL acetone under nitrogen atmosphere, and heated to reflux for 14 h (**Scheme A2.1**). After cooling to ambient temperature, the solvent was removed *via* rotary evaporation under reduced pressure, and the residue was purified by column chromatography (CH₂Cl₂:petroleum ether = 1:10), giving 1.7 g (50% yield) of 9-(4-bromobutoxy)anthracene as a white solid.

Synthesis of **AnPy**: 360 mg (1.08 mmol) **AnBr** and pyridine (3 mL) were dissolved in acetone (100 mL), and the solution was heated to reflux for 48 h under nitrogen atmosphere (**Scheme A2.1**). After cooling to room temperature, the mixture was poured into diethyl ether (300 mL). The precipitated product was filtered and washed with diethyl ether. The product was dried overnight under vacuum, giving 250 mg (57% yield).

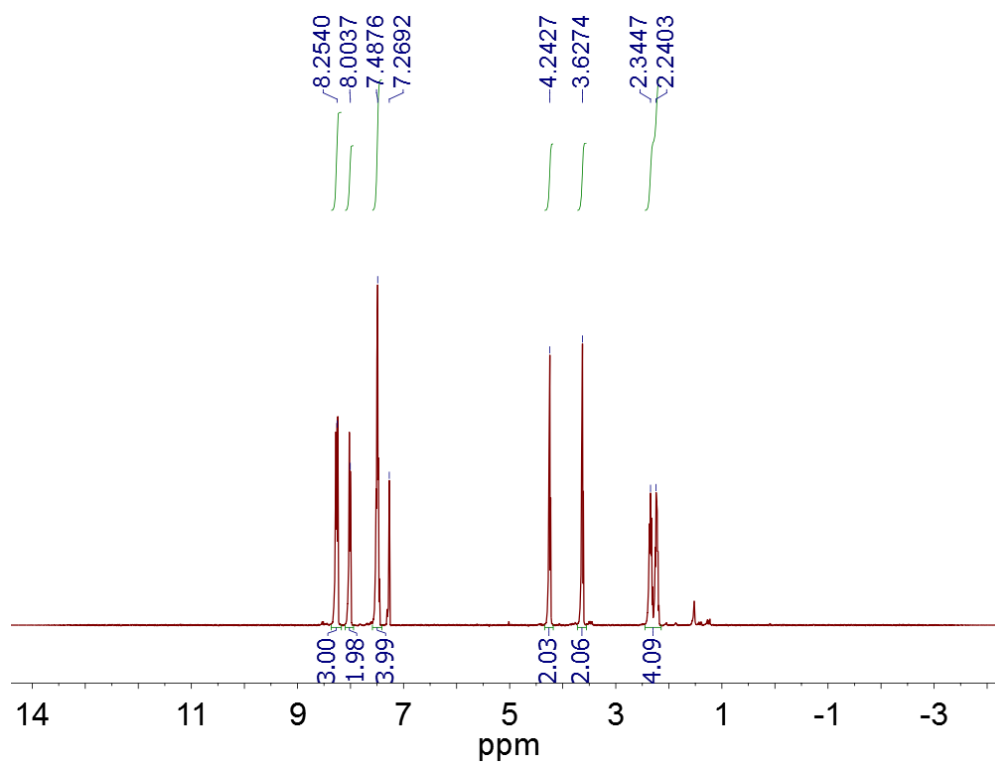


Figure A2.1 ¹H NMR spectrum of AnBr in CDCl₃.

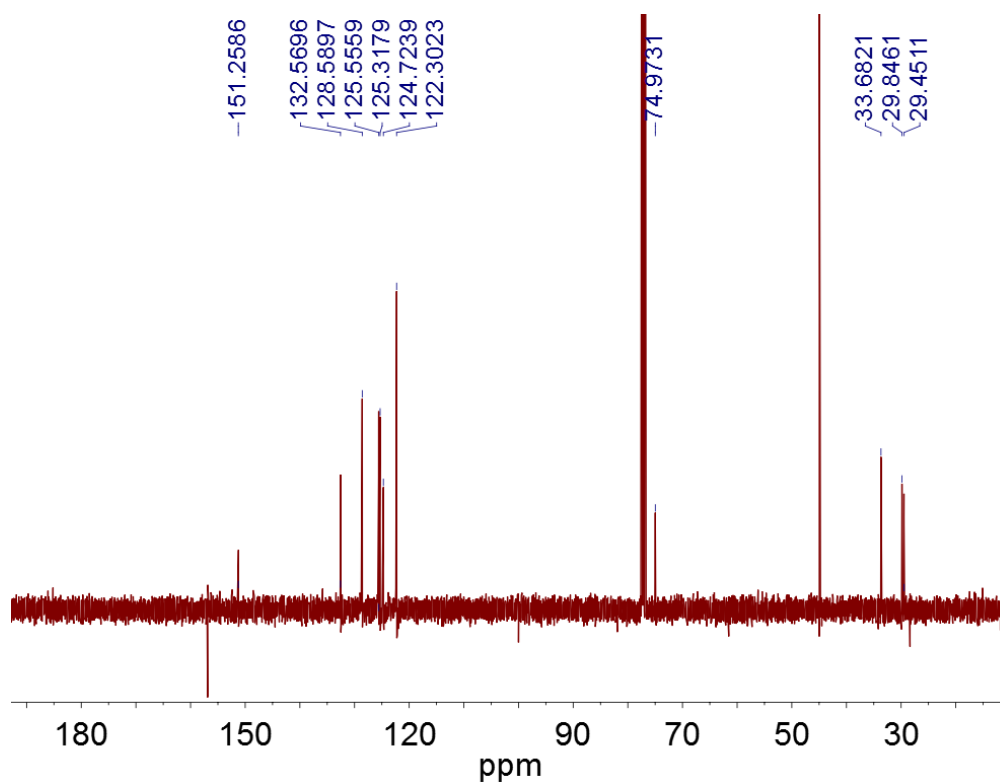


Figure A2.2 ¹³C NMR spectrum of AnBr in CDCl₃.

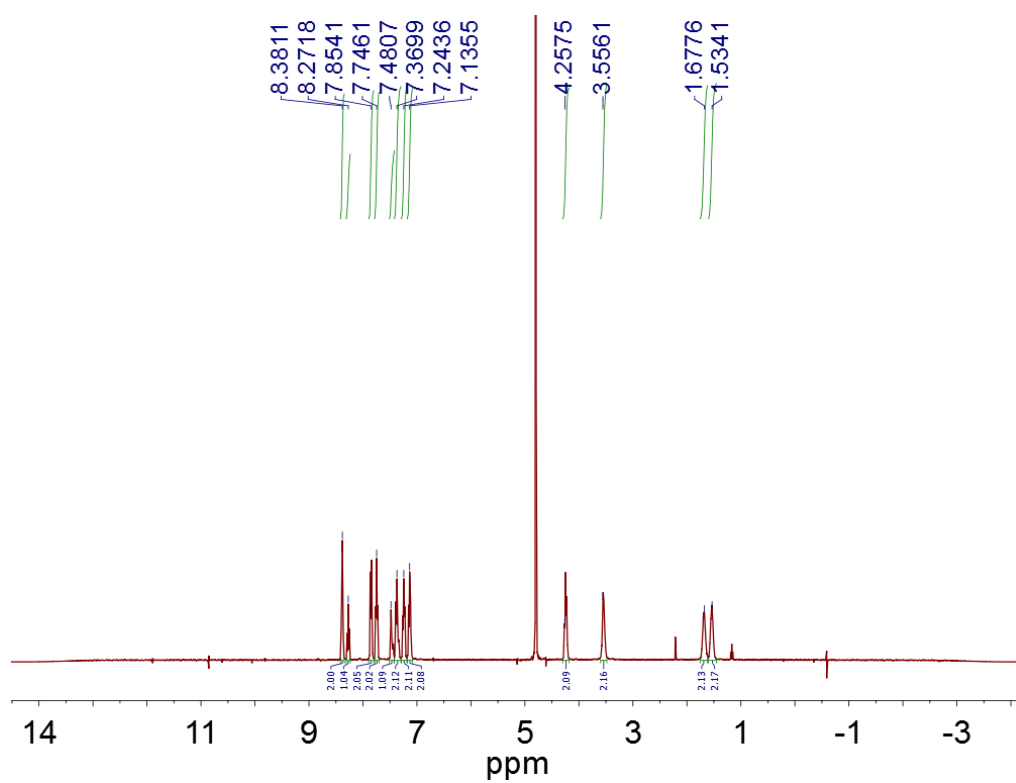


Figure A2.3 ¹H NMR spectrum of AnPy in D₂O.

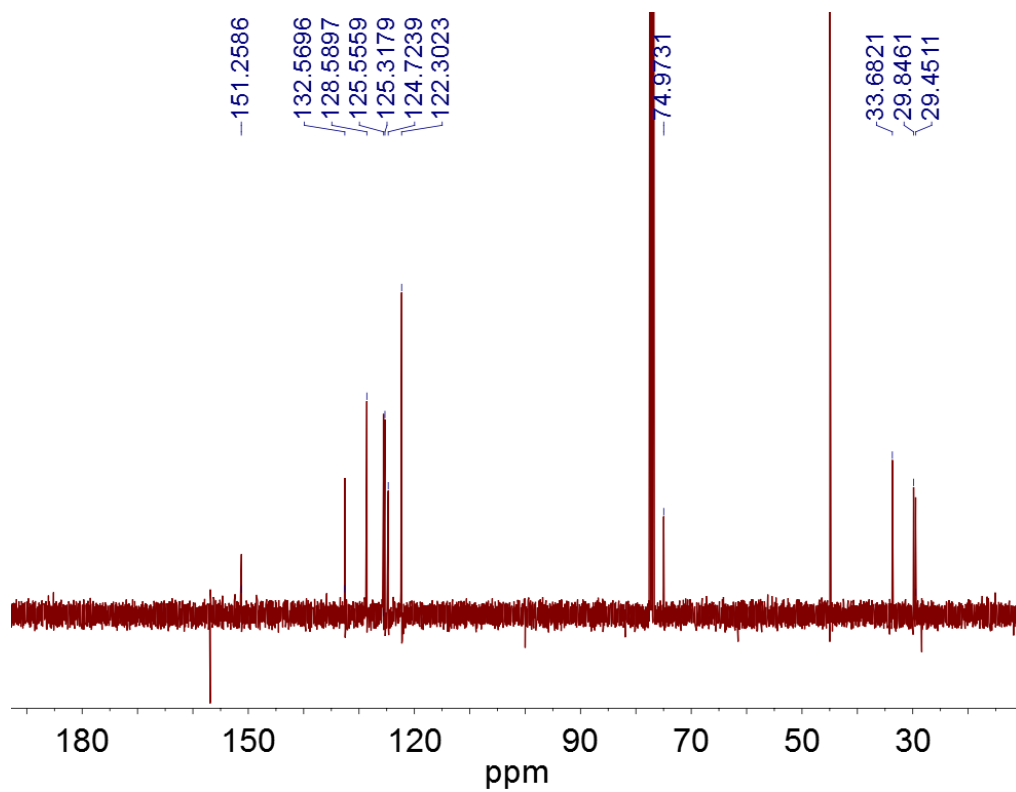


Figure A2.4 ¹³C NMR spectrum of AnPy in D₂O.

A.2.3 Job's Plots of the $\text{CB}n\bullet\text{AnPy}$ Complexes

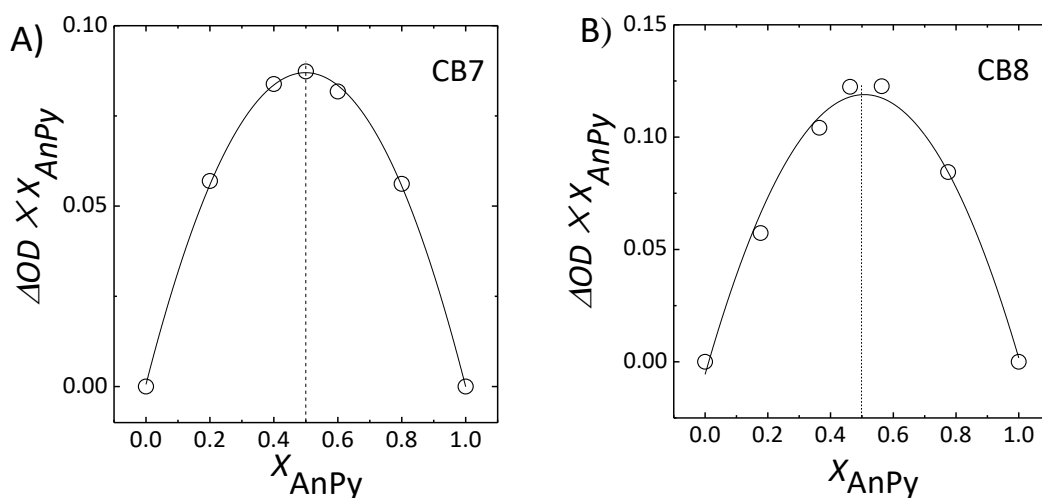


Figure A2.5 Job's plots for A) $\text{CB7}\bullet\text{AnPy}$ complex and B) $\text{CB8}\bullet\text{AnPy}$ complex.

A.2.4 ITC Experiments

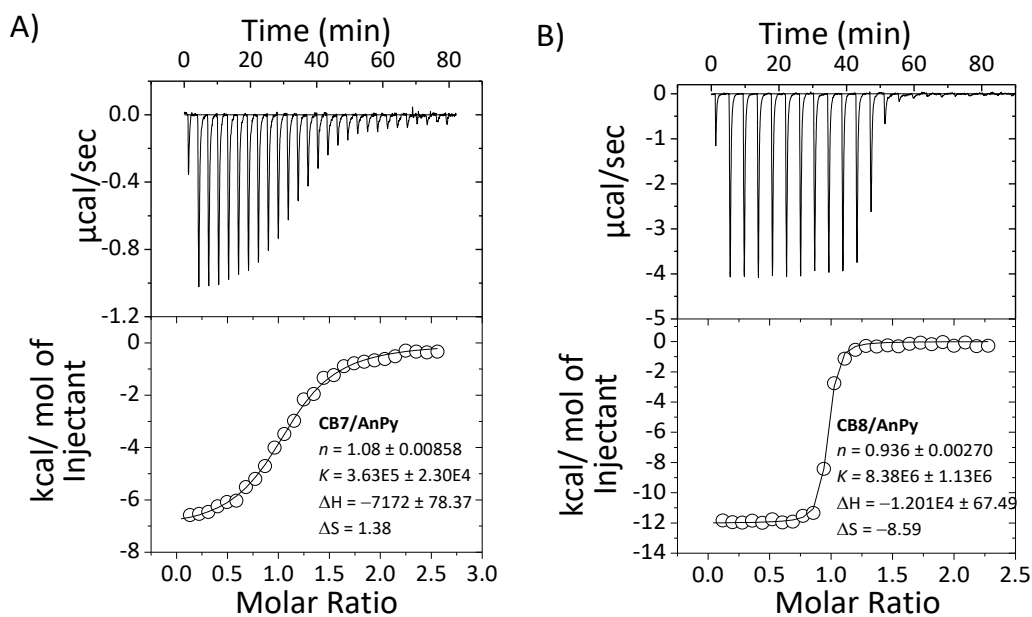


Figure A2.6 ITC isotherms for the titration of A) CB7 (0.5 mM) into a solution of 0.05 mM AnPy and B) AnPy (1.0 mM) into a solution of 0.10 mM CB8 ; experiments were done in water at 25 °C.

A.2.5 Competitive Titrations

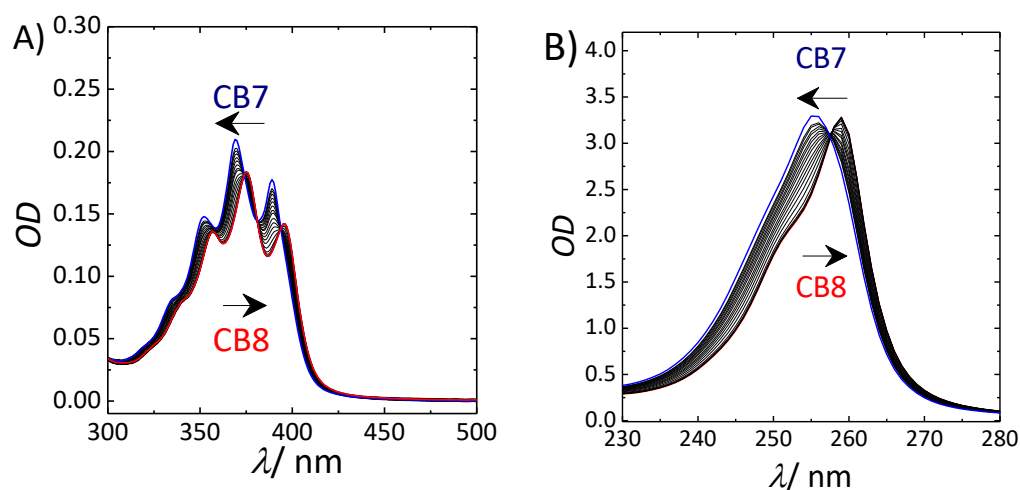


Figure A2.7 UV-Vis titrations of CB8•AnPy (35:35 μM) with CB7. A) UV-Vis change of the absorption bands of the anthracene (A) and the pyridinium residue (B).

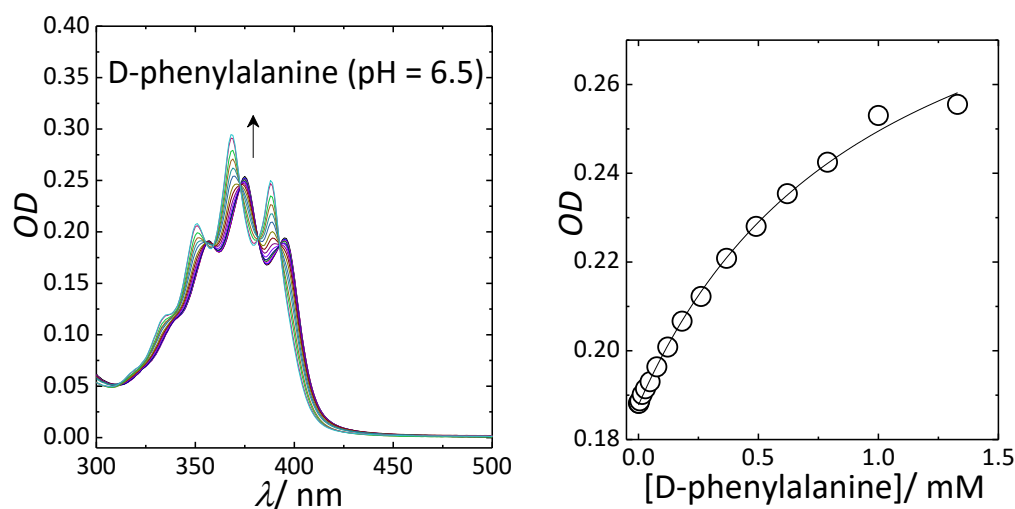


Figure A2.8 UV-Vis competitive titrations for the complexation of D-phenylalanine with the CB8•AnPy reporter pair (35:35 μM) at pH 6.5.

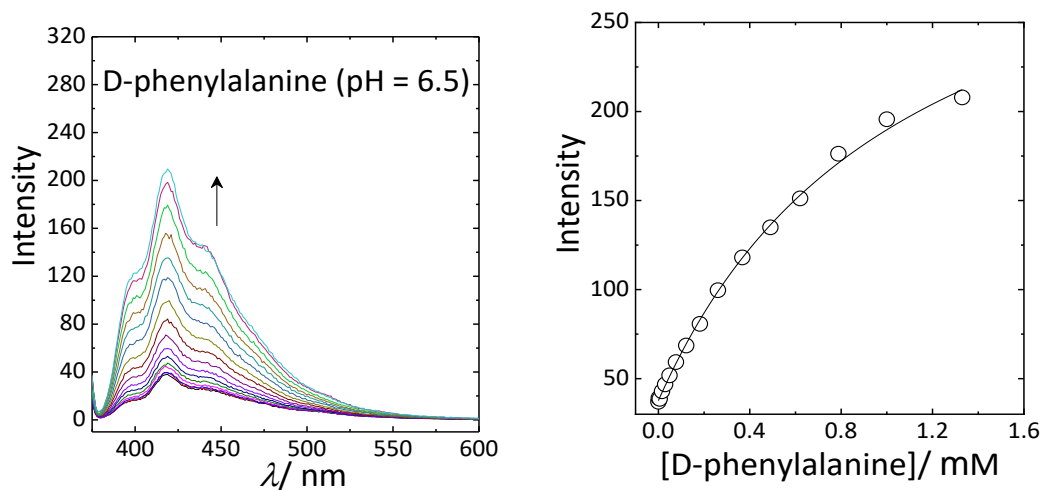


Figure A2.9 Fluorescence competitive titrations for the complexation of D-phenylalanine with the CB8•AnPy reporter pair (35:35 μM) at pH 6.5.

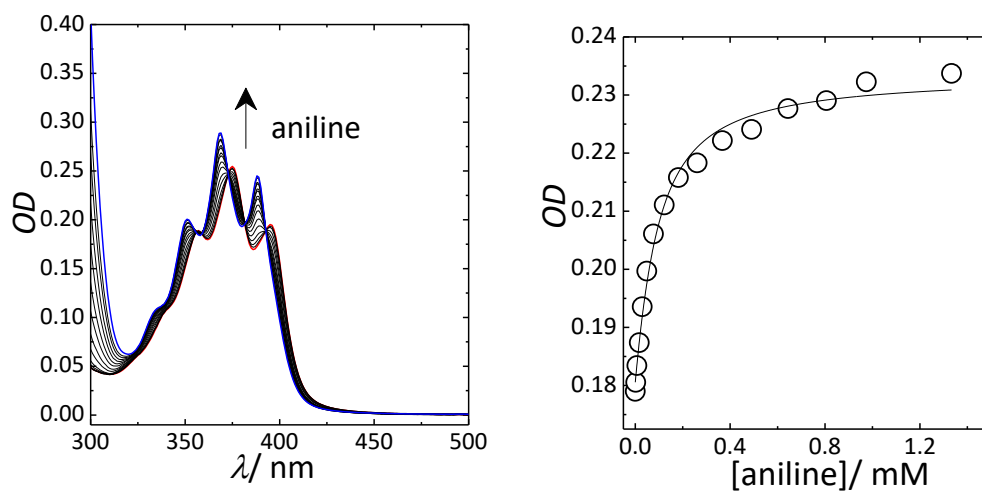


Figure A2.10 UV-Vis competitive titrations for the complexation of aniline with the CB8•AnPy reporter pair (35:35 μM) at pH 2.

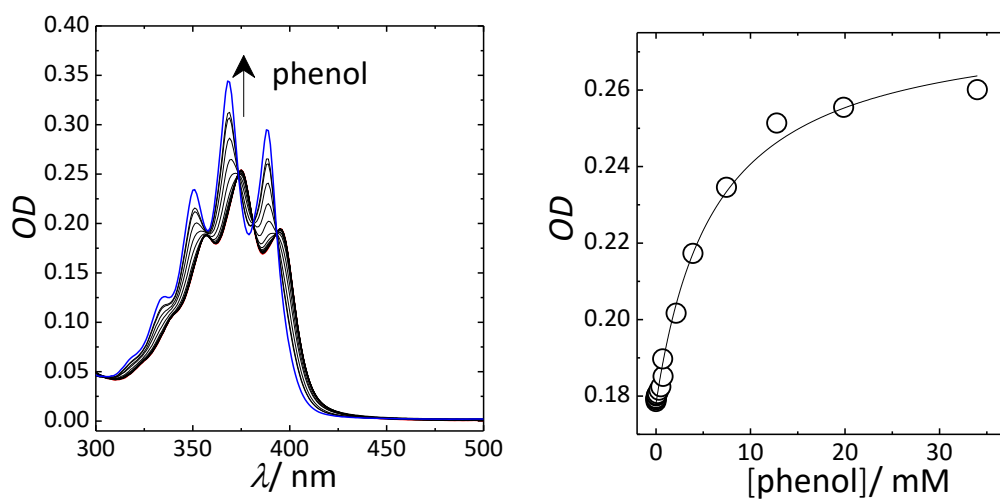


Figure A2.11 UV-Vis competitive titrations for the complexation of phenol with the CB8•AnPy reporter pair (35:35 μM) at pH 7.

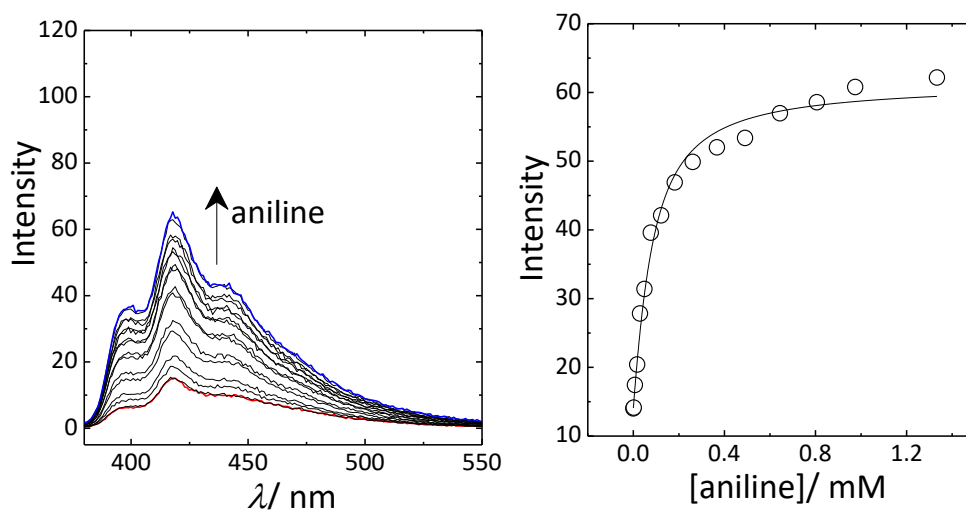


Figure A2.12 Fluorescence competitive titrations for the complexation of aniline with the reporter pair CB8•AnPy (35:35 μM) at pH 2.

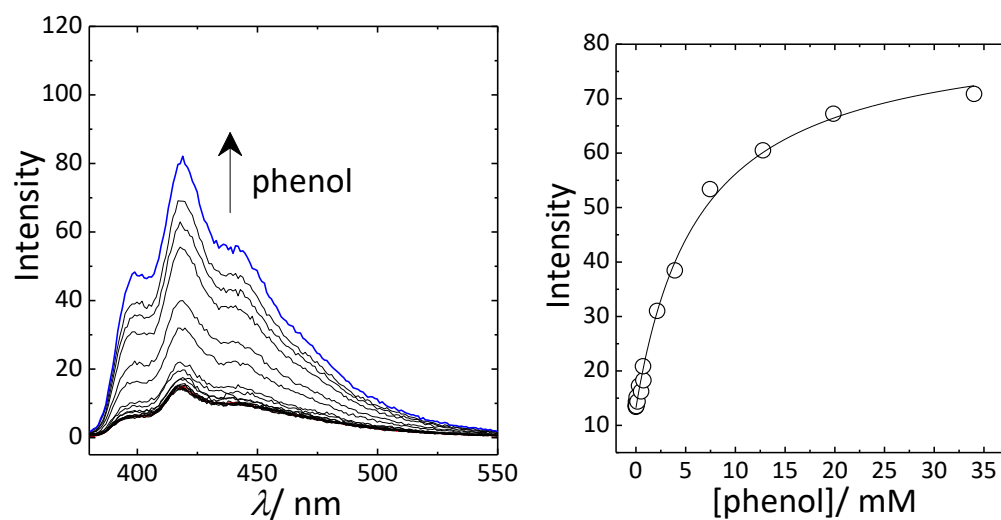


Figure A2.13 Fluorescence competitive titrations for the complexation of phenol with the reporter pair CB8•AnPy (35:35 μM) at pH 7.

A.2.6 Photo-oxidation Reaction of AnPy

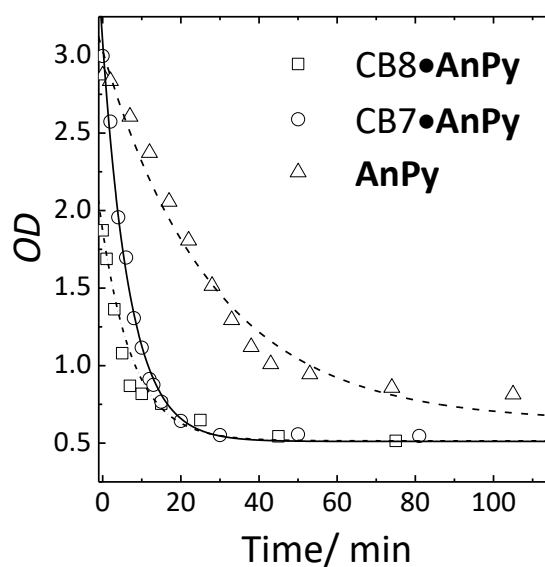


Figure A2.14 Monitoring of the photo-reaction of free (0.5 mM) and complexed AnPy (0.5 mM AnPy and 0.5 mM host) as a function of time.

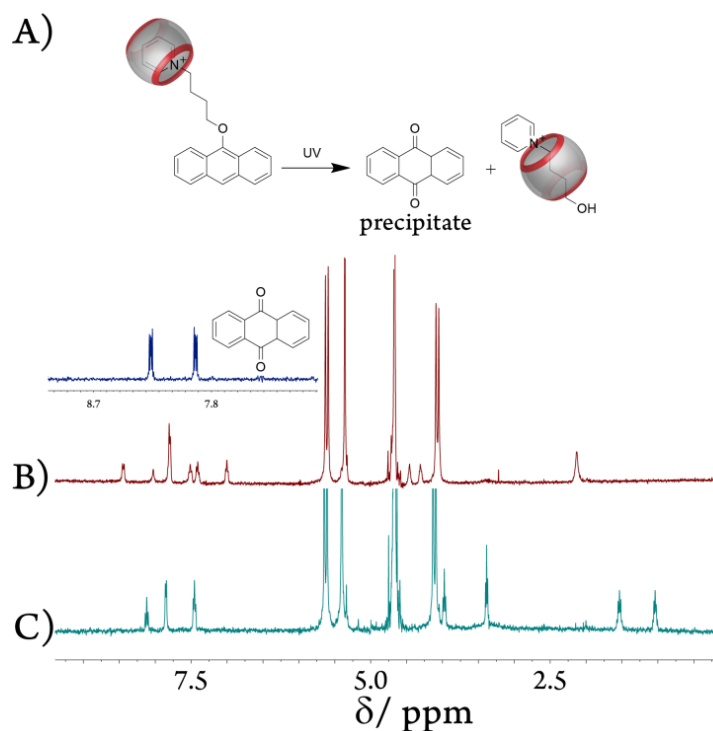


Figure A2.15 A) Photo-oxidation of AnPy upon UV-irradiation in aqueous solution. ^1H NMR spectra of CB7•AnPy (1 mM) in D_2O before (B) and after (C) UV-irradiation for 3 h. The ^1H NMR spectrum of the extracted anthraquinone in acetone- d_6 show in blue.

A.3 Supporting Information for Chapter 4

A.3.1 Materials and Instrumentation

Materials. Starting materials for synthesis and reference compounds were purchased from Sigma-Aldrich (Steinheim, Germany) or Merck (Mannheim, Germany), and Tokyo Chemical Industry (TCI) and were used without further purification. Deuterated D₂O and DCI for NMR measurements were purchased from Deutero (Kastellaun, Germany), Cucurbit[7]uril (CB7) was purchased from Strem Chemicals Inc. (Massachusetts, United States) or synthesized according to literature.^[222] For titrations in H₂O, water distilled from KMnO₄ was used or Millipore water, if not otherwise noted. The compounds (2,3-diazabicyclo[2.2.2]oct-2-enyl) methanamine and aminomethyladamantane-putrescine were synthesized according to literature procedures.^[166,223] (S)-2-(Adamantan-1-yl)-2-aminoacetic acid hydrochloride was from Ark Pharm Inc. (IL, US). All fluorescence measurements were performed at ambient temperature using PMMA cuvettes, if not noted otherwise.

Instrumentation. ¹H NMR spectra were recorded on a JEOL ECX 400 spectrometer. Fluorescence was measured with a Varian Eclipse 4000 spectrophotometer. ITC experiments were carried out on a VP-ITC from Microcal Inc. (Northampton, MA, United States) at 25 °C. The solutions were degassed and thermostatted by a ThermoVac accessory for ITC experiments. pH values were measured with a Weilheim 3110 pH meter. The pH was converted to pD by the known relation (+ 0.40 units).^[224]

A.3.2 Abbreviations

ADA: adamantylamine, AMADA: aminomethyladamantane, AMADA-aa: (S)-2-(adamantan-1-yl)-2-aminoacetic acid hydrochloride, AMADA-Put: *N*-adamantylmethylbutane-1,4-diamine, BE: berberine chloride, BODIPY: 4,4-difluoro-4-bora-3a,4a-diaza-s-indacene, CB7: cucurbit[7]uril, CBAMC: *cis*-1,4-bis(aminomethyl)-cyclohexane, CHMA: cyclohexylmethylamine, DBO-A: (2,3-diazabicyclo[2.2.2]oct-2-enyl) methylamine, FDMA: *N,N*-dimethylaminomethylferrocene, HMD: hexamethylenediamine, ITC: isothermal titration calorimetry, NMR: nuclear magnetic resonance spectroscopy, Put: putrescine, PXD: *p*-xylylenediamine, TBA: tetrabutylammonium chloride, TBAMC: *trans*-1,4-bis(aminomethyl)-cyclohexane.

A.3.3 Binding Constant Determinations and Error Calculations

In general, the error Δy of a function $y = f(x_1, x_2, \dots, x_n)$, which is dependent on more than one independent value and its respective error ($\Delta x_1, \Delta x_2, \dots, \Delta x_n$), is given by:

$$\Delta y = \sqrt{\left(\frac{\partial y}{\partial x_1}\right)^2 \Delta x_1^2 + \left(\frac{\partial y}{\partial x_2}\right)^2 \Delta x_2^2 + \dots + \left(\frac{\partial y}{\partial x_n}\right)^2 \Delta x_n^2} \quad [\text{eq.A3.1}]$$

A.3.3.1 Determination of Reference Values and Their Uncertainty

To determine the final binding constant reference value from n different binding constants, which have been determined by various methods (e.g. NMR, fluorescence, and ITC), we first, determined the average by:

$$K_{a,\text{ave}} = \frac{K_{a,1} + K_{a,2} + \dots + K_{a,n}}{n} \quad [\text{eq.A3.2}]$$

Then, the respective error for the average value is given by considering the errors of the different binding constants by:

$$\Delta K_{a,\text{ave}} = \sqrt{\frac{1}{n^2} (\Delta K_{a,1}^2 + \Delta K_{a,2}^2 + \dots + \Delta K_{a,n}^2)} \quad [\text{eq.A3.3}]$$

As a specific example, the binding constant of BE was determined by NMR, ITC, and fluorescence as $(2.40 \pm 0.22) \times 10^7 \text{ M}^{-1}$, $(2.26 \pm 0.39) \times 10^7 \text{ M}^{-1}$, and $(2.43 \pm 0.39) \times 10^7 \text{ M}^{-1}$. Then, the proposed value for the binding constant reference values is $K_{a,\text{ave}} = \frac{(2.40 + 2.26 + 2.43) \times 10^7 \text{ M}^{-1}}{3} = 2.36 \times 10^7 \text{ M}^{-1}$ and the respective error is $\Delta K_{a,\text{ave}} =$

$$\sqrt{\frac{1}{3^2} ((0.22 \times 10^7 \text{ M}^{-1})^2 + (0.39 \times 10^7 \text{ M}^{-1})^2 + (0.39 \times 10^7 \text{ M}^{-1})^2)} = 0.20 \times 10^7 \text{ M}^{-1}.$$

A.3.3.2 Error Propagation for Fluorescence Displacement Titrations

Fluorescence displacement titrations were analysed with OriginLab OriginPro 2020 as previously described.^[199] Here, we now used the global fitting routine implemented in OriginPro to simultaneously analyse more than one binding titration at the same time to obtain the best fit for all analysed binding titration curves. Unfortunately, the uncertainty of the reference binding constant value of the fluorescent dye could not be implemented in the OriginPro fitting procedure. To assess the uncertainty in a different way, the data was analysed twice considering the upper and lower limits of the error of the reference value. Herein, the proposed reference value for BE is $K_a = (2.36 \pm 0.20) \times 10^7 \text{ M}^{-1}$, such that the displacement titration data was analysed twice with a fixed binding constant parameter for BE of $K_{a,\text{BE}} = (2.36 + 0.20) \times 10^7 \text{ M}^{-1} = 2.56 \times 10^7 \text{ M}^{-1}$ and $K_{a,\text{BE}} = (2.36 - 0.20) \times 10^7 \text{ M}^{-1}$

$= 2.16 \times 10^7 \text{ M}^{-1}$. This gave two different binding constants of the competitor and a respective error, $(K_{a,\max} \pm \Delta K_{a,\max})$ and $(K_{a,\min} \pm \Delta K_{a,\min})$.

Then, the binding constant value of the competitor, $K_{a,C}$, for the fluorescence displacement titration was obtained by considering the upper end and lower end of the range given by this procedure:

$$K_{a,C} = \frac{((K_{a,\max} + \Delta K_{a,\max}) + (K_{a,\min} - \Delta K_{a,\min}))}{2} \quad [\text{eq.A3.4}]$$

The error of the binding constant was then calculated by:

$$\Delta K_{a,C} = \frac{\Delta K_{a,\max} + \Delta K_{a,\min}}{2} \quad [\text{eq.A3.5}]$$

As a specific example, the value of the binding constant for the reference compound PXD by fluorescence displacement titrations was obtained by global fitting of six fluorescence displacement using a competitive binding titration function.^[34] The data was analysed twice using a binding constant for BE of $2.56 \times 10^7 \text{ M}^{-1}$ and $2.16 \times 10^7 \text{ M}^{-1}$, which gave the values shown in **Table A3.1**.

Table A3.1 Binding constants of BE used in the fitting of the fluorescence displacement titrations for determining the binding constant of PXD and its error by global fitting.

$K_{a, \text{BE}} / \times 10^7 \text{ M}^{-1}$	2.56	2.16
$K_{a, \text{PXD}} / \times 10^{10} \text{ M}^{-1}$	2.17 ± 0.18	1.79 ± 0.14

The binding constant value of the competitor PXD was then $K_{a,C} = \frac{1}{2} \times [(2.17 + 0.18) \times 10^{10} \text{ M}^{-1} + (1.79 - 0.14) \times 10^{10} \text{ M}^{-1}] = 2.00 \times 10^{10} \text{ M}^{-1}$ and the error was $\Delta K_{a,C} = 0.35 \times 10^{10} \text{ M}^{-1}$ (see also Table 1 in main text). Note that this covers the whole range of binding constants, namely the maximum binding constant $((2.17 + 0.18) \times 10^{10} \text{ M}^{-1} = 2.35 \times 10^{10} \text{ M}^{-1})$ and the minimum binding constant $((1.79 - 0.14) \times 10^{10} \text{ M}^{-1} = 1.65 \times 10^{10} \text{ M}^{-1})$.

A.3.3.4 Error Propagation and Binding Constants by Competitive NMR

A.3.3.4.1 Relative Binding Constants by Competitive NMR

K_{rel} is the ratio of the binding constants of a reference compound, $K_{a,\text{ref}}$, and a competitor, $K_{a,C}$, where $[\text{Ref}]_{\text{free}}$ is the free concentration of the reference compound, $[\text{C}]_{\text{free}}$ is the free

concentration of the competitor, and [CB7•Ref] and [CB7•C] are the concentrations of the respective CB7 complexes (eq. A4.6).

$$K_{\text{rel}} = \frac{K_{a,C}}{K_{a,\text{ref}}} = \frac{[\text{CB7}\cdot\text{C}][\text{Ref}]_{\text{free}}}{[\text{CB7}\cdot\text{Ref}][\text{C}]_{\text{free}}} \quad [\text{eq.A3.6}]$$

The concentrations can be calculated by eqs. A3.7-A3.10 using the integrated peak areas of the ¹H NMR signals of the free reference, $I_{\text{free,ref}}$, the bound reference, $I_{\text{bound,ref}}$, the bound competitor, $I_{\text{bound,C}}$, the free competitor, $I_{\text{free,C}}$, as well as the total concentrations of reference, $[\text{Ref}]_{\text{total}}$, and the competitor, $[\text{C}]_{\text{total}}$.

$$[\text{CB7} \cdot \text{Ref}] = \frac{I_{\text{bound,ref}}}{I_{\text{bound,ref}} + I_{\text{free,ref}}} \times [\text{Ref}]_{\text{total}} \quad [\text{eq.A3.7}]$$

$$[\text{Ref}]_{\text{free}} = \frac{I_{\text{free,ref}}}{I_{\text{bound,ref}} + I_{\text{free,ref}}} \times [\text{Ref}]_{\text{total}} \quad [\text{eq.A3.8}]$$

$$[\text{CB7} \cdot \text{C}] = \frac{I_{\text{bound,C}}}{I_{\text{bound,C}} + I_{\text{free,C}}} \times [\text{C}]_{\text{total}} \quad [\text{eq.A3.9}]$$

$$[\text{C}]_{\text{free}} = \frac{I_{\text{free,C}}}{I_{\text{bound,C}} + I_{\text{free,C}}} \times [\text{C}]_{\text{total}} \quad [\text{eq.A3.10}]$$

Combining equations A3.6-A3.10 gives:

$$K_{\text{rel}} = \frac{I_{\text{bound,C}} \times I_{\text{free,ref}}}{I_{\text{free,C}} \times I_{\text{bound,ref}}} \quad [\text{eq.A3.11}]$$

This procedure was repeated n times ($n \geq 3$) by evaluating different peaks in the same NMR spectrum and gave an average binding constant according to eq.A3.2 and its error as the standard deviation:

$$\Delta K_{\text{rel}} = \sqrt{\frac{\sum n(K_{\text{rel},n} - K_{\text{rel,ave}})^2}{(n-1)}} \quad [\text{eq.A3.12}]$$

In those cases, in which no well-resolved NMR signals could be obtained, the concentrations were calculated using the law of mass conservation (equations A4.13-A4.15), where $[\text{CB7}]_{\text{total}}$ is the total concentration of CB7.

$$[\text{C}]_{\text{total}} = [\text{C}]_{\text{free}} + [\text{CB7} \cdot \text{C}] \quad [\text{eq.A3.13}]$$

$$[\text{Ref}]_{\text{total}} = [\text{Ref}]_{\text{free}} + [\text{CB7} \cdot \text{Ref}] \quad [\text{eq.A3.14}]$$

$$[\text{CB7}]_{\text{total}} = [\text{CB7} \cdot \text{C}] + [\text{CB7} \cdot \text{Ref}] \quad [\text{eq.A3.15}]$$

A.3.3.4.2 Absolute Binding Constants by Competitive NMR

With the known binding constant of the reference compound, the absolute binding constant of the competitor was then calculated by rearranging eq.A3.6, which gives eq.A3.16:

$$K_{a,C} = K_{rel} \times K_{a,ref} \quad [\text{eq.A3.16}]$$

The respective error was calculated using standard rules of error propagation (see eqs. A3.1 and 16), which gave eq.A3.17, where $\Delta K_{a,ref}$ is the error of $K_{a,ref}$ (obtained as described in Appendix 3.1), and $\Delta K_{a,C}$ is the resulting error of $K_{a,C}$.^[225]

$$\Delta K_{a,C} = \sqrt{K_{rel}^2 \times (\Delta K_{a,ref})^2 + K_{a,ref}^2 \times (\Delta K_{rel})^2} \quad [\text{eq.A3.17}]$$

Eq. A3.17 is then combined with eq.A3.16 to give eq.A3.18:

$$\Delta K_{a,C} = K_{a,C} \times \sqrt{\left(\frac{\Delta K_{a,ref}}{K_{a,ref}}\right)^2 + \left(\frac{\Delta K_{rel}}{K_{rel}}\right)^2} \quad [\text{eq.A3.18}]$$

A.3.3.4.3 Example of Binding Constant and Error Determinations by NMR

To obtain the relative affinity of different CB7 guest pairs, we measured the concentrations of each of the CB7•guest complexes and the concentration of each free guest. The concentration of CB7 is limiting quantity for all measurements. From eqs. A3.7-A3.10 and A3.13-A3.15, it becomes apparent that the equilibrium concentrations of all species can be individually calculated after integrating the relevant peaks. Within experimental restrictions, e.g. limited compound solubility or complex precipitation, the ratio of the integrated peak areas could be adjusted to easily integratable values by carefully selecting the concentrations of the reference and the competing guest.

As an example, we provide in the following details on the determination of the binding constant and its error of BE using Put as a reference compound. From eq.A3.16, we obtain in this case eq.A3.19:

$$K_{rel} = \frac{K_{a,BE}}{K_{a,Put}} = \frac{[\text{CB7} \cdot \text{BE}][\text{Put}]}{[\text{BE}][\text{CB7} \cdot \text{Put}]} \quad [\text{eq.A3.19}]$$

Using the law of mass conservation:

$$[\text{Put}] = [\text{Put}]_{\text{tot}} - [\text{CB7} \cdot \text{Put}] \quad [\text{eq.A3.20}]$$

and

$$[\text{CB7} \cdot \text{Put}] = [\text{CB7}]_{\text{tot}} - [\text{CB7} \cdot \text{BE}] \quad [\text{eq.A3.21}]$$

gives

$$K_{rel} = \frac{[\text{CB7} \cdot \text{BE}]([\text{Put}]_{\text{tot}} - [\text{CB7}]_{\text{tot}} + [\text{CB7} \cdot \text{BE}])}{[\text{BE}]([\text{CB7}]_{\text{tot}} - [\text{CB7} \cdot \text{BE}])} \quad [\text{eq.A3.22}]$$

The concentration of the CB7/BE complex can be determined by eq.A3.9, in which BE is the competitor, which gives

$$[\text{CB7} \bullet \text{BE}] = \frac{I_{\text{CB7} \bullet \text{BE}}}{I_{\text{CB7} \bullet \text{BE}} + I_{\text{BE}}} [\text{BE}] \quad [\text{eq.A3.23}]$$

Four K_{rel} values were then obtained for each measured spectrum (see Tables S2-S4) by using the integrated peak areas of the peaks labelled as 1 ($= I_{\text{BE}}$) and 1' ($= I_{\text{CB7} \bullet \text{BE}}$), 2 ($= I_{\text{BE}}$) and 2' ($= I_{\text{CB7} \bullet \text{BE}}$), 3 ($= I_{\text{BE}}$) and 3' ($= I_{\text{CB7} \bullet \text{BE}}$), and 5+11 ($= I_{\text{BE}}$) and 5'+11' ($= I_{\text{CB7} \bullet \text{BE}}$). The K_{rel} value and its error for each spectrum was then calculated as the average (eq.A3.2) and standard deviation (eq.A3.12) of these four K_{rel} values.

Table A3.2 Integrated peak areas of the proton signals used to calculate K_{rel} of BE against Put (Measurement No. 1, refers to the NMR spectrum shown in Figure 2 in the main text). $K_{\text{rel}} = 12.50 \pm 0.57$.

Proton signal used	$I_{\text{free,C}}$	$I_{\text{bound,C}}$	K_{rel}
5 + 11	0.62	0.12	12.74
2	0.31	0.61	13.16
1	0.62	1.16	11.91
3	0.64	1.21	12.16

Table A3.3 Integrated peak areas of the proton signals used to calculate K_{rel} of BE against Put (Measurement No. 2, spectrum not shown). $K_{\text{rel}} = 13.25 \pm 1.54$.

Proton signal used	$I_{\text{free,C}}$	$I_{\text{bound,C}}$	K_{rel}
5 + 11	0.64	1.12	13.91
2	0.32	0.49	11.02
1	0.63	1.08	13.53
3	0.64	1.14	14.52

Table A3.4 Integrated peak areas of the proton signals used to calculate K_{rel} of BE against Put (Measurement No. 3, spectrum not shown). $K_{\text{rel}} = 13.82 \pm 0.71$.

Proton signal used	$I_{\text{free,C}}$	$I_{\text{bound,C}}$	K_{rel}
5 + 11	0.64	1.04	13.7
2	0.34	0.52	13.7
1	0.69	1.03	13.1
3	0.67	1.07	14.8

Then, the average of the K_{rel} values of all three spectra was calculated by eq.A3.2, which gave $K_{\text{rel}} = 13.18$ and the error by eq.A3.3, which gave $\Delta K_{\text{rel}} = 0.60$. This was then converted (eq.A3.16 and A3.18) into the absolute binding constant of BE by competitive NMR, $K_{\text{a,BE}} = (2.40 \pm 0.22) \times 10^7 \text{ M}^{-1}$

A.3.5 Berberine Chloride (BE)

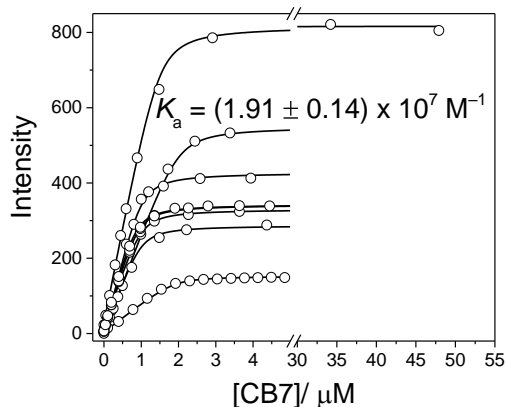


Figure A3.1 Fluorescence titration plots ($\lambda_{\text{ex}} = 420 \text{ nm}$; $\lambda_{\text{em}} = 490 \text{ nm}$) of different BE concentrations (1-2 μM) upon addition of CB7 at pH 7.0. The data was obtained by different individuals in our lab during the previous years with different commercial and self-synthesized CB7 batches. Herein, the data is re-evaluated by a global fitting procedure, which provides the best fit to all titrations as well as the respective error.

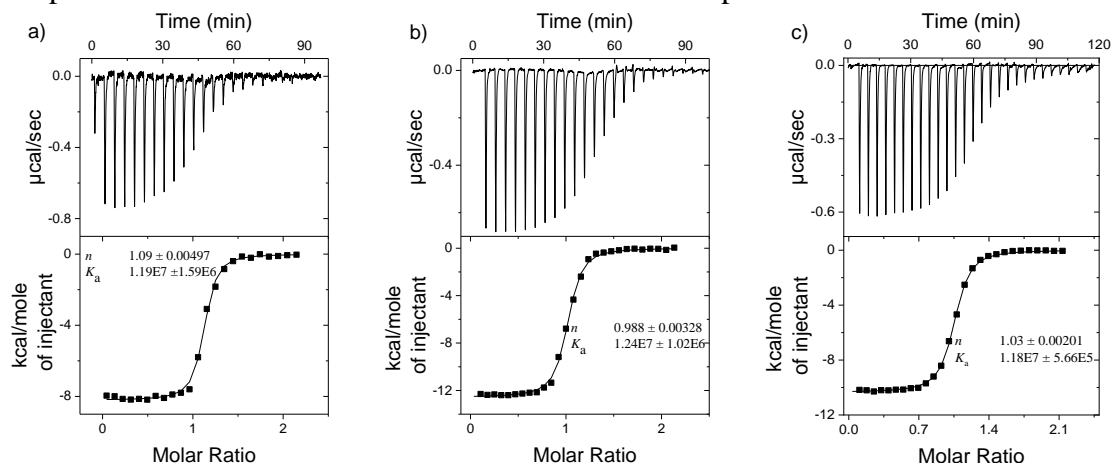


Figure A3.2 ITC titration isotherms of varying CB7 concentrations (14 μM (a), 20 μM (b), and 15 μM (c)) upon addition of BE in H_2O , pH 7.0 at 25 $^\circ\text{C}$.

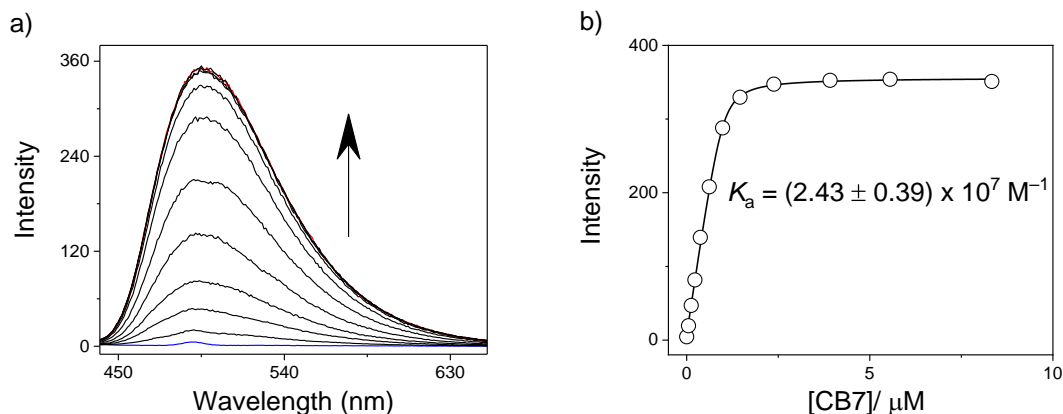


Figure A3.3 a) Fluorescence spectral changes ($\lambda_{\text{ex}} = 420 \text{ nm}$) of 1.0 μM BE upon addition of CB7 at pH 7.0 in water distilled from KMnO_4 . b) Respective titration plot ($\lambda_{\text{em}} = 490 \text{ nm}$).

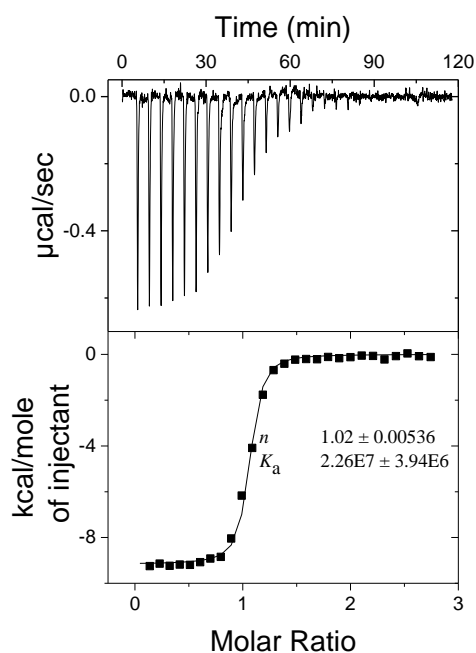


Figure A3.4 ITC isotherms on complexation of 14 μ M CB7 with BE measured in water distilled from KMnO_4 , pH 7.0, 25 $^\circ\text{C}$.

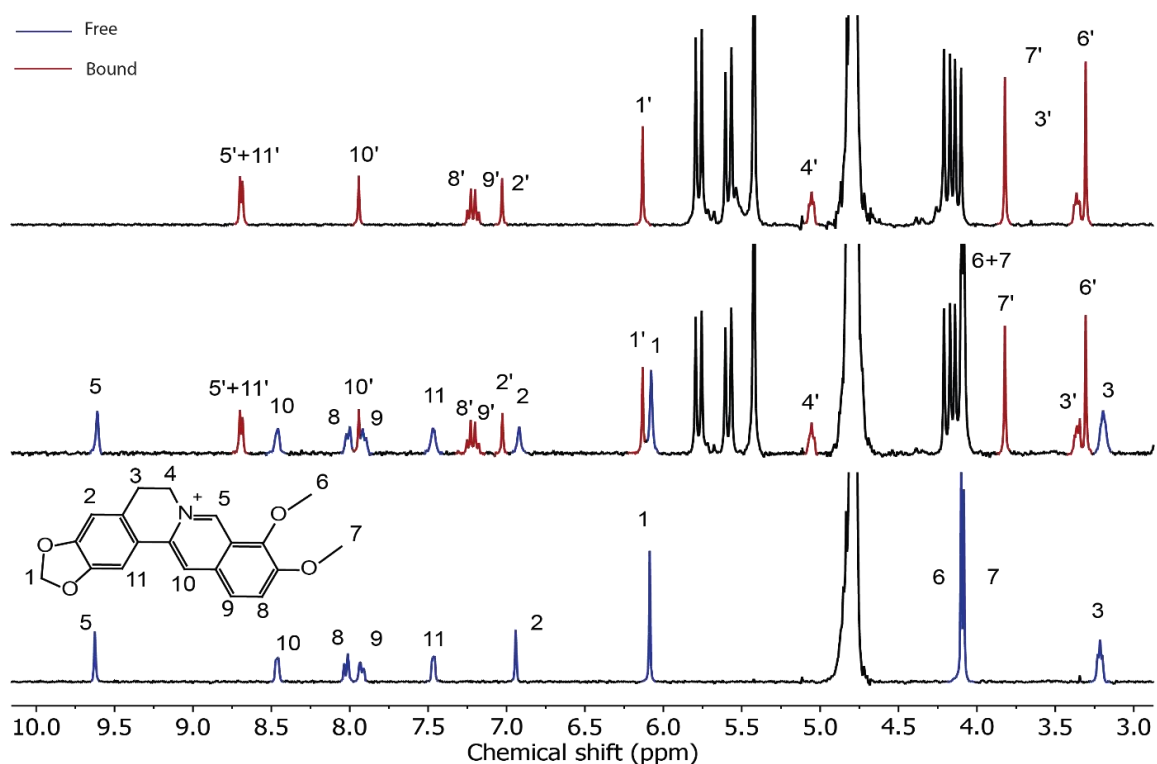


Figure A3.5 ^1H NMR spectra of 2 mM BE (bottom), 1 mM BE with 0.5 mM CB7 (middle), and 1 mM BE with 1 mM CB7 (top).

A.3.6 Hexamethylenediamine (HMD)

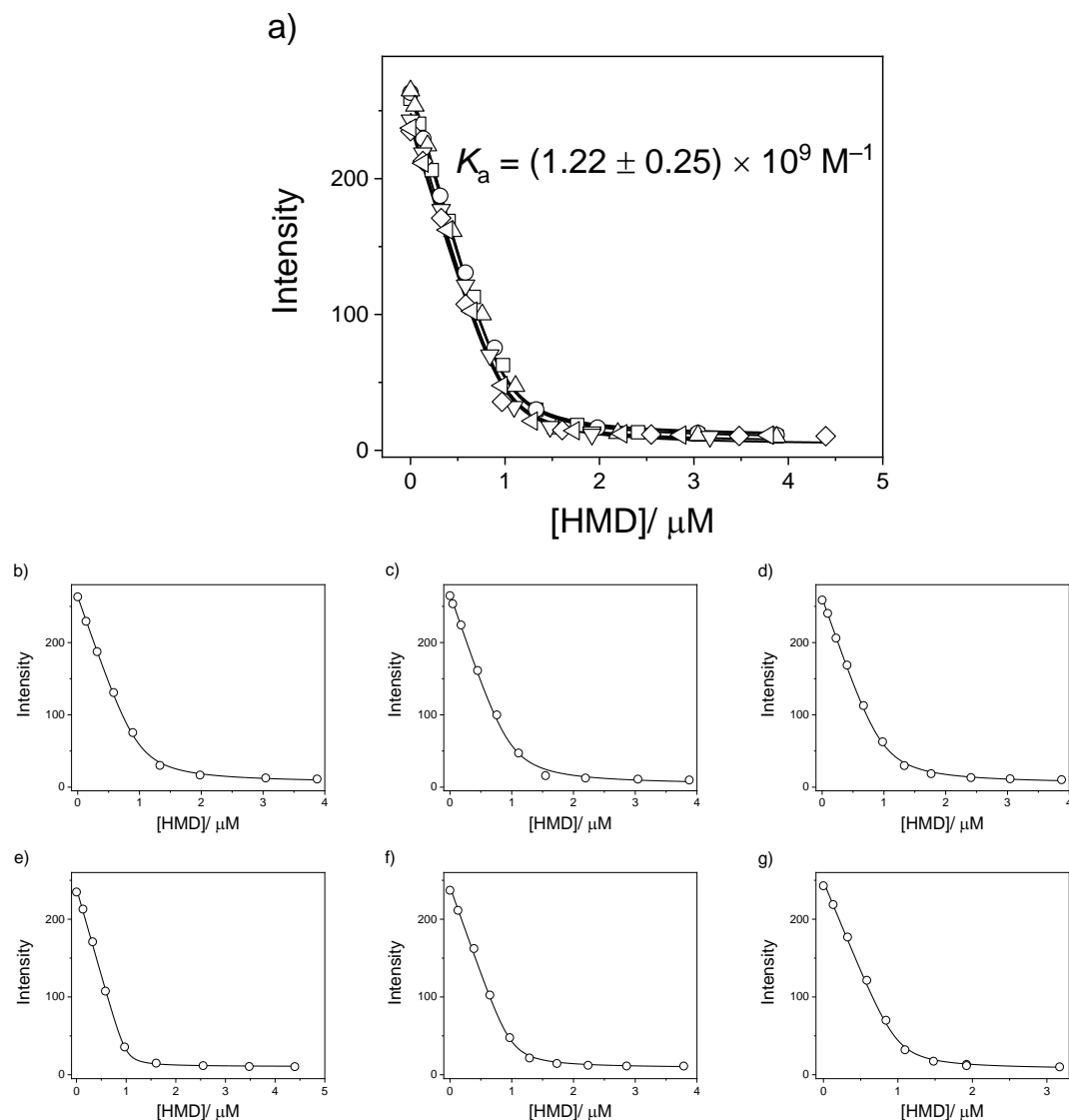


Figure A3.6 a) 1:1 Global fitting of the titration plots shown in Panels b-g. b-g) Titration plots obtained from the fluorescence spectral changes ($\lambda_{\text{ex}} = 420 \text{ nm}$, $\lambda_{\text{em}} = 490 \text{ nm}$) of $2.0 \mu\text{M}$ BE and $1.0 \mu\text{M}$ CB7 upon addition of HMD at pH 7.0 using Millipore water in b), c), and d), water distilled from KMnO_4 in e), f), and g). Note that the shape of the titration curves was independent on the type of water used. Consequently, the global fitting (Panel a) included data with both types of water, but used the reference K_a value of BE in water distilled from KMnO_4 (see also main text).

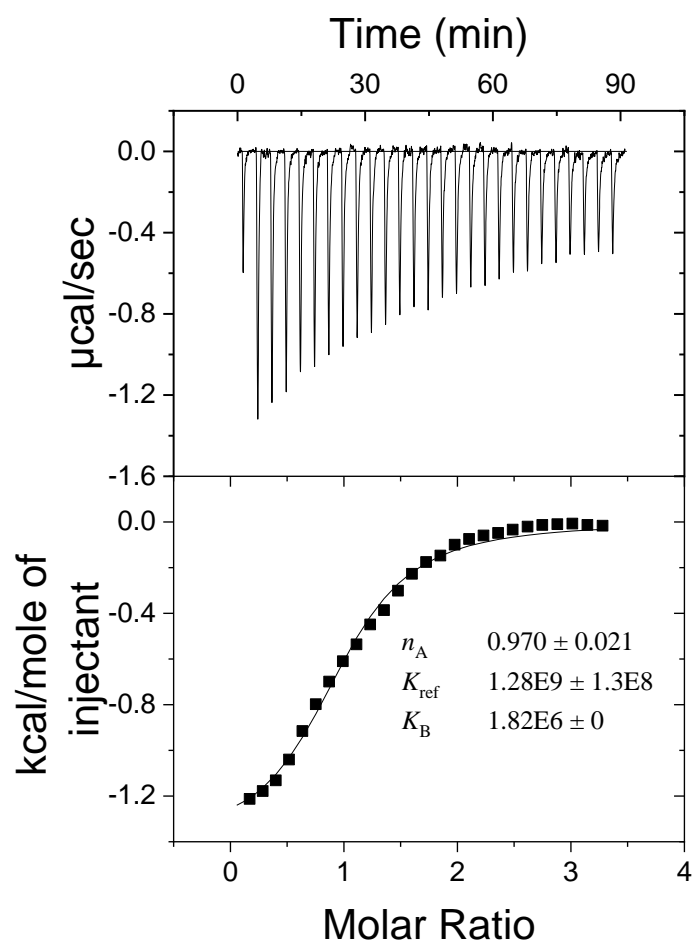


Figure A3.7 Competition ITC isotherms on complexation of 100 μM CB7 with HMD in the presence of 10 mM Put in H_2O , pH 7.0 at 25 $^\circ\text{C}$.

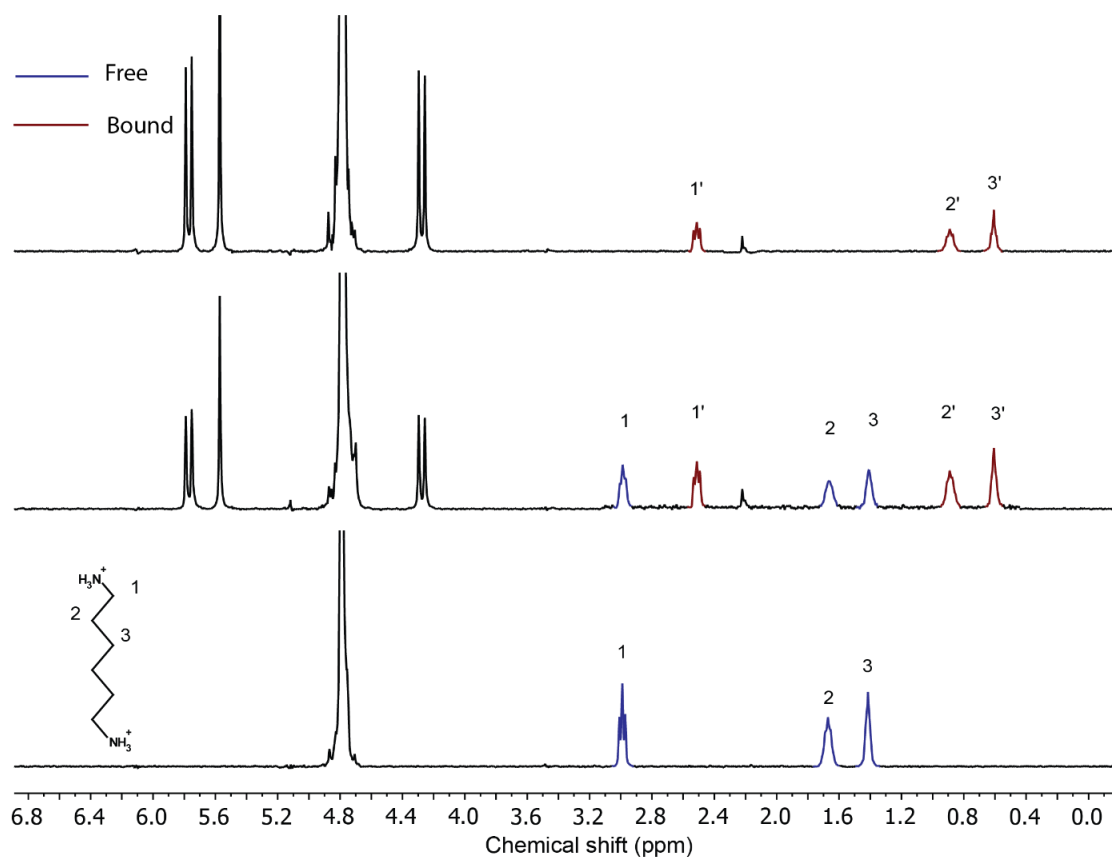


Figure A3.8 ^1H NMR spectra for 2 mM HMD (bottom), 1 mM HMD with 0.5 mM CB7 (middle), and 1 mM HMD with 1 mM CB7 (top).

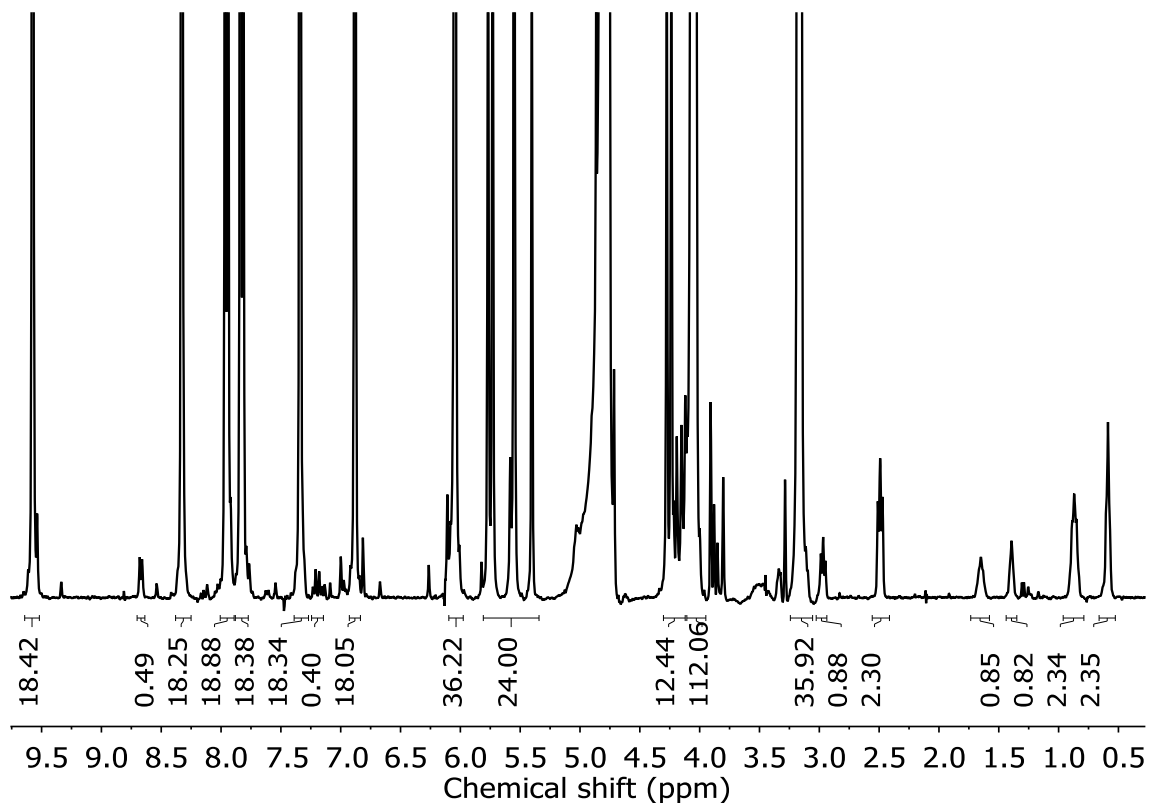


Figure A3.9 ^1H NMR spectra used to determine the K_{rel} for **BE**•CB7 and **HMD**•CB7 in D_2O at pD 7.4. Concentrations were 2 mM BE, 100 μM HMD and 100 μM CB7.

A.3.7 *p*-Xylylenediamine (PXD)

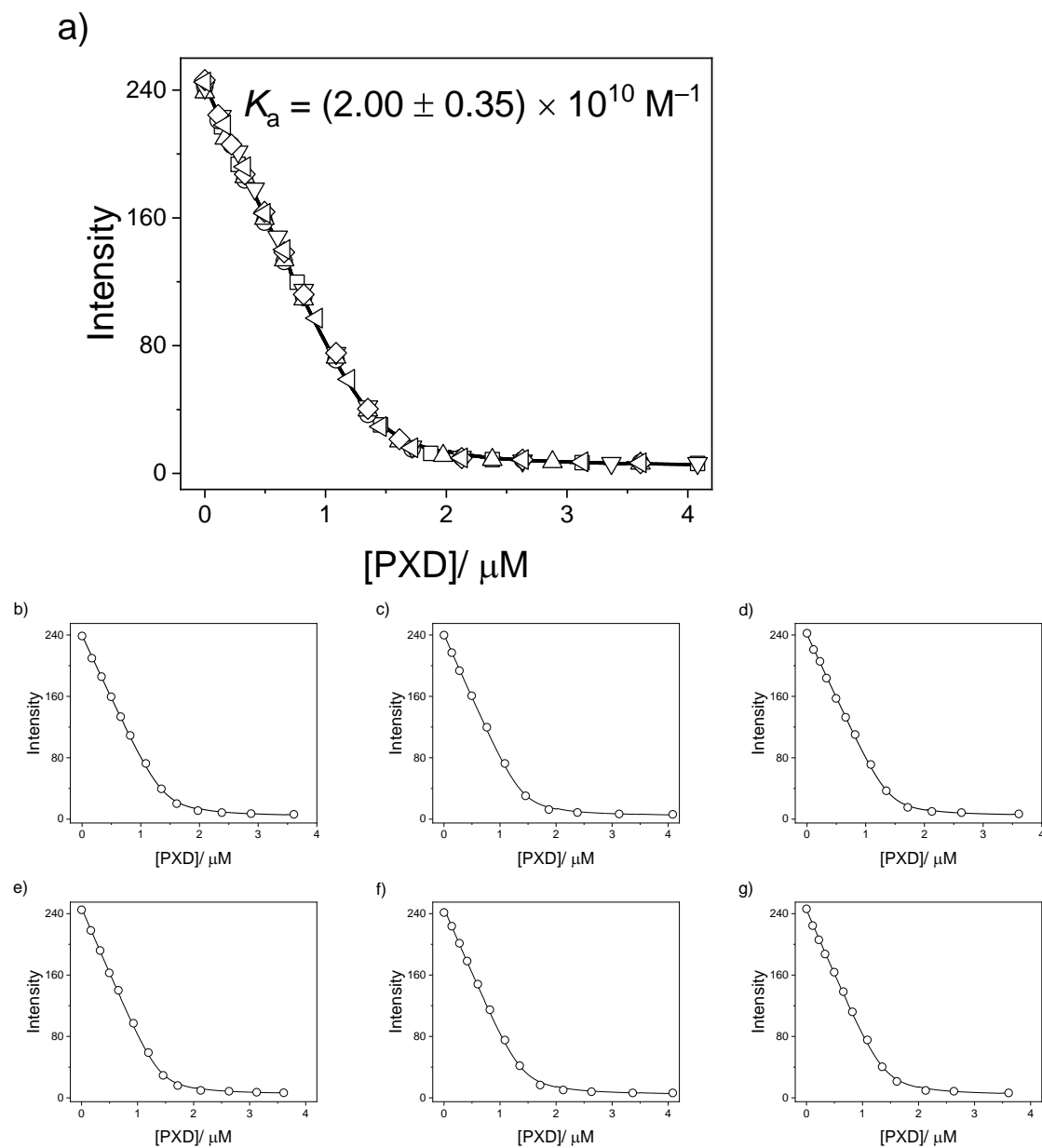


Figure A3.10 a) Global fitting of the titration plots shown in Panels b-g. b-g) Titration plots obtained from the fluorescence spectral changes ($\lambda_{\text{ex}} = 420 \text{ nm}$, $\lambda_{\text{em}} = 490 \text{ nm}$) of $25.0 \text{ } \mu\text{M}$ BE and $1.4 \text{ } \mu\text{M}$ CB7 upon addition of PXD at pH 7.0. Millipore water was used in b), c) and d), and water distilled from KMnO_4 in e), f) and g).

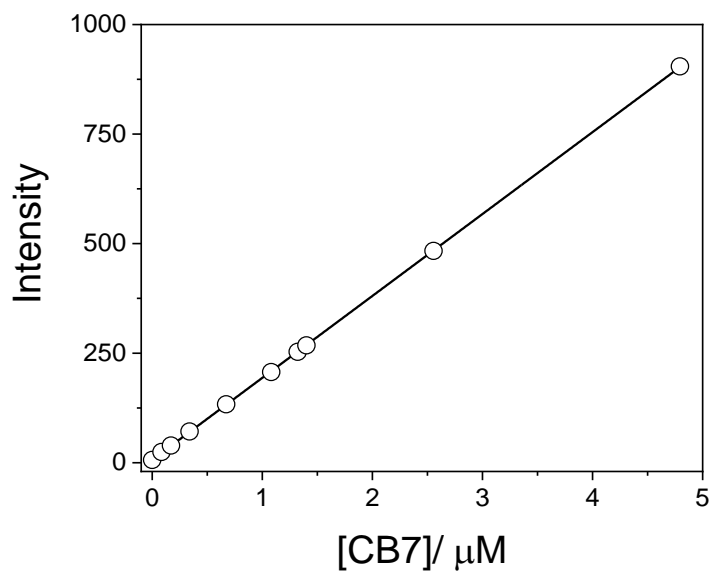


Figure A3.11 Linear response of the fluorescence intensity of 25 μM BE in a 10 \times 4 mm quartz glass cuvette towards CB7 addition.

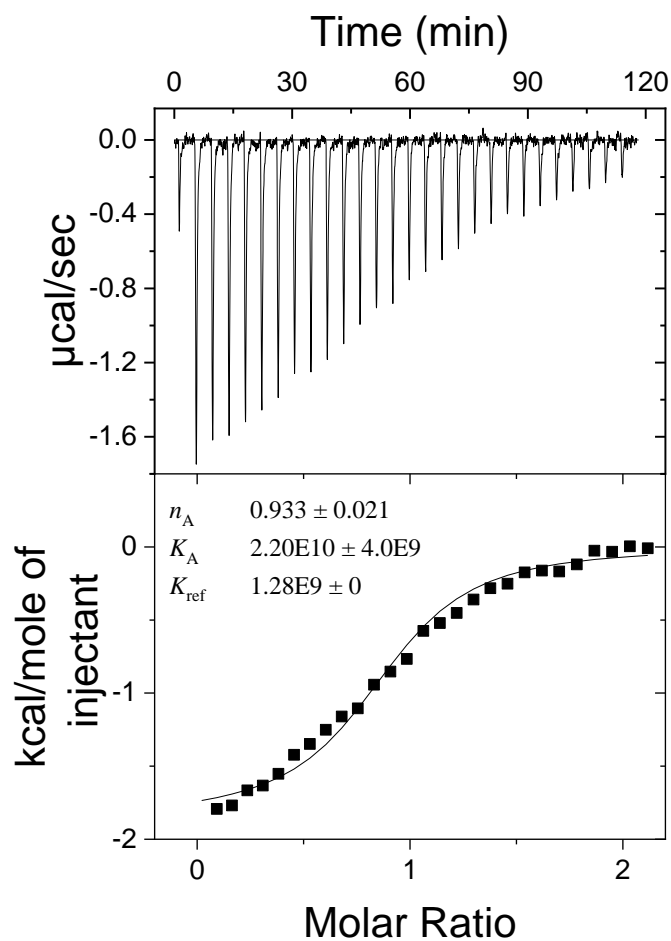


Figure A3.12 Competition ITC isotherms on complexation of 250 μM CB7 with PXD in the presence of 250 μM HMD in H_2O , pH 7.0 at 25 $^\circ\text{C}$.

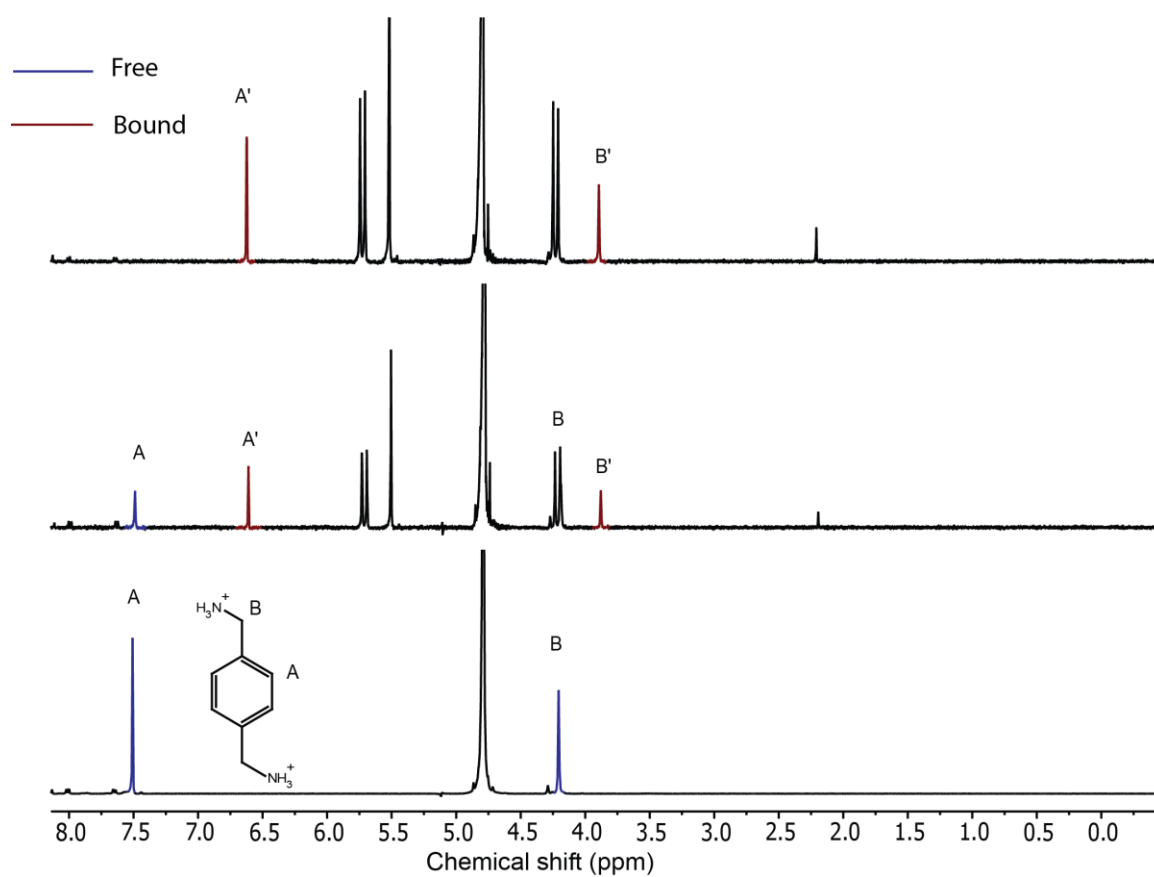


Figure A3.13 ^1H NMR spectra for 2 mM PXD (bottom), 1 mM PXD with 0.5 mM CB7 (middle), and 1 mM PXD with 1 mM CB7 (top).

A.3.8 Putrescine (Put)

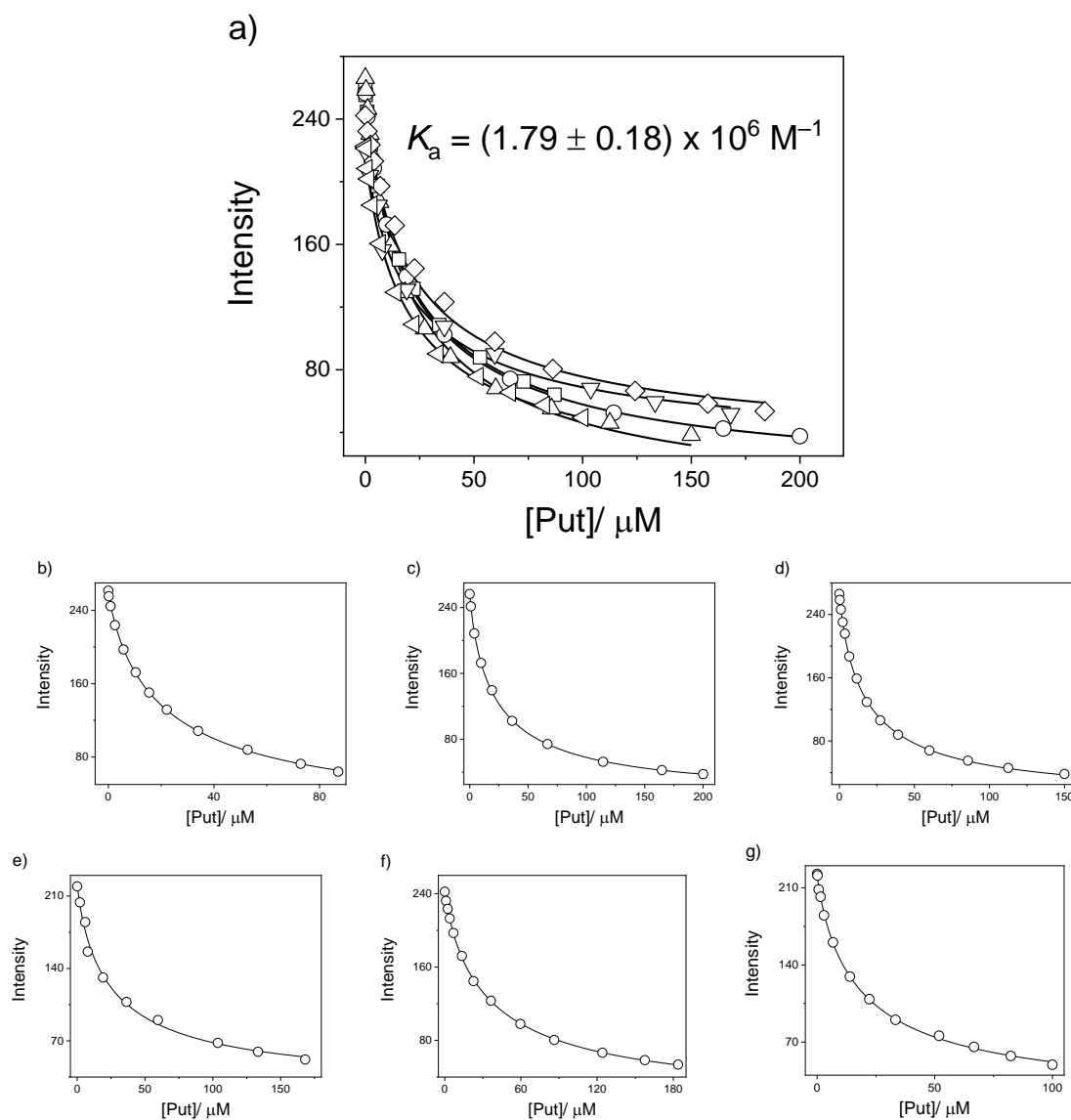


Figure A3.14 Global fitting of titration plots obtained from the fluorescence spectral changes ($\lambda_{\text{em}} = 490$, $\lambda_{\text{ex}} = 420$ nm nm) of 2.0 μM BE and 1.0 μM CB7 upon addition of Put at pH 7.0 using Millipore water and water distilled from KMnO_4 .

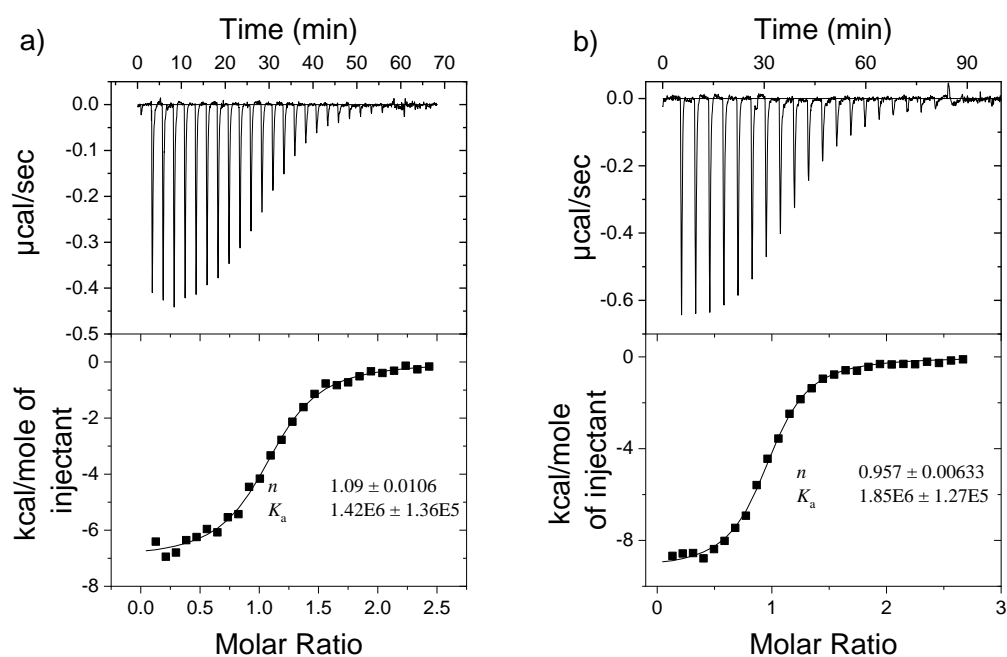


Figure A3.15 ITC isotherms on complexation of Put with a) 16 μM CB7 in Millipore water b) 20 μM CB7 in water distilled from KMnO_4 , at pH 7.0, 25 $^\circ\text{C}$.

A.3.9 Tetrabutylammonium Chloride (TBA)

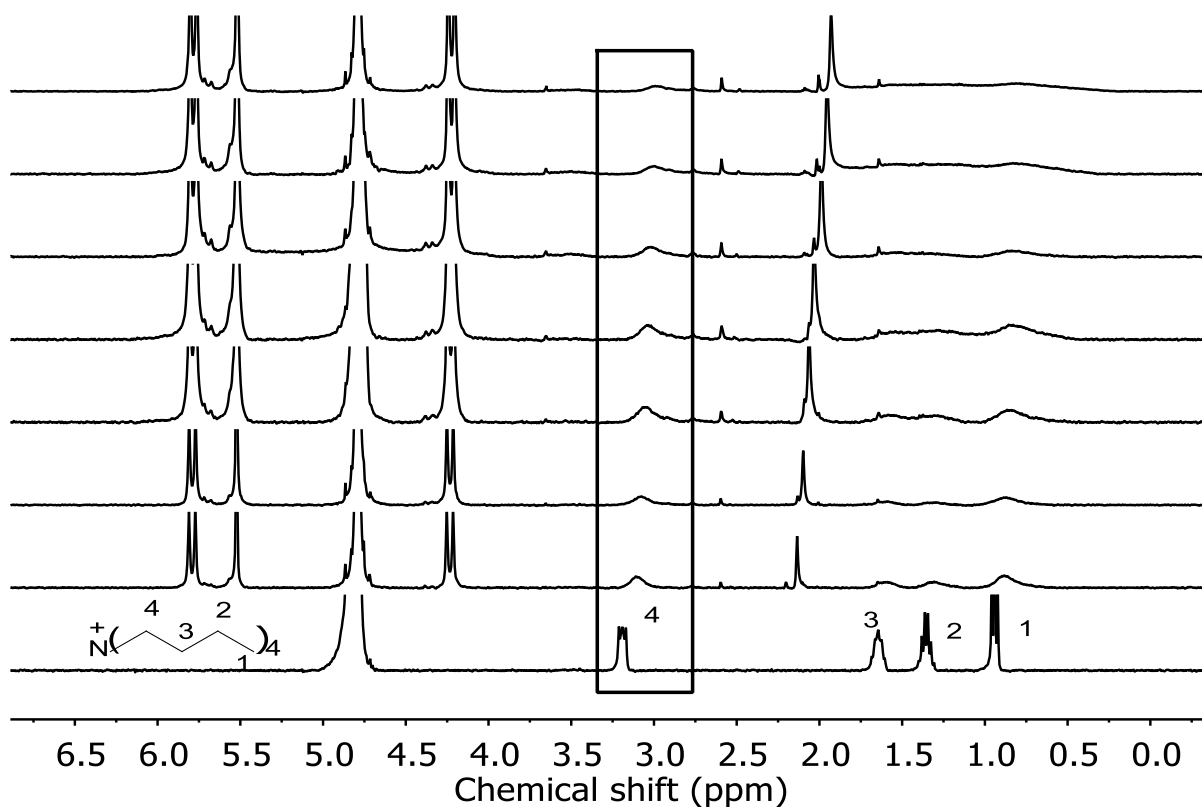


Figure A3.16 ^1H NMR titration spectra for 300 μM TBA with different (See **Figure A3.17**) CB7 concentrations at pD 7.4.

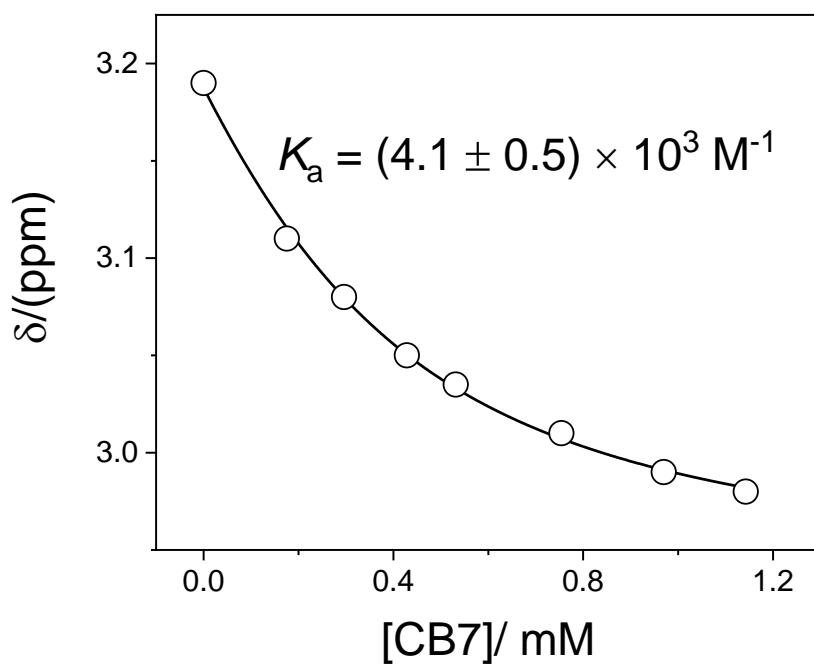


Figure A3.17 ^1H NMR chemical shift changes of the TBA proton signal (300 μM) at $\delta = 3.19$ ppm upon addition of CB7 at pD 7.4.

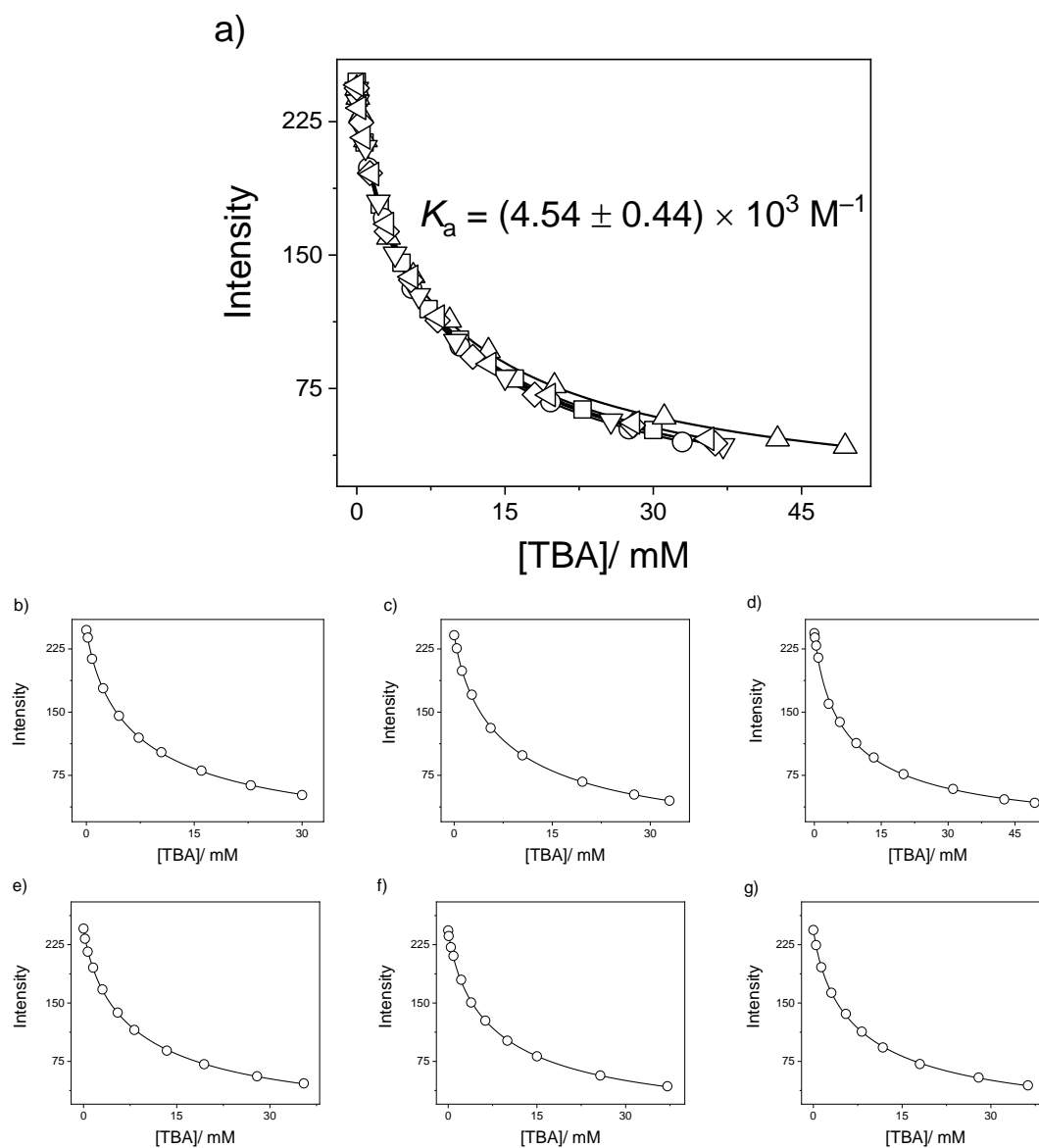


Figure A3.18 1:1 Global fitting of titration plots obtained from the fluorescence spectral changes ($\lambda_{em} = 490$, $\lambda_{ex} = 420$ nm nm) of $1.8 \mu\text{M}$ BE and $1.0 \mu\text{M}$ CB7 upon addition TBA at pH 7.0 using Millipore water and water distilled from KMnO_4 .

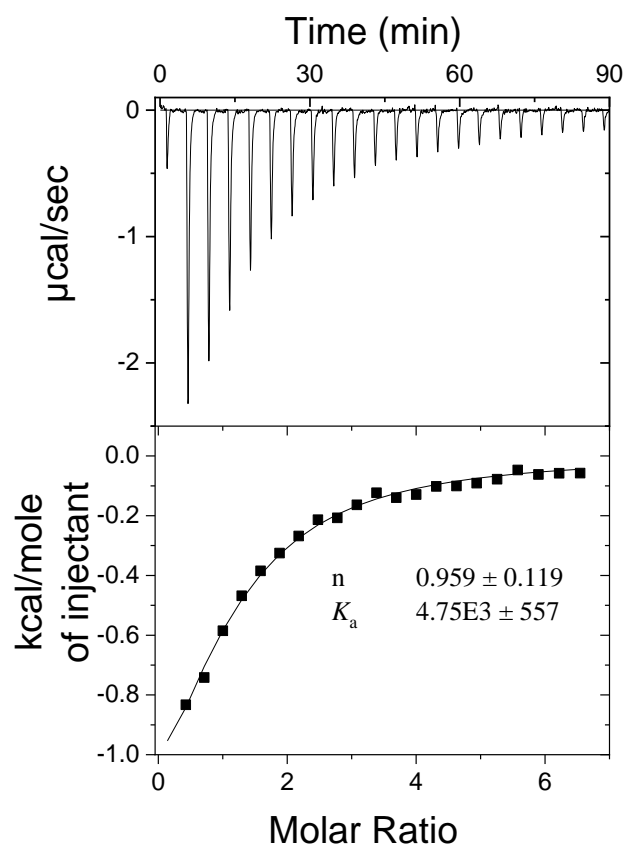


Figure A3.19 . ITC isotherms on complexation of 200 μM CB7 with TBA measured in H_2O pH 7.0, 25 $^\circ\text{C}$.

A.3.10 Cyclohexylmethylamine (CHMA)

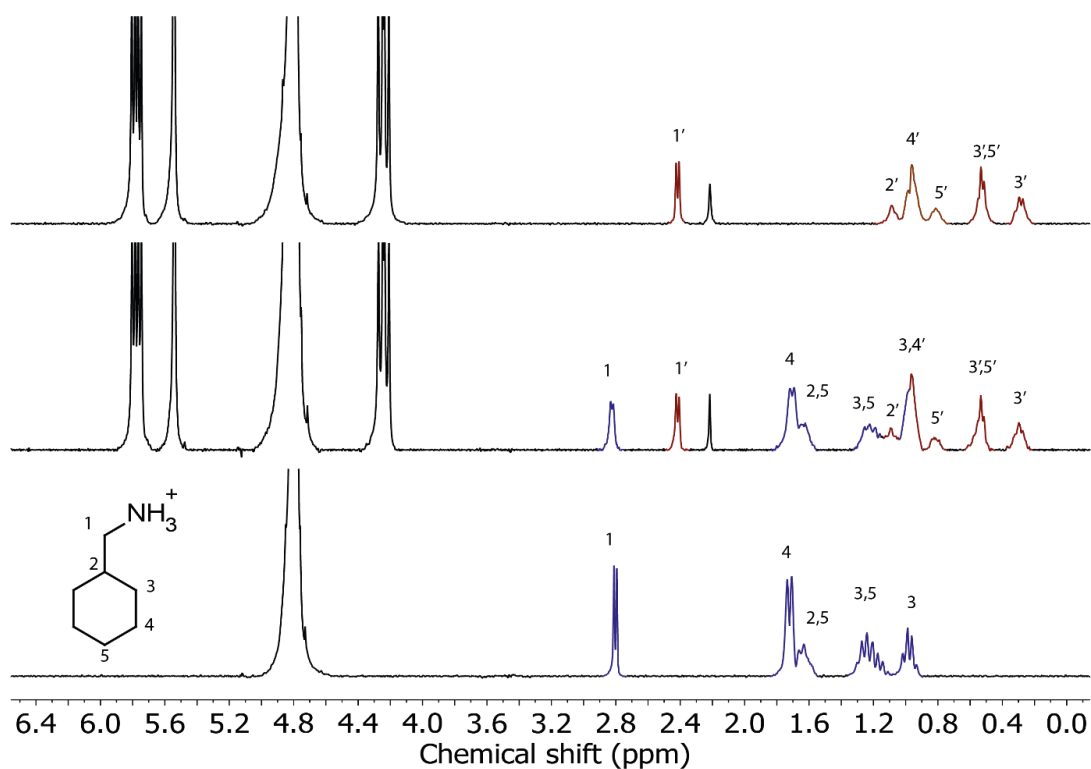


Figure A3.20 ^1H NMR spectra for 2 mM CHMA free (bottom), 1 mM CHMA with 0.5 mM CB7 (middle), and 1 mM CHMA with 1 mM CB7 (top).

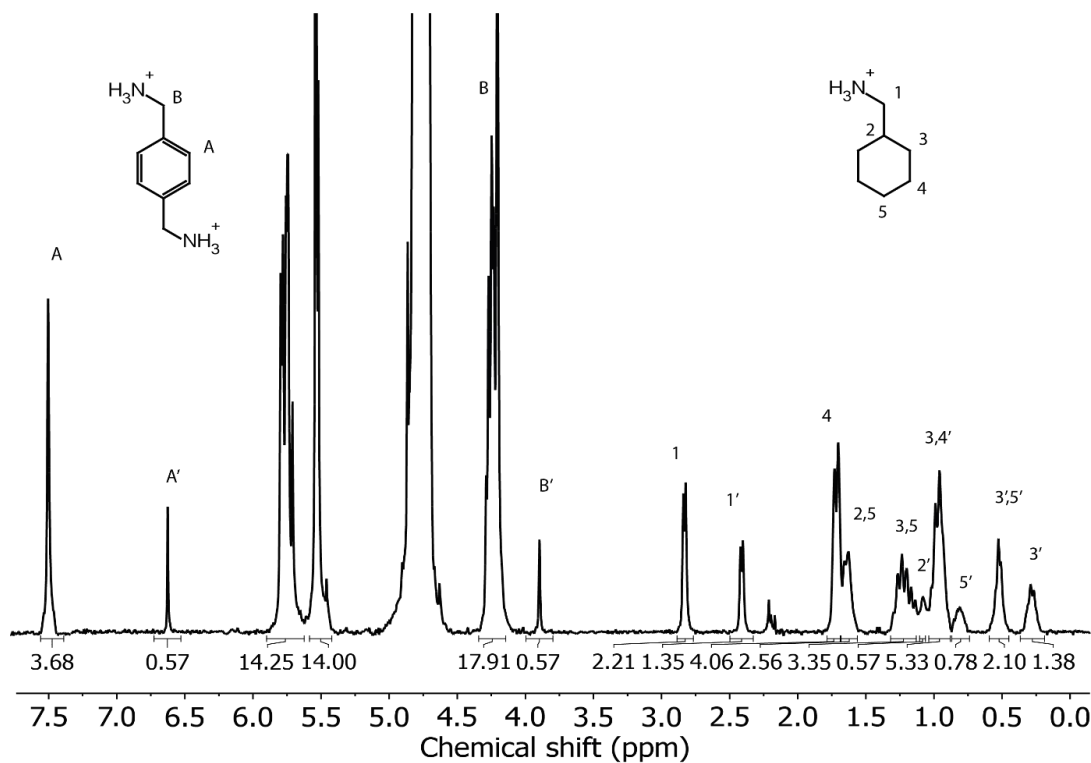


Figure A3.21 ^1H NMR spectra used to determine the K_{rel} for PXD•CB7 and CHMA•CB7 in D_2O at pD 7.4. Concentrations were 1.10 mM PXD, 1.86 mM CHMA and 1 mM CB7.

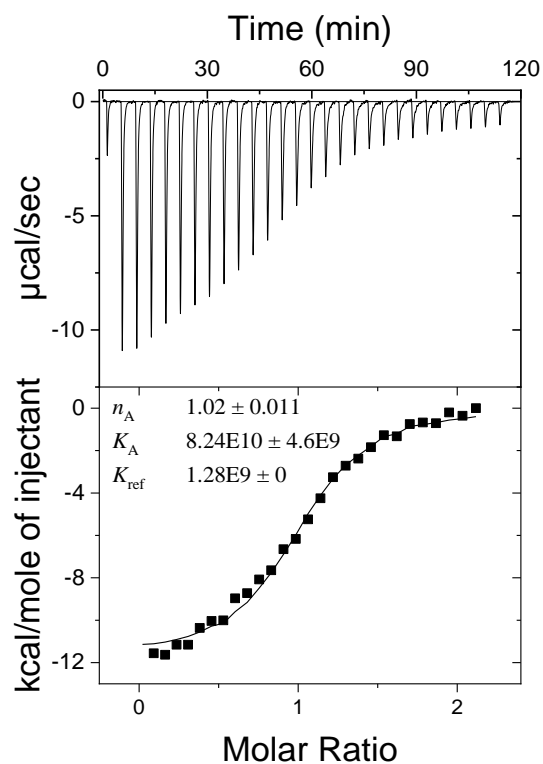


Figure A3.22 Competition ITC isotherms on complexation of 250 μ M CB7 with CHMA in the prescnce of 1.0 mM HMD in H₂O, pH 7.0, 25 $^{\circ}$ C.

A.3.11 *Cis*-1,4-Bis(aminomethyl)-cyclohexane (CBAMC)

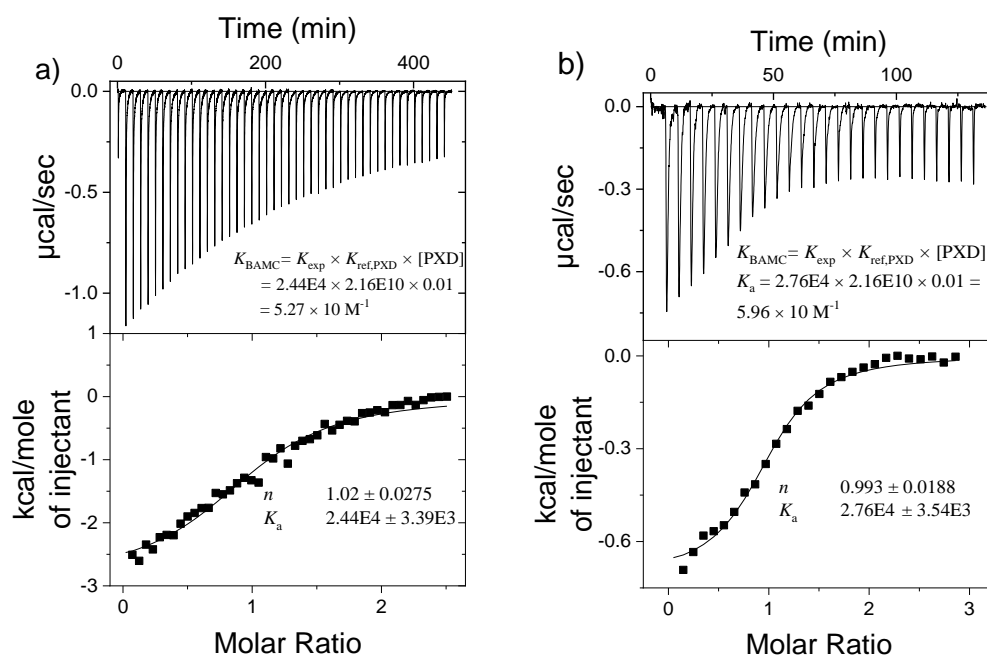


Figure A3.23 Competition ITC experiments on complexation of a) 0.25 mM and b) 0.20 mM CB7 with CBAMC with in the presence of 10 mM PXD at pH 7.0, 25 °C.

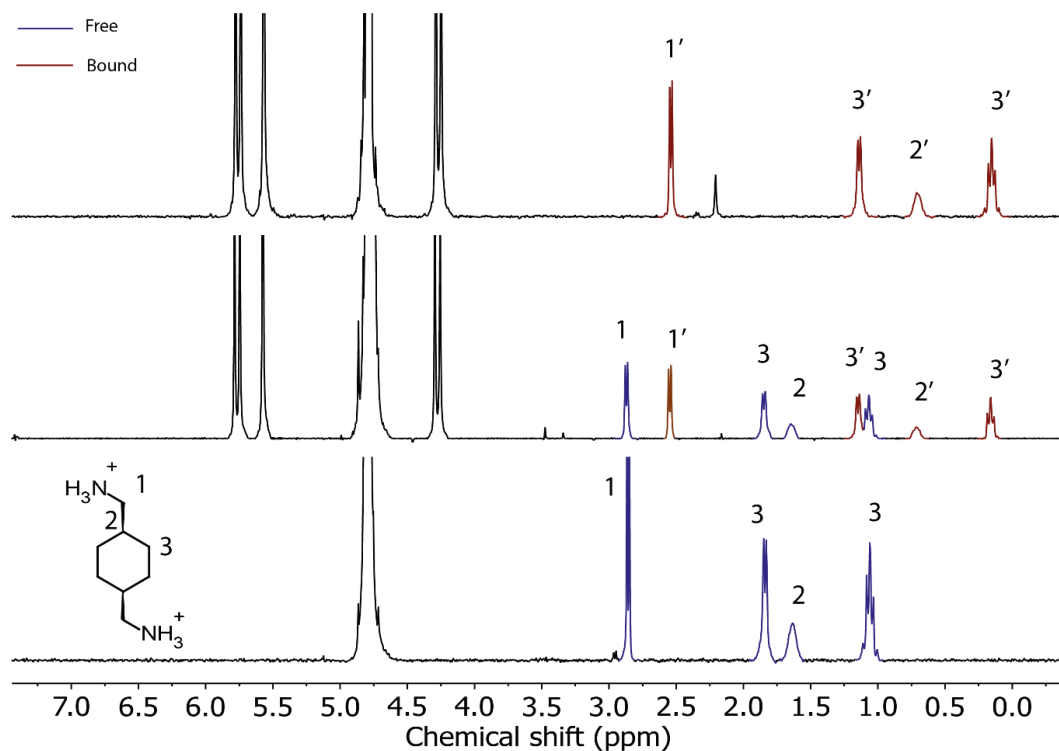


Figure A3.24 ^1H NMR spectra for 2 mM CBAMC free (bottom), 1 mM CBAMC with 0.5 mM CB7 (middle), and 1 mM CBAMC with 1 mM CB7 (top).

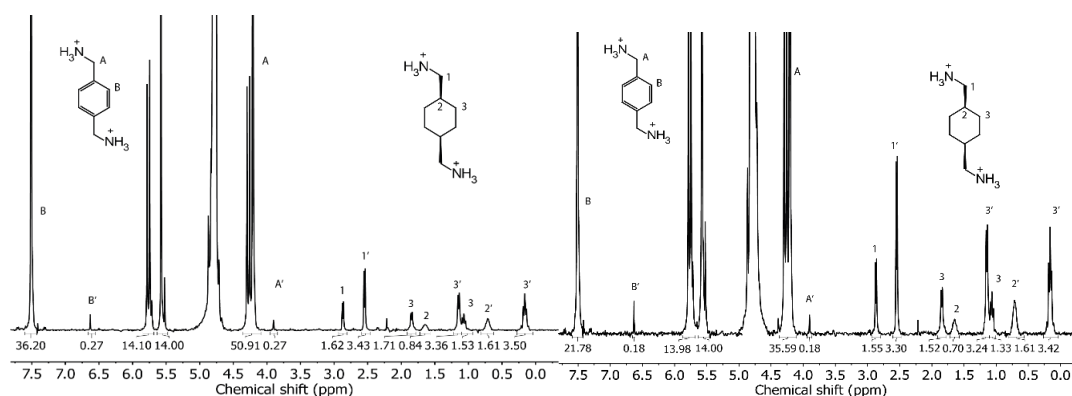


Figure A3.25 ^1H NMR spectra used to determine the K_{rel} for $\text{PXD}\cdot\text{CB7}$ and $\text{CBAMC}\cdot\text{CB7}$ in D_2O at pD 7.4. Concentrations were a) 9.2 mM PXD, 1.26 mM CBAMC and 1 mM CB7, b) 5.49 mM PXD, 1.21 mM CBAMC and 1 mM CB7

A.3.12 (2,3-Diazabicyclo[2.2.2]oct-2-enyl) Methylamine (DBO-A)

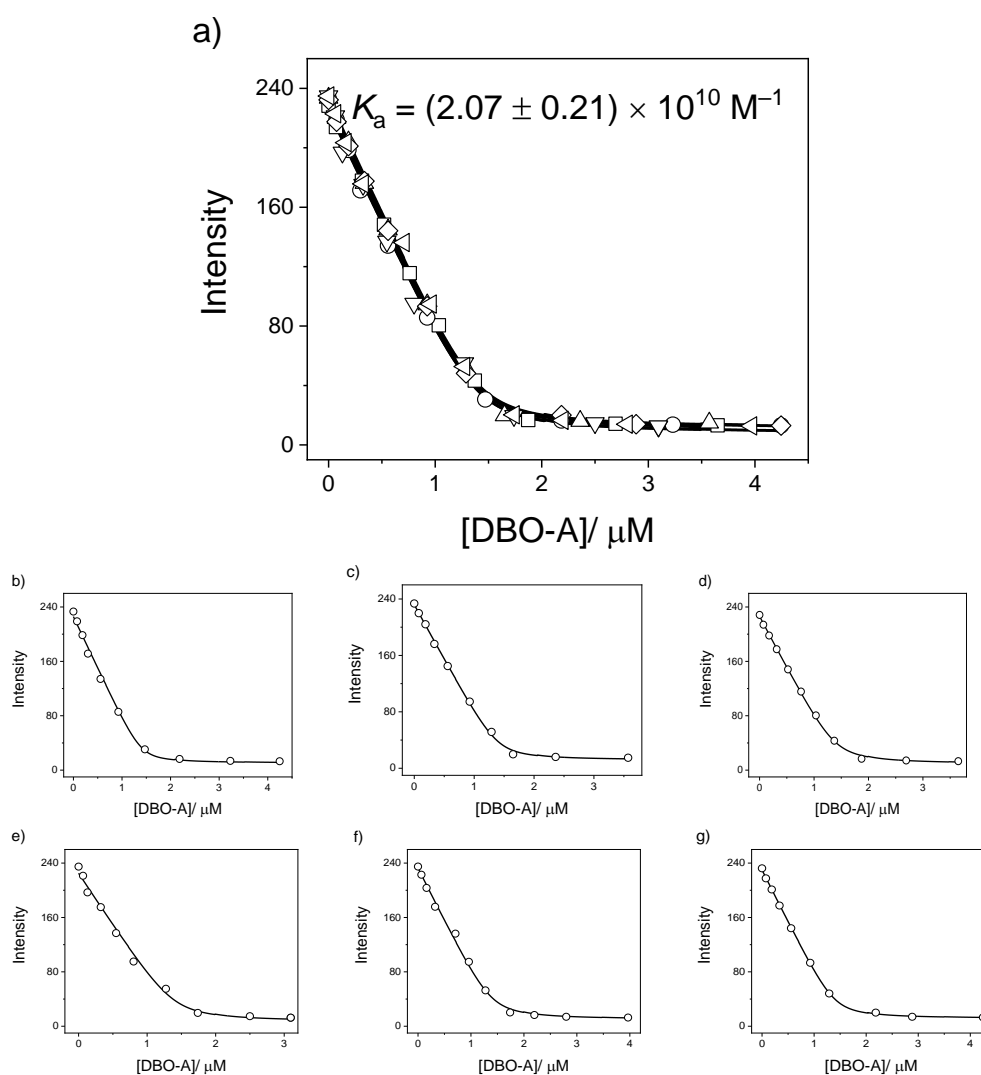


Figure A3.26 a) Global fitting of the titration plots shown in Panels b-g. b-g) Titration plots obtained from the fluorescence spectral changes ($\lambda_{\text{ex}} = 420 \text{ nm}$, $\lambda_{\text{em}} = 490 \text{ nm}$) of $25.0 \text{ } \mu\text{M}$ BE and $1.4 \text{ } \mu\text{M}$ CB7 upon addition of DBO-A at pH 7.0 in Millipore water in b), c) and d), and in water distilled from KMnO_4 in e), f) and g).

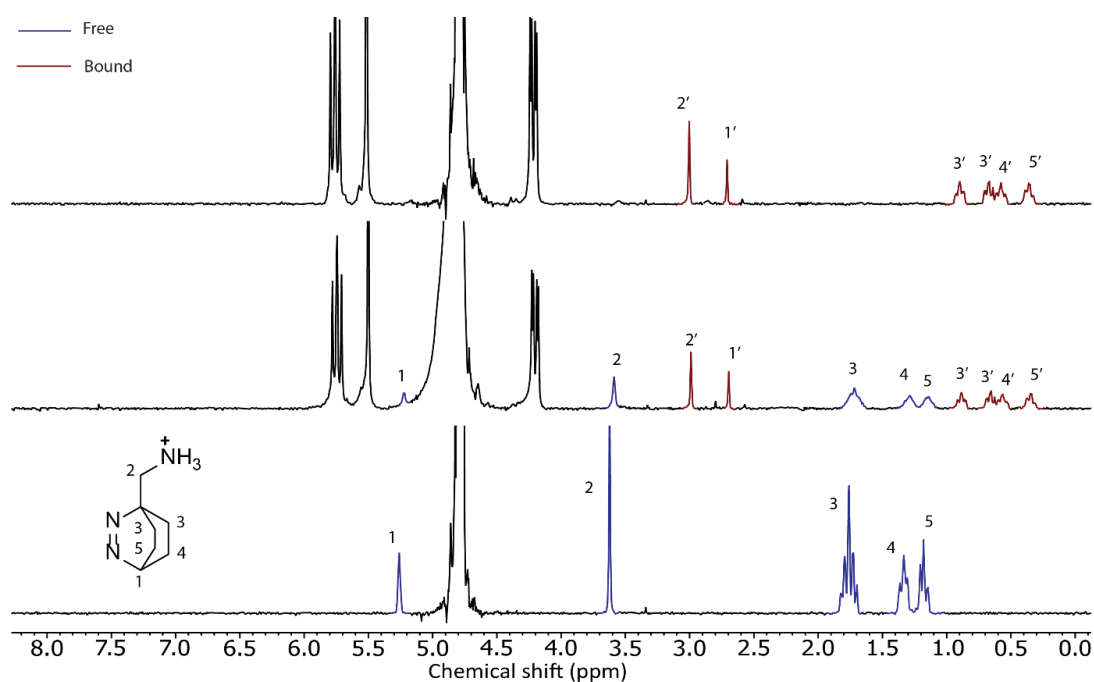


Figure A3.27 ^1H NMR spectra for 2 mM DBO-A (bottom), 1 mM DBO-A with 0.5 mM CB7 (middle), and 1 mM DBO-A with 1 mM CB7 (top).

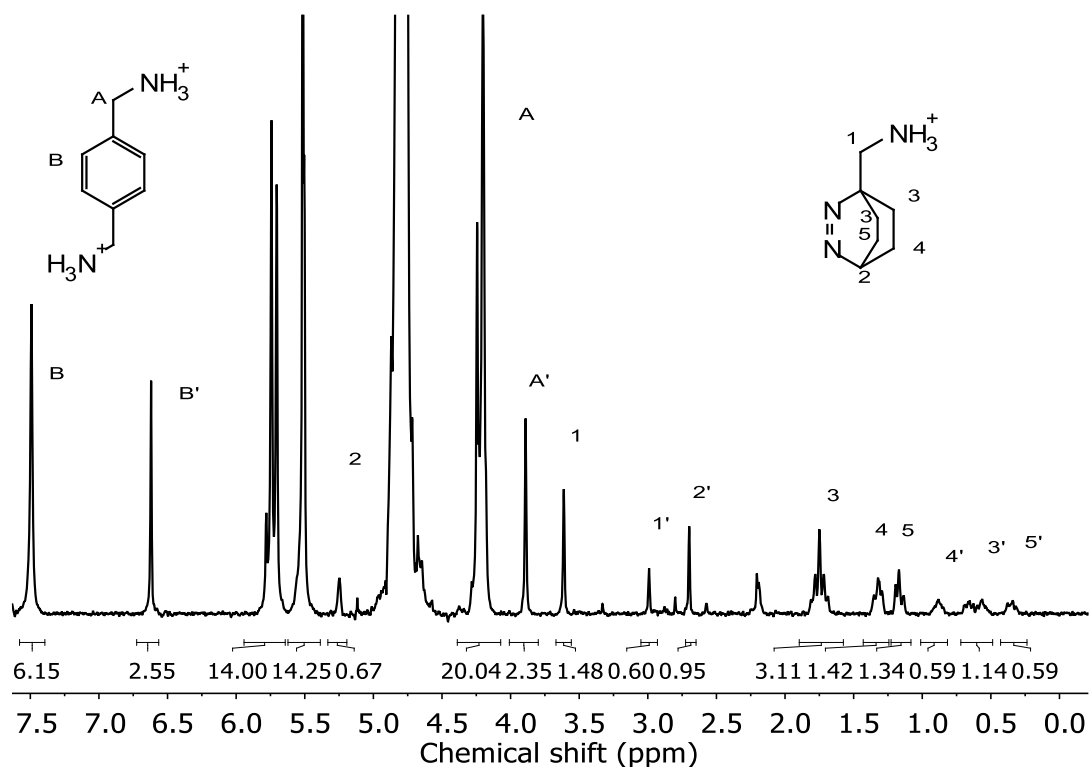


Figure A3.28 ^1H NMR spectra used to determine the K_{rel} for $\text{PXD} \cdot \text{CB7}$ and $\text{DBO-A} \cdot \text{CB7}$ in D_2O at pD 7.4. Concentrations were 2.18 mM PXD, 1.15 mM DBO-A and 1 mM CB7.

A.3.13 Adamantylamine (ADA)

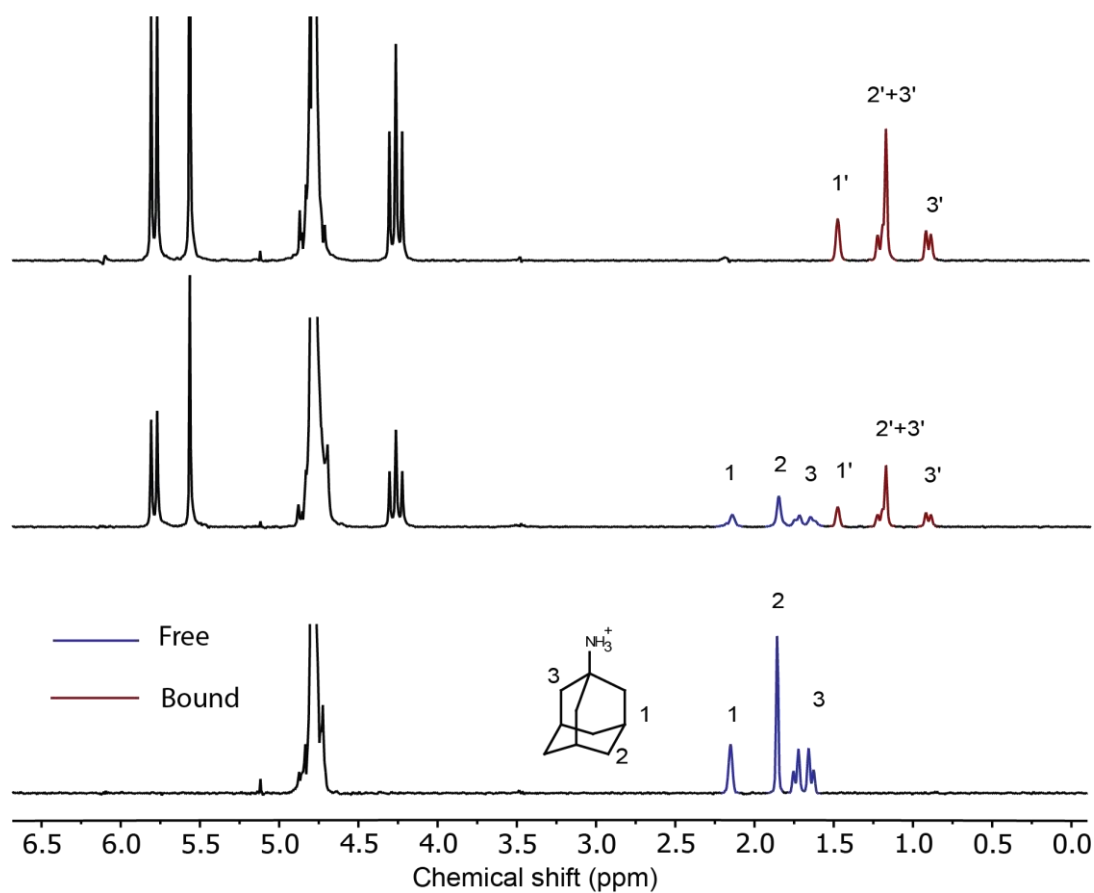


Figure A3.29 ^1H NMR spectra for 2 mM ADA free (bottom), 1 mM ADA with 0.5 mM CB7 (middle), and 1 mM ADA with 1 mM CB7 (top).

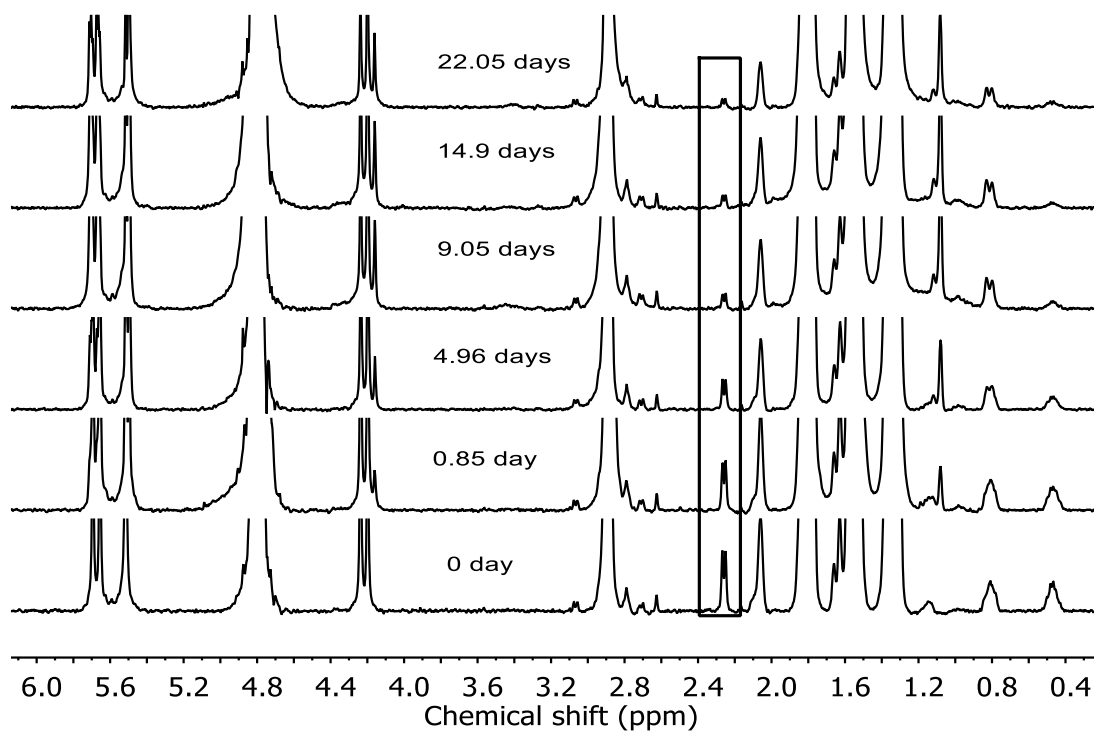


Figure A3.30 Time-dependent changes in ^1H NMR spectra of 0.74 mM of CB7 and 20 mM BAMC was prepared followed by addition of 0.74 mM ADA at pD 5.4.

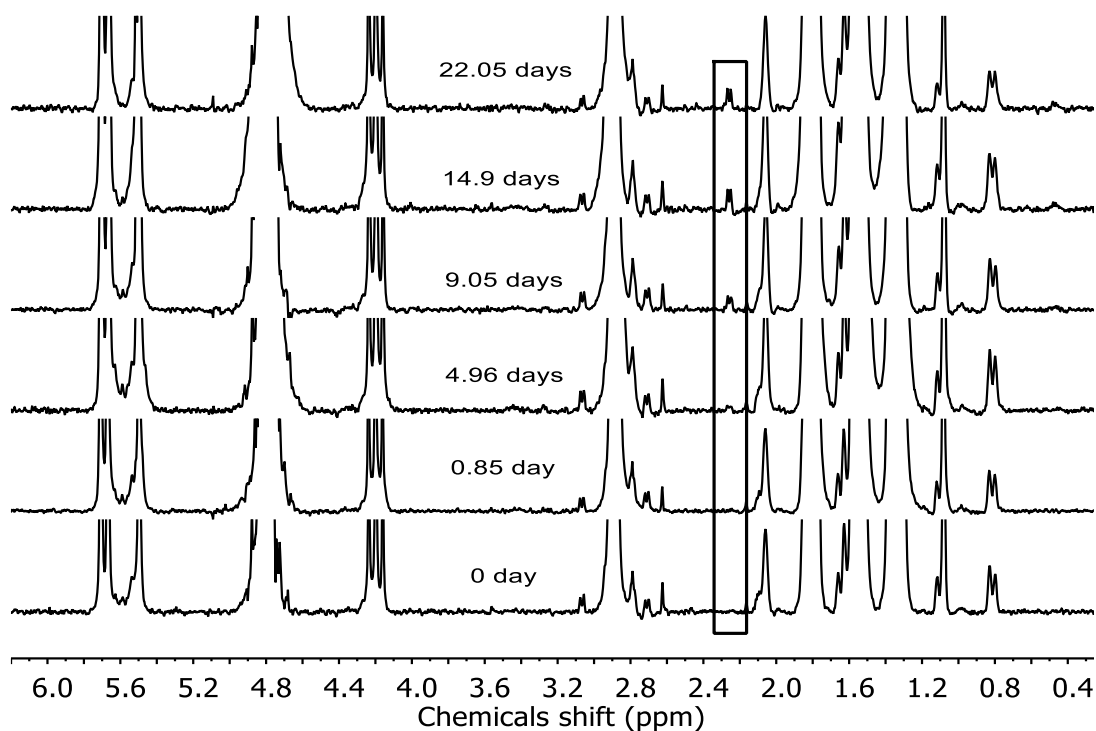


Figure A3.31 Time-dependent changes in ^1H NMR spectra of 0.74 mM of CB7 and 0.74 mM ADA was prepared followed by addition of 20 mM BAMC at pD 5.4.

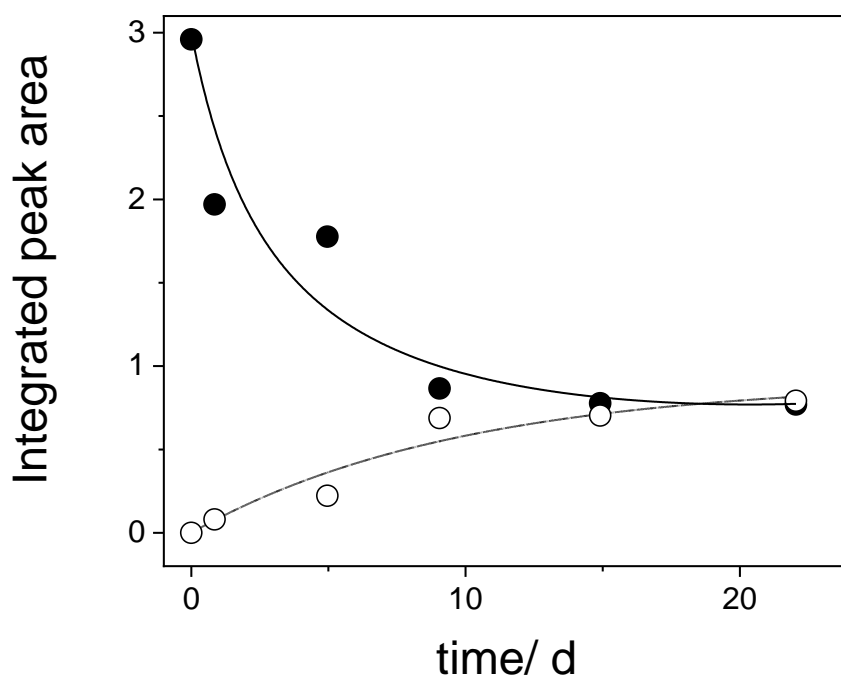


Figure A3.32 Time-dependent changes in the integrated peak area of the peak at 2.26 ppm assigned to the BAMC complex. The upper curve (●) was obtained with 0.74 mM CB7 and 20 mM BAMC after the addition of 0.74 mM ADA (**Figure A3.30**) and the lower curve (○) with 0.74 mM CB7 and 0.74 mM ADA after the addition of 20 mM BAMC (**Figure A3.31**). The lines were inserted to guide the eye.

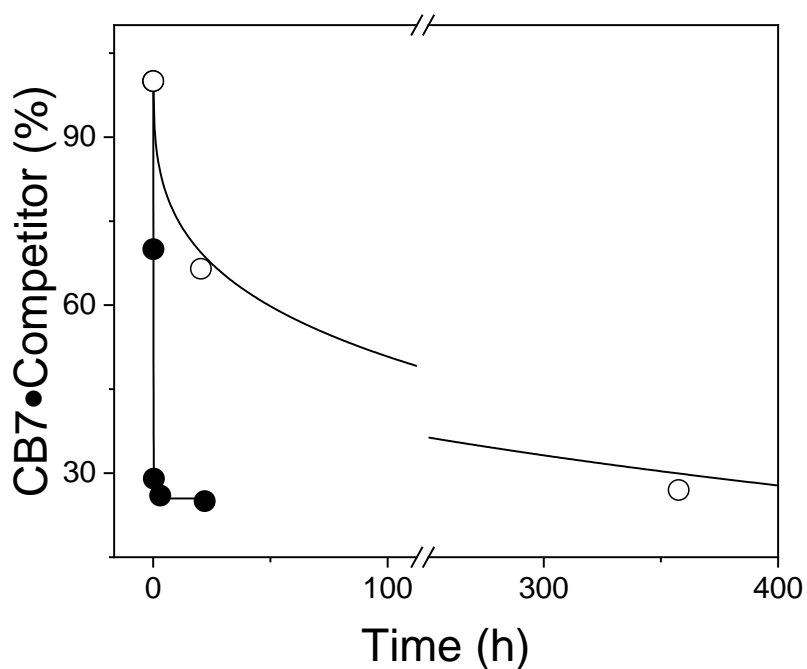


Figure A3.33 Dissociation of the pre-formed CBAMC•CB7 (○) and FDMA•CB7 (●) complexes. Therefore, 20 mM CBAMC and 0.74 mM CB7 or 17 mM FDMA and 1 mM CB7 were mixed and 1.25 mM ADA leading to dissociation of the complexes by competitive binding. The lines were inserted to guide the eye.

A.3.14 Aminomethyladamantane (AMADA)

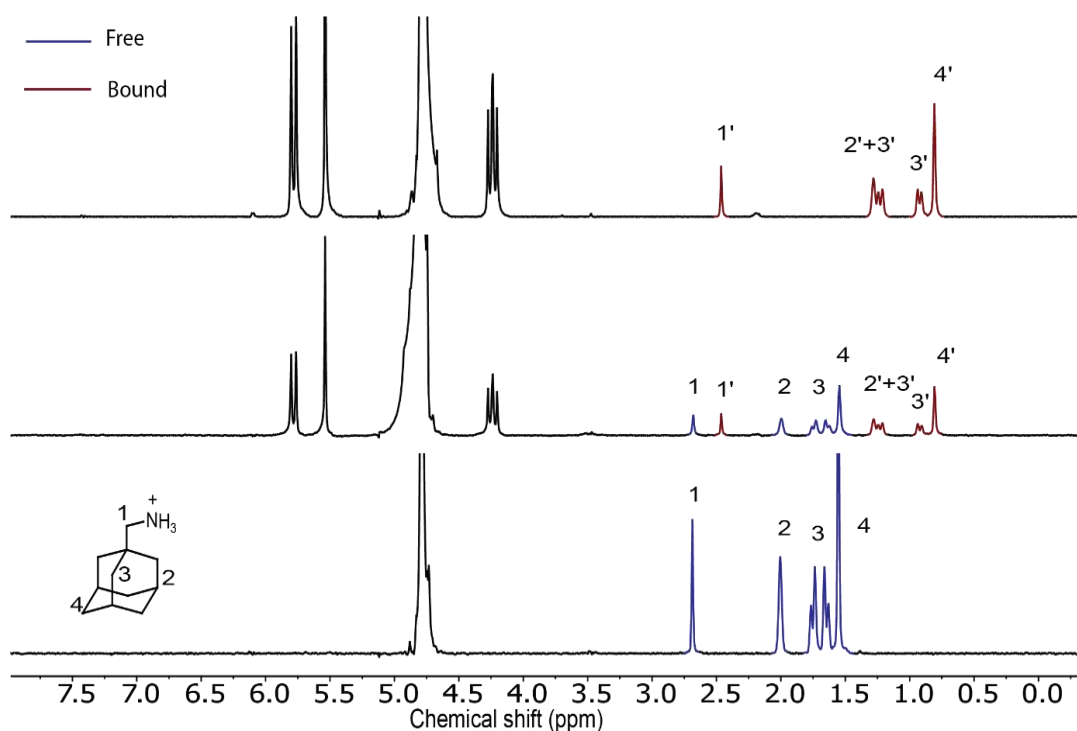


Figure A3.34 ¹H NMR spectra for 2 mM AMADA free (bottom), 1 mM AMADA with 0.5 mM CB7 (middle), and 1 mM AMADA with 1 mM CB7 (top).

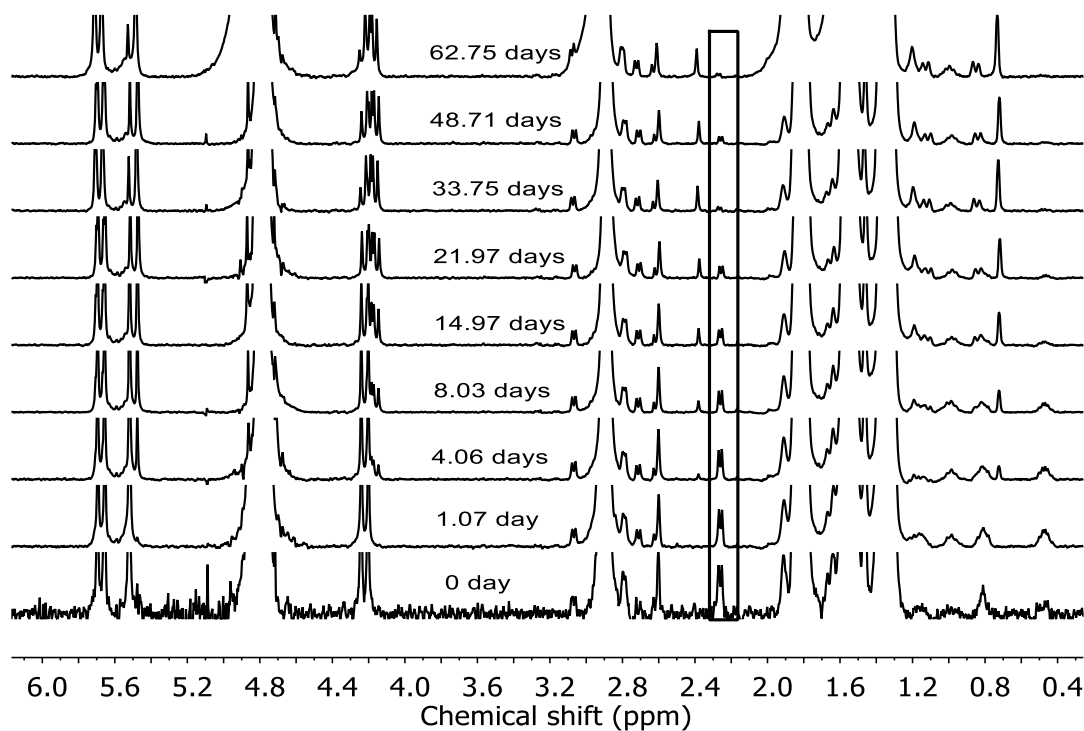


Figure A3.35 Time-dependent changes in ^1H NMR spectra of 0.56 mM of CB7 and 40 mM BAMC was prepared followed by addition of 0.56 mM AMADA at pH 7.4.

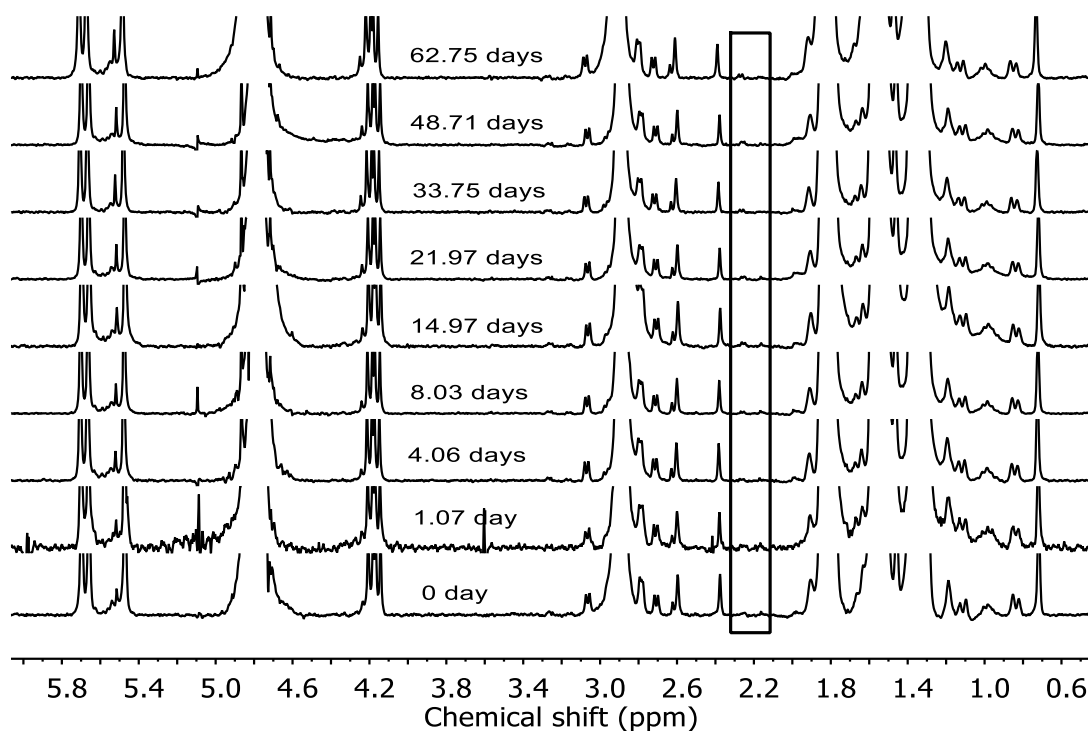


Figure A3.36 Time-dependent changes in ^1H NMR spectra of 0.56 mM of CB7 and 0.56 mM AMADA was prepared followed by addition of 40 mM BAMC at pH 7.4.

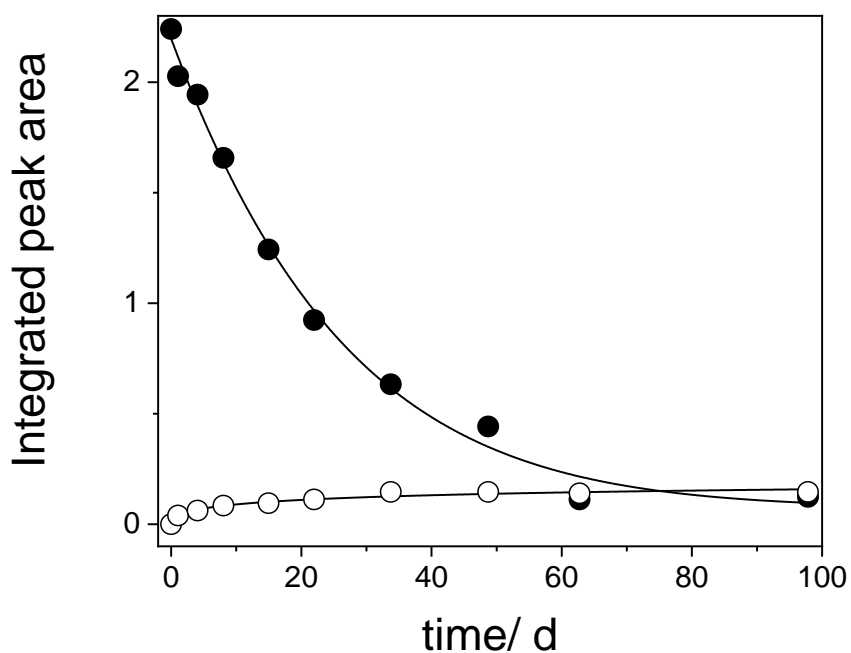


Figure A3.37 Time-dependent changes in the integrated peak area of the BAMC•CB7 complex peak at 2.26 ppm. The upper curve (●) was obtained with 0.56 mM CB7 and 40 mM BAMC after the addition of 0.56 mM ADA (**Figure A3.35**) and the lower curve (○) with 0.56 mM CB7 and 0.56 mM ADA after the addition of 40 mM BAMC (**Figure A3.36**). The lines were inserted to guide the eye.

A.3.15 *N,N*-Dimethylaminomethylferrocene (FDMA)

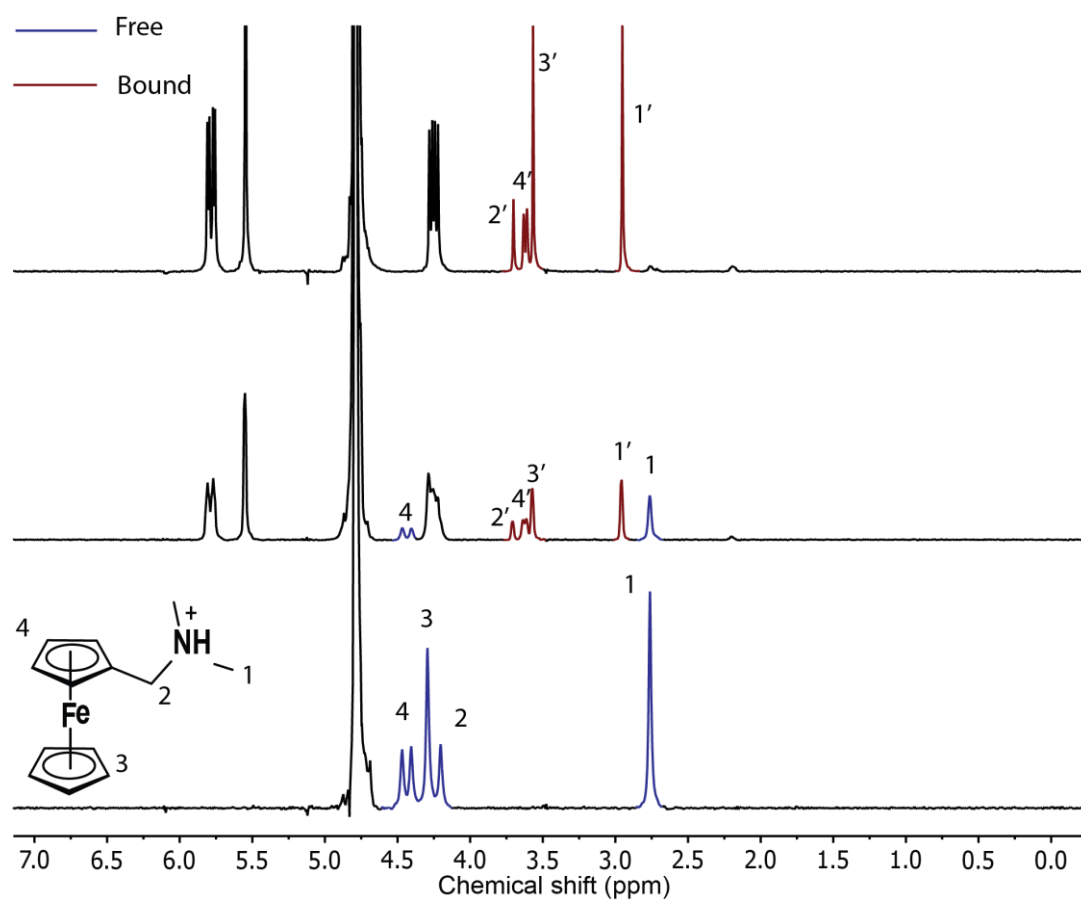


Figure A3.38 ^1H NMR spectra for 2 mM FDMA free (bottom), 1 mM FDMA with 0.5 mM CB7 (middle), and 1 mM FDMA with 1 mM CB7 (top).

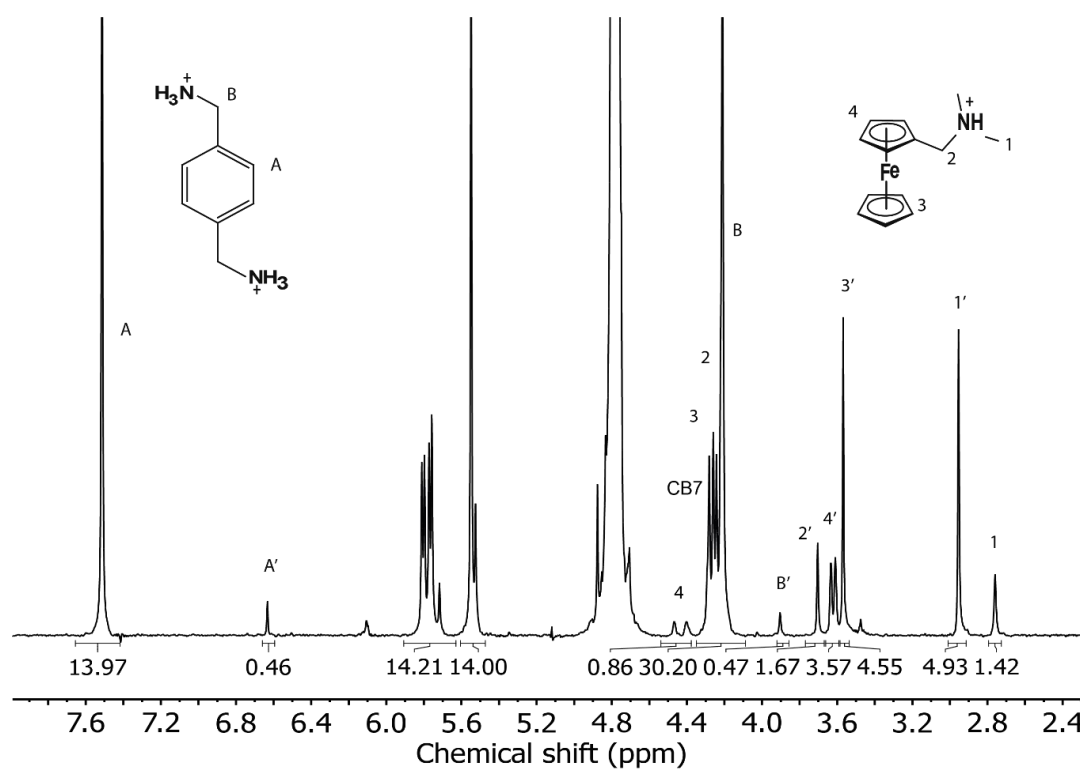


Figure A3.39 ^1H NMR spectra used to determine the K_{rel} for PXD•CB7 and FDMA•CB7 in D_2O at pH 7.4. Concentrations were 3.5 mM PXD, 1.06 mM FDMA and 1 mM CB7.

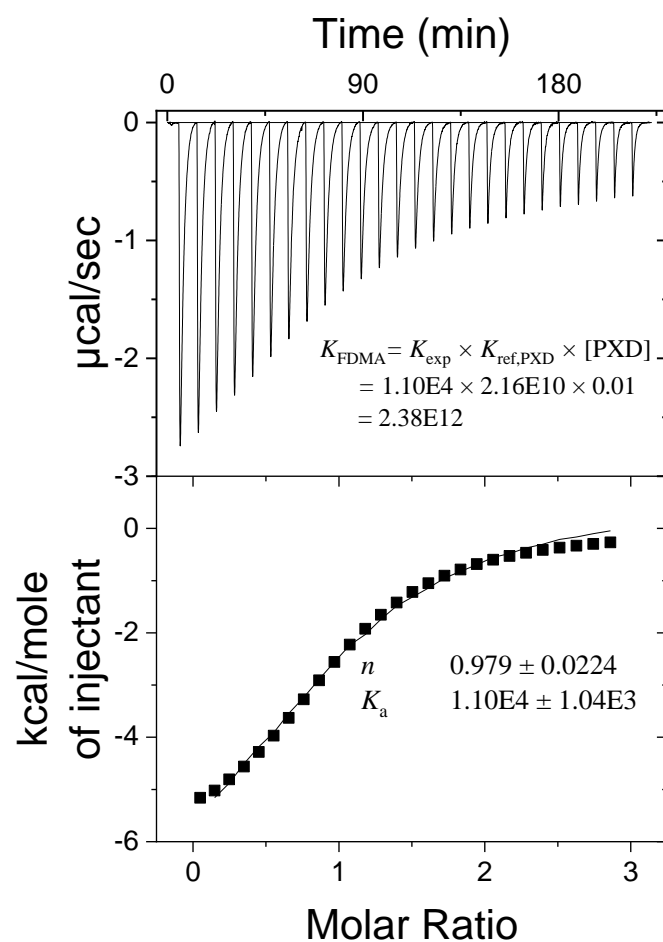


Figure A3.40 Competition ITC experiments on complexation of 0.43 mM CB7 and 10 mM PXD with FDMA as competitor at pH 7.0, 25 °C.

A.3.16 (*S*)-2-(Adamantan-1-yl)-2-aminoacetic Acid Hydrochloride (AMADA-aa)

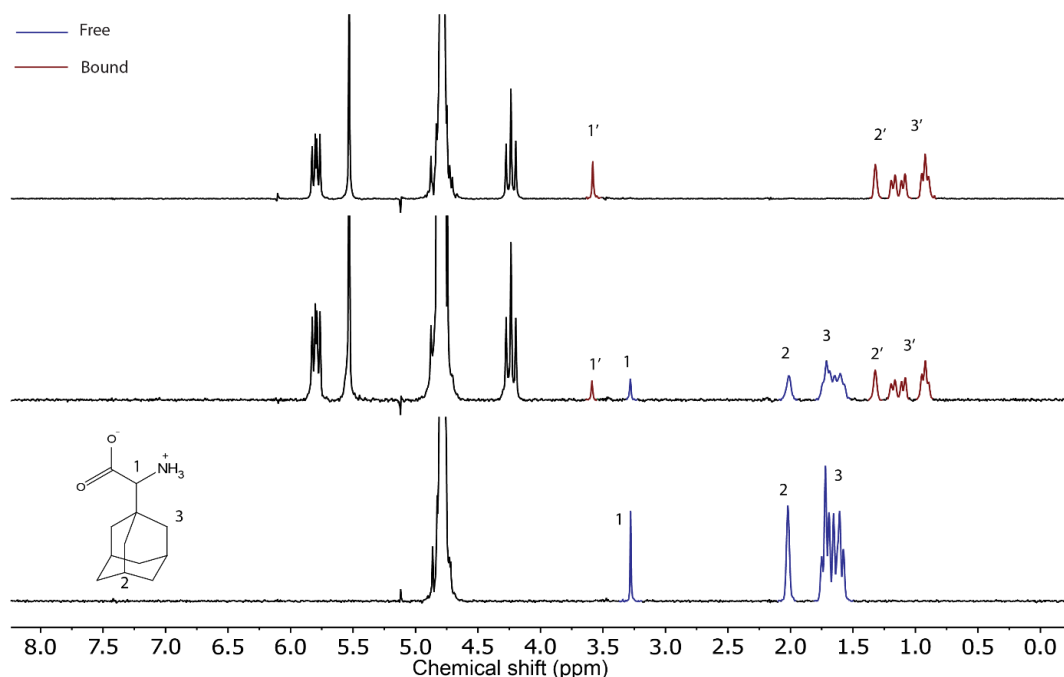


Figure A3.41 ^1H NMR spectra for 2 mM AMADA-aa free (bottom), 1 mM AMADA-aa with 0.5 mM CB7 (middle), and 1 mM AMADA-aa with 1 mM CB7 (top).

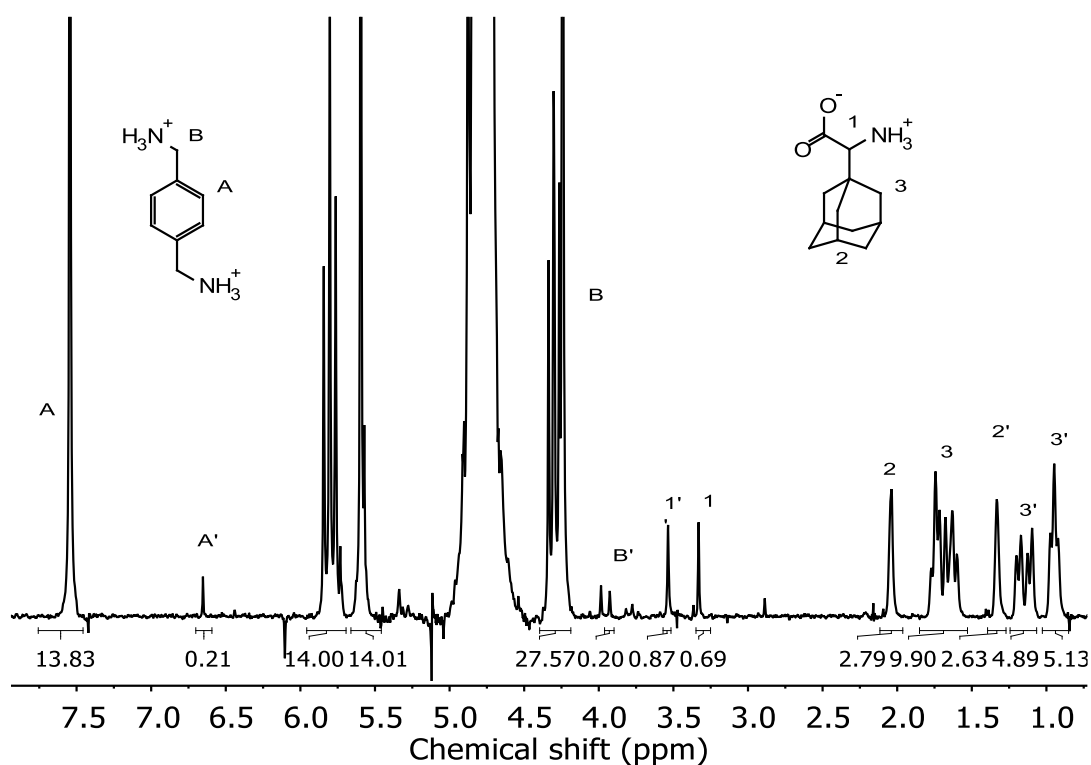


Figure A3.42 ^1H NMR spectra used to determine the K_{rel} for $\text{PXD}\cdot\text{CB7}$ and $\text{AMADA-aa}\cdot\text{CB7}$ in D_2O at pD 7.4. Concentrations were 3.5 mM PXD, 1.65 mM FDMA and 1 mM CB7.

A.3.17 Aminomethyladamantane-putrescine (AMADA-Put)

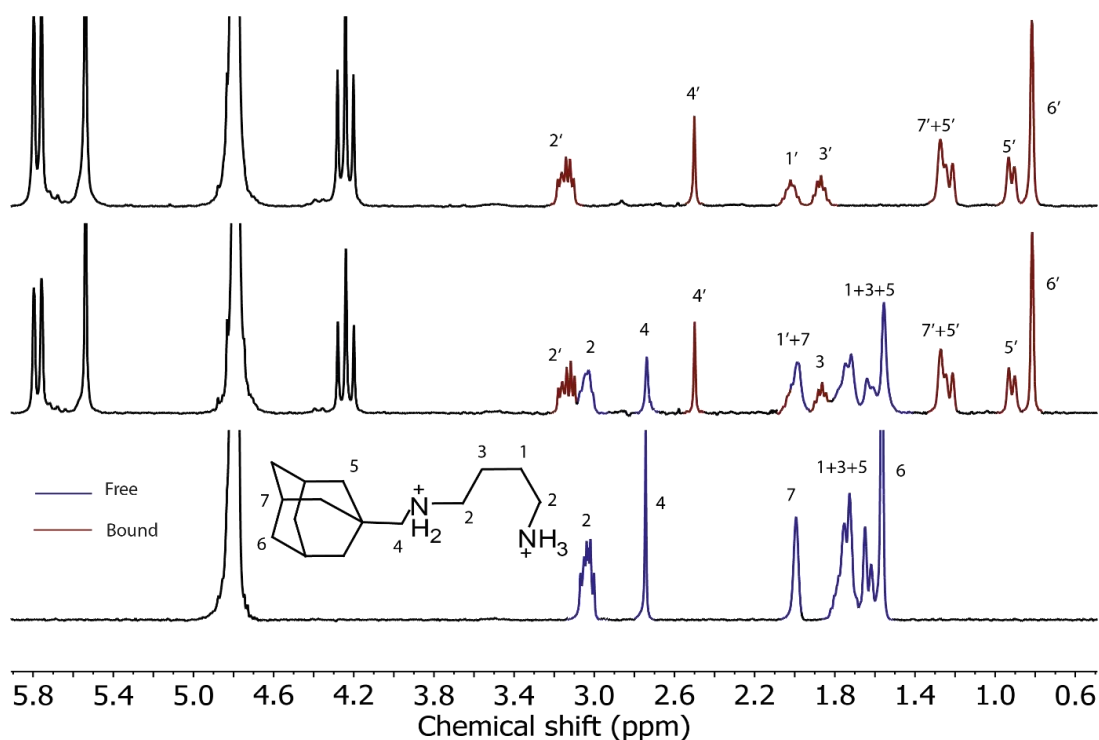


Figure A3.43 ^1H NMR spectra for 2 mM AMADA-Put free (bottom), 1 mM AMADA-Put with 0.5 mM CB7 (middle), and 1 mM AMADA-Put with 1 mM CB7 (top).

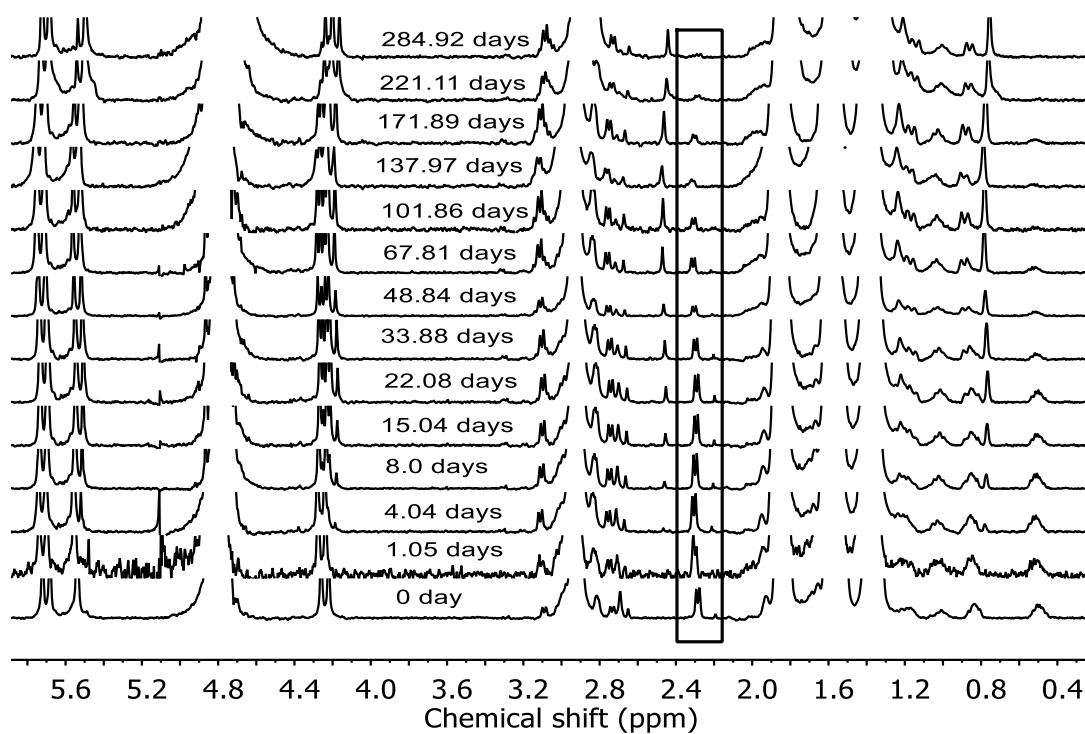


Figure A3.44 Time-dependent changes in ^1H NMR spectra of 0.56 mM of CB7 and 50 mM BAMC was prepared followed by addition of 0.93 mM AMADA-Put at pD 5.4.

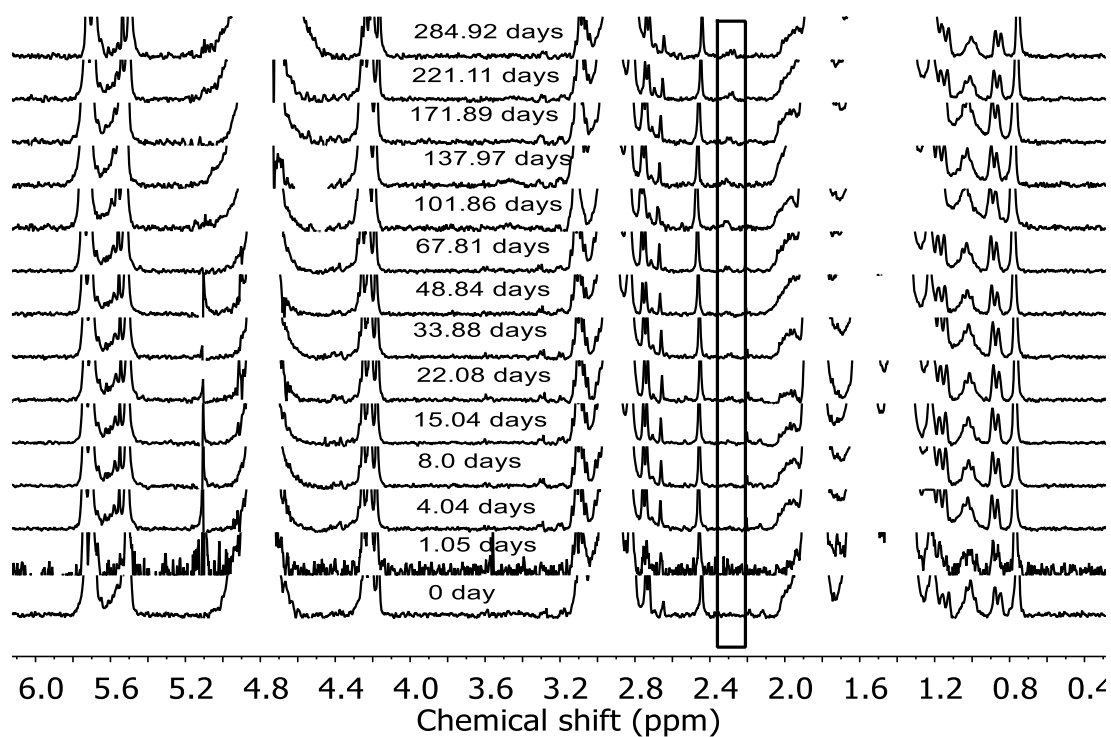


Figure A3.45 Time-dependent changes in ^1H NMR spectra of 0.56 mM of CB7 and 0.93 mM AMADA-Put was prepared followed by addition of 50 mM BAMC at pH 5.4.

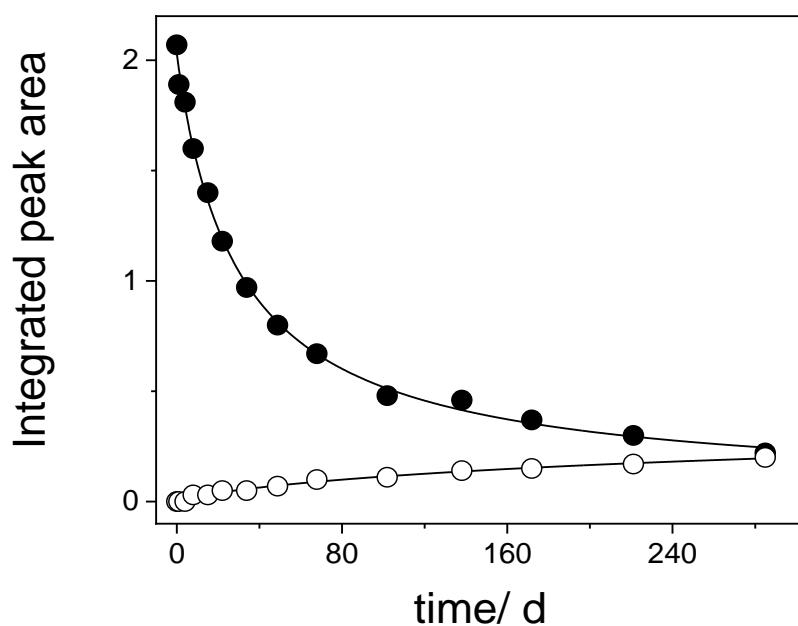


Figure A3.46 Time-dependent changes in the integrated peak area of the BAMC•CB7 complex peak at 2.26 ppm. The upper curve (●) was obtained with 0.56 mM CB7 and 50 mM BAMC after the addition of 0.93 mM AMADA-Put (**Figure A3.44**) and the lower curve (○) with 0.56 mM CB7 and 0.93 mM AMADA-Put after the addition of 50 mM BAMC (**Figure A3.45**). The lines were inserted to guide the eye.

A.3.18 *Trans*-1,4-Bis(aminomethyl)-cyclohexane (TBAMC)

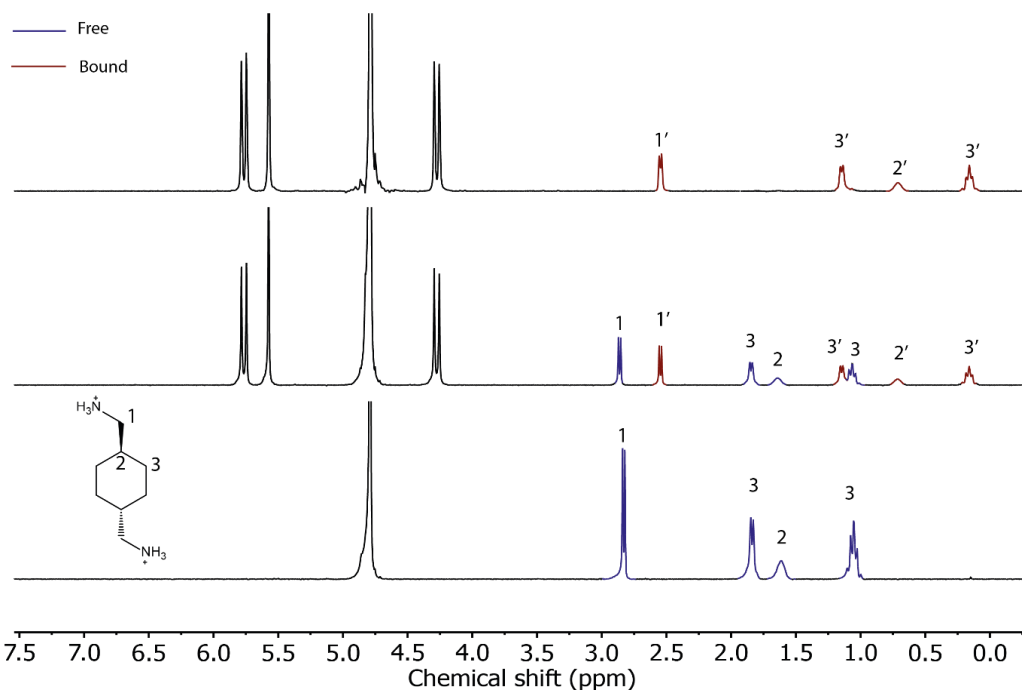


Figure A3.47 ^1H NMR spectra for 2 mM TBAMC free (bottom), 1 mM TBAMC with 0.5 mM CB7 (middle), and 1 mM TBAMC with 1 mM CB7 (top).

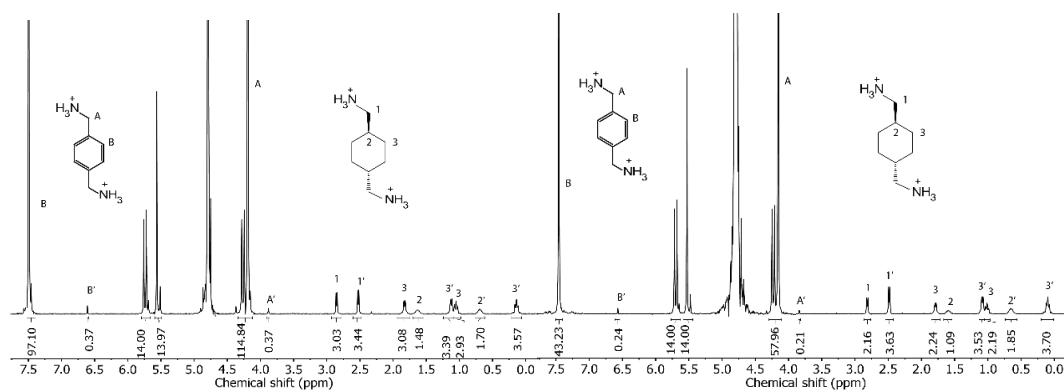


Figure A3.48 ^1H NMR spectra used to determine the K_{rel} for $\text{PXD}\cdot\text{CB7}$ and $\text{TBAMC}\cdot\text{CB7}$ in D_2O at pH 7.4. Concentrations were a) 20 mM PXD, 1.6 mM TBAMC, and 1 mM CB7 and b) 10.8 mM PXD, 1.47 mM TBAMC, and 1 mM CB7.

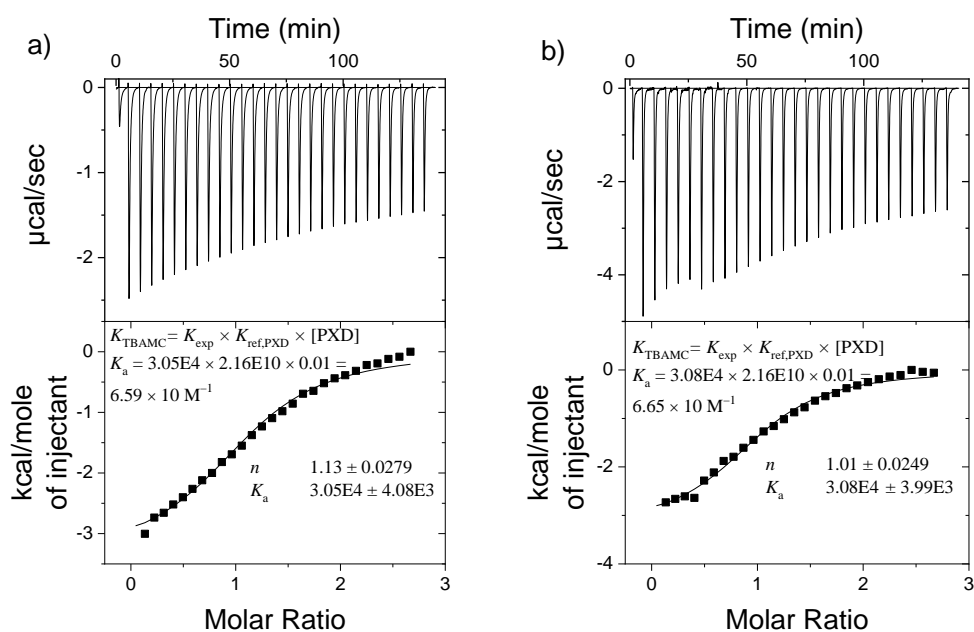


Figure A3.49 Competition ITC experiments on complexation of TBAMC with a) 0.25 mM CB7 or b) 0.20 mM CB7 in the presence of 10 mM PXD at pH 7.0, 25 °C.

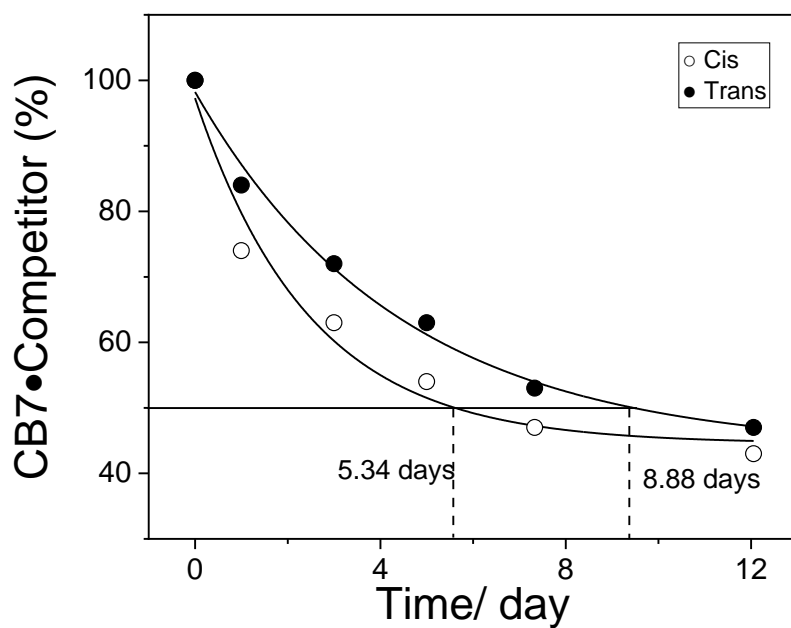


Figure A3.50 Approximation of the half-life times of the CB7 complexes of CBAMC (○), and TBAMC (●). The fraction of initial CB7 complex was monitored as a function of time with 1 mM CB7 with 33 mM CBAMC (○) and 1 mM CB7 33 mM TBAMC (●) followed by addition of 1.25 mM ADA. The lines were inserted to guide the eye.

